THESIS ON CIVIL ENGINEERING F35

Nonlinear Dynamics of Internal Gravity Waves in Shallow Seas

OXANA KURKINA

TUT PRESS

TALLINN UNIVERSITY OF TECHNOLOGY
Institute of Cybernetics
Laboratory of Wave Engineering

The dissertation was accepted for the defence of the degree of Doctor of Philosophy on 20 July, 2012

Supervisors: Prof. Tarmo Soomere
Institute of Cybernetics
Tallinn University of Technology, Tallinn, Estonia

Prof. Efim Pelinovsky
Department of Nonlinear Geophysical Processes
Institute of Applied Physics
Russian Academy of Sciences, Nizhny Novgorod, Russia

Opponents: Prof. Christian Kharif
Non-Equilibrium Phenomena Research Institute
Grande Ecole d'ingénieurs – Ecole Centrale Marseille
Marseille, France

Prof. Henrik Kalisch
Department of Mathematics
University of Bergen, Bergen, Norway

Defence of the thesis: 24 September 2012

Declaration:
Hereby I declare that this doctoral thesis, my original investigation and achievement, submitted for the doctoral degree at Tallinn University of Technology has not been submitted for any academic degree.

/Oxana Kurkina/

ISSN 1406-4766
ISBN 978-9949-23-341-0 (publication)
ISBN 978-9949-23-342-7 (PDF)

EHITUS F35

Siselainete mittelineaarne dünaamika madala vee lähenduses

OXANA KURKINA

TTÜ
KIRJASTUS

Contents

Introduction

Internal gravity waves

Internal gravity waves (IGWs), more often called internal waves (IWs), are one of the key components of both linear and nonlinear wave motions in stratified basins. The formation of IWs requires the presence of vertical density stratification of the water bodies as a critical background factor. They may be excited by a variety of external forces that disturb such a stratified fluid (surface pressure gradient, diverging or converging surface layer motion, sea-level variations, flow over topography, etc.). The restoring force is the difference between buoyancy and gravity force, frequently called net gravity. Differently from surface waves, even large-amplitude IWs in the ocean or atmosphere do not necessarily need massive amounts of energy for their generation. This is because the density differences between the water masses in natural conditions are small compared with the drastic density jump (about 1000 times) between the air and water, as for surface waves. Therefore the amplitude of IWs can easily be by one order of magnitude greater than that of surface waves with comparable energy.

IWs do not produce noticeable sea-level displacements. They still frequently become evident due to the movement of water particles: the IW motion creates convergence and divergence bands on the sea surface. Floating material and/or surfactant films are accumulated in the convergence bands, marking the existence of IWs. IWs also cause changes in the reflectivity of the sea surface (slicks and rips) due to changes in capillary wave properties owing to the associated velocity fields.

Similarly to surface waves, IWs play several important roles in the dynamics of water masses. The propagation of small-amplitude, practically linear IWs leads to a negligible impact on the water body. In natural conditions IWs usually propagate in basins of variable depth. The wave field often experiences transformation from large basin-wide scales to smaller scales. Similarly to surface waves, IWs become shorter and steeper in this process. As long as the associated changes to wave properties do not lead to wave breaking and local instability, nothing dramatic will happen. However, if a combination of vertical density gradient and shear of horizontal currents in some layers owing to the IW propagation leads to a sufficiently small Richardson number Ri ($Ri < ¼$), the lighter water will mix with the deeper heavier water, giving rise to vertical diffusion of substances into lower depths. This mixing is chiefly responsible for the ventilation of the deeper waters and the homogenization of the water through the basin depth (Babu et al., 2010; Grimshaw et al., 2011; Hutter, 2012). These processes are usually addressed in physical and dynamical oceanography or meteorology, but they play an important role also in the ecological and geological development of the basin.

Large-amplitude IWs are highly significant for sediment resuspension and transport (Bogucki and Redekopp, 1999; Stastna and Lamb, 2008; Reeder et

al., 2011) and for the biology on the continental shelf (Sandstrom and Elliott, 1984). The accompanying currents cause strong forces on marine platforms and submersibles, the associated strong distortion of the density field has a severe impact on acoustic signalling (Chin-Bing et al., 2009; Warn-Varnas et al., 2009; Sridevi et al., 2010) and their capacity to break and impact the local microstructure has major consequences for the understanding of interior ocean mixing (Muller and Briscoe, 2000).

IWs are believed to be responsible for substantial damage (Chakrabarti, 2005; Osborne 2010). Large water velocities in intense IWs can create enormous local loads and bending moments and represent a potential danger to off-shore structures, such as oil platforms, drill rigs, etc. They have been reported to displace oil platforms as much as by 200 m in horizontal direction and 10 m in vertical direction. Nonlinear IWs may cause significant (up to a factor of 2) increases in anchor tensions (Osborne et al., 1978; Song et al., 2011). The maximum force caused by such a wave associated with a peak horizontal velocity of 2.1 m/s compares with the force exerted by a surface wave with a wavelength of 300 m and a height of 18 m (Du et al., 2007). Using limited observational data of IWs in the northern South China Sea, Cai et al. (2003) conclude that intensive IWs can exert much larger forces and torques on a structure than surface waves. The danger from IWs is considered so critical that, similar to the systems of tsunami warning, the potential for automated detection systems for large-amplitude IWs (internal soliton early warning system) is being discussed now. Such systems were even tested to support drilling campaigns and guarantee the safety of drilling platforms (Stober and Moum, 2011).

An interesting phenomenon, called deadwater and known to seamen for centuries, is also directly connected to IWs. When travelling into a fiord, or near a melting ice sheet, ships seemed to come to a halt, and even at full power they would only make very slow progress. The polar explorer Fridtjof Nansen, the leader of the Norwegian North Polar expedition to the Arctic in 1893–1896 reported the following experience aboard the small research vessel *Fram*, as he was tracking the ice drift across the Arctic: 'On Tuesday, August 29th, 1893, the *Fram* got into open water in the sound between the Island of Taimyr and the Almqvist Islands and steamed in calm water through the sound to the north-east... . We took a course to ice edge to pull in to it, but the *Fram* had got into "dead-water", and made hardly any way, in spite of the engine going at full pressure. It was such slow work that I thought I would row ahead to shoot seals... . The speed must have reduced to 1–1.5 knots in the dead-water... The water at the surface was almost fresh, whereas through the bottom-cock of the engine room we got perfectly salt water' (Nansen, 2007). Later, scientists discovered the cause of this phenomenon: the radiation of energy through the so-called internal wake wave, a system of IWs created by the ship's movement similar to wake waves on the sea surface (Mercier et al., 2011).

There has been speculation that the loss of the submarine *USS Thresher* in 1969 came from an intensive IW impulse carrying the submarine rapidly into

water deeper than its crush depth. 'The nuclear submarine *USS Thresher* was lost with all hands on board. Prior to the sinking there had been no indication of equipment malfunction or unusual storm weather. While submerged, submarines attain neutral buoyancy by flooding or jettisoning seawater from a series of ballast tanks. An effective way for a submarine to avoid being detected by surface vessels is to dive and cruise silently along density pycnoclines, which tend to reflect the engine noise downward and sonar pulses from above upward. US Navy scientists speculate that the *USS Thresher* was probably cruising along a pycnocline when it encountered a large IW. Because of its neutral buoyancy, it is thought that the submarine suddenly slid down the wave's back side, down to greater depths. Unable to compensate for this sudden fall, the submarine exceeded its design depth and imploded with loss of all life' (Pinet, 1992, 2003). Osborne (2010) describes another incident in the Strait of Gibraltar. A possible explanation for the damage to the Victor class Russian submarine was that it might have been carried to the surface by an IW of positive polarity, followed by an impact with a surface ship. Although both possibilities are unconfirmed they do illustrate the potential for energetic IWs to influence submarine ballasting. Atmospheric IGWs can intensify tornado generation (http://science.nasa.gov/science-news/science-at-nasa/2008/19mar_grits/).

Solitary internal gravity waves in shallow seas

This thesis focuses on large-amplitude localized IWs, which propagate in relatively shallow areas of oceans, shelf regions or semi-sheltered seas. A fascinating feature of many waves of this kind is that they propagate for a long time without any significant change of their energy or shape as solitons do. They can be interpreted and adequately described as solitary internal waves (SIWs) and are often referred to as internal solitons. Strictly speaking, the term 'soliton' is reserved for elastically interacting solitary waves in integrable systems (Drazin and Johnson, 1989), but we will nevertheless follow the widely used custom (Soomere, 2009) and call these waves internal solitons. Such a terminology is particularly justified here because, as a first approximation, these waves can be successfully modelled by integrable equations of Korteweg–de Vries (KdV) type. Observations of large-amplitude IWs are presented in many original research papers and reviews (Ostrovsky and Stepanyants, 1989; Jeans, 1995; Grimshaw, 2002; Holloway et al., 2002; Jackson, 2004; Ostrovsky and Stepanyants, 2005; Sabinin and Serebryany, 2005; Vlasenko et al. 2005; Helfrich and Melville, 2006; Apel et al., 2007; Grimshaw et al., 2007).

Various appropriate mathematical models have been developed to describe nonlinear IWs (Grimshaw, 2002; Grimshaw et al., 2007; Pelinovsky et al., 2007). The first study of internal solitons was based on the nonlinear boundary problem for the stream function (Dubriel-Jacotin, 1932; Long, 1953). This approach is based on the Dubreil-Jacotin–Long (DJL) equation that is formally equivalent to the full set of Euler equations and remains popular in numerical simulations of large-amplitude solitons (see Vlasenko et al., 2005; Helfrich and

Melville, 2006; Dunphy et al., 2011 and references therein). The unsteady dynamics of small-amplitude soliton-like IWs was first analysed in the framework of the KdV equation (Benney, 1966). More complicated models based on the extended versions of the KdV and Boussinesq equations have been developed for moderate- and large-amplitude waves. Now the direct numerical simulation of IWs in the framework of the basic 2D and 3D Euler equations is being actively carried out (Grue et al., 1999; Lamb, 2002; Vlasenko et al., 2005, Maderich et al., 2010, 2012) to study the generation, propagation and breaking of internal solitons.

Outline of the thesis

Chapter 1 presents an overview of theoretical concepts and asymptotic techniques used to address unidirectional IWs in a stratified medium and expands further towards detailed analysis of IWs in a generic three-layer environment and in several specific cases (the Baltic Sea and the South China Sea). As the relevant derivations are usually presented in the scientific literature for specific cases, it is instructive to describe this technique in a general manner. Doing so makes it possible to naturally distinguish different balances of nonlinear and dispersive terms from a unique framework and also to specify different regimes of wave propagation. The presented material is to a large extent classical but several developments in Papers I, IV and V are highlighted as well.

In Chapter 2, based on Papers IV and V, the theory described in Chapter 1 is extended to higher orders for lower-mode IWs in one special stratified medium because of vanishing lower-order nonlinear terms, and the higher-order extension of weakly nonlinear theory is considered. A key development is the derivation of a new so-called (2+4)KdV-like equation for IWs in a symmetric three-layer fluid. Its solitary wave solutions are found and their behaviour is analysed.

Chapters 3 and 4 extend further the analysis of the properties of IWs in realistic conditions. Chapter 3 mostly follows Papers III and VI. It first presents an overview of existing observational evidence of IWs in the Baltic Sea. The key development of this chapter is a thorough description of the spatial and seasonal variability of the basic average kinematic and nonlinear parameters governing the propagation and transformation of IWs in this basin. In particular, different nonlinear wave regimes are mapped in detail together with estimates of potential values of horizontal velocities excited by various IW regimes. Finally, the basic properties of extreme surface wave conditions in the southern Baltic Sea (probably the most intense IW generation area in the Baltic) are analysed.

Chapter 4 focuses on the propagation and transformations of IWs in the Baltic Sea and two other strongly stratified basins of the World Ocean. In the South China Sea IWs are regularly excited by tidal flows while the excitation

of IWs in the Barents Sea is substantially modified by the effects of the Earth's rotation. The presentation follows the material published in Papers I and II.

Papers constituting the thesis and approbation of the results

The thesis is based on the following publications:

Papers in journals indexed by the ISI Web of Science:

I. Grimshaw, R., Talipova, T., Pelinovsky, E., Kurkina, O. Internal solitary waves: propagation, deformation and disintegration. – Nonlinear Processes in Geophysics 17; 2010, p. 633–649.

II. Kurkina O., Talipova, T. Huge internal waves in the vicinity of the Spitsbergen Island (Barents Sea). – Natural Hazards and Earth System Sciences 11; 2011, p. 981–986.

III. Kurkina, O., Pelinovsky, E., Talipova, T., Soomere, T. Mapping the internal wave field in the Baltic Sea in the context of sediment transport in shallow water. – Journal of Coastal Research SI 64(II); 2011, p. 2042–2047.

IV. Kurkina, O., Kurkin, A., Soomere, T., Pelinovsky, E., Rouvinskaya, E. Higher-order (2+4) Korteweg–de Vries-like equation for interfacial waves in a symmetric three-layer fluid. – Physics of Fluids 23 /11; 2011, Art. No. 116602, p. 1–13.

V. Kurkina, O.E., Kurkin, A.A., Rouvinskaya, E.A., Pelinovsky, E.N., Soomere, T. Dynamics of solitons in non-integrable version of the modified Korteweg–de Vries equation. – JETP Letters 95 /2; 2012, p. 91–95.

Peer-reviewed paper:

VI. Soomere, T., Kurkina, O. Statistics of extreme wave conditions in the south-western Baltic Sea. – Fundamental and Applied Hydrophysics 4 /4; 2011, p. 43–57.

The basic results described in this thesis have been presented in the following international conferences and seminars:

1. European Geosciences Union (EGU) General Assemblies, Vienna, Austria (2010–2012):
   1.1. Talipova, T., **Polukhina (Kurkina), O.** Modeling of intensive internal wave generation over the critical latitude in the Barents Sea: effects of bottom slopes. – EGU General Assembly, Vienna, Austria, May 02–07, 2010. Geophysical Research Abstracts, 12, EGU2010-1189-1, 2010.
   1.2. **Polukhina (Kurkina), O.**, Kurkin, A., Vladykina (Rouvinskaya), E. Extended modified Korteweg–de Vries equation for internal gravity waves in a symmetric three-layer fluid. – EGU General Assembly, Vienna, Austria, May 02–07, 2010. Geophysical Research Abstracts, 12, EGU2010-2998, 2010.

1.3. Giniyatullin, D., Tyugin, A., Kurkin, A., **Polukhina (Kurkina), O.** Influence of hydrological data sources upon the geographical and seasonal distribution of kinematic and nonlinear parameters of long internal gravity waves. – EGU General Assembly, Vienna, Austria, May 02–07, 2010. Geophysical Research Abstracts, 12, EGU2010-6070, 2010.

1.4. **Kurkina**, **O.,** Talipova, T., Pelinovsky, E., Soomere, T., Giniyatullin, A. Prognostic characteristics of internal waves for the Baltic Sea. – EGU General Assembly, Vienna, Austria, April 03–08, 2011. Geophysical Research Abstracts, 13, EGU2011-4559-2, 2011.

1.5. Giniyatullin, A., Tyugin, D., **Kurkina, O.**, Kurkin, A. GIS for studying internal gravity waves. – EGU General Assembly, Vienna, Austria, April 03–08, 2011. Geophysical Research Abstracts, 13, EGU2011-4361, 2011.

1.6. Ruvinskaya, E., **Kurkina, O.**, Kurkin, A., Kuzin, A., Barenboim, M. Nonlinear dynamics of intensive internal waves in bounded stratified basins. – EGU General Assembly, Vienna, Austria, April 03–08, 2011. Geophysical Research Abstracts, 13, EGU2011-4363, 2011.

1.7. Talipova, T., **Kurkina, O.** Modulation instability and hazardous internal waves in South China and Baltic Seas. – EGU General Assembly, Vienna, Austria, April 03–08, 2011. Geophysical Research Abstracts, 13, EGU2011-1975, 2011.

1.8. **Kurkina O.**, Kurkin A., Rouvinskaya, E. Higher-order weakly nonlinear theory for internal waves in three-layer fluid. – EGU General Assembly, Vienna, Austria, April 22–27, 2012. Geophysical Research Abstracts, 14, EGU2012-8429, 2012.

2. Seminar 'Nonlinear internal gravity waves: models and dynamics' by **O. Kurkina** at the Institute of Cybernetics, Tallinn University of Technology, January 31, 2011.
3. 11th International Coastal Symposium, Szczecin, Poland (2011): **Kurkina, O.**, Pelinovsky, E., Talipova, T., Soomere, T. 2011. Mapping the internal wave field in the Baltic Sea in the context of sediment transport in shallow water. – Abstracts of the 11th International Coastal Symposium (Szczecin, Poland, May 9–13, 2011).
4. 8th Baltic Sea Science Congress, St. Petersburg, Russia (2011): **Kurkina, O.E.**, Kurkin, A.A., Dorokhov, D.V., Gorbatsky, V.V., Morozov, E.G., Pankratov, A.S. Distribution, vertical structure and seasonal variability of horizontal currents near the Curonian Spit in south-eastern Baltic Sea in 2010. – Book of Abstracts of 8th Baltic Sea Science Congress (August 22–26, 2011, St. Petersburg, Russia), p. 272.

Acknowledgements

I wish to thank my supervisor Prof. Tarmo Soomere for his guidance, support and substantial contribution to this thesis.

I am very grateful to my supervisor Prof. Efim Pelinovsky for motivation, advice and support, which made this work possible.

I would like to express my warm gratitude to all of my co-authors for interesting ideas and fruitful collaboration.

My sincere thanks to all colleagues at the Institute of Cybernetics for their support and help. I very much appreciate the invisible support from the Centre of Excellence in Non-linear Studies and especially the models and simulated data made available by the BalticWay team. These activities were both supported by the European Union through the European Regional Development Fund and through the BONUS+ cooperation. Many activities during the preparation of the thesis were also supported by the targeted financing by the Estonian Ministry of Education and Research (Grant No. SF0140007s11) and by the Estonian Science Foundation (Grant No. 9125).

Particular thanks to my colleagues from Nizhny Novgorod State Technical University, Russian Federation, and from National Research University Higher School of Economics, Russia, for their efforts that made possible my visits to Estonia.

Finally, I wish to thank my family for love, understanding, encouraging and believing in me.

1 Theoretical models for nonlinear internal waves in shallow seas

In this chapter the basic theory of weakly nonlinear unidirectional IGWs in shallow and coastal waters, properties of SIWs and velocity fields induced by them are briefly reviewed in the framework of equations of the KdV family. Although a large part of the material is classical, the relevant derivations are usually presented in the scientific literature in much narrower context. One of the aims of this chapter is to describe the appropriate asymptotic technique in a general and systematic manner. The theory was used and the relevant results are presented in Papers I and III.

The derivation of equations of the KdV family in the context of IGWs propagating over a horizontally homogeneous sea and in a variable background is shortly reproduced in Section 1.1. Single-soliton solutions of the specified integrable equations are given in Section 1.2. The structure of local currents induced by these waves is discussed in Section 1.3.

1.1 Weakly nonlinear models of unidirectional internal waves based on equations of the KdV family

The main advantage of weakly and moderately nonlinear models of IWs in the stratified basins based on the KdV-family equations is the use of average properties of the water column to understand the wave motion. The operation of averaging eliminates the vertical coordinate and leads to certain (1+1)-dimensional [(1+1)D] equations that depend only on the horizontal coordinate and time. In the case of the unidirectional wave propagation, the main properties of nonlinear IWs can be analysed analytically. Numerical simulation in the framework of such models does not require excessive computational time, and various scenarios of the IW dynamics taking into account the variable depth, horizontal variability of the density stratification and wave energy dissipation can be studied.

In general, one has to consider a nonstationary three-dimensional (3D) hydrodynamic problem for the description of IWs in realistic conditions. It is well known that for idealized conditions (in particular, for basins of constant depth) the IW field can be presented as a superposition of wave components with different vertical structure (modes) and propagating with different speeds. If the generation of IWs has a local character, the different modes far from the generation area will be separated from one another due to dispersion (the difference in propagation speeds). Therefore, they will not interact any more and can be analysed independently. This property makes it possible to eliminate the dependence of the particular wave component on the vertical coordinate. Consequently, the evolution equation describing the dynamics of a selected mode with a fixed vertical structure includes only the horizontal

coordinates and time and is incommensurably simpler than the initial (3+1)D hydrodynamic system.

This idea to simplify the hydrodynamic equations is employed in this section for unidirectional IW propagation. The basic model here is the Gardner equation (an extended version of the KdV equation). While the KdV equation contains one quadratic nonlinear term, the Gardner equation contains a quadratic and a cubic nonlinear term. The main properties of the nonlinear IWs can be analysed analytically in the framework of the Gardner equation. In this model a travelling IW in the stratified water can have various shapes such as solitary wave (soliton) of elevation or depression, multi-soliton pulse or oscillating wave packet (breather). They can appear from various initial finite-length disturbances.

For the interpretation of the observed dynamics of IWs it is necessary to take into account the variable depth, horizontal variability of the vertical stratification in density and shear flow. Such effects are incorporated in the theoretical model leading to the variable-coefficient Gardner equation. Interesting effects become evident here when the coefficients (one or both) at the nonlinear terms of the Gardner equation vanish. For example, the soliton solution is generally destroyed at such critical points and looses its identity.

Derivation of the Korteweg–de Vries equation and its extensions for unidirectional IWs in a horizontally homogeneous sea. Weakly nonlinear models for long IWs are actively used to describe IW propagation in seas and lakes. They are based on the KdV equation and its generalizations (Benney, 1966; Kakutani and Yamasaki, 1978; Lamb and Yan, 1996; Holloway et al., 2001; Grimshaw et al., 2002). Such equations are derived by using a multiple scale method (Engelbrecht et al., 1988; Nayfeh, 2004) for an asymptotic analysis of the governing Euler equations for an inviscid incompressible stratified fluid. We shortly bring here the procedure of the derivation of the KdV-like equations in 2D (vertical plane) geometry (Pelinovsky et al., 2000; Grimshaw et al., 2002). A similar procedure is applied in Papers IV and V for the derivation of more complicated equations for certain specific situations.

The Euler equations for an inviscid incompressible stratified fluid in terms of the stream function ψ and buoyancy b are written as

$$\frac{\partial \Delta\psi}{\partial t} - \frac{\partial b}{\partial x} = J(\psi, \Delta\psi), \tag{1.1}$$

$$\frac{\partial b}{\partial t} + N^2(z)\frac{\partial \psi}{\partial x} = J(\psi, b), \tag{1.2}$$

where $(u,v) = (\partial\psi/\partial z, \partial\psi/\partial x)$ are the horizontal and the vertical components of the velocity field, respectively, $b = \rho'/g\rho_0$ is density disturbance (often called buoyancy parameter), the z-axis is vertical and positive against the direction of the gravity force, g is the gravity acceleration, $\rho_0(z)$ is the

undisturbed density of fluid, $J(A,B)=A_xB_z-A_zB_x$ is the Jacobian and $N(z)$ is the buoyancy (Brunt-Väisälä) frequency

$$N(z)=\sqrt{-\frac{gd\rho_0}{\rho_0 dz}}\,. \tag{1.3}$$

The fluid (Fig. 1.1) is assumed to be confined between two rigid boundaries: $z=-h$ (bottom) and $z=0$ (free surface). In fact, the 'rigid lid' assumption on the free surface works very well in natural water basins due to the weak variation of the water density compared with the density jump on the surface. Thus, the boundary conditions for Eqs. (1.1) and (1.2) have the form:

$$\frac{\partial\psi}{\partial x}(z=0)=\frac{\partial\psi}{\partial x}(z=-h)=0\,. \tag{1.4}$$

It is convenient to introduce the isopycnal (Lagrangian) coordinate

$$y=z-\zeta(x,z,t)\,, \tag{1.5}$$

where $\zeta(x,z,t)$ is the vertical displacement of a fluid particle from its rest position. Thus, the density $\rho(x,z,t)=\rho_0(y)$ is 'frozen' in this representation. Vertical coordinates *y* and *z* coincide in an undisturbed state and are equivalent to represent background quantities. We also assume that the horizontal velocity field $u(x,z,t)$ can be decomposed into the unperturbed horizontal shear flow velocity $U(y)$ and its perturbation $u'(x,z,t)$: $u=U+u'$.

Considerable simplifications of Eqs. (1.1) and (1.2) are possible if waves are relatively small and long. Let us consider the weakly nonlinear limit when the wave amplitude a is finite and small relative to the water depth h, equivalently, when $\varepsilon=a/h<<1$. Another small parameter $\overline{\mu}=h/L$ (L is the characteristic wavelength), or more convenient $\mu=\overline{\mu}^2$, characterizes the weak

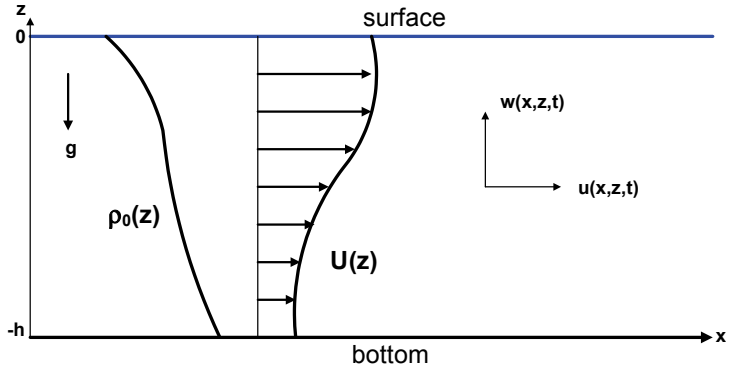

Fig. 1.1. Coordinate system and the background flow showing the undisturbed density distribution $\rho_0(z)$, the horizontal velocity $U(z)$, the coordinates *x*, *z* and the components of the velocity field, *u* and *w*

dispersion of the long waves. These parameters can be naturally used to define the slow variables: $X = \bar{\mu} x$, $T = \bar{\mu} t$. It is well known that the leading nonlinear and dispersive corrections to the linear wave equation are of the same order of magnitude (smallness) when

$$\varepsilon = \mu .$$

This relationship is sometimes called the KdV scaling. In order to construct a hierarchy of higher-order corrections, we introduce the set of new temporal variables $\tau_i = \varepsilon^i T$ in powers of ε of the slow time *T*. The relevant derivatives are:

$$\frac{\partial}{\partial T} = -c\frac{\partial}{\partial s} + \varepsilon\frac{\partial}{\partial \tau}, \quad \frac{\partial}{\partial \tau} = \frac{\partial}{\partial \tau_1} + \varepsilon\frac{\partial}{\partial \tau_2} + \cdots, \qquad \frac{\partial}{\partial X} = \frac{\partial}{\partial s}, \quad s = X - cT . \tag{1.6}$$

The co-moving coordinate s contains the linear long-wave speed *c*, which is yet to be determined and is treated as a constant in what follows.

After tedious but straightforward calculations it is possible to reduce Eqs. (1.1) and (1.2) to one equation with respect to the vertical displacement ζ:

$$\frac{\partial}{\partial y}\left\{\rho_0 (c-U)^2 \frac{\partial^2 \zeta}{\partial s \partial y}\right\} + \rho_0 N^2 \frac{\partial \zeta}{\partial s} = R . \tag{1.7}$$

Here $N(y)$ is the Brunt–Väisälä (buoyancy) frequency profile described by (1.3) and *R* is a complicated expression containing nonlinear and dispersive terms of different orders, see for instance (Grimshaw et al., 2002). The boundary conditions for Eq. (1.7) are $\zeta_{y=-h} = 0$ at the bottom and on the surface $\zeta_{y=0} = 0$.

Next, we assume that the isopycnal displacement ζ is represented by the asymptotic series

$$\zeta(s, y, \tau) = \varepsilon A(s, \tau)\Phi(y) + \varepsilon^2 \zeta_2(s, y, \tau) + \varepsilon^3 \zeta_3(s, y, \tau) + \cdots . \tag{1.8}$$

The unknown functions $\zeta_i(s, y, \tau)$ can be subsequently determined by substituting series (1.8) into Eq. (1.7) and collecting the terms of the same order of ε. To the lowest order, the linear eigenvalue problem for the modal function $\Phi(y)$ is

$$L\Phi \equiv \frac{d}{dy}\left[(c - U(y))^2 \frac{d\Phi}{dy}\right] + N^2(y)\Phi = 0 , \tag{1.9}$$

with zero boundary conditions on the bottom and the surface of the fluid. Equation (1.9) may be further simplified by using the Boussinesq approximation $\rho_0(y) \equiv \rho_0$. Physically, this means neglecting the weak density variation and setting the density constant in most of the natural water column. Doing so is usually acceptable in relatively shallow water (except for the jump layers) and will be used hereafter.

Real solutions (stable IWs) of Eq. (1.9) can be obtained only for 'supercritical' values of the Richardson number $Ri = N^2 / U_z^2 > 1/4$ (see, for instance, (Miropolsky, 2001; Vlasenko et al., 2005)). It is well known that the eigenvalue problem (1.9) has, in general, a countable infinite sequence of modes $\Phi_n^{\pm}$ with corresponding linear wave speeds (eigenvalues) $c_n^{\pm}$ ($n = 0, 1, 2, ...$). Here it is understood that $c_n^{\pm}$ characterizes the wave propagation speed with respect to the background current. A formal theory can be developed for any of these modes, but the amplitudes of wave components belonging to higher modes gradually decrease due to the energy transfer to radiated shorter lower-mode dispersive waves (Akylas and Grimshaw, 1992). This is why theories are developed mainly for solitary waves of the lowest ($n = 0$) mode only[1], which has the greatest speed *c*. The corresponding modal function $\Phi(y)$ is defined by Eq. (1.9). We choose the normalization of the modal function in a way that its extreme value is unity, i.e. $\Phi_{\max} = 1$ at $y_{\max}$.

The compatibility conditions to solve on each order of the inhomogeneous problem (1.7) (their physical meaning is avoiding secular terms) give the moving coordinate s for the wave amplitude to different orders of accuracy. At the $O(\varepsilon^2)$ level, we obtain the famous KdV equation, derived first in this context in (Benney, 1966),

$$\frac{\partial A}{\partial \tau} + \alpha A \frac{\partial A}{\partial s} + \beta \frac{\partial^3 A}{\partial s^3} = 0, \tag{1.10}$$

where

$$\alpha = \frac{3}{2I} \int_{-h}^{0} (c-U)^2 (d\Phi/dy)^3 dy, \quad \beta = \frac{1}{2I} \int_{-h}^{0} (c-U)^2 \Phi^2 dy, \quad I = \int_{-h}^{0} (c-U)(d\Phi/dy)^2 dy \tag{1.11}$$

and all integrals are calculated over the fluid depth. The KdV equation is a popular model in the physics of nonlinear waves. It is often applied in physical oceanography and limnology to demonstrate the soliton properties of both the surface and IW field in oceans, seas and lakes.

[1] In some basins the second and third modes of internal waves have also been observed (Boegman et al., 2003; Vidal et al., 2005; Yang et al., 2010).

After solving the compatibility condition for Eq. (1.7) at $O(\varepsilon^2)$ one obtains for ζ_2 the expression

$$\zeta_2 = A^2 T_n(y) + \frac{\partial^2 A}{\partial s^2} T_d(y), \tag{1.12}$$

in which $T_n(y)$ is the first nonlinear and $T_d(y)$ the first dispersion correction to the modal structure $\Phi(y)$ of the IW. These two functions are solutions of corresponding inhomogeneous boundary problems, namely:

$$LT_n = -\alpha \frac{d}{dy}\left[(c-U)\frac{d\Phi}{dy}\right] + \frac{3}{2}\frac{d}{dy}\left[(c-U)^2\left(\frac{d\Phi}{dy}\right)^2\right], \tag{1.13}$$

and

$$LT_d = -2\beta \frac{d}{dy}\left[(c-U)\frac{d\Phi}{dy}\right] - (c-U)^2\Phi, \tag{1.14}$$

with zero boundary conditions at the bottom and the surface of the fluid. In these expressions, L is the Sturm–Liuville operator given by Eq. (1.9). It is important to note that solutions of the boundary-value problems (1.13) and (1.14) are unique only up to additive multiples of Φ. It is convenient to let $A(s,\tau)$ represent the isopycnal displacement at level $y_{\max}$. Hence, we choose the auxiliary conditions $T_n(y_{\max}) = T_d(y_{\max}) = 0$. In this case, at level $y = y_{\max}$ series (1.8) gives:

$$\zeta(s, y_{\max}, \tau) = \varepsilon A(s,\tau) + O(\mu^3). \tag{1.15}$$

Other normalizations can be also used if convenient (Lamb and Yan, 1996).

Along with Eqs. (1.6) and (1.10), the compatibility condition for (1.7) at $O(\varepsilon^3)$ leads to the second-order KdV equation:

$$\frac{\partial A}{\partial \tau} + \alpha A \frac{\partial A}{\partial s} + \beta \frac{\partial^3 A}{\partial s^3} + \varepsilon\left(\alpha_1 A^2 \frac{\partial A}{\partial s} + \beta_1 \frac{\partial^5 A}{\partial s^5} + \gamma_1 A \frac{\partial^3 A}{\partial s^3} + \gamma_2 \frac{\partial A}{\partial s}\frac{\partial^2 A}{\partial s^2}\right) = 0. \tag{1.16}$$

The new coefficients may be expressed as quadratures of the modal function Φ and its corrections T_n and T_d; for example

$$\alpha_1 = \frac{1}{2I}\int_{-h}^{0} dy\Big\{3(c-U)^2\left[3(dT_n/dy) - 2(d\Phi/dy)^2\right](d\Phi/dy)^2$$
$$+ \alpha(c-U)\left[5(d\Phi/dy)^2 - 4(dT_n/dy)\right](d\Phi/dy) - \alpha^2(d\Phi/dy)^2\Big\}. \tag{1.17}$$

The next terms towards an extended KdV equation are important if coefficients of Eq. (1.10) become small. The coefficient of dispersion β is

always positive, see (1.11). However, the coefficient of quadratic nonlinearity α can have either sign and may vanish (Djorjevich and Redekopp, 1978; Kakutani and Yamasaki, 1978; Koop and Butler, 1981; Liu et al., 1985; Liu, 1988). Such a situation is typical for ocean shelves (Holloway et al., 1997; Grimshaw et al., 2007), especially at river estuaries (Pelinovsky et al., 1995). It is also frequent for inland seas and lakes (Ivanov et al., 1992; Talipova et al., 1998; Boegman et al., 2005).

In the limit $\alpha \to 0$, when the above scaling in Eq. (1.16) is violated, we have $\alpha = \varepsilon\chi$, where χ is $O(1)$. With the new scalings for the length and time

$$S = \sqrt{\varepsilon}s\,, \qquad \widetilde{T} = \varepsilon\sqrt{\varepsilon}\tau\,, \tag{1.18}$$

Eq. (1.16) is replaced by

$$\frac{\partial A}{\partial \widetilde{T}} + \left(\chi A + \alpha_1 A^2\right)\frac{\partial A}{\partial S} + \beta\frac{\partial^3 A}{\partial S^3} + \varepsilon\left(\gamma_1 A\frac{\partial^3 A}{\partial S^3} + \gamma_2\frac{\partial A}{\partial S}\frac{\partial^2 A}{\partial S^2}\right) + \varepsilon^2\beta_1\frac{\partial^5 A}{\partial S^5} = 0\,. \tag{1.19}$$

It is evident that the terms representing nonlinear dispersion and dispersion of the 5th degree are $O(\varepsilon)$ and $O(\varepsilon^2)$, respectively. In the zeroth order of ε we may keep only the term with the cubic nonlinearity from among the higher-order terms. After keeping $O(1)$ terms with respect to the small coefficient ε and returning to the usual notation we obtain the following equation in its recognized form (Holloway et al., 1999):

$$\frac{\partial \eta}{\partial t} + (c + \alpha\eta + \alpha_1\eta^2)\frac{\partial \eta}{\partial x} + \beta\frac{\partial^3 \eta}{\partial x^3} = 0\,, \tag{1.20}$$

in which A is replaced by η, χ by α and $(S, \widetilde{T})$ by (x,t). This equation is called the extended KdV equation with combined nonlinearity or the Gardner equation. The coefficients of this equation are calculated as integrals (1.11) and (1.17) depending on the eigenmode Φ of the problem (1.9) and its nonlinear correction T_n, a solution of Eq. (1.13). Both functions must be calculated in the undisturbed state of the stratified fluid, i.e. when $y \equiv z$. Therefore further on we shall consider Φ and T_n as functions of the vertical coordinate z.

The long-wave eigenvalue problem for Eq. (1.9) can yield nearly identical sets of eigenvalues for different background density profiles (Llewellyn Smith and Young, 2002; Dunphy et al., 2011). However, numerical experimentations described in (Dunphy et al., 2011) showed that a near match between long-wave speeds does not guarantee that parameters α, β and α_1 are even close for lower-mode IWs. Nevertheless, they were able to find matches between several sets of qualitatively different density profiles to provide very close values of c, α and β. The numerical simulations showed qualitatively different IW dynamics for these backgrounds, even though they were nearly identical from the point of view of weakly nonlinear theory in the KdV

approximation. The use of the Gardner equation (1.20) can improve the situation, but it is far from clear now whether the Gardner theory would yield the same result as the one found via the DJL theory for fully nonlinear stationary localized solutions.

Variable-coefficient Korteweg–de Vries-like models for IWs in waters with variable background. Variable depths are usual in natural basins. Their presence leads to a much more complex behaviour of wave fields due to transformation, refraction and diffraction. Moreover, vertical profiles of water density and background flow may vary in different domains. Formally, it is straightforward to account for a variable depth in Eqs. (1.1)–(1.4): only the bottom boundary condition (1.4) must be replaced by a condition of no water penetration through the bottom $z = -h(x)$. It is convenient to choose the x-axis on the unperturbed water surface (Fig. 1.2). In this case Eq. (1.4) should be replaced by

$$w - \vec{u}\nabla h = 0, \tag{1.21}$$

where $\vec{u} = (u, v)$, as above, contains horizontal and vertical components of the velocity field.

A much more complicated problem is to account for ambient velocities and density patterns, which may vary in the horizontal and/or vertical directions. In the context of the Euler equations the gravity force provides a stationary vertical inhomogeneity of the density and background motions. In general, a consistent inclusion of external forces (to parameterize the real physical factors, such as geostrophic currents, circulation, wind stress, slow waves like Rossby waves) into the governing equations is necessary to produce and maintain horizontal non-uniformities. For this reason, in most numerical models of the

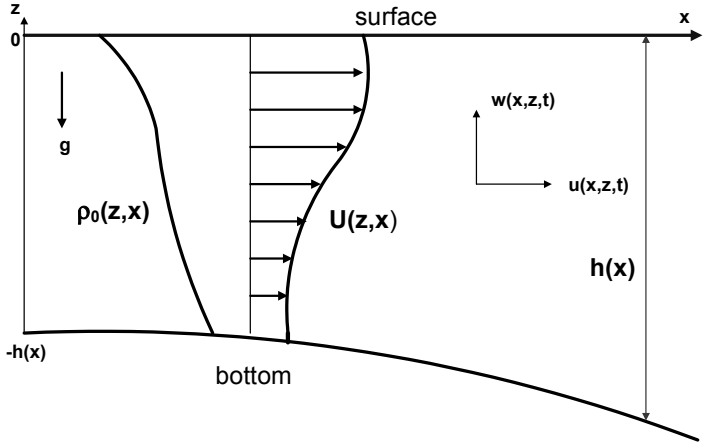

Fig. 1.2. Schematic of the coordinate system and the background flow on a variable bottom showing the undisturbed density distribution $\rho_0(z)$, the horizontal velocity $U(z)$, the coordinates x, z and the components of the velocity field, u and w

basic hydrodynamic equations for wave motions in a stratified fluid only the variable depth is usually accounted for, but not the horizontal variability of the density and velocity fields (Lamb, 1994; Vlasenko and Hutter, 2002; Vlasenko et al., 2005).

A considerable simplification to this problem is possible if the water density, background flow and basin depth vary in the horizontal direction slowly and very smoothly on a wavelength scale. This frequently happens under common natural conditions. The advantage of the use of asymptotic methods, usually based on the energy balance equation, to explore such cases is that it is not necessary to know the nature of the external forces but only to suppose their presence. Let us illustrate this point by a simple example of a long linear IW (Pelinovsky et al., 1994).

Assuming that the horizontal inhomogeneities in the density stratification and depth are sufficiently smooth, one can neglect the wave reflection[2] and consider wave propagation in one direction only. In a smooth, weakly inhomogeneous non-moving medium, the wave energy flux through any cross-section must be constant. This is one of the basic physical principles, which is not violated by the asymptotic theory (see for details, (Miropolsky, 2001)). For long linear IWs, the energy flux S through a cross-section is

$$S = \int_{-h}^{0} pudz \,. \tag{1.22}$$

Locally, the relationship between the horizontal velocity u of the water particles and the wave pressure p can be expressed based on the linear theory of long IWs in a fluid with horizontally constant density stratification. On the one hand, from the linear Euler equation

$$\rho_0 \frac{\partial u}{\partial t} + \frac{\partial p}{\partial x} = 0 \tag{1.23}$$

for a wave propagating with a speed c, it follows that

$$p = \rho_0 cu \,. \tag{1.24}$$

On the other hand, from the continuity equation and the definition of the vertical velocity through the isopycnal displacement in the linear long wave approximation we find:

$$u = c\frac{\partial \zeta}{\partial z} \,. \tag{1.25}$$

Restricting consideration in Eq. (1.8) to the lowest (linear) order and further re-scaling, we use the classical *ansatz* of separating the variables

[2] In fact, wave reflection can be very weak on certain bottom profiles even when they are not smooth (Krauss, 1966; Pelinovsky and Talipova, 2010).

$$\zeta(x,z,t) = \eta(x,t)\Phi(z)\,. \tag{1.26}$$

Note that due to the smooth horizontal inhomogeneity, the modal function Φ is also a slowly varying function of the horizontal coordinate. Finally, we obtain the relations

$$u = c\eta\frac{d\Phi}{dz}\,, \qquad p = \rho_0 c^2 \eta\frac{d\Phi}{dz}\,. \tag{1.27}$$

Of course, Eqs. (1.27) can be obtained from the formulations of the zeroth order approximation in the framework of the asymptotic method. After substitution of Eqs. (1.27) into Eq. (1.22), the energy flux conservation can be expressed (in the Boussinesq approximation) as

$$S = \rho_0 c^3 M\eta^2 = \text{const}\,, \tag{1.28}$$

where

$$M(x) = \int_{-H}^{0}\left(\frac{d\Phi}{dz}\right)^2 dz\,. \tag{1.29}$$

By virtue of the conservation of S along the x-axis, relation (1.28) can be converted to the partial differential equation

$$\frac{\partial\eta}{\partial x} + \eta\frac{\partial(Mc^3)/\partial x}{2Mc^3} = 0\,. \tag{1.30}$$

So, the equation for IWs in a horizontally smoothly inhomogeneous basin can be obtained without an exact description of the specific physical nature responsible for this variability. Using the speed of propagation c in a smoothly non-uniform medium, Eq. (1.30) can be rewritten more formally with the introduction of the small parameter ε, which now characterizes the smoothness of the horizontal inhomogeneity (it is of the same order as parameters of nonlinearity and dispersion):

$$\frac{\partial\eta}{\partial t} + c(X)\frac{\partial\eta}{\partial x} + \varepsilon\left(\frac{\eta}{2Mc^2}\frac{d(c^3M)}{dX}\right) = 0\,, \tag{1.31}$$

where $X = \varepsilon x$ is a slow coordinate. Equation (1.31) is the basic tool for the analysis of long linear IWs in a basin with variable depth and smoothly variable density field.

Accounting for nonlinearity and dispersion leads to the Gardner equation (1.20) for IWs in a basin with a fixed vertical density stratification, which in the present coordinate system is as follows:

$$\frac{\partial\eta}{\partial t} + c\frac{\partial\eta}{\partial x} + \varepsilon\left((\alpha\eta + \alpha_1\eta^2)\frac{\partial\eta}{\partial x} + \beta\frac{\partial^3\eta}{\partial x^3}\right) = 0\,. \tag{1.32}$$

It is clear now that simultaneous consideration of weak nonlinearity, dispersion and smooth density inhomogeneity in the first approximation must lead to certain additional small terms in the equations. Thus, Eqs. (1.31) and (1.32) must be combined to give:

$$\frac{\partial \eta}{\partial t} + c(X)\frac{\partial \eta}{\partial x} + \varepsilon\left((\alpha(X)\eta + \alpha_1(X)\eta^2)\frac{\partial \eta}{\partial x} + \beta(X)\frac{\partial^3 \eta}{\partial x^3} + \frac{\eta}{2Mc^2}\frac{d(c^3 M)}{dX} \right) = 0 . \qquad (1.33)$$

In a reference frame co-moving with the linear long-wave variable speed c we have:

$$\tilde{s} = \int \frac{dx}{c(X)} - t . \qquad (1.34)$$

Finally, after eliminating the small parameter, the evolution equation appears in the equivalent form:

$$\frac{\partial \eta}{\partial X} + \left(\frac{\alpha(X)}{c^2(X)}\eta + \frac{\alpha_1(X)}{c^2(X)}\eta^2 \right)\frac{\partial \eta}{\partial \tilde{s}} + \frac{\beta(X)}{c^4(X)}\frac{\partial^3 \eta}{\partial \tilde{s}^3} + \frac{\eta}{2Mc^3}\frac{d(c^3 M)}{dX} = 0 . \qquad (1.35)$$

Equation (1.35) is called the generalized Gardner equation. All its coefficients are calculated using the local undisturbed stratification structure and depth, so that it is not necessary to change the procedure of their computation for moving disturbances.

The physical, heuristic approach was used here to derive the nonlinear evolution equations (Pelinovsky et al., 1994). The governing equations can, of course, be corroborated by systematic perturbation analyses in the framework of the asymptotic theory (Pelinovsky et al., 1977; Djordjevic and Redekopp, 1978).

The presence of a horizontal shear flow leads to a modification of the function M in Eq. (1.35) (Zhou and Grimshaw, 1989; Holloway et al., 1999) (compare e.g. with (1.29)):

$$M = \int_{-h}^{0} \left(1 - \frac{U(z)}{c} \right) \left(\frac{d\Phi}{dz} \right)^2 dz . \qquad (1.36)$$

The last term in the left-hand expression of Eq. (1.35) governs wave behaviour in the framework of the linear non-dispersive theory. Therefore it is convenient to perform the change of variable

$$\eta(\tilde{s}, X) = Q(X)\xi(\tilde{s}, X) , \qquad (1.37)$$

where

$$Q(X) = \sqrt{\frac{(Mc^3)_0}{Mc^3}} \qquad (1.38)$$

is the amplification factor of long linear waves along the way of propagation. The variables with zero subscript correspond here to their initial values at $X = 0$. After substitution of Eq. (1.37) into Eq. (1.35) we reach the variable-coefficient Gardner equation:

$$\frac{\partial \xi}{\partial X} + \left(\frac{\alpha(X) Q(X)}{c^2(X)} \xi + \frac{\alpha_1(X) Q^2(X)}{c^2(X)} \xi^2 \right) \frac{\partial \xi}{\partial \tilde{s}} + \frac{\beta(X)}{c^4(X)} \frac{\partial^3 \xi}{\partial \tilde{s}^3} = 0 . \qquad (1.39)$$

This equation is not integrable (except when it can be reduced to an equation with constant coefficients); however, it has two important conservation laws: mass flow

$$\int_{-\infty}^{+\infty} \xi(\tilde{s}, X) d\tilde{s} = \int_{-\infty}^{+\infty} \xi(t, X) dt = \int_{-\infty}^{+\infty} \eta(t,0) dt \qquad (1.40)$$

and energy flux

$$\int_{-\infty}^{+\infty} \xi^2(\tilde{s}, X) d\tilde{s} = \int_{-\infty}^{+\infty} \xi^2(t, X) dt = \int_{-\infty}^{+\infty} \eta^2(t,0) dt . \qquad (1.41)$$

Let us briefly discuss the applicability of the variable-coefficient Gardner equation. The most important condition is that the horizontal nonuniformities of the density stratification must be smooth and slow, so that the linear wave speed $c(x)$ would change slowly on a scale of the typical wavelength of the IWs. In this case wave reflection in such an inhomogeneous medium can be neglected. The wave speed cannot vanish (e.g. when a wave propagates into unstratified waters or approaches the shore). Such a situation is singular. Physically, the wave must either be reflected or destroyed (analogously to surface wave reflection, run-up or breaking). Formally, the remaining coefficients of the Gardner equation can change arbitrarily, even very rapidly. Unlike the wave speed, they may vanish. The zero-crossing points of some coefficients are critical for the propagation of solitons since solitary waves can be destroyed at such points. The presence of such points does not affect the applicability of the variable-coefficient Gardner equation.

In general, for an arbitrary stratification the eigenvalue problem (1.9) (which determines the modal structure and linear long-wave speed) and all the coefficients of the Gardner equation have to be evaluated numerically. The same applies to the boundary problem (1.13) for the nonlinear correction to the linear mode. In studies of IWs in geophysical water bodies, the assumption of piece-wise constant density and shear flow is popular and the parameters of the nonlinear evolution equation can be considered as explicit functions of background conditions.

For the important case of two-layer stratification (without shear flow) explicit expressions of the coefficients are known (Djorjevich and Redekopp, 1978; Kakutani and Yamasaki, 1978; Koop and Butler, 1981). The analytical estimate of the influence of shear flow on the parameters of IWs in a two-layer

flow whose upper layer is moving with constant velocity was considered in detail in (Pelinovskii et al., 2000) for a Boussinesq fluid with the rigid lid assumption. The set of examples of analytical expressions for the coefficients of the Gardner equation is very limited. A few cases are given in (Grimshaw et al., 1997, 2002).

1.2 Solitary internal waves

Solitons, defined as solitary waves that are stable not only when propagating but also when interacting with each other, are fascinating examples of nonlinear wave processes. Internal solitons are an important part of nonlinear wave motion in natural stratified basins. They have been frequently observed in nature; see for instance reviews and books (Ostrovsky and Stepanyants, 1989; Vlasenko et al., 2005) and references therein. As it was shown above, internal solitons in shallow water can be described, to the leading order, by the KdV equation and its extended versions. As discussed in Section 1.2, the coefficients at both quadratic and cubic nonlinear terms can have either sign, depending on the fluid stratification, while the dispersive coefficient is always positive. In the framework of the Gardner equation the possibility of a sign change for the cubic nonlinearity results in a variety of wave regimes.

The Gardner equation (1.20) is an integrable nonlinear evolutionary equation, which possesses stationary localized solutions (solitary waves) for all combinations of the signs of the nonlinearities (except when both are zero, and one must move to a higher-order approximation). Its multi-soliton solutions can be found using modern techniques of nonlinear waves such as the inverse scattering method, Hirota–Darboux transformation, etc. (Slyunyaev and Pelinovsky, 1999; Slyunyaev, 2001; Grimshaw et al., 2002a, 2010). This equation also possesses one more type of localized solution, the breather, which is a periodically pulsating, or oscillating, isolated wave form (Pelinovsky and Grimshaw, 1997; Chow et al., 2005).

Below we shall frequently speak about solitons of certain equations, having in mind the relevant soliton (or solitonic) solutions to these equations. The properties of solitons of the KdV equation (which contains only one quadratic nonlinear term) are well known. The inclusion of a cubic nonlinearity into this equation substantially modifies the appearance of its soliton solutions. The single-soliton solution of the Gardner equation (1.20) is given by the formula:

$$\eta(x,t) = \frac{A}{1 + B\cosh(\gamma(x - Vt))}. \tag{1.42}$$

The soliton velocity $V = c + \beta\gamma^2$ is expressed through the inverse width γ of the soliton. The parameters A and B depend on the coefficients of Eq. (1.20) and determine the soliton amplitude a or the extreme of the function (1.42):

$$a = \frac{A}{1+B}, \quad A = \frac{6\beta\gamma^2}{\alpha}, \quad B^2 = 1 + \frac{6\alpha_1\beta\gamma^2}{\alpha^2}. \tag{1.43}$$

The possible combinations of the signs of the nonlinear coefficients in the Gardner equation correspond to different wave propagation regimes.

1) Zero cubic nonlinearity: soliton of the KdV equation

When the quadratic nonlinear term is nonzero and the cubic nonlinear term vanishes ($\alpha_1 = 0$), solution (1.42) will transform into

$$\eta(x,t) = a\,\mathrm{sech}^2\left[\sqrt{\frac{\alpha a}{12\beta}}\left(x - ct - \frac{\alpha a}{3}t\right)\right]. \tag{1.44}$$

The polarity of the KdV soliton is defined by the sign of the quadratic nonlinearity coefficient α. In particular, for the lowest IW mode, when $\alpha > 0$, the isopycnals of the solitary wave are shifted upwards (and we have a soliton of elevation, or of positive polarity). On the other hand, when $\alpha < 0$, the isopycnals of the solitary wave are shifted downwards (soliton of depression, or of negative polarity). By contrast, solitary surface waves in shallow water described by the KdV equation can have only positive polarity as the quadratic nonlinearity coefficient for surface waves is always positive.

2) Zero quadratic nonlinearity: soliton of the modified KdV equation

When quadratic nonlinearity[3] vanishes ($\alpha = 0$) and cubic nonlinearity is positive, soliton (1.42) will reduce into a soliton solution of the modified KdV (mKdV) equation (Lamb, 1980):

$$\eta(x,t) = a\,\mathrm{sech}\left[\sqrt{\frac{\alpha_1 a^2}{6\beta}}\left(x - ct - \frac{\alpha_1 a^2 t}{6}\right)\right]. \tag{1.45}$$

It can have either polarity.

No soliton solutions on nonzero pedestal exist when the coefficient of cubic nonlinear term in the mKdV equation is negative.

3) Negative cubic nonlinearity

When the coefficient α_1 at the cubic nonlinearity is negative (this is the case for a two-layer fluid), soliton solutions of a single polarity, with $\alpha\eta > 0$, exist with amplitudes between zero and a limiting value

[3] For brevity, the expressions 'quadratic nonlinearity' etc. are used to denote the values of coefficients at the relevant terms in various equations.

$$a_{\lim} = -\frac{\alpha}{\alpha_1}. \tag{1.46}$$

The shapes of solitons for different combinations of signs of the nonlinear parameters are shown in Fig. 1.3. This family corresponds to $0 < B < 1$. At small amplitudes ($B \to 1$) soliton (1.42) transforms into a KdV soliton (1.44). An increase in the soliton amplitude to the limiting value (1.46) when $B \to 0$ leads to an unlimited increase in its width. The solitary wave becomes 'wide' or 'table-shaped'. It has a flat crest and its slopes are shock-like waves or kinks.

The inclusion of only one (cubic) nonlinear term into the governing equation gives rise to several principally new phenomena that do not occur in the KdV environment. While the increase in the energy for the KdV soliton is associated with a higher and narrower wave profile, a similar process for the relevant class of solutions of the Gardner equation results in a widening of the wave profile and in the formation of a plateau-like entity with a steep front and back and a very gently sloping upper part. Such appearance of large-amplitude solitary waves has been repeatedly observed in both laboratory and field conditions (Michallet and Barthelemy, 1998; Holloway et al., 1999; Talipova et al., 1999).

4) Positive cubic nonlinearity

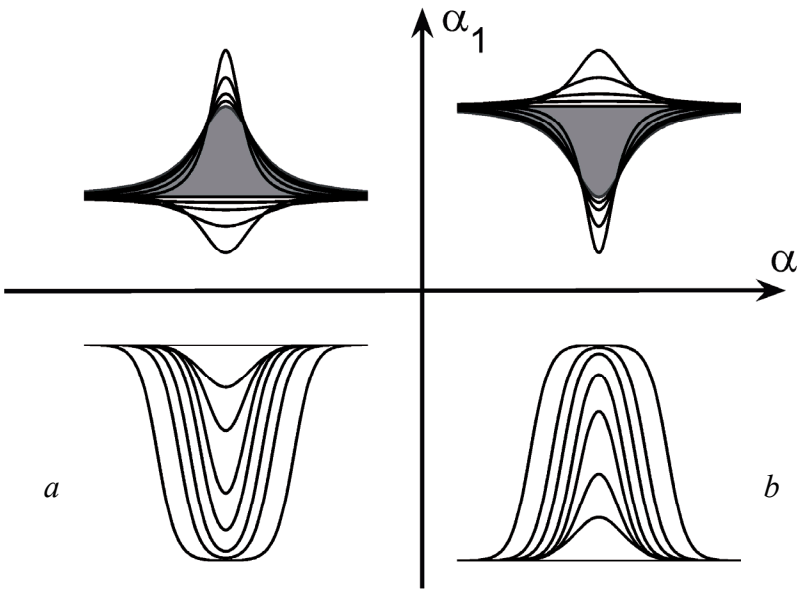

Fig. 1.3. Gardner equation soliton shapes for different combinations of the signs of nonlinear coefficients. Situations with a positive cubic nonlinearity correspond to panels (a) and (b) in the upper half-plane and with a negative cubic nonlinearity correspond to panels (c) and (d) in the lower half-plane

If $\alpha_1 > 0$, solitons of either polarity exist (Fig. 1.3a, b, upper half-plane). One of these families with $\alpha\eta > 0$ has $1 < B < \infty$; therefore, its amplitude is not bounded. In the limit of small amplitudes these solitons also become KdV solitons (1.44). For large amplitudes ($B \to \infty$) the solitons become similar to the solitons of the mKdV equation (1.45).

Another family of solitons (with $\alpha\eta < 0$) corresponds to $-\infty < B < -1$. If $B \to -\infty$, the soliton will transform into an mKdV soliton (2.9). However, the waves of this family have a minimum amplitude

$$a_{\text{alg}} = -2\frac{\alpha}{\alpha_1}. \tag{1.47}$$

At the near-critical amplitude (when $B \to -1$) soliton (1.42) acquires power-law tails and tends to the so-called algebraic soliton, which (in a reference system moving with the linear wave speed) is given by

$$\eta(x) = \frac{a_{\text{alg}}}{1 + \alpha^2 x^2 / 6\beta}, \qquad V = 0. \tag{1.48}$$

The algebraic soliton (1.48) is structurally unstable (Pelinovsky and Grimshaw, 1997).

No soliton family of (1.42) similar to the above-described structures exists if $-1 < B < 0$. In this range, when the polarity of the soliton is opposite to the sign of the quadratic nonlinearity (filled areas in Fig. 1.3a, b), only breathers exist (Pelinovsky and Grimshaw, 1997; Grimshaw et al., 2010). This type of solution of the Gardner equation (1.20) exists when $\alpha_1 > 0$. It has no limitations on its amplitude.

1.3 Velocity field induced by solitary internal waves

With the use of the Gardner equation (1.20), or its variable-coefficient forms (1.35) and (1.39), the velocity components (u, w) of fluid particles in the vertical section (x, z) can be expressed as follows:

$$u(x,z,t) = c\eta(x,t)\frac{d\Phi}{dz} + \left(\frac{\alpha}{2}\frac{d\Phi}{dz} + c\frac{dT_n}{dz}\right)\eta^2, \tag{1.49}$$

$$w(x,z,t) = -c\frac{\partial \eta}{\partial x}\Phi(z) - \left(\alpha\Phi(z) + 2cT_n(z)\right)\eta\frac{\partial \eta}{\partial x}. \tag{1.50}$$

The horizontal velocity *u* gives the greatest contribution into the local current speed. This is a typical property of long waves. This feature of an IW field may greatly contribute to the local sediment transport and/or resuspension (Reeder et al., 2011).

The first terms in Eqs. (1.49) and (1.50) correspond to the leading order of the asymptotic expansion. The remaining additives reflect the first nonlinear correction in the asymptotic series. Thus, to forecast the local current speed one has to determine (i) the isopycnal displacement $\eta(x,t)$ at the level of $z_{\max}$ (see

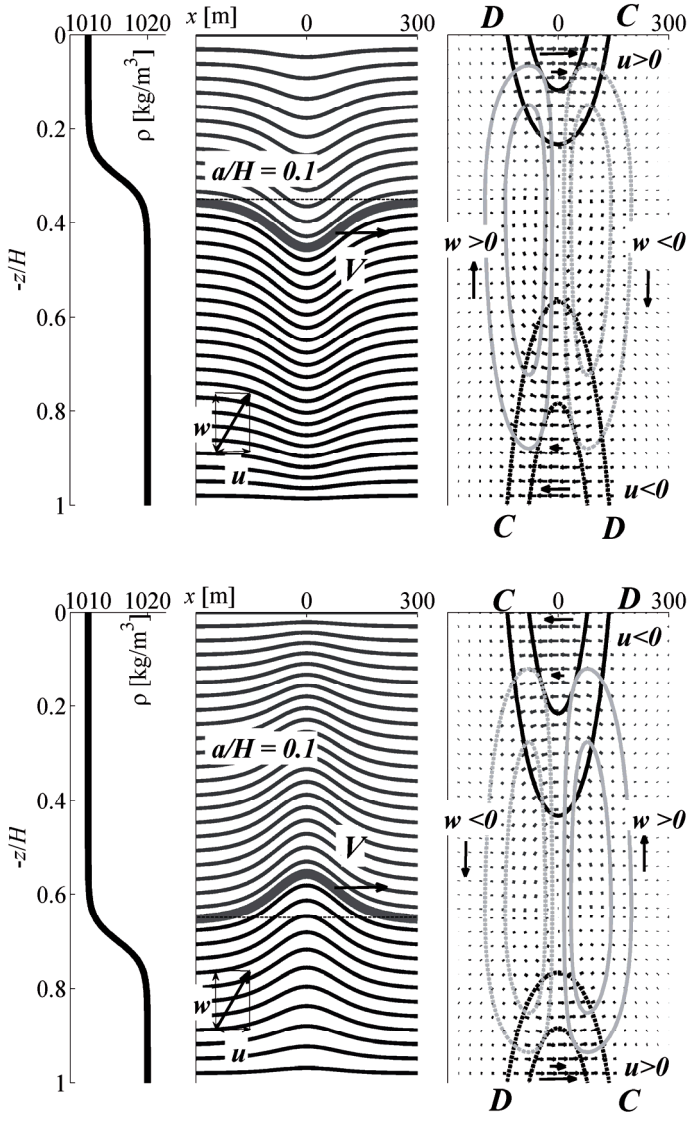

Fig. 1.4. Velocity field in a long SIW with a nondimensional amplitude a/H = 0.1 in almost two-layer water ($\rho = \rho_0 - \Delta_\rho \tanh[(z - z_0)/d]$, ρ_0 = 1015 kg/m^3, Δ_ρ = 5 kg/m^3, d = 5 m, total depth H is 100 m): upper panel (modified from (Lamb. 1997)) – negative polarity of SIW (shallow pycnocline, z_0 = –30 m), lower panel – positive polarity of SIW (deep pycnocline, z_0 = –70 m)

Eq. (1.15)), (ii) the vertical IW mode $\Phi(z)$ and (iii) its nonlinear correction $T_n(z)$. The amplitude of $\eta(x,t)$ is not known a priori. It depends upon background conditions of IW generation and can be found by means of a detailed simulation.

The velocity field induced by a SIW was studied in (Lamb, 1997) in the context of larval migrations on the sea surface. If the density variation is predominantly in the upper half of the fluid column, SIWs are waves of depression. The largest horizontal currents associated with these waves are at the surface where they are in the direction of wave propagation and at the bottom where the direction is the opposite.

Both the surface current $u_s(x,t)$ and the wave propagation speed V are typically of the order of 10–100 cm/s (sometimes up to 300 cm/s for deep areas or strong stratifications). Bottom currents are weaker for this type of

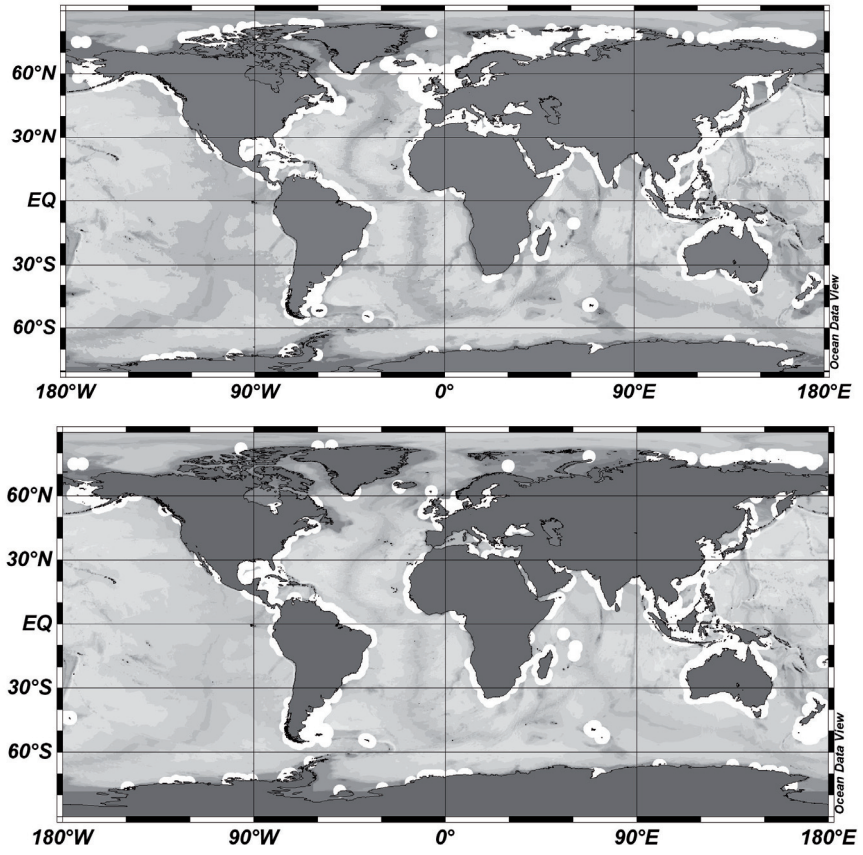

Fig. 1.5. Maps of the geographical locations (white points) where the pycnocline (position of maximum buoyancy frequency (1.3)) is situated in the lower half of the water column: upper panel – January, lower panel – July. Hydrological data to calculate the density and buoyancy profiles are from the climatological atlas GDEM V3.0 (Teague et al., 1990)

stratification. Surface currents associated with the wave will carry objects near the surface forward with the wave. This will increase the amount of time the objects are in the wave, which is an important factor in increasing their advection distance. Objects near the bottom are swept back and out of the wave, resulting in smaller advection distances. A scheme of such a SIW in a continuously stratified but almost two-layer fluid is given in Fig. 1.4a. The maximum of surface and near-bottom currents occurs at the centre of the wave (equivalent to the crest or trough of surface waves). Ahead of the wave centre the near-bottom currents are divergent and behind the wave center they are convergent. Solitary waves are symmetric at about the vertical line passing through their centre.

The change in the polarity of such a SIW gives patterns reflected with respect to half-depth (Fig. 1.4b). Such density stratifications often occur in shelf regions and especially in shallow seas (such as the Baltic Sea) and coastal waters when the pycnocline (the location of the maximum of buoyancy frequency (1.3)) is situated in the lower half of the fluid (Fig. 1.5)[4]. For this situation the strongest horizontal currents are at the bottom, and objects near the bottom are extensively carried by the wave. Therefore IWs propagating in domains where the pycnocline is located relatively close to the seabed can strongly affect bottom sediments. Confirming this, instrumental observations of very large subaqueous sand dunes on the upper continental slope of the South China Sea generated by episodic, shoaling SIWs were recently reported (Reeder et al., 2011). Such a situation apparently is typical in autumn and winter for many parts of the Gulf of Finland (Soomere et al., 2008; Leppäranta and Myrberg, 2009).

The contribution from second-order terms into the horizontal velocity in Eq. (1.49) can be estimated for the model of three-layer stratification. Such a situation again frequently occurs in the Baltic Sea. The water masses in its central part often consist of a mixed upper layer, a well-defined seasonal thermocline at a depth of about 20–40 m, an intermediate layer and the main halocline at a depth of about 80–100 m. In many cases the total depth is 120–140 m and density changes between the layers are more or less equal (Soomere, 2003). We model this sort of three-layer density profile using the formula

$$\rho = \rho_0 - \Delta_{\rho_1} \tanh \frac{z - z_1}{d_1} - \Delta_{\rho_2} \tanh \frac{z - z_2}{d_2}, \tag{1.51}$$

where the parameters are chosen to reproduce the profiles presented in (Soomere, 2003): $\rho_0 = 1007$ kg/m^3, $\Delta_{\rho 1} = \Delta_{\rho 2} = 2$ kg/m^3, $d_1 = 3$ m, $d_2 = 10$ m, $z_1 = -20$ m, $z_2 = -80$ m, total depth H is 130 m.

The density, buoyancy, mode $\Phi(z)$ and correction $T_n(z)$ profiles for the chosen parameters are illustrated in Fig. 1.6. Such background conditions give

[4] The maps here and further are drawn using Ocean Data View software (Schlitzer, 2004).

positive signs of both nonlinear parameters (α, α_1), and solitons of both polarities can exist. The isopycnal displacements and horizontal velocity contours induced by the passage of the lowest-mode solitons (1.42) of positive and negative polarities with approximately equal amplitudes ($a \cong 13.4$ m) are demonstrated by Fig. 1.6, lower panel, and Fig. 1.7. The horizontal velocity fields have a quasi-three-layer structure with thin transition layers of thicknesses d_1 and d_2. The fields of horizontal velocities in elevation and depression solitons are positive and negative, respectively, in the lower near-bottom layer, and have the reversed direction in the middle and the upper layer. Near-bottom and near-surface velocities have the greatest values whereas the velocity in the mid-layer is insignificant.

The influence of the nonlinear correction manifests itself firstly in the

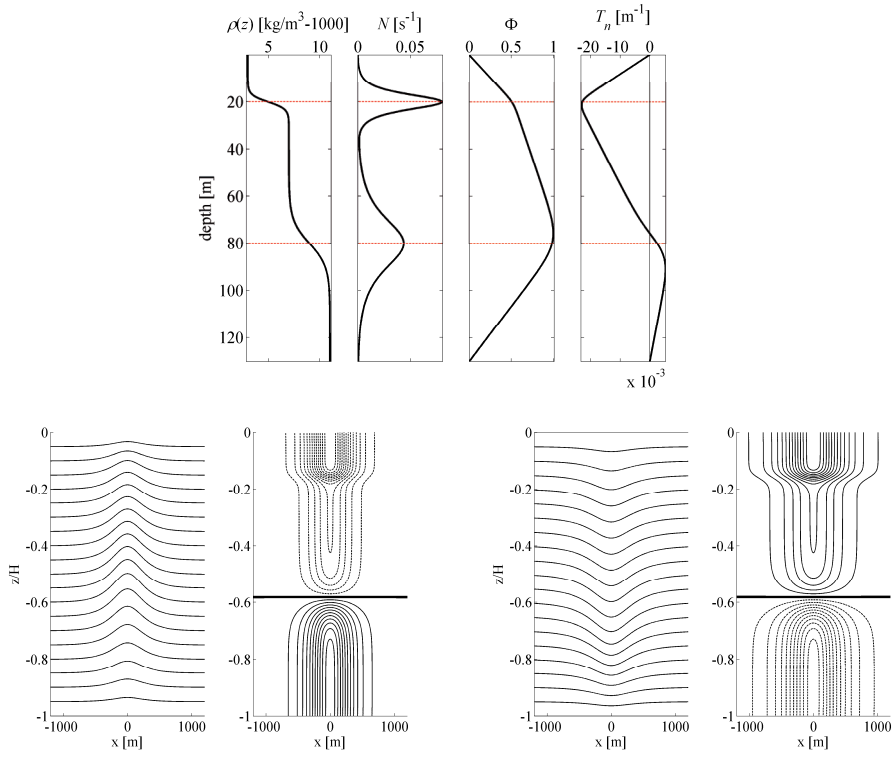

Fig. 1.6. Upper panel: model of an almost three-layer density stratification and the corresponding profiles of buoyancy frequency $N(z)$, lowest vertical mode $\Phi(z)$ and its nonlinear correction $T_n(z)$. Lower panel: isopycnal displacement and horizontal velocity contours (for the leading order of Eqs. (1.8) and (1.49)) while the soliton of positive(left half)/negative(right half) polarity propagates. Contour interval is $H/20$ for isopycnals and $0.025c$ for velocity. Solid/dashed lines correspond to positive/negative values of velocity, thick lines are the lines of zero horizontal velocity. The velocity is positive when the fluid particles move in the direction of soliton propagation (to the right) and negative in the opposite case

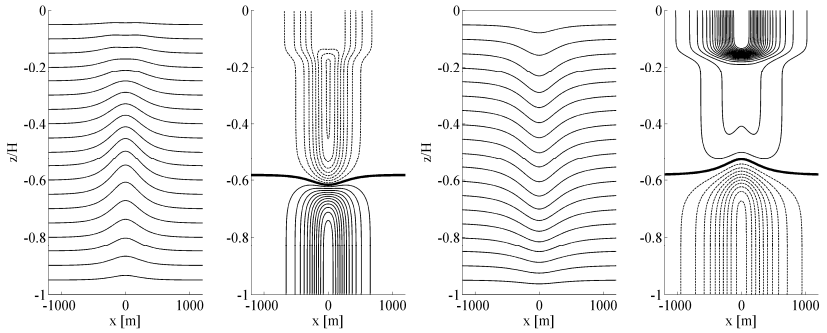

Fig. 1.7. Isopycnal displacement and horizontal velocity contours (when the nonlinear correction terms are taken into account in Eqs. (1.8), (1.12) and (1.49)) while the soliton of positive(left half)/negative(right half) polarity propagates. Notations are the same as for Fig. 1.6, lower panel

shape of the lines of zero horizontal velocity: they are curved in the opposite direction to the soliton polarity while for the leading-order wave field they are horizontal. Also the wavefield accounting for the nonlinear correction has smaller maximal absolute values of negative velocities (near-surface for the soliton of elevation, and near-bottom for the soliton of depression) and larger maximums of positive velocities.

The accuracy of the approximate expressions (1.49) and (1.50) from the point of view of near-bottom and near-surface IW-induced currents was estimated in (Vlasenko et al., 2000; Rouvinskaya et al., 2011), where the vertical structure of fully nonlinear SIWs was compared to weakly nonlinear solitary wave solutions for KdV and mKdV models, respectively, for different profiles of sea water density stratification. It was shown that for SIWs of positive polarity weakly nonlinear theory overestimates the near-bottom velocities and underestimates the near-surface current. For solitary waves of negative polarity, which are the most typical for hydrological conditions of low and middle latitudes, the situation is the opposite. For the Gardner equation no such estimations are available.

Concluding remarks

Although contemporary numerical methods and fully nonlinear approaches such as the method of conjugate flows allow for extensive studies into properties of highly nonlinear IWs, many specific features can still be recognized, analysed and understood using classical methods for analytical studies into IWs in the weakly nonlinear framework. Such fully analytical methods make it possible to exactly establish the qualitative appearance of disturbances of different shapes and amplitudes, and, more importantly, to understand the specific features of the behaviour of waves corresponding to the situation where a substantial change in the overall regime of wave propagation is possible.

2 Higher-order (2+4) Korteweg–de Vries-like equation for interfacial waves in a symmetric three-layer fluid

The properties of internal solitons are addressed in this chapter in the framework of the widely used concept of layered fluid. Models of wave motion for such environments are attractive for both theoretical research and applications because of their ability to mirror the basic properties of the actual IW systems using model equations of stratified media containing small number of parameters and in many cases allowing for extensive analytical studies of the properties of solutions.

Here, the theory described in Chapter 1 is extended to higher orders in one special (but frequent in natural conditions) stratified medium because of vanishing lower-order nonlinear terms in the commonly used IW equations. The presentation follows Papers IV and V. The chapter is organized as follows. Section 2.1 describes the state-of-the-art of the relevant research and describes a frequently occurring situation in some basins of the World Ocean that requires more detailed analysis. Section 2.2 presents the basic equations of motion for the three-layer model and then focuses on the modification of the derivation of the mKdV equation towards expressing the balance between nonlinear and dispersive terms in the case the coefficients of both the leading nonlinear terms vanish. The basic properties of solitary solutions to the resulting equation and their nonlinear interactions are discussed in Section 2.3. Discussion and conclusions are presented at the end of this chapter.

2.1 Failure of the Gardner equation for a symmetric three-layer environment

The need for systematically accounting for higher nonlinearities stems from the nature of the nonlinear evolutionary equations for IWs. While the coefficients of similar equations in some other environments can be expressed in terms of simple combinations of governing scales for the particular problem (Ablowitz and Clarkson, 1991; Gorshkov et al., 2004), the coefficients of nonlinear evolution equations for IWs are defined by the particular vertical distribution of water density, properties of shear flow and boundary conditions at the water surface (Funakoshi, 1985; Lamb and Yan, 1996; Pelinovsky et al., 2000; Grimshaw et al., 2002a). A specific property of such equations is that some coefficients at the nonlinear terms may vanish for certain symmetric situations (Kakutani and Yamasaki, 1978; Grimshaw et al., 1997). In such cases it is necessary to account for higher-order nonlinearities to adequately describe the motion. This process not only leads to the necessity of inclusion of some additional terms into the governing equations but naturally highlights a variety of qualitatively new phenomena in the dynamics of localized, solitonic (non-

radiating) IWs – solutions to such equations (Grimshaw et al., 1999, 2002b, 2010; Slyunyaev and Pelinovsky, 1999; Slyunyaev, 2001).

The simplest system basically representing the key properties of IWs is the two-layer model. Various properties of IWs in this approximation have been addressed in numerous analytical and numerical studies as well as by means of in situ observations and laboratory experiments (Kakutani and Yamasaki, 1978; Koop and Butler, 1981; Funakoshi, 1985; Funakoshi and Oikawa, 1986; Mirie and Pennel, 1989; Choi and Camassa, 1996, 1999; Pullin and Grimshaw, 1998; Craig et al., 2004; Guyenne, 2006; Zahibo et al., 2007; Camassa et al., 2010). These studies cover a wide range of different regimes of wave motion from ideally linear systems and weakly nonlinear models up to fully nonlinear phenomena.

The two-layer model and the KdV equation and its generalizations have been widely used as a simple but instructive model to demonstrate the richness of IW phenomena compared to long weakly nonlinear surface waves. For example, for IWs the coefficient at the quadratic nonlinearity in the KdV equation vanishes for the naturally occurring symmetric situation when the layers have equal thicknesses in the Boussinesq approximation. The leading nonlinear term in almost symmetric situations is the cubic one and the Gardner equation (or its generalizations) has to be used to describe the wave motion (Benney and Ko, 1978; Kakutani and Yamasaki, 1978; Miles, 1979, 1981; Koop and Butler, 1981; Gear and Grimshaw, 1983; Funakoshi and Oikawa, 1986).

The two-layer fluid is, in fact, quite a simplified representation of the natural stratified flows. For example, in many areas of the World Ocean the vertical stratification has a clearly pronounced three-layer structure with well-defined seasonal thermocline at a depth of ~100 m and the main thermocline at much larger depths (Knauss, 1996; Yang et al., 2010). Several basins such as the Baltic Sea host more or less continuously a three-layer vertical structure (Leppäranta and Myrberg, 2009). In order to reveal the basic features of the IW field in such environments it is necessary to introduce a three-layer model. Such models are considerably more complex than the two-layer systems; however, they allow for much more analytical progress compared to the arbitrary stratified situation.

A generalization of the mKdV equation for the three-layer stratification, presented in this chapter based on Paper IV, is basically straightforward, albeit cumbersome and technically complicated. The resulting equation admits solitary wave solutions for a certain range of parameters. The focus of the study is an almost symmetric situation in which the lower-order nonlinear terms vanish and higher-order contributions govern the behaviour of wave phenomena in the system. A simple symmetric situation corresponds to the equal thicknesses of the uppermost and the lowermost layers provided the density differences between the layers are also equal. This situation can naturally occur in shallow strongly stratified seas like the Baltic Sea where the interplay of fresh water discharge to the surface and irregular salt water

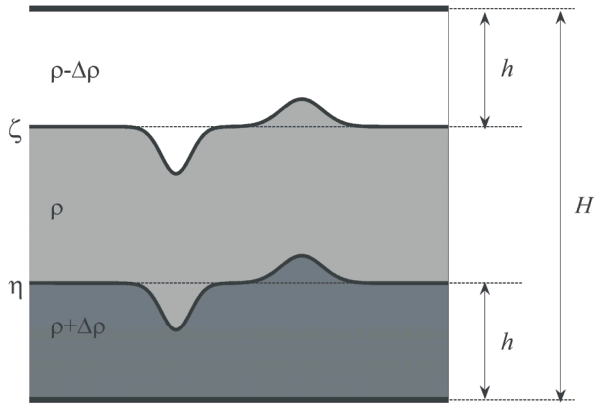

Fig. 2.1. Definition sketch of a symmetric three-layer fluid

intrusion in the bottom layers frequently gives rise to two density jumps of comparable size and sharpness and an almost symmetric three-layer structure (Leppäranta and Myrberg, 2009) and may lead to the vanishing of several interactions between baroclinic Rossby waves (Soomere, 2003).

The key difference of such an environment from those addressed in previous studies is the possibility of having the cubic nonlinearity with a positive coefficient. This is impossible in the two-layer medium. Moreover, this coefficient may change its sign in different domains and may even vanish under certain conditions (Grimshaw et al., 1997). As a result, the dynamics of IWs in such environments is much richer in content and reveals several features that cannot become evident in two-layer flows. In particular, the possibility of the simultaneous vanishing of the coefficients at both the quadratic and cubic nonlinear terms makes it possible to naturally generalize the mKdV equation towards accounting for the quadratic nonlinearity and towards even more detailed analytical description of the properties of the IW dynamics in layered fluids.

2.2 Nonlinear equations of motion and an extended version of mKdV equation

Let us consider a model situation of irrotational motions in a three-layer inviscid fluid of total thickness H overlying a flat horizontal bottom in the approximation of a rigid lid on the surface of the fluid (Fig. 2.1). We consider the symmetric case in which the thicknesses h of the surface and the bottom layer are equal and assume that the density differences between the layers are also equal; then the densities in the layers are $\rho_1 = \rho + \Delta\rho$, $\rho_2 = \rho$, $\rho_3 = \rho - \Delta\rho$, where ρ is the density in the middle layer. As usual, we employ the Boussinesq approximation and assume that densities in the layers differ

insignificantly ($\Delta\rho/\rho \ll 1$). In this case, the equations of the motion are Laplace equations for the velocity potential in each layer:

$$\nabla^2\Phi_i = 0\,,\ i = 1,2,3\,. \tag{2.1}$$

The vertical velocities at the bottom and at the fixed upper boundary will obviously vanish:

$$\Phi_{1z}(z=0) = 0\,,\ \Phi_{3z}(z=H) = 0\,, \tag{2.2}$$

where the subscript x, y or z denotes a partial derivative. The classical kinematic and dynamic boundary conditions at the interfaces between the layers complete the setup of the problem:

$$\left.\begin{array}{c} \eta_t + \Phi_{1x}\eta_x - \Phi_{1z} = 0, \quad \eta_t + \Phi_{2x}\eta_x - \Phi_{2z} = 0 \\ \rho_1\left(\Phi_{1t} + \frac{1}{2}(\nabla\Phi_1)^2 + g\eta\right) = \rho_2\left(\Phi_{2t} + \frac{1}{2}(\nabla\Phi_2)^2 + g\eta\right) \end{array}\right\} z = h + \eta(x,t)\,,$$

$$\left.\begin{array}{c} \zeta_t + \Phi_{2x}\zeta_x - \Phi_{2z} = 0, \quad \zeta_t + \Phi_{3x}\zeta_x - \Phi_{3z} = 0 \\ \rho_2\left(\Phi_{2t} + \frac{1}{2}(\nabla\Phi_2)^2 + g\zeta\right) \\ = \rho_3\left(\Phi_{3t} + \frac{1}{2}(\nabla\Phi_3)^2 + g\zeta\right) \end{array}\right\} z = H - h + \zeta(x,t)\,. \tag{2.3}$$

Here the unknown functions $\eta(x,t)$ and $\zeta(x,t)$ denote the instantaneous position of the interface between the bottom and the middle layer and between the upper and the middle layer, respectively.

We consider long waves with a small amplitude (as compared to the depth of the fluid) and introduce small parameters of nonlinearity ($\varepsilon = a/H$) and dispersion ($\overline{\mu} = H/L$, $\mu = \overline{\mu}^2$), where a is the characteristic scale of the amplitude of displacements of the interfaces between the layers and L is the characteristic horizontal scale of wave motions. There are two modes of IGWs in a fluid with a symmetric three-layer stratification, which can also be found established in the most general form for a three-layer fluid by Rusas and Grue (2002) and Mercier et al. (2011).

The details of the asymptotic expansion of Eqs. (2.1)–(2.3) can be found in Paper IV and in (Rouvinskaya et al., 2010). For the lowest mode (interfaces for which are displaced in the same direction), the quadratic nonlinearity coefficient and one of the nonlinear dispersion coefficients are identically zero for any combination of the thicknesses of the layers. The vanishing of the quadratic nonlinearity coefficient means that the classical hierarchy of small terms in the asymptotic expansion is no more valid. To derive a refined (extended) mKdV equation using asymptotic expansions for symmetric stratifications, the standard scaling (i.e., the relationship $\varepsilon = \mu$ between small

nonlinearity and dispersion parameters) of the KdV equation should be modified to $\varepsilon^2 = \mu$ in order to balance the dispersion and nonlinear effects. In this case, the role of the next nonlinear terms in the asymptotic expansion of the wave field should increase. Performing scaling with the relation $\varepsilon^2 = \mu$ between the small parameters, we arrive at the equation:

$$\begin{aligned} &\zeta_t + c\zeta_x + \alpha_1\zeta^2\zeta_x + \beta\zeta_{xxx} + \varepsilon\left(\alpha_2^*\zeta^3\zeta_x + \gamma_2^*\zeta_x\zeta_{xx}\right) \\ &+ \varepsilon^2\left(\alpha_3\zeta^4\zeta_x + \gamma_{31}\zeta_x^3 + \gamma_{32}\zeta\zeta_x\zeta_{xx} + \gamma_{33}\zeta^2\zeta_{xxx} + \beta_1\zeta_{5x}\right) + O\left(\varepsilon^3\right) = 0, \end{aligned} \tag{2.4}$$

where the coefficients are given in Paper IV. Equation (2.4) contains not only the terms of the mKdV equation but also higher-order ($O(\varepsilon)$ and $O(\varepsilon^2)$) correction terms (representing nonlinearity, nonlinear dispersion and linear dispersion). The equation for $\eta(x,t)$ differs from Eq. (1.55) only in the opposite signs of the coefficients marked with an asterisk.

The cubic nonlinearity coefficient α_1 vanishes at $h = h_{cr} = 9H/26$. Expanding the expressions for the coefficients of Eq. (2.4) into a Taylor series near the point h_{cr} ($\Delta = (h - h_{cr})/H$) and changing again the scaling of the parameters for the balance between nonlinearity and dispersion, we obtain the following extended mKdV equation with combined nonlinearity:

$$\zeta_t + \alpha_1\zeta^2\zeta_x + \alpha_3\zeta^4\zeta_x + \beta\zeta_{xxx} = 0\,. \tag{2.5}$$

Note that to account for dispersion and nonlinear effects on the same order for the stratification parameters close to those considered here, the relationship between small parameters Δ and ε should have the form $\Delta = \varepsilon^2$. The coefficients in Eq. (2.5) are as follows:

$$\alpha_1 H^2/c = -\frac{3(26l-9)}{8l^3}, \qquad \alpha_3 H^4/c = \frac{9(1324l^3 - 1508l^2 + 513l - 45)}{128l^7},$$

$$\beta/(cH^2) = \frac{4l^2 - 3l}{12},$$

and $l = h/H$. The fourth-order nonlinearity coefficient α_2 changes sign at $h = h_{cr}$ and is small near this point. In the described scaling, the term with the coefficient α_2 is of a higher smallness order than the terms retained in Eq. (2.5).

The auxiliary equations such as Eq. (2.4) derived in the process of the asymptotic analysis have different appearances for different interfaces. Remarkably, Eq. (2.5), as well as the classical mKdV equation for symmetric three-layer stratification, is universal, i.e. identical for both interfaces. Equation (2.5) more accurately describes the wave dynamics near the point of zero cubic nonlinearity ($\Delta << 1$) owing to the fifth-order nonlinear term. Continuous stratifications with similar properties also occur under natural conditions (Leppäranta and Myrberg, 2009).

Equation (2.5) differs from the classical Gardner equation (1.20) (which is frequently used for motions in situations containing zero-crossing of the coefficient at the quadratic nonlinearity, e.g. in two-layer media with almost equal layers) in the absence of quadratic nonlinearity and the presence of quintic nonlinearity. This equation belongs to the family of generalized Gardner equations (Hamdi et al., 2011a, b) used to describe different properties of IWs. Following the nomenclature of different extensions of the KdV equation, Eq. (2.5) may be called 2+4 Korteweg–de Vries-like equation, abbreviated 2+4KdV.

As equations $\zeta_t + \zeta^n \zeta_x + \zeta_{xxx} = 0$ with $n > 2$ are nonintegrable (in particular, with respect to the Zakharov–Shabat method (Novikov et al., 1984; Ablowitz and Segur, 2000)), it is likely that Eq. (2.5) is also nonintegrable. The question about its integrability is, however, out of the scope of the current study. In spite of nonintegrability, it always conserves the mass $M = \int_{-\infty}^{\infty} \zeta \, dx$ and energy $E = \int_{-\infty}^{\infty} \zeta^2 \, dx$, which are generally not conserved in Eq. (2.4). The signs of the coefficients of the nonlinear terms in Eq. (2.5) are important for wave dynamics. In particular, the cubic nonlinearity coefficient α_1 changes sign at $h \approx h_{cr} / H$ whereas the coefficient at the fifth-order nonlinearity α_3 is negative near this point.

2.3 Solitary solutions of the 2+4KdV equation and their interactions

An important feature of Eq. (2.5) is that it has solitary wave solutions. The relevant analysis of their existence and appearance (incl. the impact of the quintic nonlinearity on their shape compared to that of the classical mKdV equation) follows material in Papers IV and V.

It is known that the solitary solutions of KdV-hierarchy equations containing a higher-order nonlinearity $\zeta_t + \zeta^n \zeta_x + \zeta_{xxx} = 0$ are unstable for $n \geq 4$ (Ablowitz and Segur, 2000). For such equations, smooth localized initial conditions evolve to singular perturbations in a finite time (or at a finite distance). Equation (2.5) contains combined nonlinearity (third- and fifth-order terms). At the time of writing this thesis no investigations of the integrability and/or stability of solitons for an equation of this form existed in the scientific literature. Hamdi et al. (2011a, b) obtained two partial invariants and single-soliton solutions for a more general class of equations including Eq. (2.5). However, the general properties of such equations have not been established. Nevertheless, all numerical calculations of the evolution of smooth localized initial conditions performed for Eq. (2.5) demonstrate fairly stable wave dynamics without any singularities or collapses. A natural conjecture is that cubic nonlinearity in this equation plays a stabilizing role, but the problem undoubtedly requires a stricter theoretical consideration.

Localized steady solutions $\zeta_s(x-Vt)$ of Eq. (2.5) are expressed in terms of the integral

$$Y - Y_0 = \sqrt{\beta}\int_{v_0}^{v_S}\left(V\zeta^2 - \frac{\alpha_1}{6}\zeta^4 - \varepsilon\frac{\alpha_3}{15}\zeta^6\right)^{-1/2} d\zeta \ , \tag{2.6}$$

where V is the velocity of the wave and $Y = x - Vt$. This integral at $\alpha_1 > 0$ can be calculated analytically

$$\zeta(Y) = \pm\sqrt{\frac{60V}{5\alpha_1 + \sqrt{25\alpha_1^2 + 240\alpha_3 V}\cosh\left(2Y\sqrt{V/\beta}\right)}} \ . \tag{2.7}$$

It is easy to demonstrate that Eq. (2.7) describes localized (solitonic) solutions to Eq. (2.5) with an amplitude

$$a = \sqrt{\frac{60V}{5\alpha_1 + \sqrt{25\alpha_1^2 + 240\alpha_3 V}}} \ . \tag{2.8}$$

Similarly to the solutions of the Gardner equation, the propagation speed of such solutions

$$V = \frac{\alpha_1}{6}a^2 + \frac{\alpha_3}{15}a^4$$

depends on their amplitude a. The natural limit for the wave speed for physically meaningful solutions stems from the request that the expressions under the inner square root in Eqs. (2.7) and (2.8) must be non-negative. This condition means that the wave speed V has an upper limit

$$V_{\lim} = -\frac{5\alpha_1^2}{48\alpha_3} . \tag{2.9}$$

Consequently, the amplitude of the solutions is also limited by the following value:

$$a_{\lim} = \frac{1}{2}\sqrt{\frac{5\alpha_1}{-\alpha_3}} . \tag{2.10}$$

The limiting amplitude in Eq. (2.10) can be expressed using the relative thickness $l = h/H$ (the ratio of the lower and upper layers thickness to the total fluid depth):

$$\frac{a_{\lim}}{H} = \frac{2}{3}l^2\sqrt{15}\sqrt{\frac{9-26l}{1324l^3 - 1508l^2 + 513l - 45}} . \tag{2.11}$$

The limiting amplitude reaches a maximum value of $a_{\lim} \approx 0.0864H$ when $h/H \approx 0.286$. The highest possible position of the lower interface $h + a_{\lim}$ for such a soliton of elevation corresponds to $z \approx 0.397H$. In this case, $h \approx 0.3243H$, i.e., very close to h_{cr}.

Figure 2.2 shows the profiles of solitary waves of the mKdV equation (1.45) and solitons (2.7) for various amplitudes of the velocity V for the following parameters of the medium: total depth $H = 100$ m, depth of the uppermost and lowermost layers $h = 30$ m and the relative change in the density $\Delta\rho/\rho = 0.01$. For such a stratification the coefficients of Eq. (2.5) and the parameters of its solitary wave solutions are given in Table 2.1. For low velocities, solutions of Eq. (2.5) are similar to the classical solitons of the mKdV equation. For larger wave speeds (larger amplitudes) the two sets of solutions considerably differ from each other. The key difference is that large-amplitude solutions to Eq. (2.5) form a table-like wide signal that may, theoretically, infinitely widen in the process $V \to V_{\lim}$ whereas their amplitude asymptotically tends to $a_{\lim}$. Solitary wave solutions of both positive and negative polarity are possible for $\alpha_1 > 0$ in Eq. (2.5).

Similar table-like solutions are characteristic for some other equations containing higher-order nonlinear terms. For example, they exist for the Gardner equation (1.20). Its soliton, given by Eq. (1.42), describes motions in the two-layer fluid where the cubic nonlinearity is of the leading order. The existence of such wide table-like solitons and the possibility of their propagation in combinations with other solitons have been demonstrated for several other classes of nonlinear wave models (Miyata, 1988, 2000; Mirie and Pennel, 1989; Michallet and Barthelemy, 1998).

The described table-like appearance of relatively large-amplitude and rapidly moving solutions with steep fronts may have substantial consequences

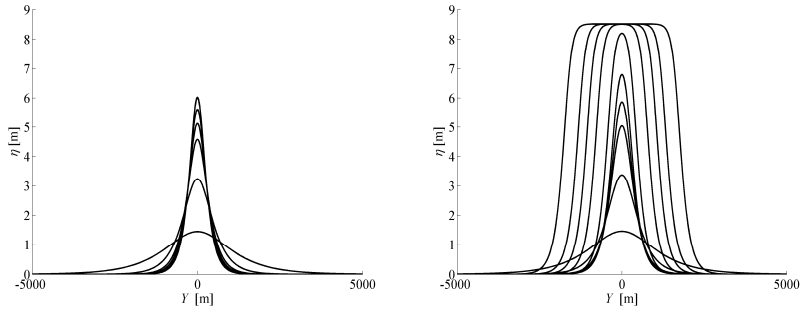

Fig. 2.2. The shape of solitary wave solutions (1.45) to the classical mKdV equation (a) and (2.7) for Eq. (1.56) (b), for solitary wave speeds of V = 0.001, 0.005, 0.01, 0.0125, 0.015, 0.0172, 0.017294, 0.01729412, 0.01729412063 and 0.01729412063364 m/s. The smaller speeds correspond to the lower-amplitude waves. Note that several lines for large-amplitude waves in panel (a) are not separable from one another

Table 2.1. Values of kinematic and nonlinear parameters of IWs in a symmetric three-layer fluid used for numerical modelling

Parameter	Value
c, m/s	1.72
α, 1/s	0.0
β, m^3/s	771.98
α_1, 1/(m·s)	0.002859
α_3, $1/(m^3 \cdot s)$	–0.00004924
a_{lim}, m	8.5194
V_{lim}, m/s	0.01729

in practical applications. Their propagation is similar to the motion of smooth bores, which poses a considerable danger to objects on their way. Such horizontal motions (sometimes called conjugate flows) are frequent in vertically inhomogeneous fluids (Benjamin, 1971; Makarenko, 2004; Makarenko et al., 2009). The performed analysis shows that such flows can naturally occur in three-layer fluids for some combinations of the layers' thicknesses and density variations.

Generally speaking, interactions and collisions of solitary solutions to nonintegrable evolution equations are inelastic. It is, therefore, not unexpected that solitary solutions to Eq. (2.5) interact inelastically with each other and with the background wave fields. As a demonstration of this feature, we present an example of numerically simulated collision of two solitonic solutions corresponding to the values of coefficients given in Table 2.1.

The numerical code used to integrate the 2+4KdV equation (2.5) employs an implicit pseudo-spectral method (Fornberg, 1998) that conserves the mass M and energy E. The spatial domain was chosen based on the analytically estimated propagation speed of solitons and interaction time, and was extended as occasion required. The numerical code was tested against exact analytical multi-soliton solutions to the classical mKdV equation and by means of long-term tracking of the propagation of exact solitary solutions to Eq. (2.5) in the absence of other disturbances. The results of the latter test did not change when the spatial step was decreased by a factor of two. For simplicity, we use the nondimensional form of Eq. (2.5):

$$q_\theta + q^2 q_\chi - q^4 q_\chi + q_{\chi\chi\chi} = 0\,, \tag{2.12}$$

where

$$\theta = \left|\frac{\alpha_1^3}{\alpha_3}\right|^{3/4} (\beta)^{-1/2} t\,, \quad \chi = \left|\frac{\alpha_1^3}{\alpha_3}\right|^{1/4} (\beta)^{-1/2} x\,, \quad q = \left|\frac{\alpha_1}{\alpha_3}\right|^{1/2} \varsigma\,. \tag{2.13}$$

The space and time steps were $\Delta\chi = 0.2$ and $\Delta\theta = 0.1$, respectively. The numerical accuracy of the scheme with the chosen parameters is of the order of 10^{-6} (the small parameter μ was not less than 0.04).

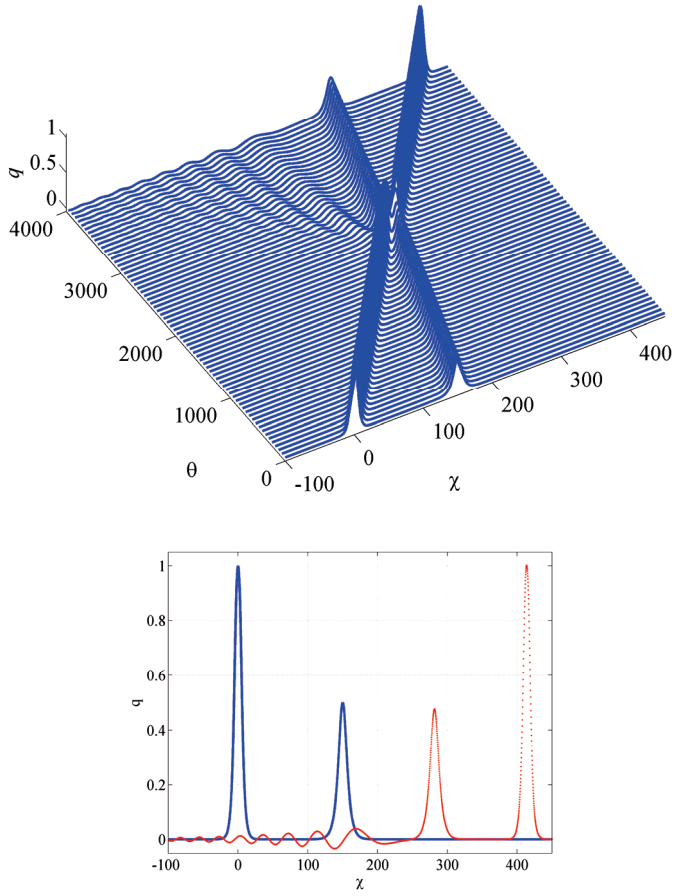

Fig. 2.3. Interaction of solitary wave solutions of elevation to Eq. (1.63) in nondimensional coordinates: space–time plot (above); cross-section of the wave field at $\theta = 0$ (solid lines) and after the collision ($\theta = 4000$, dotted line, below)

The initial state was composed of two solitary waves with nondimensional amplitudes 1 and ± 0.5. The nondimensional limiting amplitude for the parameters in use is $\sqrt{5}/2 \approx 1.118$. The corresponding dimensional amplitudes would have been 7.62 m and ± 3.81 m, respectively. The evolution of each of the counterparts was first integrated until $\theta = 4000$. During this interval, the total error of the numerical solution (caused, e.g., by small distortions of the amplitude of the numerical solution owing to its discrete representation and by radiation of wave energy) did not exceed 1×10^{-6}. The initial state for studies of the interaction of these solitary waves was composed simply as a linear superposition of the counterparts. The smaller wave was placed ahead of the larger one, at a distance (counted as the distance between the relevant maximums) of 150 nondimensional units of length. The simulation was

performed until $\theta = 4000$, that is, quite a long time after the interaction of the highest parts of the waves terminated (Figs. 2.3, 2.4).

The evolution of solitary waves of elevation resembled the typical scenarios for similar soliton interactions in the classical KdV and mKdV frameworks in which the higher wave overtakes the smaller one (Drazin and Johnson, 1989; Soomere, 2009). The counterparts usually lose their identity and merge into a composite structure at a certain instant. After a while, the counterparts emerge again whereas it is impossible to say whether they propagate through each other as waves do or collide as particles do. The interaction process is accompanied, as in the case of KdV solitons, by a clear decrease in the amplitude of the composite structure during the merging phase and by a substantial phase shift.

Differently from processes governed by integrable equations, the numerically simulated collision was accompanied by the generation of a very long and almost stationary localized depression area. The entire process was

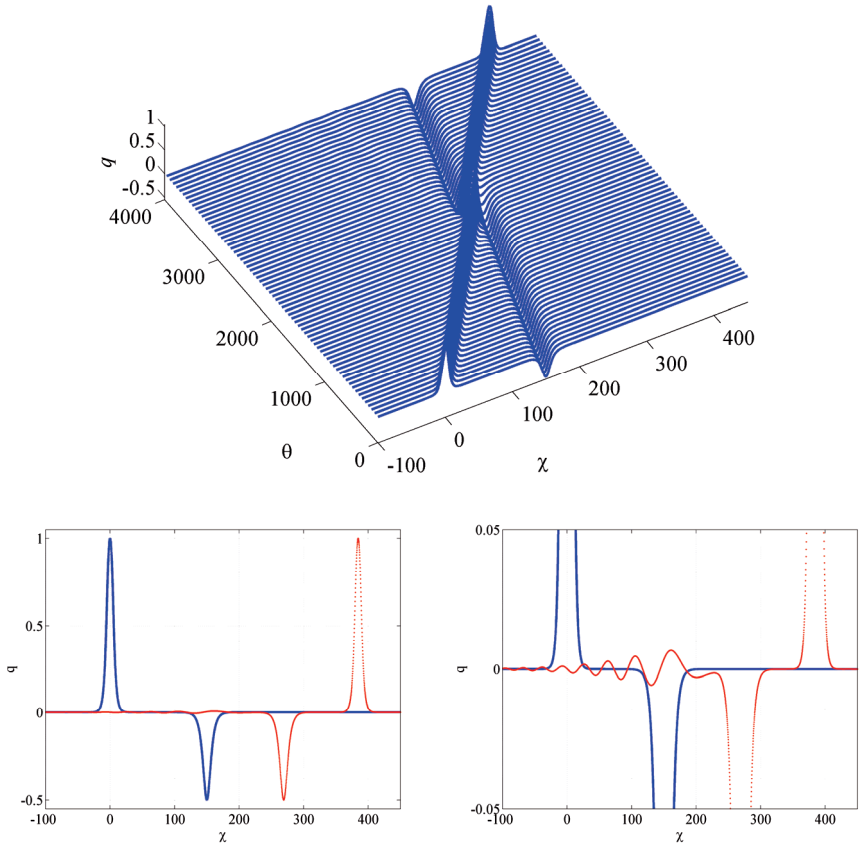

Fig. 2.4. Interaction of solitary waves of different polarity in the framework of Eq. (1.63) in nondimensional coordinates: space–time plot (above); cross-section of the wave field at $\theta = 0$ (solid lines) and after the collision ($\theta = 4000$, dotted line, below). The right bottom panel is a zoomed version of the left bottom panel

also accompanied by a modest radiation of wave energy from the interaction region. The amplitude of wavelike disturbances was about 4×10^{-2}, that is, by several orders of magnitude larger than the level of numerical errors ($<1\times10^{-6}$). This level of wave generation signifies the effects of dispersion on the evolution of the system. Note that the amplitude of the disturbances matches the magnitude of the relevant dispersive terms $O(\mu) = O(\Delta)$, which is also about 4×10^{-2}.

The collision of solitary waves of different polarity has a similar appearance. Both the counterparts largely survive the collision but the phase shift for the wave of depression is more pronounced (Fig. 2.4). The amplitude of radiated waves is much smaller than in the above case and does not exceed 1×10^{-2}. Test simulations with a twice higher spatial resolution led to practically identical results. Therefore, the described side effects such as wave radiation in both cases and the formation of a long depression area in the collision of waves of elevation evidently are an inherent part of interactions of solitary waves in the framework of Eq. (2.5).

Consequently, collisions of solitary wave solutions of Eq. (2.5) are basically of inelastic nature although both the intensity of wave radiation and changes in the amplitudes of the solitons are fairly minor. The collision of waves of elevation led to an increase in the nondimensional amplitude of the higher soliton from 1 to 1.002 and to an accompanying decrease in the smaller soliton from 0.5 to 0.477. The collision of waves of different polarity led to much smaller changes: the post-collision amplitudes of the waves were 1.001 and –0.499, respectively. Note that this effect does not exceed the order of $O(\mu)$ either. The effects caused by interactions of different solitary waves with

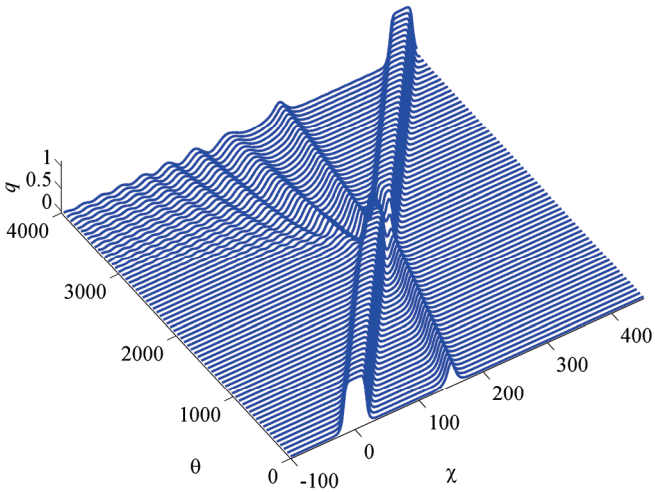

Fig. 2.5. Space–time plot of interacting solitary waves of the same polarity one of which has amplitude close to the limiting value in the framework of Eq. (1.63) in nondimensional coordinates

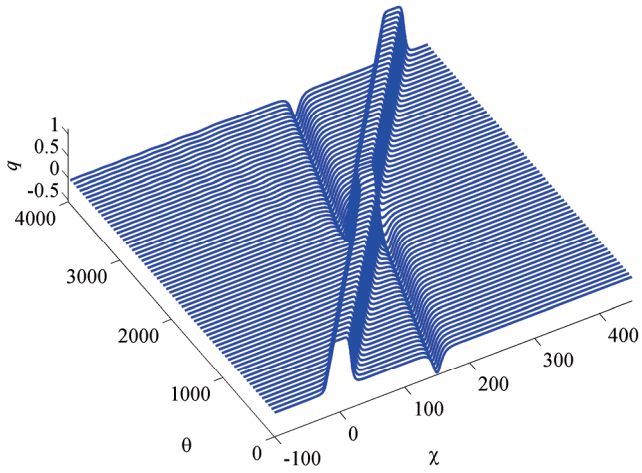

Fig. 2.6. Space–time plot of interacting solitary waves of different polarity one of which has amplitude close to the limiting value in the framework of Eq. (1.63) in nondimensional coordinates

similar entities and background could, of course, be much larger during longer time intervals and/or caused by multiple collisions. As expected for non-integrable equations, such interactions should finally lead to the decay or damping of solitary waves to a level at which they are either practically linear and/or are governed by a different balance of nonlinear and dispersive terms.

To simulate interactions of a wide soliton with a moderate-amplitude soliton, the time and space steps were reduced to $\Delta\theta = 0.01$ and $\Delta\chi = 0.1$, respectively. The numerical error in the simulation of the propagation of the wide soliton throughout the calculation region does not exceed 10^{-6}. The interaction of solitary waves of the same polarity (Fig. 2.5), one of which has an amplitude close to the limiting value, differs from the case considered above. First, the smaller solitary wave changes its polarity during passing over the crest of the wide soliton. Second, the change in the amplitude of the smaller wave is about 40% (from 0.5 to 0.298), which is much larger than that in the preceding cases. The amplitudes of the waves emitted in the process of interaction are comparable with the amplitude of the smaller soliton.

In the interaction of solitons of different polarities (Fig. 2.6), one of which has an amplitude close to the limiting value, the change in the amplitude of the smaller soliton with negative polarity is somewhat larger (from 0.5 to 0.498) than that in the calculations for solitons with amplitudes far from the limiting value. The amplitudes of the waves emitted in the interaction are about 8×10^{-3}, which does not exceed the small parameter.

As already mentioned, the interaction of solitons of Eq. (2.5) is accompanied by the shift of their phases. The change in the phases of solitons of the same polarity occurs according to the classical scenario for the KdV-hierarchy equations (Lamb, 1980). The phase shift of the faster soliton in the

interaction of solitons of different polarity can have a different sign depending on its amplitude. For small amplitudes, the dynamics is close to the mKdV case and the shift is positive. For large amplitudes, when the soliton becomes wide, the change in its phase is negative (Figs. 2.4, 2.6).

Concluding remarks

The performed analytical investigation of different regimes of wave propagation in a relatively simple but frequently occurring in nature symmetric three-layer environment (Papers IV, V) reveals several interesting features of wave shapes that are usually hidden in the analysis of nonsymmetrical situations. The key development is the derivation of a new nonlinear evolution equation that describes the wave motion in situations where all the leading-order nonlinear terms in the classical mKdV equation vanish simultaneously. Such situations may often happen in relatively shallow nontidal strongly stratified basins such as the Baltic Sea. In this case the evolution equation governing wave motion contains two nonlinear terms (cubic and quintic nonlinearities) of the same magnitude. This equation is obtained using the basically standard asymptotic procedure that is widely used in similar problems and is of the second order of accuracy as the mKdV equation for the nonsymmetrical situation.

The resulting equation differs from the mKdV equation in two important aspects. First, it reflects a different balance between the (higher-order) nonlinear terms and the dispersive terms compared to that used in the mKdV equation. More importantly, this equation contains two nonlinear terms of the same magnitude: the cubic and quintic nonlinearities, the latter distinguishing the resulting equation from the mKdV equation. The resulting equation has solitary wave solutions. As this equation probably is not integrable, the possible solitonic nature of these solutions and the existence of multi-soliton solutions are a subject of further research.

The presence of quintic nonlinearity does not substantially modify the shape of the solitons of relatively small amplitude but leads to radical changes in the appearance of larger-amplitude solitary waves. Their amplitude and propagation speed are limited. Larger-amplitude solitons have a table-like shape with very steep fronts. The motion of such solitary waves may be accompanied by high water speeds and strong hydrodynamic loads in the areas where the structure of the medium is favourable for their existence. It is likely that the classical solitary solutions to the mKdV equation are transformed into such structures when they approach sea areas where the coefficients at the lower-order nonlinear terms vanish.

Numerical calculations confirm that the collision of solitons of the derived equation is inelastic. Inelasticity is the most pronounced in the interaction of unipolar pulses. The direction of the shift of the phase of the higher-amplitude soliton owing to the interaction of solitons of different polarities depends on the amplitudes of the pulses.

3 High-frequency internal waves in the Baltic Sea

The material presented in chapters 1 and 2 vividly demonstrates that not only the formal appearance of IWs but specifically their impact on the bottom sediments, coastal and offshore engineering structures and the marine ecosystem substantially depends on the typical stratification in the particular sea area. The key property of the marine environment here is the potential asymmetry of the location of the pycnoline(s). This asymmetry naturally generates an associated asymmetry in the velocity field excited by IWs. Further, it underlines the importance of regional aspects in IW studies as the vertical stratification of the ocean is highly inhomogeneous in the horizontal direction.

One of the most interesting basins in this aspect is the Baltic Sea. It is quite a shallow shelf sea with predominant depths from 40 to 100 m (Leppäranta and Myrberg, 2009). The presence of a particularly strong stratification and associated buoyancy effects cause extensive mesoscale variability of hydrological fields with typical horizontal scales of 5–20 km. The mesoscale dynamics is particularly complex in the Gulf of Finland and in the south-western Baltic Sea where the typical values for the baroclinic Rossby radius are well below 5 km (Alenius et al., 2003; Osinski et al., 2010). As it is micro-tidal but strongly influenced by wind forcing (in terms of frequent local storm surges and occasionally occurring severe windseas), various wind-driven phenomena are the most probable source of IWs in this basin.

The focus of this chapter is the geographical and seasonal distributions of kinematic parameters of long IWs derived from the Generalized Digital Environmental Model (GDEM) climatology in the Baltic Sea region. This data set reflects the climatology of the temperature and salinity of the global oceans. The key outcome is an express estimate of the expected IW parameters for different regions of the Baltic Sea. A complementary topic is the variability in the surface wave fields in this basin, in particular, extreme surface wave fields in strongly stratified shallow-water domains where IW generation by surface waves is feasible.

The chapter reflects the results published in Papers III and VI. Some results from Paper I are provided occasionally for comparison. Section 3.1 describes some existing (remote sensing and in situ) observations of IWs in the Baltic Sea. The behaviour of prognostic kinematic and nonlinear characteristics of IW field in the Baltic Sea is examined in Section 3.2. Branches of SIWs and their amplitudes, which are possible in this basin, are discussed in Section 3.3. Near-bottom and near-surface horizontal velocities induced by IWs are mapped and analysed in Section 3.4. Statistics of surface wave conditions in the south-western Baltic Sea based on waverider data and two long-term numerical simulations is described in Section 3.5.

3.1 Observations of IWs in the Baltic Sea

Since the stratification of the Baltic Sea is stable, IWs must be a common feature there, even though the number of studies into such waves is relatively small (Leppäranta and Myrberg, 2009). Several kinds of IWs can exist in this water body because of the variety of forcing factors and the complexity of its bathymetry. The relevant field data are limited. In the existing studies the generation of IWs in the Baltic Sea is mainly explained by the strong winds.

Tidal oscillations of the Baltic Sea level are extremely small: from 4 cm (Klaipeda) up to 10 cm in some sections of the Gulf of Finland (Alenius et al. 1998). The associated current speed, however, cannot be neglected. It reaches about 10 cm/s in the middle of the Gulf of Finland (Lilover, 2012) but still remains much below the level of motions driven by IWs. Generation of IGWs

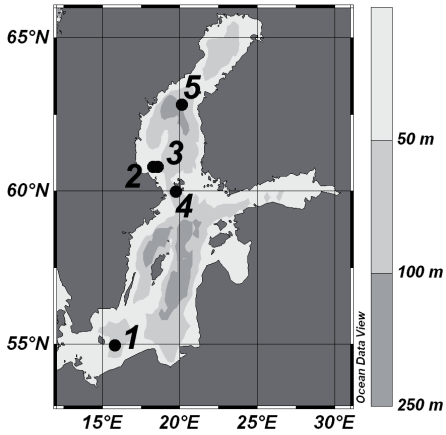

Fig. 3.1. Locations of observations 1–5 (Table 3.1) of surface manifestations of IWs on satellite SAR images of the Baltic Sea on the background of bathymetry.

Table 3.1. Parameters of IW packets detected on satellite radar images of the Baltic Sea in 2009–2010.

	Date and time, UTC	Coordinates of the center of the packet	Maximal wavelength [m]	Front length of the leading wave [m]	Number of waves in the packet
1	05/08/2009 09:03:28	54°57′57″ N 15°46′58″ E	900	23 500	4
2	01/07/2009 09:03:50	60°47′34″ N 18°15′26″ E	875	16 500	3
3	12/07/2010 20:13	60°48'10" N 18°33'50" E	300	14 600	3
4	24/07/2010 09:07	59°58'53" N 19°43'00" E	900	15 800	4
5	30/07/2010 09:20	62°49'00" N 20°06'11" E	760	15 500	3

in microtidal seas is possible due to several other dynamic processes such as the development and relaxation of coastal upwelling, vortices of different scales, surge phenomena, oscillations of hydrological fronts, etc. Several studies are devoted to in situ observations and numerical modelling of the generation and propagation of short-period IWs in microtidal and nontidal seas, based on experimental data obtained by contact probes (Ivanov et al., 1987; Vlasenko et al., 1998; Ivanov and Lisichenok, 2002).

In recent years the number of **remote sensing observations** of surface manifestations of IWs has increased significantly, including observations for nontidal seas (Mityagina and Lavrova, 2009, 2010; Lavrova et al., 2009, 2010, 2011). These observational data suggest that:

1) although IWs in non-tidal seas are less intense compared with IWs generated by the tidal flow on oceanic shelves, mechanisms of their origin are much more diverse;
2) significant seasonal and interannual variability of both the IW activity and its manifestations is evident in the Synthetic Aperture Radar (SAR) images of the sea surface;
3) a clear correlation exists between the frequency of occurrence of surface manifestations of IWs in SAR images and the pycnocline position: frequent occurrence of surface manifestations of IWs corresponds to a sharp and shallow pycnocline.

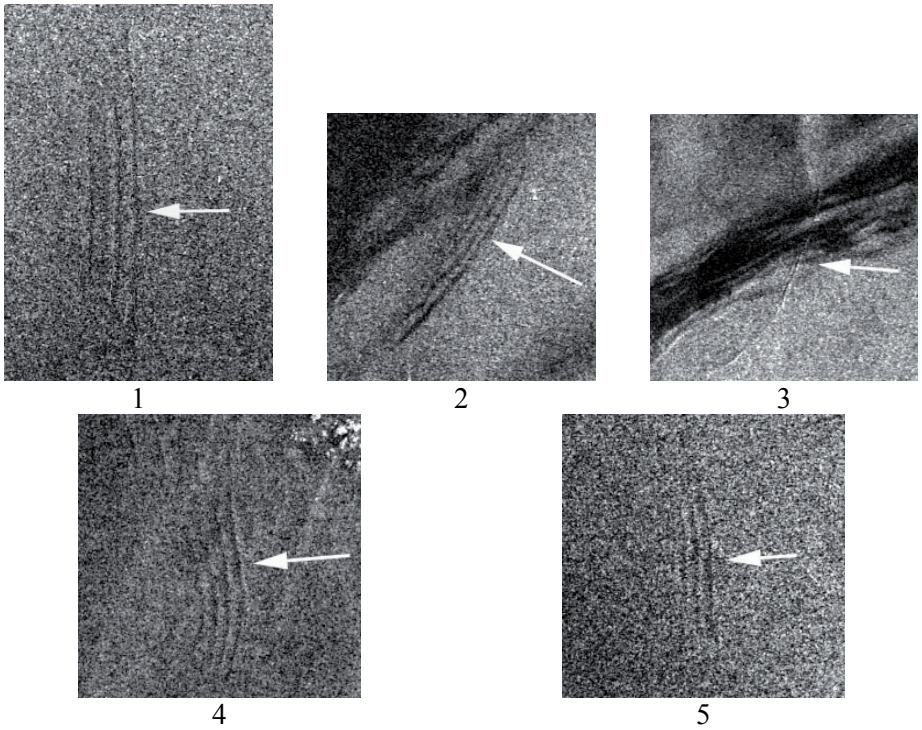

Fig. 3.2. Surface manifestations of IWs (subimages of Envisat ASAR images from http://www.iki.rssi.ru/asp/iw_images/index.html) in Table 3.1

SAR observations of surface manifestations of IWs over the Baltic Sea area are quite difficult because of unstable meteorological conditions. A number of factors such as intensification or weakening of wind (calm, windless regions), development of choppiness, rough sea, algal blooms, heavy precipitation, passage of sharp atmospheric and wind fronts or appearance of atmospheric

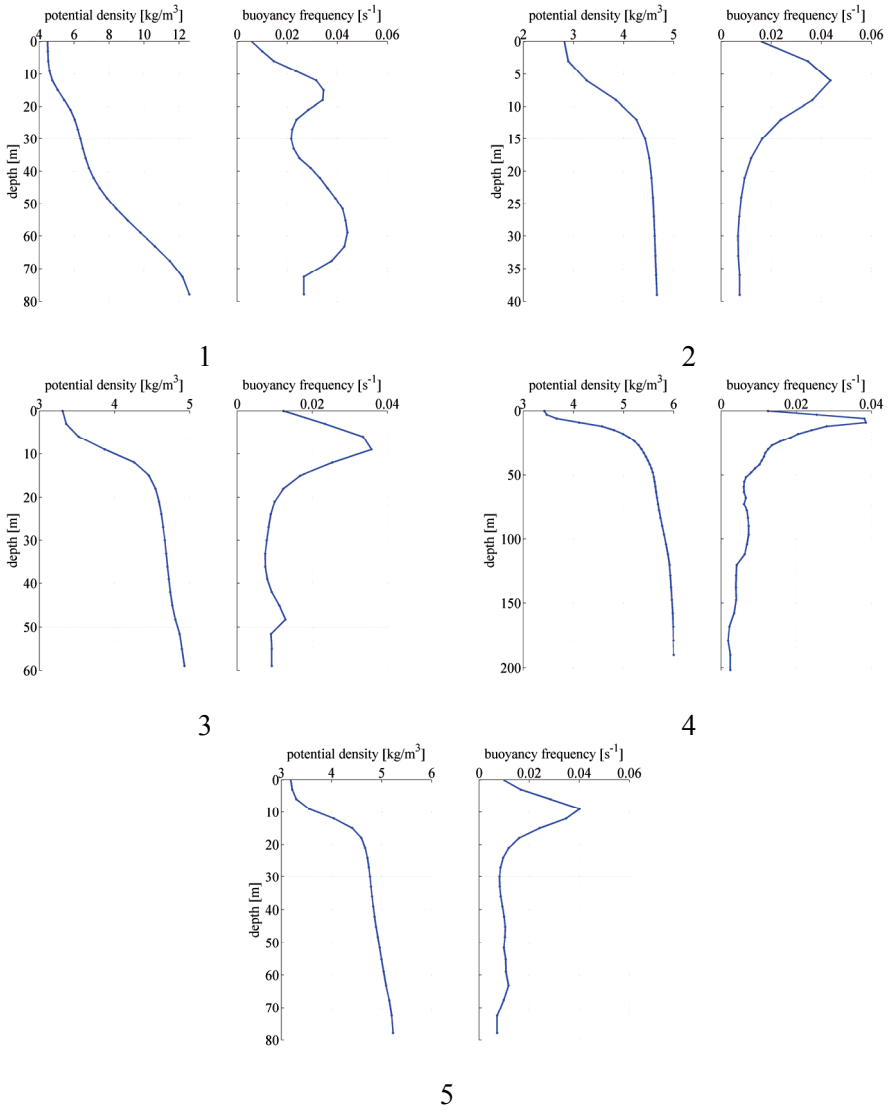

Fig. 3.3. Density and buoyancy profiles for the locations in Table 3.1

IWs undermine the identification of surface manifestations of sea IWs. They can be masked by the processes in the near-water layer of the atmosphere (Mityagina and Lavrova, 2010). Therefore it is not surprising that events of surface manifestations of IWs are relatively rare for the Baltic Sea, and that only a few of them were detected from satellite SAR images.

As an example, the main characteristics of five IW events reconstructed from SAR images are presented (Table 3.1, Figs. 3.1, 3.2). Density and buoyancy profiles for geographical locations of these observations (Fig. 3.3) are calculated from the monthly averaged long-term temperature and salinity fields calculated using the Rossby Centre Ocean circulation model (Meier et al., 2003; Meier, 2007; Soomere et al., 2011). Note that four of the five stratification profiles have quite a sharp and shallow pycnocline (5–10 m from the surface, while the total depth was 40–200 m).

Lavrova et al. (2010) detected 11 events of surface manifestations of IWs in the Baltic Proper and in the Gulf of Bothnia and 12 events in the Danish Straits in 2009–2010. The IWs in the Danish Straits are generated by tides. The number of waves in the trains was usually ≤ 10, maximal wavelength did not exceed 1 km, and the length of the leading wave front was less than 25 km. In July 2010 surface manifestations of IWs were periodically detected in the southern part of the Gulf of Bothnia and to the north and north-west of Gotland.

In situ measurements in the Baltic Sea show fluctuations in current velocities and motions of isotherms on different timescales (Leppäranta and Myrberg, 2009). Periods of 1–30 min have been observed in the Kiel Bight, while periods of 5–6 h have been reported from the Gulf of Finland, the Arcona Basin and the Darss Sill area. The resulting temperature (Fig. 3.4) and velocity (Fig. 3.5) variations can be quite large. The largest changes are usually found at the pycnocline. When there is both a thermocline and a halocline, two IW structures can be observed in the resulting three-layer medium.

Cyclones providing winds of 10−15 m/s in the Baltic Sea cause the generation of IWs with amplitudes of 11–15 m. The associated current velocities in the upper layer are about 11–15 cm/s and in the lower layer about 5–8 cm/s (Chernysheva, 1987). The characteristics of IWs and internal seiches

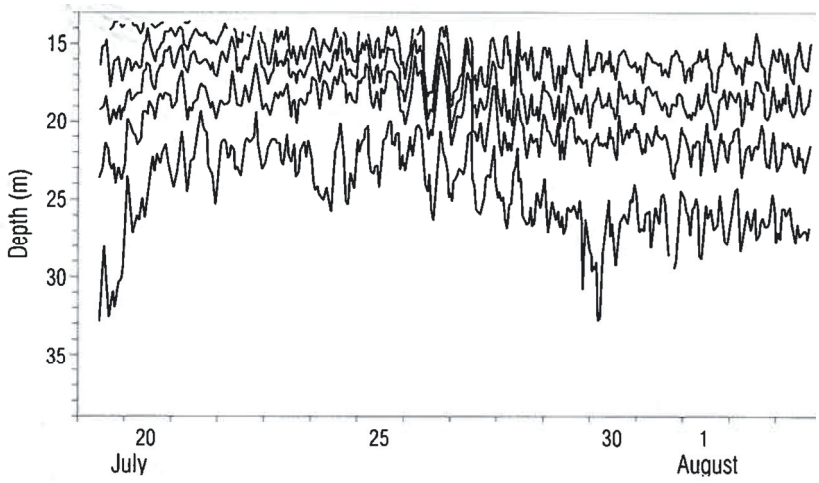

Fig. 3.4. Isotherms for a 16-day period in July-August 1978 in the Sea of Bothnia, from (Leppäranta and Myrberg, 2009)

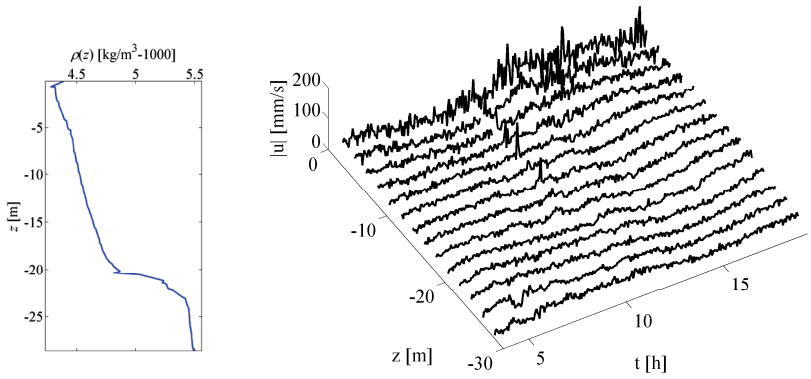

Fig. 3.5. Density profile (left) and records of the absolute value of horizontal velocity (right) on 16 June, 2010 near the coast of Curonian Spit in the south-eastern part of the Baltic Sea (Kurkina et al., 2011).

measured in the Baltic Sea are given in (Kol′chitskii et al., 1996; Golenko and Mel′nikov, 2007). In particular, IWs with periods of 0.1–1 h, observed in the central part of the Gotland Deep formed IW trains with duration of several hours and current amplitudes of about 3 cm/s. IWs in the inertial frequency range can induce currents reaching 20 cm/s.

3.2 Average kinematic and nonlinear parameters of IWs in the Baltic Sea

Horizontal variability of hydrological fields is represented in the weakly nonlinear IW theory as spatial variation of the coefficients of the corresponding nonlinear evolution equations (1.35) and (1.39). These coefficients (the propagation speed, the coefficients at the quadratic and cubic nonlinearities and the dispersion term) govern the kinematic and nonlinear characteristics of the IW field. Horizontal variability of vertical stratification is especially pronounced in the shelf zone and shallow-water basins of estuarine type.

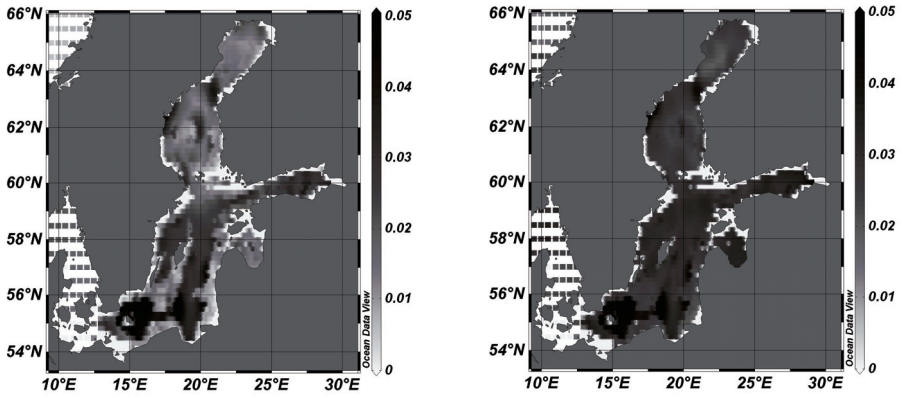

Fig. 3.6. Maps of the maximal value in the buoyancy frequency profile N_{max} [s^{-1}] (left panel: January, right panel: July)

When IWs are modelled numerically, an important problem is to specify the hydrological conditions that govern the density variations with depth to initialize the numerical models. An adequate way is to use gridded temperature–salinity data from international hydrological atlases. This approach allows reproducing the internal wave 'climate' of the considered basin, because hydrological atlases represent the long-term mean density stratification.

The first such estimations for the Baltic Sea are given in (Talipova et al., 1998) for the region of the Gotland Basin. Analogous maps for specific regions of interest can be found in (Ivanov et al., 1994) for the Black Sea, in (Pelinovsky et al., 1995) for the coast of Israel, in (Poloukhin et al., 2003, 2004) for the Arctic Sea (the last paper also accounts for the background currents) and in Paper I for the South China Sea.

We used long-term mean temperature and salinity profiles from GDEM-V3.0 (Teague et al., 1990) to calculate density stratification for the Baltic Sea. The GDEM climatology at a 10′ resolution has been developed for selected regions (incl. the Baltic Sea) where the data are sufficient to support this high resolution.

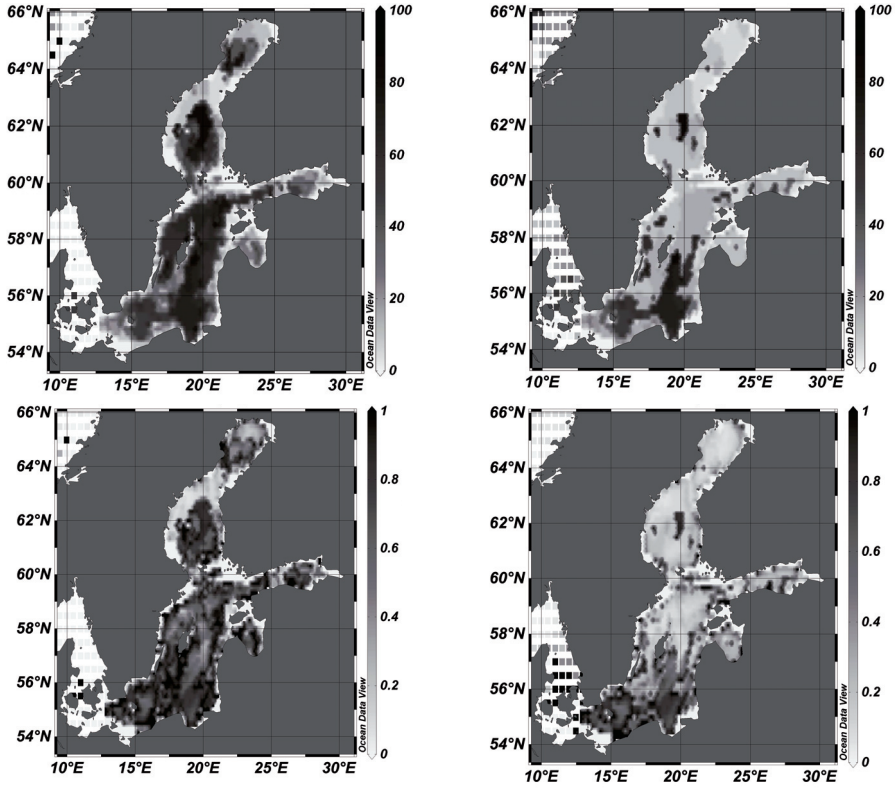

Fig. 3.7. Top: depth p_d [m] of the maximal value in the buoyancy frequency profile; bottom: maps of its values p_d/h normalized by the total sea depth (left column: January, right column: July)

Mean density profiles for each month were computed from temperature and salinity profiles using the International Equation for State of Sea Water (Fofonoff and Millard, 1983). With these density profiles, the speed of propagation and dispersive and nonlinear parameters of the Gardner equation for IWs of the lowest mode were presented in the form of charts with a resolution of $10' \times 10'$ along latitudes and longitudes in Paper III. This paper also discusses spatial and seasonal (July and January) variations in these parameters.

The eigenvalue problem (1.9) was solved numerically at each grid point for the first eigenvalue c (long linear IW phase speed for the lowest vertical mode IWs) and the first eigenfunction $\Phi(z)$ (vertical structure of a wave). The dispersion and quadratic nonlinearity parameters were evaluated next from Eq. (1.11). Further, the boundary-value problem (1.13) for the nonlinear correction $T_n(z)$ was solved numerically by the method of variation of parameters. Finally, the coefficient at the cubic nonlinearity (1.17) was calculated.

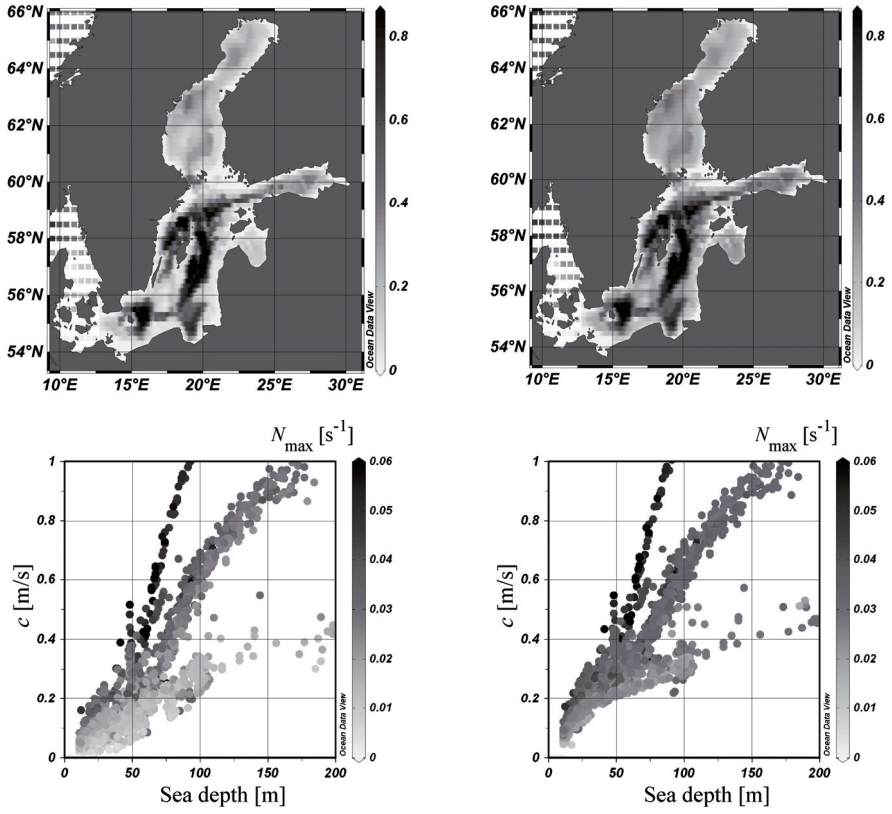

Fig. 3.8. Top: maps of long linear IW speed c [m/s]; bottom: scatterplots of c as a function of sea depth, colours indicate values of N_{max} [1/s] for the corresponding grid point (left column: January, right column: July)

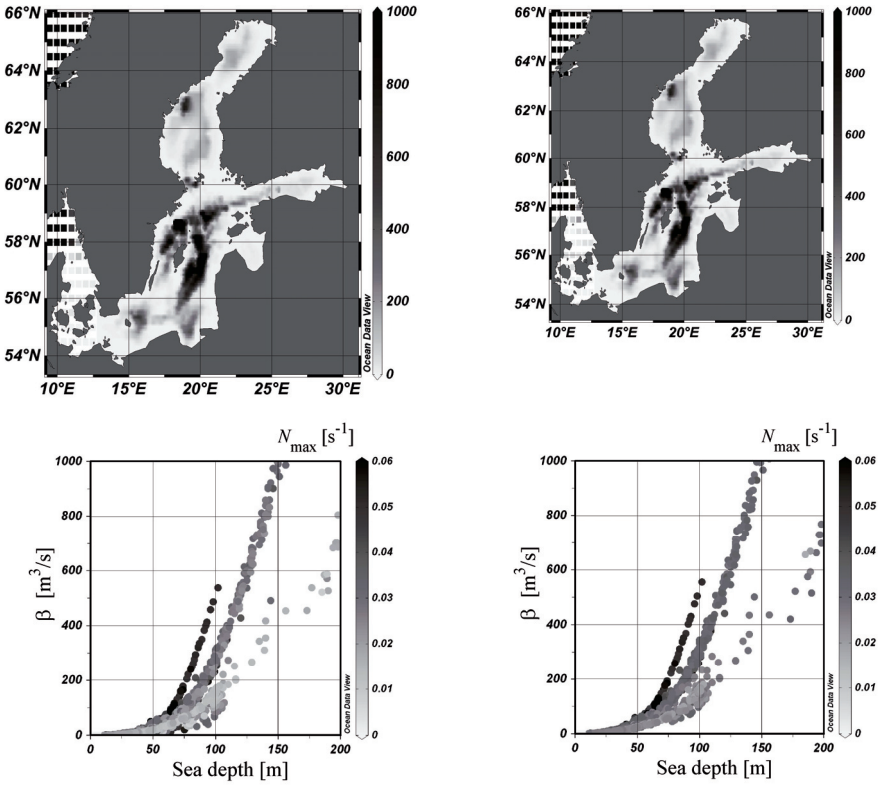

Fig. 3.9. Top: maps of the long linear IW dispersion parameter β [m^3/s]; bottom: scatterplots of β as a function of sea depth, colours indicate values of $N_{\max}$ [s] for the corresponding grid point (left column: January, right column: July)

The bathymetry of the Baltic Sea (Fig. 3.1) and charts representing the magnitude of seasonal variability in the density stratification in terms of maximums of buoyancy frequency $N_{\max}$ (Fig. 3.6), the depth p_d where the maximum of buoyancy frequency occurs (usually equivalent to the depth of the main pycnocline) and its value p_d/h normalized by the total water depth (Fig. 3.7) can help in the interpretation of obtained results and in explaining the features of the geographical distribution of kinematic and nonlinear parameters of the IW field. Consistently with the extensive seasonal variation in the Baltic Sea dynamics the stratification data strongly depend on the particular season. An interesting feature is the increase in the maximal buoyancy frequency values during summer simultaneously with a decrease of their depths. In the light of the above research, one can expect an increase in the impact of IWs upon bottom sediments in shallow-water regions of the Baltic Sea in late summer and autumn.

Seasonal variations in the linear parameters c and β (the relevant coefficients at the linear terms in Eqs. (1.20), (1.35), (1.39); Figs. 3.8 and 3.9) are not very significant.

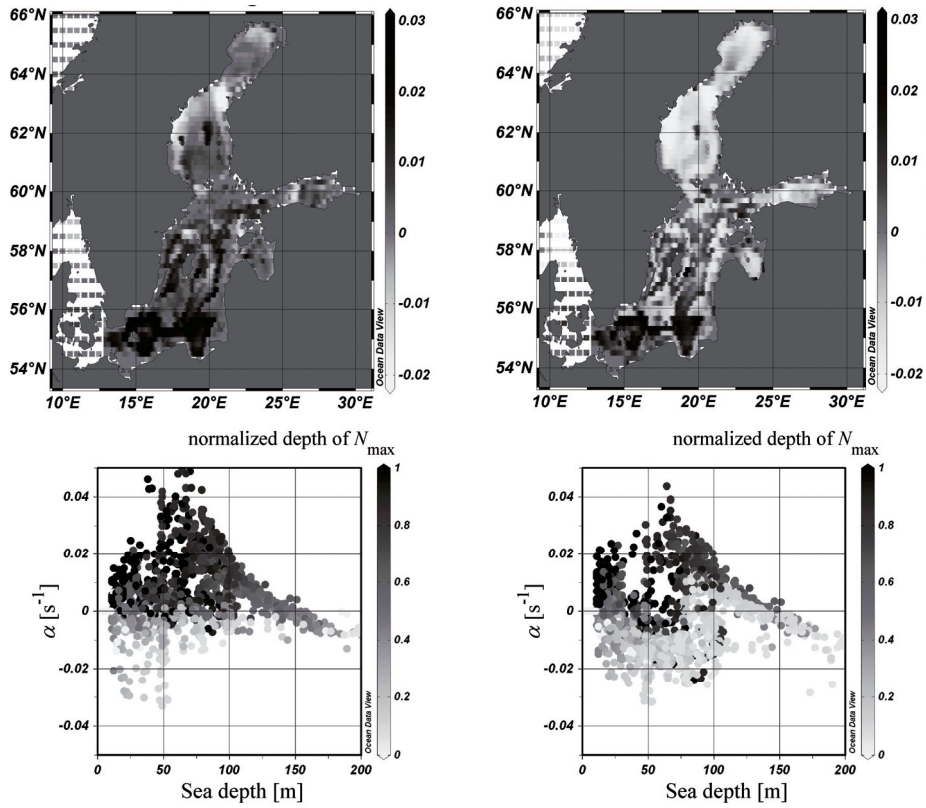

Fig. 3.10. Top: maps of the quadratic nonlinearity parameter α [1/s]; bottom: scatterplots of α as a function of sea depth, colours indicate values of p_d/h for the corresponding grid point (left column: January, right column: July).

The main features of their geographical distribution almost do not change from season to season. The maximal value of c is about 90 cm/s. These parameters apparently are mostly determined by the bathymetry. As expected, the linear phase speed and the linear dispersive coefficient scale approximately with power laws of the total sea depth (Figs. 3.8 and 3.9). Hence, as is well known, the SIWs of the largest amplitude will generally be found in shallow areas, including the coastal zone. For the Baltic Sea conditions the sets of data points for $c(h)$ and $\beta(h)$ form three clearly expressed branches depending on the values of $N_{\max}$ and signifying the presence of three different populations of IWs.

The nonlinear parameters α and α_1 (the relevant coefficients at the nonlinear terms; Figs. 3.10 and 3.11) are more sensitive with respect to the fine structure of the density stratification. They show considerable variability. Their seasonal variability is significant, and they can even change their signs at the same place from season to season. The presence of many sign changes emphasizes once more the importance of determining the critical points.

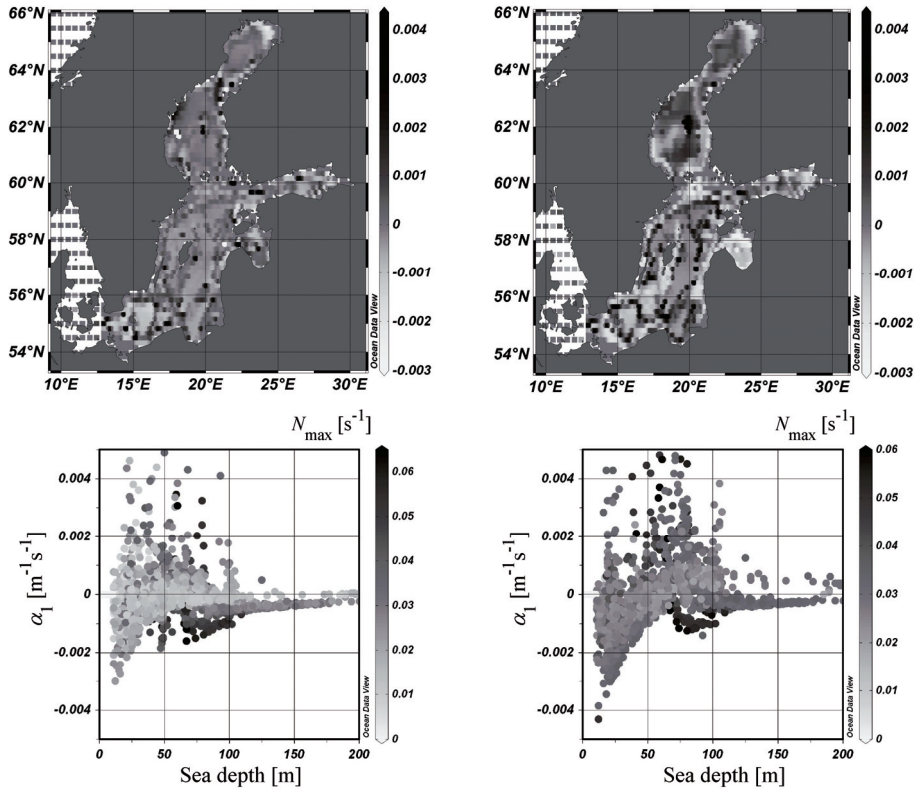

Fig. 3.11. Top: maps of the cubic nonlinearity parameter α_1 [1/(m·s)]; bottom: scatterplots of α_1 as a function of sea depth, colours indicate values of N_{max} [1/s] for the corresponding grid point (left column: January, right column: July)

The quadratic nonlinearity parameter (Fig. 3.10) changes from –0.02 to 0.03 1/s. For July it is mainly positive in the southern part of the Baltic Sea (the Arcona Basin, the Bornholm Basin and the Slupsk Furrow). In the central part (the Gotland Basin) there are spots with different signs of α. The Gulf of Finland and the Bothnian Sea are characterized by negative values of this parameter. In the winter season the zone of positive values of α broadens and includes the central part of the Baltic Sea and most of the Gulf of Finland.

The plots of the quadratic nonlinearity parameter (Fig. 3.10) show the tendency for its absolute value to decrease with the increasing depth (for depths of 100 m and more). Negative values of α are mainly observed for depths over 150 m. Larger absolute values of α are typical for the locations with larger values of N_{max}. From Fig. 3.10 it follows that in January the normalized pycnocline depth p_d/h is mainly responsible for the sign of the quadratic nonlinearity coefficient: $\alpha < 0$ if the pycnocline is situated near the surface (small p_d/h) and normally $\alpha > 0$ for deeper locations of the pycnocline. In July (Fig. 3.10) this relationship is not so clearly expressed because of a more complex pattern of density profiles.

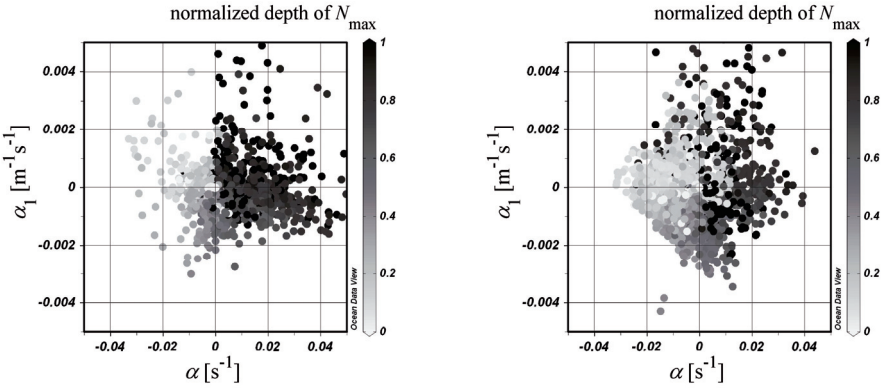

Fig. 3.12. Parameters (α, α_1) for different areas of the Baltic Sea. Colours of the points indicate values of p_d/h for the corresponding grid point (left panel: January, right panel: July)

The cubic nonlinear parameter (Fig. 3.11) changes in the range from –0.003 to 0.004 1/(m·s) in the Baltic Sea (Paper III). Its spatial distribution has a spotty character with interspersed zones with positive and negative values, with a certain predominance of negative values in winter and of positive values in the Bothnian Sea in summer. The scatterplots of this quantity against water depth show that sufficiently deep ($h > 100$ m) locations have small absolute values of this coefficient ($< 10^{-3}$ 1/(m·s)) where it is mainly negative in January, and can have both signs in July. No clear pattern is evident for α_1 against $N_{\max}$, p_d or p_d/h.

3.3 Nonlinear wave regimes

Combinations of nonlinear parameters (α, α_1) are shown in Fig. 3.12 for hydrological conditions in the Baltic Sea in January and July. A comparison with Fig. 1.3 reveals the possibility for all the branches of soliton solutions of different polarities of the Gardner equation (see Section 1.2) to exist in the Baltic Sea either in winter or in summer. Therefore, various dynamic scenarios for IW interactions and transformations are possible here. In addition, there exist a number of cases with very small values of both α and α_1. The IW field in such cases cannot be described by the Gardner equation, and certain higher-order nonlinear terms have to be taken into account to properly describe the SIWs.

Figures 3.13 and 3.14 illustrate geographical distributions of amplitudes $a_{\lim}$ (Eq. (1.46)) for the points with $\alpha_1 < 0$ and a_{alg} (Eq. (1.47)) for the points with $\alpha_1 > 0$ in the Baltic Sea. The range for the values of these amplitudes is about ± 40 m.

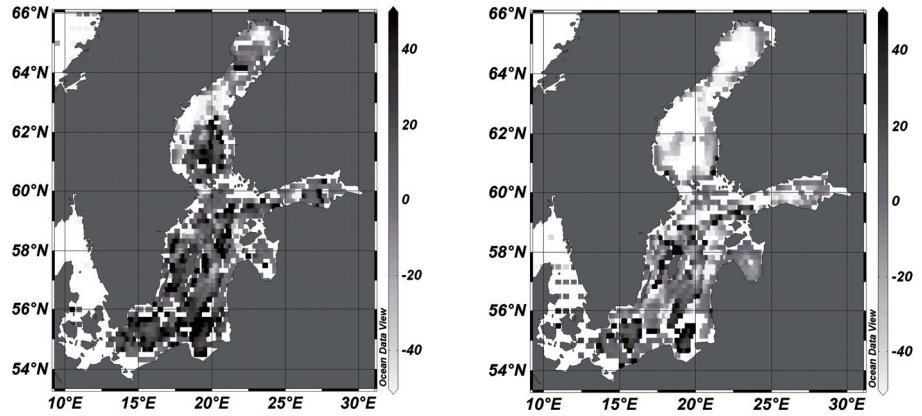

Fig. 3.13. Limiting amplitudes [m] of 'top-table' solitary waves (for negative cubic nonlinearity values, left panel: January, right panel: July)

Note that KdV, mKdV and GE+ (Gardner equation with positive cubic nonlinearity) equations, formally, do not restrict the amplitude of large-amplitude SIWs (1.44), (1.45) and (1.42). The only restriction is that the amplitude must be small enough for the equations to be applicable.

To understand the role of the nonlinearity (is it weak or not) in the IW dynamics, three values should be compared: c, αa and αa^2, where a is the amplitude of the soliton. In deep water nonlinear effects are usually small, but in the coastal waters they can be comparable with and even exceed the linear term. Nevertheless, the Gardner model may be used as demonstrated in (Maderich et al., 2009, 2010). Consequently, the relevant soliton solutions can have amplitudes at which waves break for any stratification, including those for which solutions of the DJL equation broaden and reach the limit of a flat centred solitary wave well below breaking. The amplitude of the solutions to the GE– (Gardner equation with negative cubic nonlinearity) is bounded, but the limitation is not always physically adequate: the amplitude may even

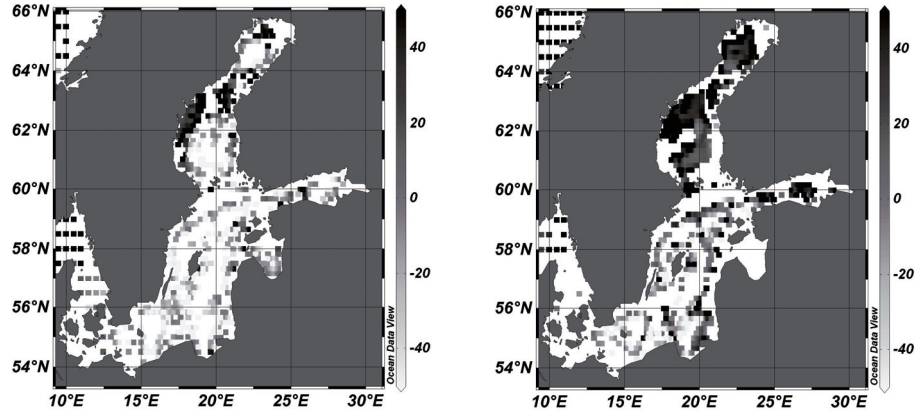

Fig. 3.14. Amplitudes [m] of algebraic solitons (left panel: January, right panel: July)

exceed the total sea depth.

A reasonable upper bound for the amplitude of SIWs can be found from the condition that the wave does not break:

$$\frac{U_{\max}}{V} \le 1, \tag{3.1}$$

where $U_{\max} = \max\, u(x,z,t)$ is maximal horizontal velocity induced by the internal soliton (see Eq. (1.49)) and V is the propagation speed of this soliton. The latter is the propagation speed c of a linear long IW plus a nonlinear correction, whose formulation depends on the approximation used (KdV, mKdV or GE) and which is always expressed through the amplitude and the parameters of nonlinearity:

$$V_{\mathrm{KdV}} = c + \frac{\alpha a}{3}, \qquad V_{\mathrm{mKdV}} = c + \frac{\alpha_1 a^2}{6}, \qquad V_{\mathrm{GE}} = c + \frac{\alpha a}{3} + \frac{\alpha_1 a^2}{6}. \tag{3.2}$$

For the largest-amplitude soliton Eq. (3.1) reduces to $U_{\max} = V$. As was discussed in Section 1.3, the maximum horizontal velocity excited by a lower-mode weakly nonlinear soliton is attained on the bottom or on the surface, therefore

$$\begin{aligned} U_{\max} &= \max_{z=\{0;-h\}} \left\{ c\eta(x-Vt)\frac{d\Phi}{dz} + \left(\frac{\alpha}{2}\frac{d\Phi}{dz} + c\frac{dT_n}{dz} \right) \eta^2 (x-Vt) \right\} \\ &= \max_{z=\{0;-h\}} \left\{ ca\frac{d\Phi}{dz} + \left(\frac{\alpha}{2}\frac{d\Phi}{dz} + c\frac{dT_n}{dz} \right) a^2 \right\}, \end{aligned} \tag{3.3}$$

where only the leading-order term is appropriate for the KdV approximation. A continuation of the research towards establishing more exact estimations for such limiting amplitudes is planned for the future.

3.4 Horizontal velocity in internal waves

Velocity components in IWs of the lowest mode are described in Section 1.3 for two- and three-layer examples of vertical density profiles. Horizontal velocity is the most significant component. It can be calculated using Eq. (1.49). The largest horizontal currents associated with these waves are at the surface or at the bottom depending on the vertical location of the most significant density variations. Such wave-induced near-surface and near-bottom currents can provide an effective means of particle transport, affecting pollutants, admixtures, nutrients, sediments etc. and having an impact on eco- and biosystems, offshore structures and their mooring devices.

The central characteristic of an IW field is the near-bottom velocity in IWs in areas where the density jump layers are located in the vicinity of the seabed. In such areas IWs are the major driver of sediment resuspension and erosion processes (Stastna and Lamb, 2008; Carr et al., 2010). They may be also

responsible for destroying the laminated structure of the sedimentation regime in affected areas. As the pycnocline is in many cases located at a depth of only a few metres in some areas of the Baltic Sea during spring and summer (Leppäranta and Myrberg, 2009), the impact of IWs on sedimentation processes frequently extends to the coastal zone and overlaps with the nearshore affected by surface waves. Such a situation often happens in partially sheltered sub-basins of the Baltic Sea like the Gulf of Finland where the role of high near-bottom velocities, eventually created by high-amplitude IWs, has been systematically underestimated in engineering applications (Erm et al., 2010).

For the analysis of the geographical features of the near-bottom and near-surface velocity distribution it is convenient to consider a normalized quantity u/η (Figs. 3.15 and 3.16). To the leading order, it is independent of η.

The largest values of normalized near-bottom velocities (Fig. 3.15) can be expected along the coasts, in the eastern part of the Gulf of Finland and especially in the south-western part of the Baltic Sea (the Arcona Basin and the Bornholm Basin) with the tendency for small values to increase in the warm

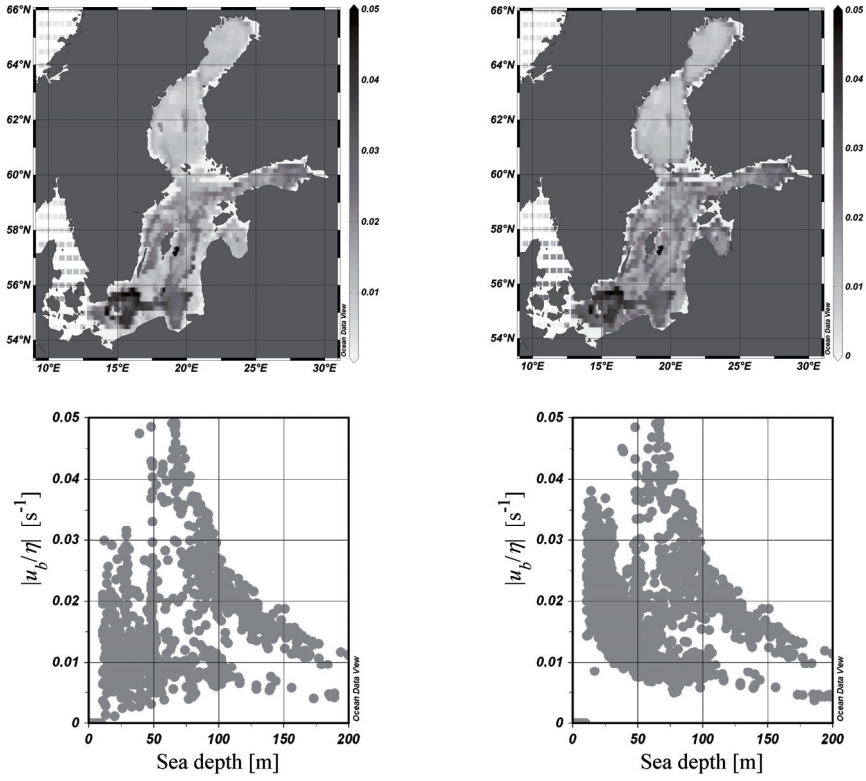

Fig. 3.15. Top: maps of leading-order normalized near-bottom velocity u_b/η [1/s], in the IW field; bottom: scatterplots of u_b/η as a function of sea depth (left column: January, right column: July)

season.

The largest values of normalized near-surface velocities (Fig. 3.16) are found in the central part of the Baltic Proper (eastern Gotland Basin, in the domains to the north, north-east and north-west of the Gotland Island), in the deepest part of the Gulf of Bothnia, and to the east and north-east of Bornholm Island. They also increase noticeably in summer.

The scatterplots of u_b/η against sea depth (Fig. 3.15) show a general decrease in this quantity for increasing depths in the Baltic Sea, while u_s/η (Fig. 3.16) exhibits a contrary trend to increasing for larger depths. Thus, for IWs of equal amplitude the wave-induced horizontal currents predominate near the bottom in shallow regions and near the surface in deep basins.

A specific feature for many relatively shallow regions of the Baltic Sea is that the normalized near-bottom velocities in IWs are almost twice as large as the corresponding near-surface velocities. This follows from the property of many winter-time density profiles. In January the pycnocline is usually located in the lower part of the water column (Fig. 3.7) and this affects the shape of $\Phi(z)$. Stratification in July is usually characterized by quasi-three-layer

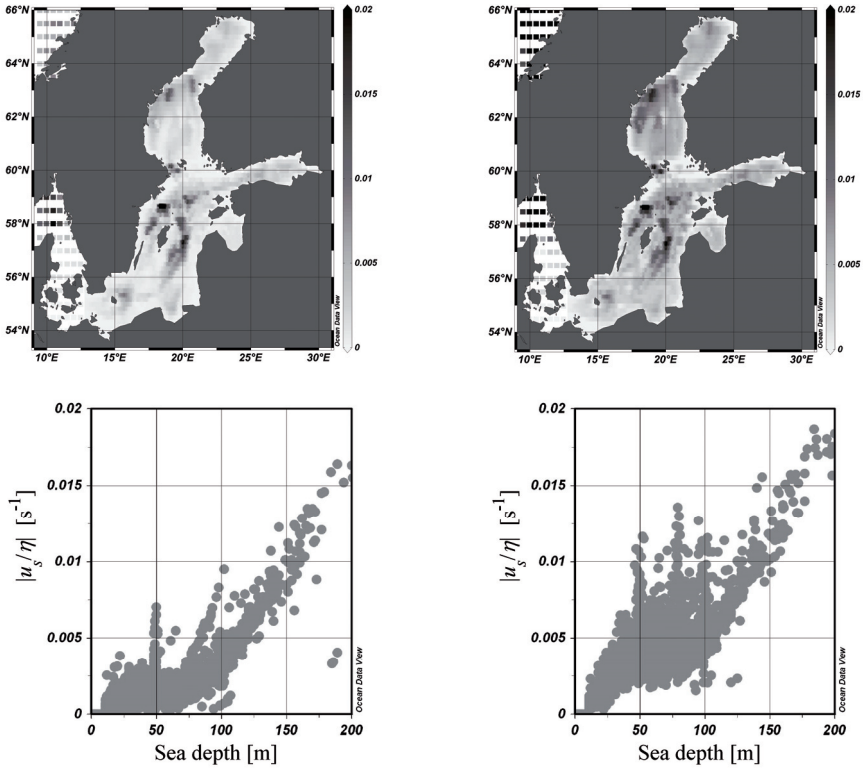

Fig. 3.16. Top: maps of leading-order normalized near-surface velocity u_s/η [1/s], in the IW field; bottom: scatterplots of u_s/η as a function of sea depth (left column: January, right column: July)

density profiles with two pronounced pycnoclines with comparable values of N (see, for example, Fig. 3.3, panel 1). Therefore, even for a relatively strong upper pycnocline the vertical mode $\Phi(z)$ can have larger gradient near the bottom.

It is interesting to note that three points of IW observations (points 1, 4, 5) out of the five in Fig. 3.1 are located near the local maximums of normalized near-surface velocity (Fig. 3.16).

3.5 Statistics of extreme surface waves in the south-western Baltic Sea

The local surface wave climate of the Baltic Sea is analysed in Paper VI on the example of the Darss Sill area, south-western Baltic Sea, based on 20 years (1991–2010) of waverider data and results of two long-term numerical simulations. This analysis is particularly important in the context of establishing potential sources of IWs in this basin. The key outcome is the demonstration that high-frequency hydrodynamic activity, which could partially replace the tidal IW generation, is quite large in the Baltic Sea.

Wave measurements have been carried out at a 20 m deep location (54°41.9' N, 12°42.0' E, Fig. 3.17) in the area of the Darss Sill since 29 January 1991 using a Datawell directional waverider. The device is operated by the Institute for Coastal Research, the Helmholtz-Zentrum Geesthacht, Germany. An overview of the recorded wave data and their climatological analysis is

Fig. 3.17. Location scheme of the wave measurement site at the Darss Sill in the SW Baltic Sea

presented in (Soomere et al., 2011).

The measured wave data are compared with two numerically simulated wave data sets, both calculated using the third generation wave model WAM (Komen et al., 1994) covering the entire Baltic Sea with a spatial resolution of about three nautical miles (5.5 km × 5.5 km) and a directional resolution of 15°. One of the simulations (called AW below) was peformed for the period of 1958–2002 using 28 frequency bins ranging from about 0.05 to 0.66 Hz (Augustin, 2005; Weisse et al., 2009). The model was forced by wind fields derived from a reconstruction using a regional atmosphere model (Feser et al., 2001) driven by the NCEP/NCAR (National Center for Environmental Prediction and the National Center for Atmospheric Research) weather reanalysis (Kalnay et al., 1996, Kistler et al., 2001). The model considered wave fields from a corresponding North Sea hindcast (Weisse et al., 2007) as lateral boundary conditions.

Another set of simulations (called RS below) was performed for 1970–2007 for the Baltic Sea only (Räämet and Soomere, 2010) using adjusted geostrophic winds and assuming that the wave energy flux through the Danish Straits can be ignored. This hindcast used an extended frequency range up to about 2 Hz (wave periods down to 0.5 s, 42 frequencies) to ensure realistic wave growth rates in low wind conditions after calm situations (Soomere, 2005). Wave data for comparisons are calculated for the grid point with coordinates 54°42' N; 12°42' E for both models. The basic integrated wave parameters such as significant wave height, mean wave direction, and different wave periods are available every hour for each of the models. As the RS simulations with using relatively low-resolution wind information (once in 3 or

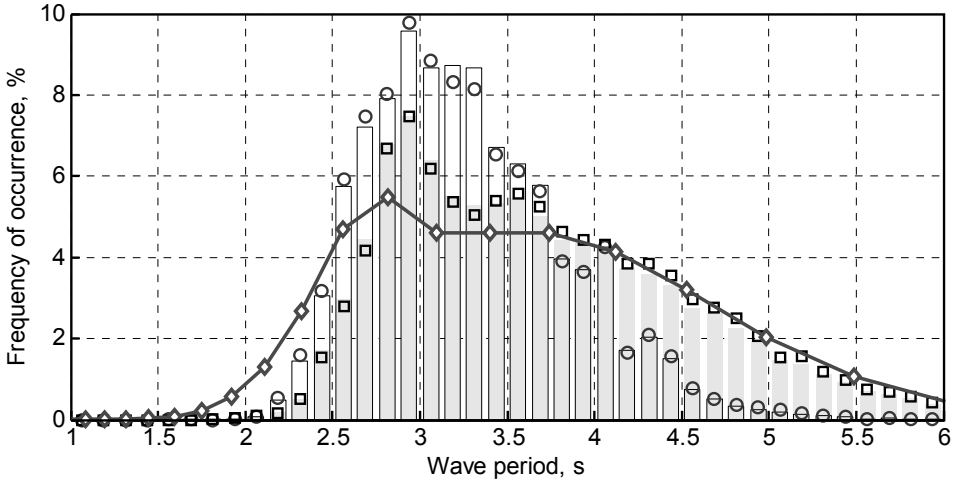

Fig. 3.18. Frequency of occurrence of different mean wave periods based on all measurements (1991–2011, white framed bars) and RW modelling results (1957–2002, grey bars). Circles and squares indicate the relevant values of these data sets for the overlapping period of 1991–2002. Rhombuses indicate the frequency of occurrence of peak periods reduced by 15% from AR simulations for 1970–2007

6 h), the timing of the simulated and measured wave events was poor but the wave statistics was reconstructed adequately.

The wave climate of the Darss Sill region (Fig. 3.17) reveals several well-known features of the Baltic Sea waves in semi-sheltered basins of this water body: relatively modest long-term wave heights, periods usually in the range of 2–4 s (Fig. 3.18) and the most frequent wave heights around 0.5 m (Fig. 3.19). Contemporary wave models reasonably reproduce both the average wave heights and the distributions for the frequency of occurrence of different wave heights (Fig. 3.19). Also, the detailed temporal course of the wave heights is adequately reproduced by the AW simulations. Models forced by low-resolution (e.g. geostrophic) wind data also reproduce the basic wave statistics although they frequently fail to reflect wave fields in strong storms. Therefore, wave data modelled even using low-resolution wind fields can be successfully used for such applications that rely exclusively on the statistical distributions of wave parameters (e.g. estimates of the intensity of coastal processes or the net longshore transport of sediment using the CERC method).

There is a major discrepancy between the measured and modelled distributions of wave periods (Fig. 3.18), especially for periods occurring in

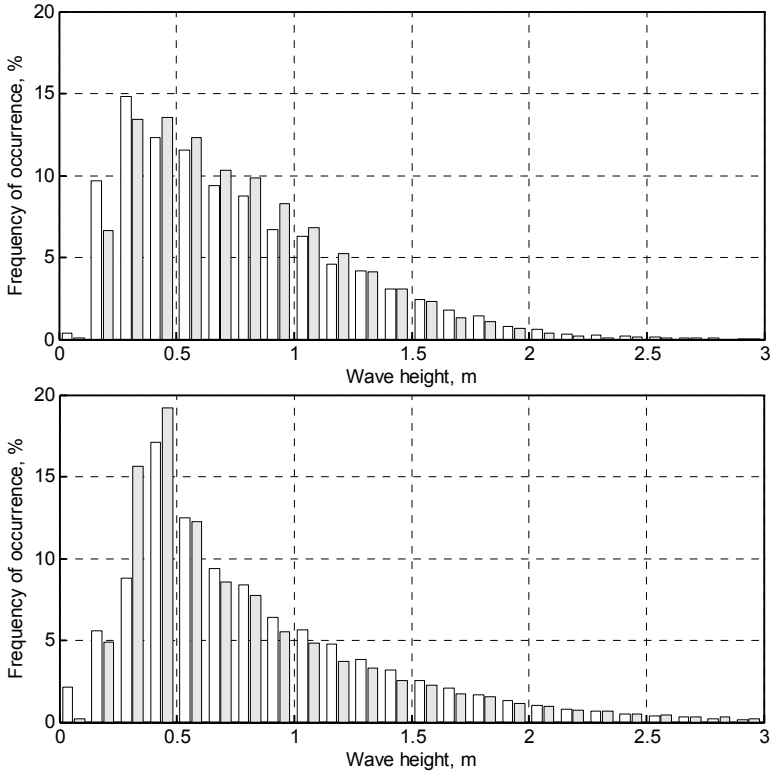

Fig. 3.19. Frequency of occurrence of different wave heights at the Darss Sill with a step of 0.125 m. Above: based on all measurements (white bars) and daily average wave heights (grey bars); below: AW simulations (white bars) and RS simulations (grey bars)

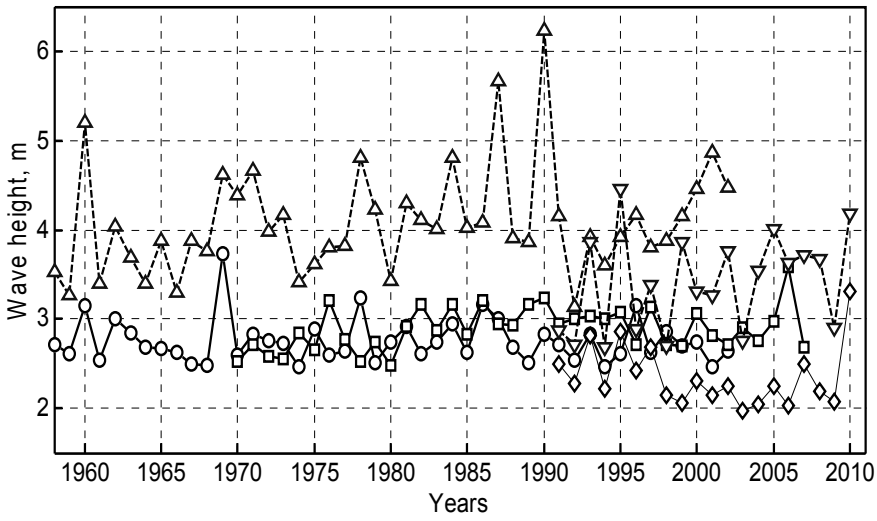

Fig. 3.20. Annual maximums of measured (downward-looking triangles) and modelled (upward-looking triangles) wave heights and annual thresholds for the highest 1% of the measured waves (99%-ile, rhombuses) and for AW simulations (circles) and for RS simulations (squares)

relatively rough wave conditions. The difference between measured and modelled periods in strong storms is up to 2 s, which may considerably affect the estimates of wave–bottom interactions and refraction patterns for certain depths and, consequently, the estimates of the frequency of nonlinear interactions between crossing wave systems.

The sawtooth-like behaviour of the modelled annual highest waves (Fig. 3.20), although it contains a large level of interannual variability, suggests that a major shift in storm properties occurred in the southern Baltic Sea at the beginning of the 1990s. Given 6.23 m as the maximum modelled wave height in RS simulations and the match of modelled and measured wave conditions in many storms, the sea area in question apparently hosts more severe wave climate than, for example, the Gulf of Riga or even the Gulf of Finland. The basic reason is that, differently from these basins, the Darss Sill area and the adjacent Arkona Basin are oriented along the wind directions prevailing during strong storms. This feature becomes evident as an about 20% difference of the all-time highest waves (5.2 m measured in the Gulf of Finland, 6.23 m hindcast in the Darss Sill area) and has a potential for even larger wave heights in the Arkona Basin.

Another highly interesting feature is the mismatch between the temporal changes in the average wave heights, typical properties of modestly high waves (the threshold for the top 10% of the waves) and the properties of the highest waves. While the properties of average and modestly high waves have shown identifiable changes over the last half-century (Soomere et al., 2011), the threshold for the 1% of the highest waves, estimated from measurements, has considerably decreased over the two latter decades. This process is opposite to

the recently identified increase in this threshold in the north-eastern Gulf of Finland (Soomere et al., 2010) on the background of no changes in the average wave heights. Still, both the patterns of changes are consistent with the gradual increase in the frequency of south-western and western winds at the 'expense' of other wind directions (Jaagus, 2009; Lehmann et al., 2011) in a large section of the Baltic Sea basin: the Darss Sill. The analysis also shows some evidence (albeit statistically not significant) that the wave heights in the strongest storms have not changed over the last 20 years whereas the frequency of storms exciting very severe waves might have increased.

Concluding remarks

The presented overview of the spatial variability of the basic parameters and several interesting features of the underlying hydrophysical fields (such as the depth of the maximal value in the buoyancy frequency profile and the maximal values of the buoyancy frequency over such profiles for different months) and the derived average values of the coefficients of the Gardner equation allow producing the estimations of nonlinear IW shapes and limiting amplitudes before numerical simulations. The critical points (where the coefficients at the quadratic or the cubic nonlinear term vanish) define the locations of special interest where SIWs may undergo dramatic transformation, often involving a polarity change and disintegration into a wave train. The spatial and seasonal distributions of the kinematic and nonlinear parameters governing the IW field in a frame of the Gardner equation are constructed on a $10' \times 10'$ grid from the GDEM V3.0 climatological average hydrographic data set for the Baltic Sea in Paper III. Geographical variations of the climatological averages of parameters together with the effects of stratification and water depth apparently describe the main elements of the distributions of IW features in the Baltic Sea.

Seasonal (January and July) maps indicate that seasonal variations in the hydrophysical fields are insignificant for the linear (phase speed and dispersion) parameters. The coefficients at nonlinear terms of the Gardner equation α and α_1 are less stable. Their relatively strong variations and even changes in their sign are possible. The presented data and technique enable to systematically estimate limiting amplitudes for SIWs and to highlight the possible soliton branches. As an application of the technique of the Gardner equation, maps of the leading-order near-bottom and near-surface amplitude-scaled horizontal velocities have been constructed. This descriptive study as well as the database of IW parameters for the Gardner model in the Baltic Sea will eventually provide a useful resource for a variety of dynamic studies. The established kinematic parameters can be used for express evaluations of the possible polarities and shapes of solitary IWs, their limiting amplitudes, propagation speeds etc. They also can help to set up and initialize more complex full nonlinear multidimensional models for IGWs.

The properties of extreme waves in relatively shallow domains of the Baltic Sea are analysed on the example of the Darss Sill area, SW Baltic Sea, based

on 20 years (1991–2010) of waverider data and results of numerical simulations. The largest measured significant wave height is 4.46 m. Numerical modelling indicates that wave heights over 6 m have occurred in this area within the last half-century. A major discrepancy (difference up to 2 s) is identified between the measured and modelled distributions of wave periods. The temporal course of the modelled annual highest waves has sawtooth-like behaviour, with gradual increase for 1958–1990 from about 4 m to about 5 m, a drastic decrease in 1991–1992 and an increase since then again. These changes may be reflected in the field of IWs in the Baltic Sea.

4 Propagation of nonlinear internal waves in shallow seas

This chapter presents several examples of modelling of IWs in realistic conditions based on results published in Papers I and II. The central goal is to demonstrate how the theoretical results presented in Chapter 1 can be applied for realistic oceanic conditions, such as those found in the South China Sea.

SIW transformations in the framework of models presented in Chapter 1 in zones including sign changes of nonlinear parameters are described in Sections 4.1 and 4.2 for the South China Sea and the Baltic Sea, respectively. Although the Baltic Sea is situated in middle and rather high latitudes, these calculations do not account for the Earth's rotation effects, which are discussed in Section 4.3. The relevant impact is negligible because the considered waves are relatively short in comparison with tidal and inertial waves, and we do not solve the problem of the generation of such waves. This approach is not applicable at even higher latitudes as described in Section 4.3. The situation presented in Section 4.4 requires another approach in modelling based on the direct solving of primitive Euler equations for a rotating basin, because the evolution of long tidal IWs is considered in supercritical latitudes in the Barents Sea.

4.1 Transformations of solitary internal waves in the South China Sea

In a typical oceanic situation, where there is a relatively sharp near-surface pycnocline, a SIW of depression is generated in the deep water and it propagates shorewards along generally decreasing depth until it reaches a critical point. For a simple two-layer model, the pycnocline at such a location is close to the mid-depth (Koop and Butler, 1981). The theory (Grimshaw et al., 1998) predicts that this wave will be destroyed in the vicinity of the critical

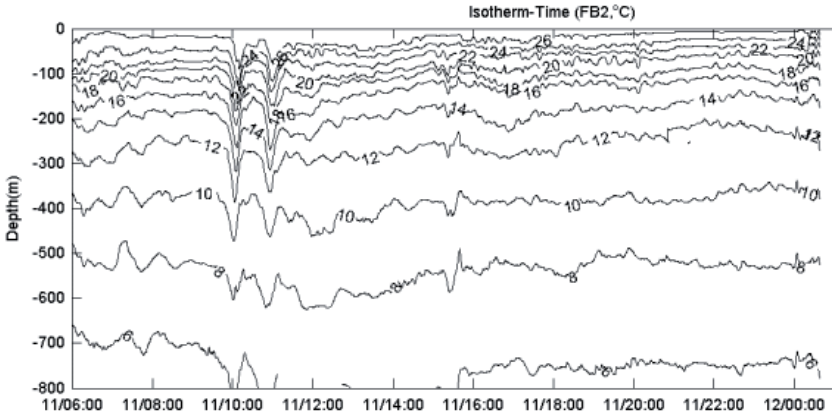

Fig. 4.1. Displacement of the isotherms as measured in the South China Sea, from (Liu et al., 2006)

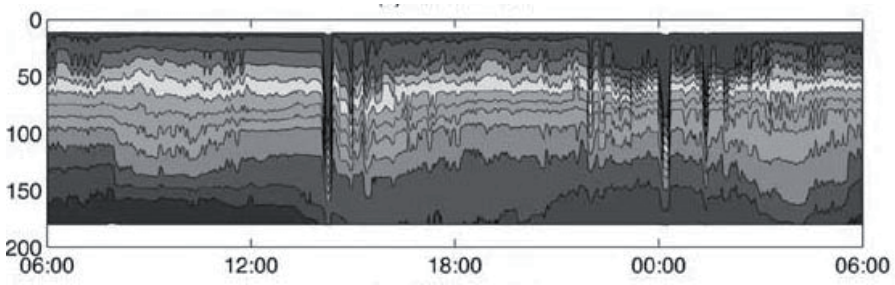

Fig. 4.2. Time series of IWs in the South China Sea, from (Duda et al., 2004)

point. It will be replaced in the shallow water shorewards of the critical point by one or more SIWs of elevation riding on a negative pedestal. This basic scenario has been observed many times in several places in the ocean, in lakes and in estuaries. Elsewhere in the ocean, where there are no such critical points, the shoreward propagating small-amplitude SIWs are expected to deform adiabatically (at least within the framework of the Gardner equation). Examples of this behaviour often occur. See Paper I for detailed references of both the scenarios.

The South China Sea is well known as a location where SIWs have been commonly observed. The dynamics of IWs in this basin has been intensively studied both experimentally and through numerical simulations (Paper I). Typically, large-amplitude IWs are generated by barotropic tidal currents, possibly combined with the extension of the Kuroshio Current, interacting with the topography in Luzon Strait. Solitary waves with amplitudes up to 80 m (in sea areas with a water depth of 300 m) have been observed at two underwater mountain ridges in Luzon Strait. The resulting wave field in Fig. 4.1 is taken from (Liu et al., 2006). These waves cross the deep basin and then shoal on the continental shelf where the water depth is 400–200 m. See, for example, the reports of the ASIAEX experiment (Duda et al., 2004; Liu et al., 2004; Ramp et al., 2004). Wave amplitudes can reach 100 m and their shapes compare well with theoretical solitary wave shapes. See (Klymak et al., 2006) and Fig. 4.2 from Liu et al. (2006).

Numerical modelling of the SIW transformation on the continental slope

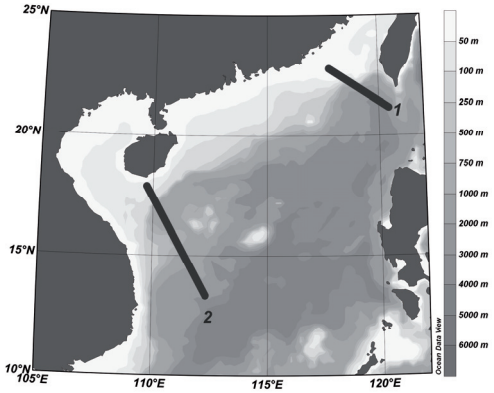

Fig. 4.3. Bathymetry of the South China Sea, with the chosen cross-sections

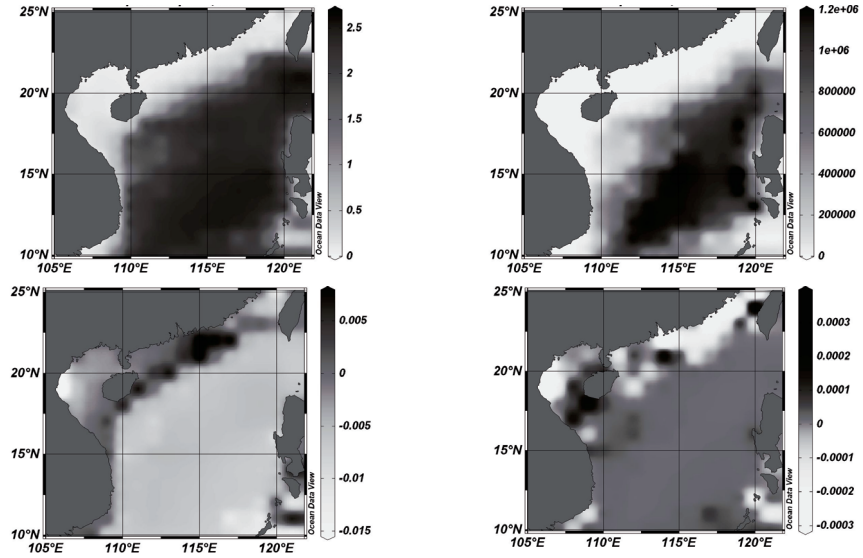

Fig. 4.4. Contour maps of the coefficients of the variable-coefficient Gardner equation for the South China Sea. The plots are those for the phase speed c, the dispersion coefficient β (upper panels), the quadratic coefficient α and the cubic coefficient α_1 (lower panels)

and shelf of the South China Sea has often been based on the variable-coefficient KdV and Gardner models, using mainly two-layer representations of the density stratification. The results have been used to interpret the observed solitary wave evolution and especially the polarity changes (Liu et al., 1998, 2004; Orr and Mingerey, 2003; Zhao et al., 2003, 2004). There are also a few numerical simulations that use the full Euler equations for stratified flow (Buijsman et al., 2008; Du et al., 2008; Scotti et al., 2008; Warn-Varnas et al., 2010; Vlasenko et al., 2010).

A set of numerical simulations of the variable-coefficient Gardner equation (1.39) for two typical cross-sections of the South China Sea (Fig. 4.3) is performed in Paper I. One cross-section is close to the conditions for ASIAEX 2001, where the SIWs are generated by westward tidal currents in Luzon Strait (Liu et al., 2006; Zhao and Alford, 2006). The other cross-section is chosen to have a positive cubic nonlinear coefficient along the whole wave path. Contour maps of the linear long wave speed, the coefficients at the quadratic and cubic nonlinear terms and the coefficient at the linear dispersive term in the variable-coefficient Gardner equation (1.33) are shown in Fig. 4.4. They are based on the vertical density profiles from the GDEM database for January, while the bathymetry is taken from the GEBCO database. As expected, the linear wave speed c and the dispersion coefficient β correlate well with the depth h (Talipova and Polukhin, 2001; Polukhin et al., 2003). The quadratic nonlinear coefficient α is negative in the deep part of the South China Sea but changes to positive on the continental slope of the South China Sea (Orr and Mignerey, 2003; Zhao et al., 2003, 2004). The coefficient at the cubic nonlinearity α_1 is

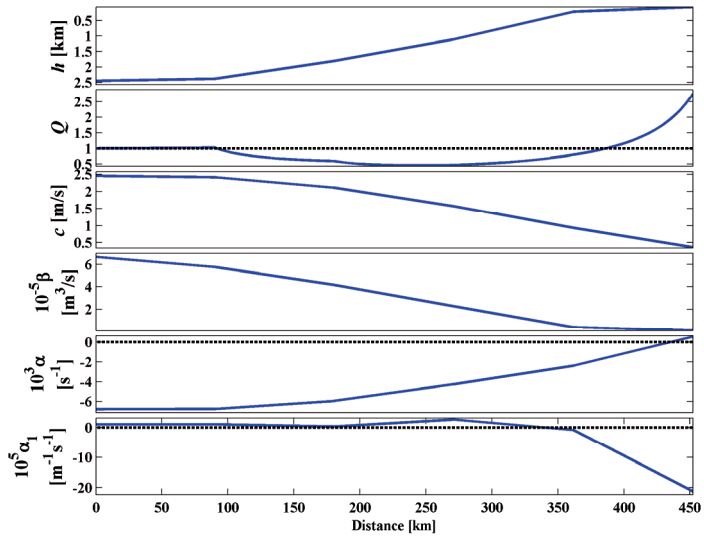

Fig. 4.5. Coefficients of the variable-coefficient Gardner equation (1.39) along cross-section 1

very small and positive in the deep part of the sea, but its sign changes in some parts of the continental slope to negative, while in other places it stays positive and grows in absolute value.

To understand the role of quadratic and cubic nonlinearity in the IW dynamics three values should be compared: c, αa and $\alpha_1 a^2$. In the deep part of the South China Sea, the wave speed $c = 2.5$ m/s and even if the IW amplitude is taken as 80 m (it is usually much less in deep water), $\alpha a = 0.48$ m/s and $\alpha_1 a^2 = 0.13$ m/s. Hence, nonlinear effects are small in the deep part of the South China Sea. But on the continental slope c is less than 0.5 m/s and for the same IW amplitude of about 80 m, $\alpha a = 0.48$ m/s, comparable with c, and $\alpha_1 a^2 = 1.28$ m/s, which is much larger than the quadratic nonlinear term. Thus in the shelf zones the waves are strongly nonlinear. Indeed, the ratio of the nonlinear terms to the speed of propagation is about 3.5. Although the Gardner model may be still used in such conditions as demonstrated by Maderich et al. (2009, 2010), several other higher-order KdV-type models have been proposed (Apel et al., 2007) to more adequately describe the IW dynamics.

Numerical results for cross-section 1. The wave path is close to the conditions of the ASIAEX 2001 experiment on the shelf (Ramp et al., 2004) and is here extended to Luzon Strait to the site where the westward propagating solitary waves were observed (Liu et al., 2006; Zhao and Alford, 2006). The model coefficients are shown in Fig. 4.5. The depth decreases from 2.5 km to 200 m, the linear long wave speed c varies from 2.5 m/s to 0.2 m/s, the linear modification factor Q is equal to 1 initially, then decreases to 0.5 at the location $x = 250$ km, before increasing to 2.5 on the shelf. Corresponding to the change

in depth, the dispersion coefficient β decreases along the cross-section. The nonlinear quadratic coefficient α is negative for most of the wave path, but changes sign once only at a depth of about 100 m. The cubic nonlinear coefficient α_1 is positive in the deep water and becomes negative at a depth of about 400 m. Hence there are two critical points here, both on the shelf. The amplitude of the initial solitary wave (1.42) is chosen as 49 m at $x = 0$ in Figs. 4.6 and 4.7. This is less than that mentioned by Liu et al. (2006) where the amplitude of an observed solitary wave was estimated at 140 m but large enough for our purposes.

During the solitary wave evolution (Fig. 4.6) the leading wave amplitude has decreased by a factor of 2 at $x = 220$ km, from 49 m to 25 m. Over this same distance, the cubic nonlinear coefficient is almost constant, the quadratic nonlinear coefficient and the dispersive coefficient have decreased, and the

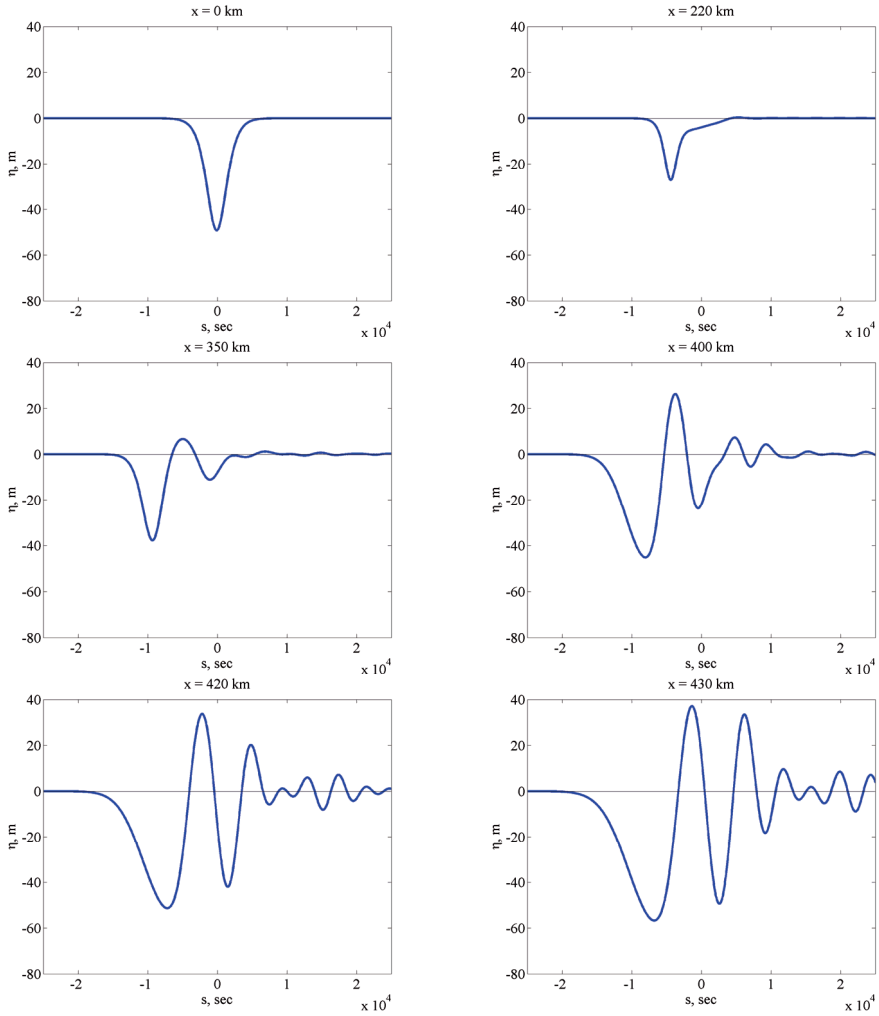

Fig. 4.6. Transformation of a SIW along cross-section 1

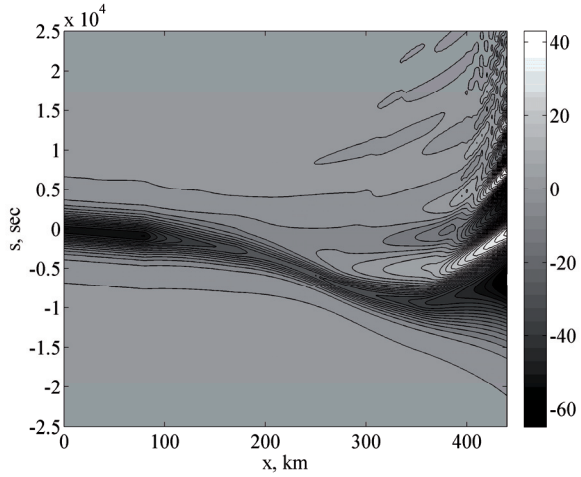

Fig. 4.7. Contour plot in the space–time domain of a SIW transformation along cross-section 1

linear modification factor has decreased by a factor of 1.5; together these have the effect that the initial wave has started to deform with the formation of a trailing tail. At the location $x = 350$ km the linear modification factor is decreasing, the cubic nonlinear coefficient changes sign and the quadratic nonlinear coefficient tends to zero. The leading solitary wave now has an amplitude of about 35 m and is wider than at the location $x = 220$ km. At $x = 400$ km the quadratic nonlinear coefficient changes sign. At this location the typical destruction of the solitary wave of depression takes place, followed by the generation of several solitary waves of elevation. The space–time contour plot of this IW transformation is shown in Fig. 4.7.

Numerical results for cross-section 2. On this cross-section, the initial point is in deep water (depth $h = 3$ km), and the last point lies near Hainan Island. The cubic nonlinear coefficient is positive everywhere, while the quadratic nonlinear coefficient changes sign on the shelf (Fig. 4.8). The depth decreases from 3 km to 200 m non-monotonically, producing analogous tendencies for the dispersion coefficient β and the linear long wave speed c. The linear modification factor Q is initially close to one, and then decreases before increasing after the location $x = 700$ km. The quadratic coefficient α grows after $x = 400$ km in absolute value. After $x = 580$ km it tends to zero, changing sign at $x = 700$ km. The cubic coefficient α_1 is positive everywhere, but grows by an order of magnitude.

This is a scenario when we might expect the formation of a breather from a solitary wave at the location of the zero-crossing of the quadratic nonlinearity coefficient, provided the leading wave amplitude is large enough. Two runs with initial solitary wave amplitudes of 23 m and 41 m were performed to verify the conjecture.

The solitary wave transformation for the first run is shown in Fig. 4.9. Due to the increase in the cubic nonlinearity coefficient the initial solitary wave becomes narrower and a trailing tail emerges, developing oscillations after

$x = 600$ km. This occurs without a significant change in the leading wave amplitude because the modification factor increases slowly. At the location $x = 700$ km a 'sech'-like solitary wave is developed. Then, at $x = 730$ km the quadratic nonlinear coefficient changes sign. The leading wave amplitude is not large enough for the transformation into a 'sech'-like solitary wave of depression that would correspond to a positive coefficient of quadratic nonlinearity. Instead, the wave disintegrates and at $x = 760$ km we see the formation of secondary solitary waves of opposite polarity. The space–time contour plot of this run is shown in Fig. 4.10.

The initial disturbance in the second run (Fig. 4.11) has an amplitude of 41 m. Again a 'sech'-like solitary wave emerges (this time at the location $x = 500$ km) and its amplitude grows to 60 m. At $x = 600$ km a secondary

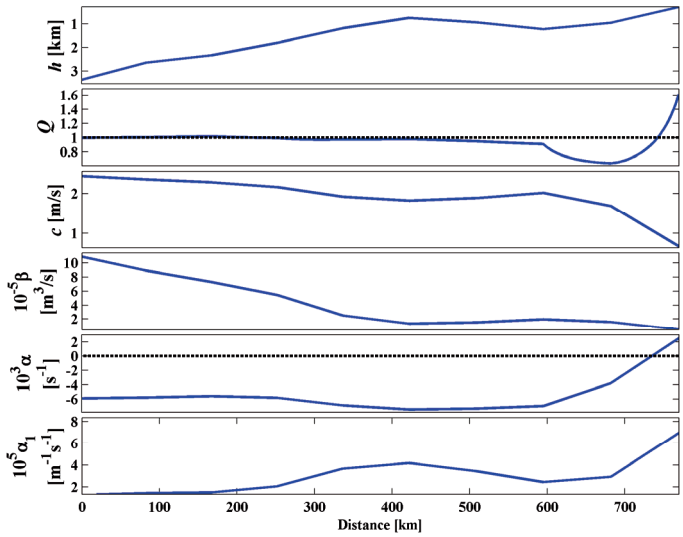

Fig. 4.8. Coefficients of the generalized Gardner equation (1.39) along cross-section 2

solitary wave begins to form. Due to the increase in the linear modification factor Q, the amplitude of the leading wave decreases to about 45 m. Then, as the coefficient of quadratic nonlinearity tends to zero, the cubic nonlinear coefficient grows rapidly, and the destruction of the leading solitary wave begins around the location $x = 700$ km. Until the location $x = 750$ km there is a strong indication that an internal breather has formed in association with an oscillatory trailing wave train. The division of the initial solitary wave into two entities is evident in the space–time contour plots (Fig. 4.12). This happens at a section from $x = 400$ km to the location $x = 650$ km, with breather formation after $x = 700$ km.

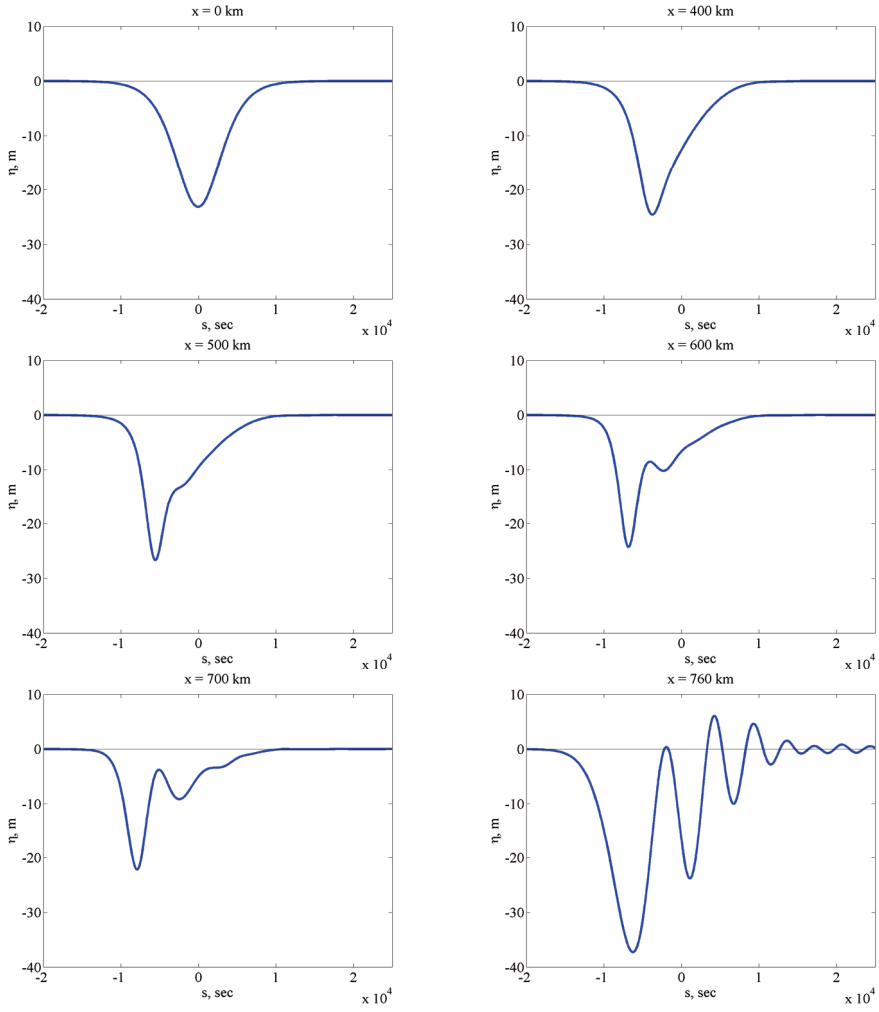

Fig. 4.9. Transformation of a SIW along cross-section 2, initial amplitude 23 m

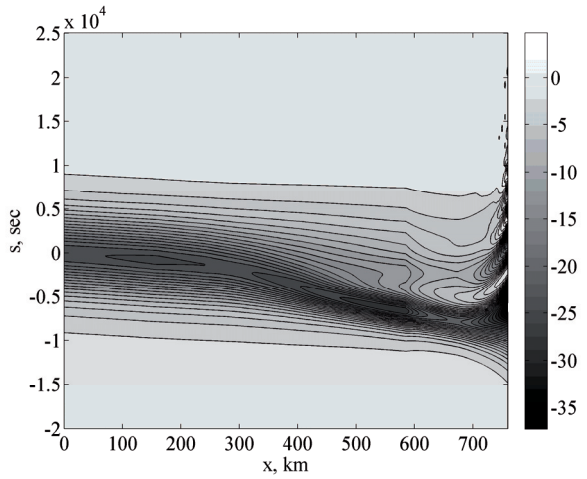

Fig. 4.10. Contour plot in the space–time domain of a SIW along cross-section 2, initial amplitude 23 m

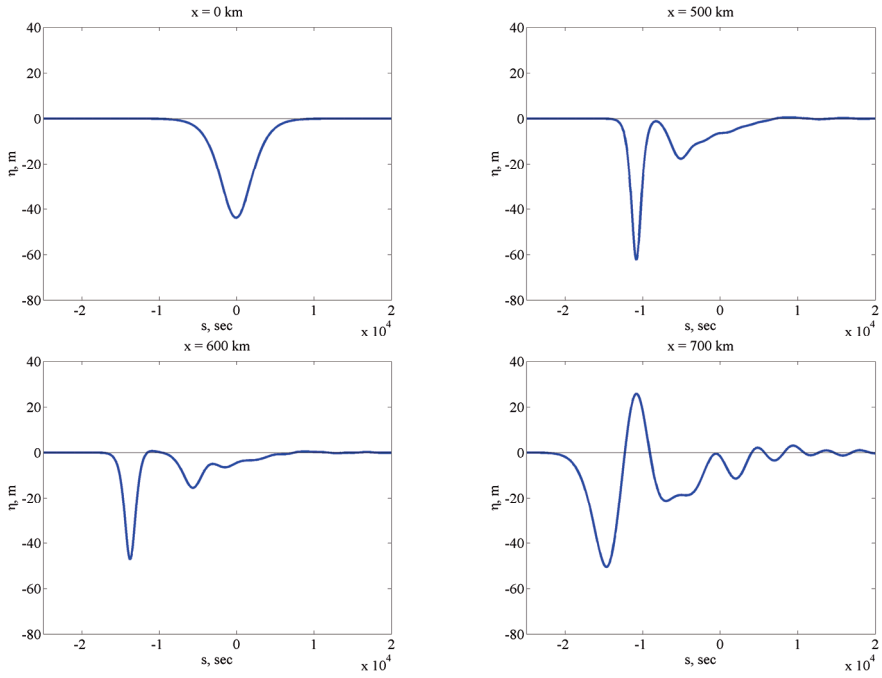

Fig. 4.11. Transformation of a SIW along cross-section 2, initial amplitude 41 m

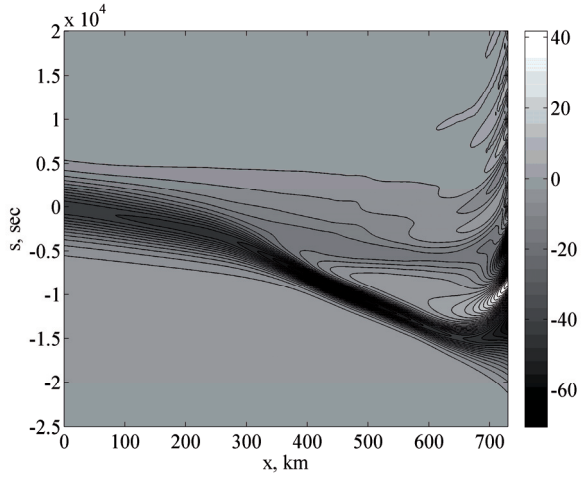

Fig. 4.12. Contour plot in the space–time domain of a SIW transformation along cross-section 2, initial amplitude 41 m

4.2 Solitary internal wave evolution in the Baltic Sea

It is feasible to derive examples of possible SIW transformations in the Baltic Sea from the existing databases. The hydrological data for the sections are taken from the GDEM database for July. The sections are choosen so as to show changes of signs for nolinear coefficients (passage through critical points). As the Baltic Sea is an almost nontidal sea and does not host major jet-like currents with substantial horizontal or vertical shear (Leppäranta and Myrberg, 2009), the direction of IW propagation depends almost entirely on the source of their generation listed in Section 3.1 and on refractive properties of bathymetry. Therefore a large variety of paths of IW propagation in the Baltic Sea may exist, and we are not limited in the choice of sections for the modelling. Furthermore, each transformation of a SIW can be inverted to demonstrate the possibility of a reverse metamorphosis: focusing of a wave train into a SIW. An example of the transformation of IW group with a moderate amplitude along a cross-section in the Baltic Sea with a specific behaviour of cubic nonlinearity can also be found in the recent paper by Talipova et al. (2011) where the effect of the modulation instability of wavepackets is shown to occur in natural conditions and lead to the appearance of anomalously large internal rogue waves.

Calculations of the conditions for IW propagation were performed for the sections in the Baltic Sea shown in Fig. 4.13. The initial problem for the variable-coefficient Gardner equation was solved using an implicit pseudo-spectral numerical scheme with periodic boundary conditions in the variable $\widetilde{s}$. The atlases of IW kinematic and nonlinear parameters for July described in Chapter 3 were used.

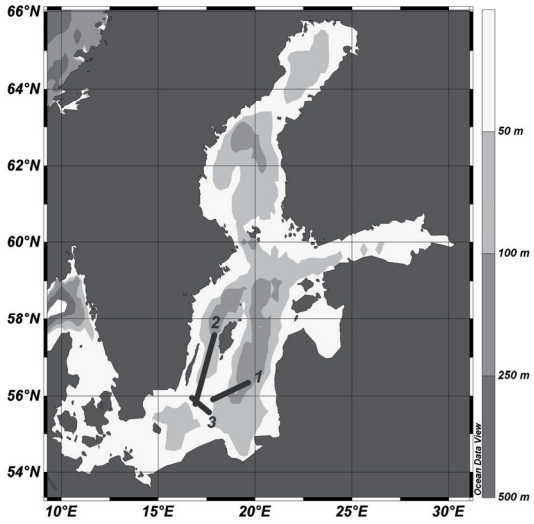

Fig. 4.13 Bathymetry of the Baltic Sea, with the chosen cross-sections

An example of variable environmental parameters for the modelling of IWs in the framework of Eq. (1.39) along cross-section 1 is demonstrated in Fig. 4.14. This cross-section of approximately 100 km length has depths in the range 50–125 m and is characterized by a gradual increase of the depth after a 25 km long segment of a small decrease of the depth. The linear amplification factor Q, which is equal to 1 in the initial point of the cross-section, then increases, and after $x = 25$ km decreases to 0.4, as consistent with the depth changes along the cross-section. The linear IW parameters, long wave phase speed c and dispersion coefficient β, correlate well with the depth, increasing from $x = 25$ km.

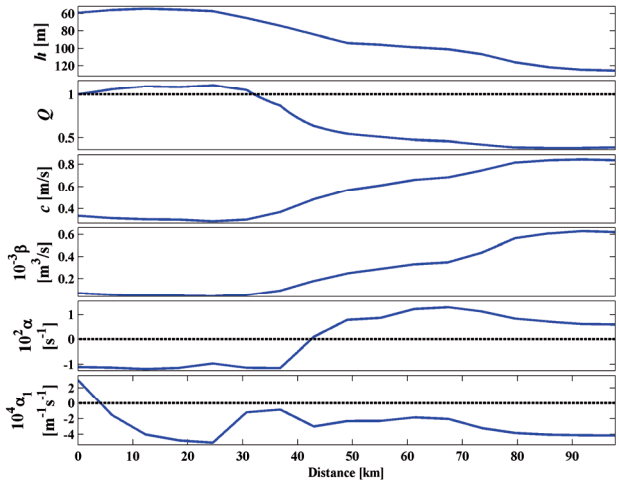

Fig. 4.14. Coefficients of the variable-coefficient Gardner equation (1.39) along cross-section 1

The nonlinear parameters α and α_1, determining the solitonic regime in the framework of the Gardner equation (see Section 1.2), are very sensitive to the shape of density stratification and therefore they have a complex behaviour along the cross-section. The coefficient of quadratic nonlinearity α is negative at the beginning of the cross-section and is almost constant about -1×10^{-2} 1/s upto $x = 38$ km, then it rapidly decreases in absolute value, changes the sign around $x = 43$ km, and stays then positive with the values of about 1×10^{-2} 1/s. The cubic nonlinearity parameter α_1 is positive along a small segment at the beginning of the cross-section, then it almost linearly decreases, changes sign around $x = 4$ km and stays negative thereafter. It has a few local maximums and minimums along the cross-section. As $\alpha < 0$ and $\alpha_1 > 0$ at the initial point of the cross-section, two soliton branches are possible here. One of the branches has polarities corresponding to the sign of α, and the other branch has the opposite polarity. The latter family has a lower limit in the amplitude. This is physically inappropriate for the chosen conditions: the solitons of this family must have the amplitude $a \geq 166$ m. Therefore for the initial condition the former branch was taken: soliton (1.42) of negative polarity with the amplitude of $a = -7$ m.

The transformation of this disturbance is shown in Figs. 4.15 and 4.16 in the reference frame $(\tilde{s}, x)$. The soliton of negative polarity weakly changes until the point where $\alpha = 0$, i.e. over almost 40 km, but then it transforms into a dispersive oscillating wave tail, propagating over a negative pedestal. The amplitude of the wav field gradually decreases after the transformation from the initial value of 7 m to 1 m at the end of the cross-section. In terms of IW-induced near-surface currents these amplitudes correspond to velocities of 0.15 and 0.04 m/s, respectively. The velocities of the near-surface currents can be used in studies of surfactant dynamics in a field of IWs or for estimations of hydrodynamic contrasts of the sea surface. They also provide effects used by the remote sensing to detect the IW surface manifestations.

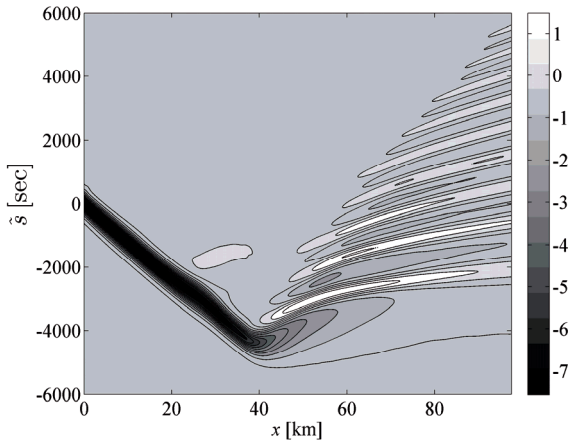

Fig 4.15. Contour plot in the space–time domain of a SIW along cross-section 1

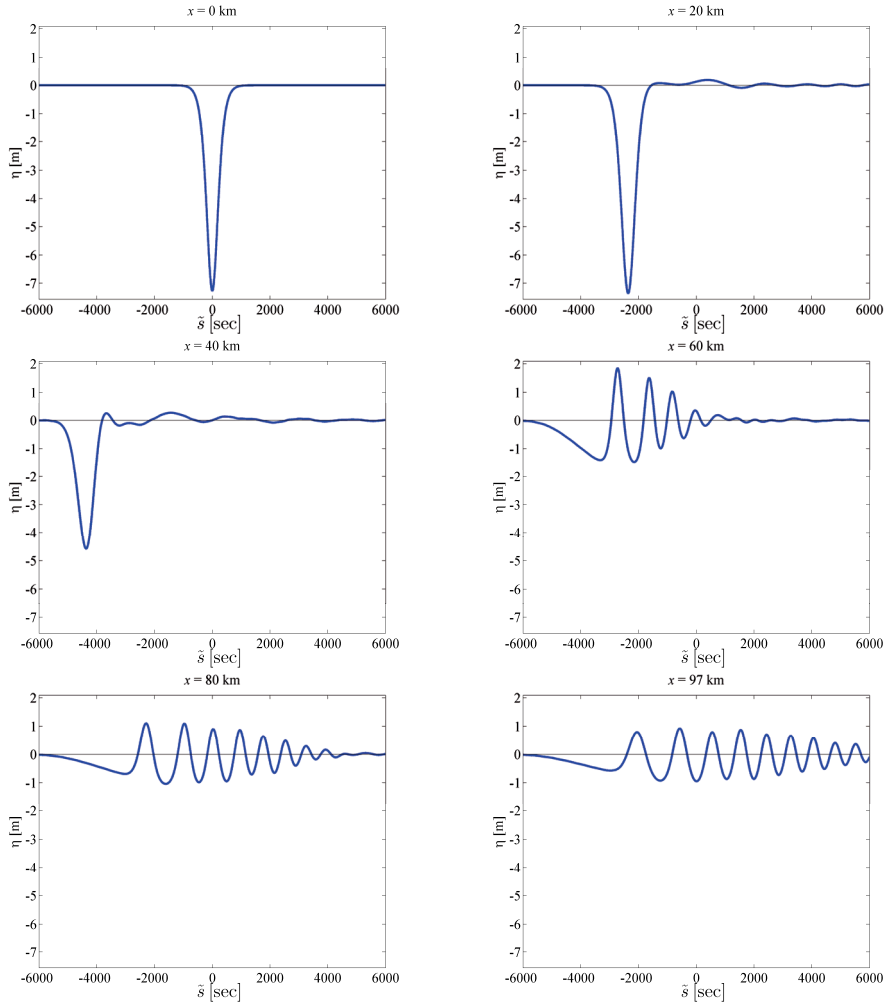

Fig. 4.16. Transformation of a SIW along cross-section 1

Variability of the coefficients of the generalized Gardner equation (1.39) for the cross-sections 2 and 3 is shown in Figs. (4.17) and (4.18), respectively. The numerical results of simulations for IW propagation along them are shown in Figs. (4.18), (4.19) and (4.21), (4.22). The complex behaviour of IWs can be observed there, including adiabatic adjustment, wave amplification, transformation of a wide solitary wave into a sequence of narrow ones, change of their polarity, appearance of multiple breather-like disturbances and radiation of oscillatory dispersive tails of small amplitude. All of these nonstationary and nonlinear effects developed due to the inhomogeneity of the environment lead to the formation of complex field of IW-induced currents, which can be easily reconstructed and further used as an input for models of the near-bottom boundary layer, as well as for advective–diffusive models of pollution dynamics.

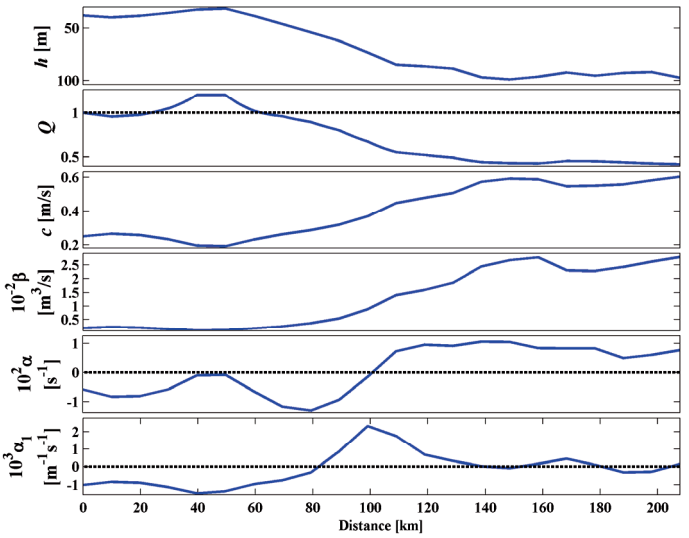

Fig. 4.17. Coefficients of the Gardner equation (1.39) along cross-section 2

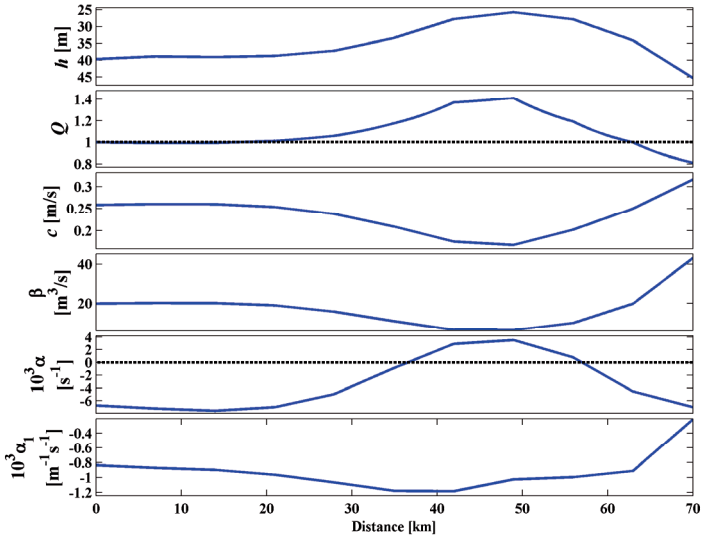

Fig. 4.18. Coefficients of the generalized Gardner equation (1.39) along cross-section 3

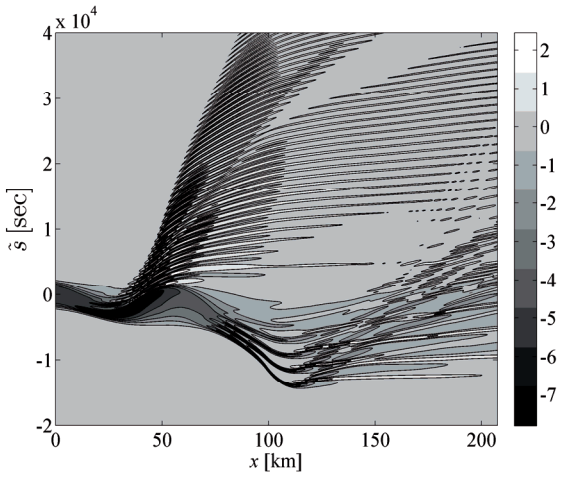

Fig. 4.19. Contour plot in the space–time domain of a SIW along cross-section 2

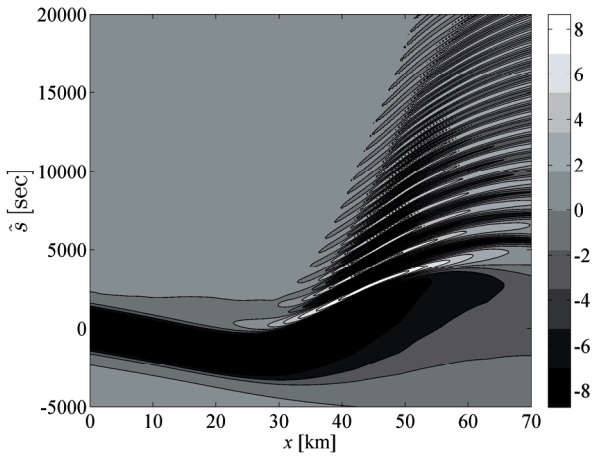

Fig. 4.20. Contour plot in the space–time domain of a SIW along cross-section 3

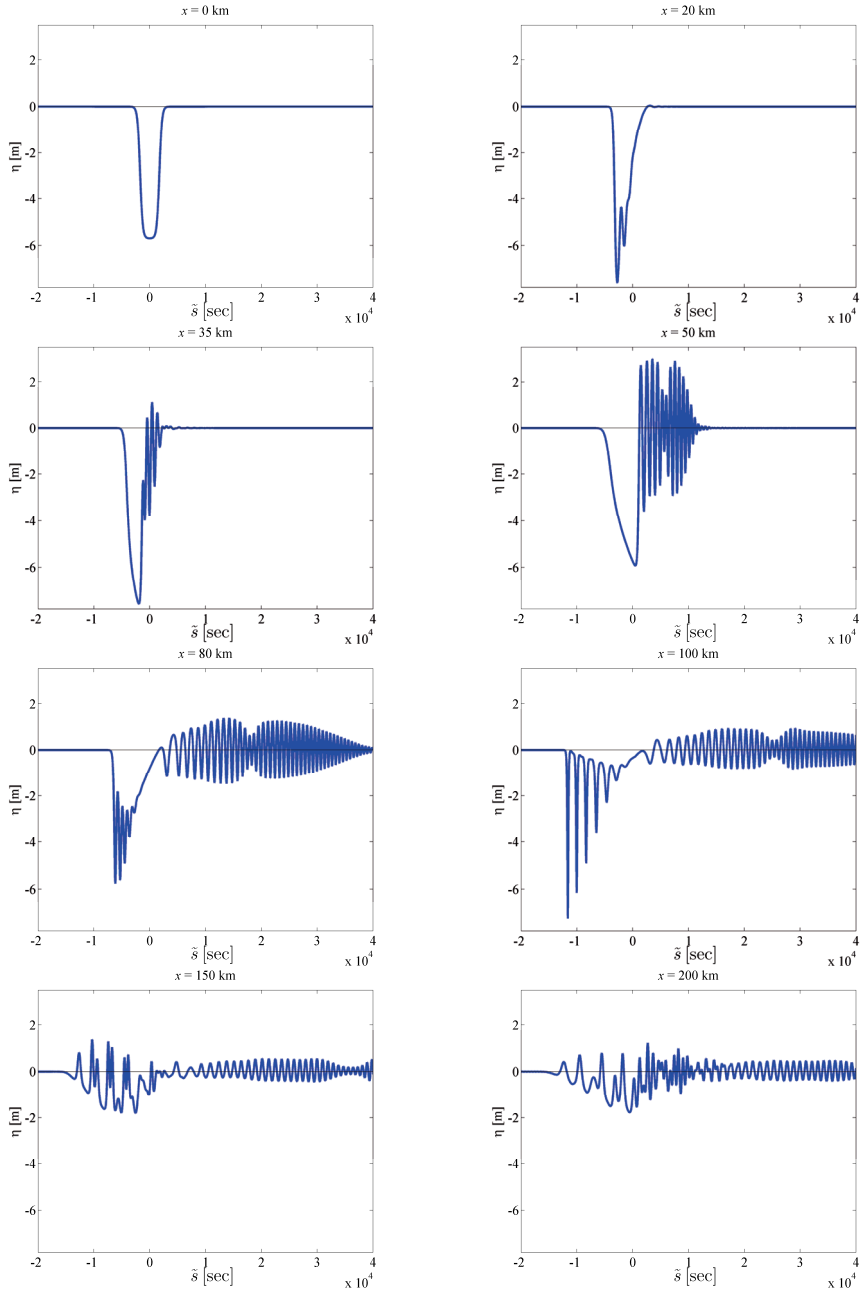

Fig. 4.21. Transformation of a SIW along cross-section 2

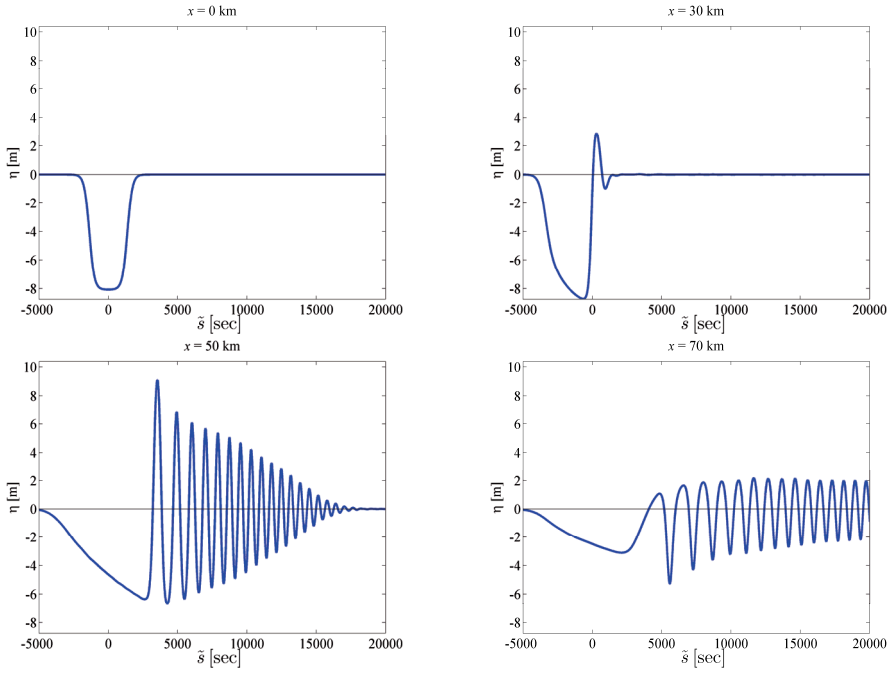

Fig. 4.22. Transformation of a SIW along cross-section 3

4.3 Effect of the Earth's rotation for internal waves

Several important issues affecting the propagation of SIWs have not been included into the standard theoretical models described in Section 1.2. Most notably, the stability, transverse structure, the effect of the background Earth rotation and the effect of friction may modify their appearance. Technically, all the listed issues can be incorporated into weakly-nonlinear models (Craig, 1991; Holloway et al., 1997; Grimshaw, 2001; Holloway et al., 2001) but their joint analysis is extremely complicated.

The majority of the results presented in this thesis have been derived for relatively short-period (with periods less than 2 h) IGWs. One of the main mechanisms of their generation is the transformation of internal tides (Vlasenko et al., 2005). Therefore, a proper theoretical IGW model should be able to describe this process of transformation of long waves into a train of short waves. An important point here is that the Earth's rotation can notably affect these initially long waves. This impact apparently is particularly large at higher latitudes and in the case of wave propagation over long distances. The effect of background rotation generally causes a solitary wave to decay through the radiation of inertia-gravity waves, see the review (Helfrich and Melville, 2006) and the recent studies (Grimshaw and Helfrich, 2008; Sanchez-Garrido and Vlasenko, 2009). In practice, the time scale for this decay is one or two inertial periods.

Several studies (Ostrovsky, 1978; Holloway et al., 1997, 1999, 2001; Talipova et al., 1999) address theoretical models that include rotational effects on the same level (of weakness) as effects of nonlinearity and dispersion. An extension of the variable-coefficient Gardner model (1.39) that accounts for the Coriolis forcing due to the Earth's rotation is the Gardner–Ostrovsky (GO) equation (also known as the extended rotation-modified KdV equation):

$$\frac{\partial \xi}{\partial X} + \left(\frac{\alpha Q}{c^2} \xi + \frac{\alpha_1 Q^2}{c^2} \xi^2 \right) \frac{\partial \xi}{\partial \tilde{s}} + \frac{\beta}{c^4} \frac{\partial^3 \xi}{\partial \tilde{s}^3} = \frac{f^2}{2c} \int \xi \, d\tilde{s} \ , \tag{4.1}$$

where f is the Coriolis parameter, which depends on the period of the Earth's rotation T_e = 24 h and the geographical latitude φ:

$$f = \frac{4\pi}{T_e} \sin \varphi \ . \tag{4.2}$$

The question of the applicability of Eq. (4.1) for basins at different latitudes is worth a more detailed discussion. In the framework of the linear theory, the exact dispersion relation for IWs is determined from the eigenvalue problem

$$\frac{d^2 \Phi}{dz^2} + \frac{N^2 - \omega^2}{\omega^2 - f^2} k^2 \Phi = 0 \tag{4.3}$$

with zero boundary conditions at the sea surface and bed. Here ω is the wave frequency and k is the horizontal wavenumber. We consider only long waves. At this limit $\omega << N$, and Eq. (4.3) can be simplified as follows:

$$\frac{d^2 \Phi}{dz^2} + \frac{N^2}{c^2} \Phi = 0 \, , \tag{4.4}$$

where

$$c^2 = \frac{\omega^2 - f^2}{k^2} \, . \tag{4.5}$$

Obviously in this limit the eigenvalue problem for Eq. (4.4) does not depend on the Coriolis parameter and coincides with the eigenvalue problem for Eq. (1.9) considered in Section 1.2. In the framework of Eq. (4.4) the long-wave linear phase speed c can be calculated numerically for arbitrary stratification. However, the dispersion relation will be a more complex relationship when the Earth's rotation is taken into account:

$$\omega^2 = c^2 k^2 + f^2 \, , \tag{4.6}$$

or

$$k = \frac{\sqrt{\omega^2 - f^2}}{c}. \tag{4.7}$$

Thus for the rotating and non-rotating environments the eigenvalue problems and the eigenvalues themselves are identical, but the dispersion relations are different.

Let us consider now the linear version of Eq. (4.1) in the original variables:

$$\frac{\partial}{\partial x}\left(\frac{\partial \xi}{\partial t} + c\frac{\partial \xi}{\partial x}\right) = \frac{f^2}{2c}\xi. \tag{4.8}$$

By substituting the monochromatic wave solution

$$\xi = a\exp(\omega t - kx), \tag{4.9}$$

into Eq. (4.8) the corresponding dispersion relation can be obtained in the form

$$\omega = ck + \frac{f^2}{2ck}. \tag{4.10}$$

Equation (4.10) represents two lowest-order terms in the Taylor expansion of the exact dispersion relation (4.6) in terms of the small parameter f/ω. Therefore, the problem of a correct description of the Earth's rotation can be reduced to a simpler problem of comparison of the exact and approximate dispersion relations.

It is convenient to rewrite Eq. (4.10) in another form with the same accuracy

$$k = \frac{\omega}{c}\left(1 - \frac{f^2}{2\omega^2}\right), \tag{4.11}$$

which also corresponds to the Taylor expansion of the exact dispersion relation (3.7).

The ratio of wavenumbers obtained from the exact (3.7) and approximate (3.11) dispersion relations is

$$\frac{k_{\text{appr}}}{k_{\text{exact}}} = \left(1 - \frac{f^2}{2\omega^2}\right) \Big/ \sqrt{1 - \frac{f^2}{\omega^2}}. \tag{4.12}$$

Apparently, the difference is not large for high-frequency waves but it may increase considerably for longer waves of low frequencies (e.g. such as internal tides with the basic M_2 period $T_t = 12.4$ h). For waves with a period of T relationship (3.12) can be written in the form:

$$\frac{k_{\text{appr}}}{k_{\text{exact}}} = \frac{(1 - 2T^2 \sin^2 \phi / T_e^2)}{\sqrt{1 - 4T^2 \sin^2 \phi / T_e^2}}. \tag{4.13}$$

Thus the accuracy of the model equation (4.1) depends only on the geographical latitude where IWs propagate. Due to the difference between the period of the Earth's rotation T_e and M_2 tidal period T_t the exact dispersion relation (4.7) can be solved for latitudes less than 74.5°. This is a well-known critical latitude for tidal IWs (LeBlond and Mysak, 1978). Internal M_2 tides cannot propagate to even higher latitudes and they also rapidly decay with the distance from the continental slope or underwater ridges. The relationship (4.13) is shown in Fig. 4.23 for periods T_t = 12.4 h and T = 6 h. For tidal IWs at latitudes lower than 55° the difference does not exceed 20%, and the approximate dispersion relation is acceptable. For this reason the above-described model based on Gardner-Ostrovsky equation was successfully used for the modelling of internal tide transformation on Australian and European shelves. For latitudes higher than 63° the difference between the solutions to the dispersion relations exceeds 47%, and the use of approximation (4.11) is unacceptable. The described effect is minor for shorter waves. For example, for waves with the period of 6 h the error of approximation does not exceed 1% for any latitude; therefore short-period waves can be investigated using Eq. (4.1).

There are two possible ways of improving the theoretical models for the description of IWs in high-latitude basins. One of them is related to the direct numerical solution of primitive equations of hydrodynamics for stratified fluids (Wood and Grue, 2002). This approach is used below for the study of baroclinic wave motions in the Barents Sea (Section 4.4).

Another approach can be developed to adapt the existing IW model (4.1) for the conditions of Arctic basins. The basic idea is to introduce a phenomenological coefficient q into the term that describes the Earth's rotation

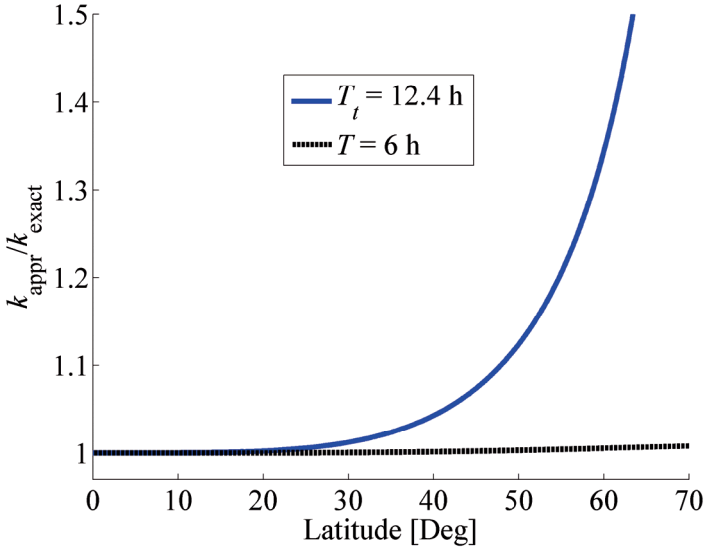

Fig. 4.23. Ratio of approximate and exact dispersion relations for waves with periods of 12.4 h and 6 h

$$k = \frac{\omega}{c}\left(1 - \frac{qf^2}{2\omega^2}\right). \tag{4.14}$$

The particular values of this adjustable parameter do not affect the dispersion curve in the high-frequency domain, thus all the properties of high-frequency IWs, including SIWs, hold true. Its role is important in the domain of tidal frequencies. For example, at $q = 2$ both the exact (Eq. (4.7)) and the phenomelogical (Eq. (4.14)) dispersion relations give the same value of wavenumber ($k = 0$) at $\omega \to f$. An optimum choice of the adjustable parameter q can be made through the minimization of the functional representing the squared difference between the curves specified by Eqs. (4.7) and (4.14):

$$\varepsilon^2 = \int_f^\infty \left[\frac{qf^2}{2\omega} - \left(\omega - \sqrt{\omega^2 - f^2}\right)\right]^2 d\omega. \tag{4.15}$$

This procedure yields the following expression:

$$q = 2\int_1^\infty \left(1 - \sqrt{1 - \frac{1}{\xi^2}}\right) d\xi. \tag{4.16}$$

This integral can be estimated numerically to give $q = 1.14$. The variations of the values of q in the range 1–1.14 influence the dispersion curve only in the vicinity of the Coriolis frequency f. The actual dispersion of IWs due to the Earth's rotation is very strong in the neighbourhood of this point. In the framework of the approximate dispersion relation this dispersion is much weaker. It can result in strengthening the possible nonlinear effects in the framework of the Gardner–Ostrovsky equation (4.1). In this sense one can produce upper bounds from the point of view of nonlinear effects for long IW evolution using this model equation.

4.4 Numerical modelling of baroclinic motions at high latitudes

The focus in this section is the Barents Sea and the IWs generated to the north of the critical latitude (74.5°N) for the semidiurnal (M_2) tide. As it was mentioned above, the critical latitude is determined as the latitude φ where the tidal frequency is equal to the local inertial frequency $f = 2\Omega_E \sin\varphi$ (cf. Eq. 4.2), where $\Omega_E = 0.00007292$ 1/s is the frequency of the Earth's rotation. The linear theory of baroclinic tide generation predicts that no baroclinic wave generation should occur to the north of this latitude (LeBlond and Mysak, 1978). Nevertheless, observations show the existence of IWs of very large amplitudes here.

We reproduce briefly the description of results in (Pisarev, 1996; Morozov and Pisarev, 2002). Special measurements of IWs with distributed temperature sensors were carried out from drifting ice in 1983 in Saint Anna Trough and in

1986–1989 in Franz Victoria Trough. The latitude of the measurements was 80°–81° N and the depths were in the range 200–500 m. In addition to the other phenomena, very short and localized semidiurnal IWs were found. Their lengths were within 2–6 km. They propagated from the slope of the trough and their amplitudes reached 40 m. When the measuring instruments drifted from the slopes of the trough to a distance of 20–40 km toward flat bottom regions, the amplitude of these waves significantly decreased. Under certain stipulations, these semidiurnal waves were classified as internal tides.

The possibility of the generation of internal tidal waves by the topography to the north of the critical latitude was demonstrated in (Nakamura et al., 2000) with the use of the fully nonlinear nonhydrostatic model. These waves are generated and trapped by the barotropic tidal flow at the lee side of a sill. They were called unsteady lee waves. Their amplitudes depend on the amplitude of the tidal flow speed and the steepness of the bottom topography. Nonlinear generation of IWs near and to the north of the critical latitude was first modelled in (Vlasenko et al., 2003) for the Barents Sea conditions (near Bear Island) and propagating short nonlinear IWs with amplitudes of about 20 m was demonstrated.

The aim of this section is to explain the nature of large-amplitude baroclinic motions observed over the critical latitude in the Franz Victoria Trough, using the numerical results in the framework of the fully nonlinear Euler equations for stratified water, and to forecast dangerous underwater events for this region.

The **numerical model** by Lamb (1994) is applied in Paper II for simulating the generation and propagation of IWs in the Barents Sea. The model equations are two-dimensional (vertical section) fully nonlinear Euler equations on a rotating *f*-plane under the Boussinesq approximation. The coordinates are defined as follows: *x* is along the section, *y* is perpendicular to the section, and *z* is the vertical axis. The equations of the model are

$$\begin{aligned} &\vec{V}_t + \left(\vec{V}\nabla\right)\vec{V} - f\vec{V}\times\vec{k} = -\nabla P - \vec{k}\rho g\,, \\ &\rho_t + \vec{V}\nabla\rho = 0\,, \qquad \nabla\vec{V} = 0\,, \end{aligned} \tag{4.17}$$

where $\vec{V}(u,v,w)$ is the velocity vector, ∇ is the 3D gradient operator, subscript t denotes the time derivative, ρ is the density, P is the pressure, g is the gravitational acceleration, $f = 1.425\times10^{-4}$ 1/s is the Coriolis parameter for the latitude of 78.5º and $\vec{k}$ is the unit vector along the *z*-direction. The normal to the section velocity is included in the model, but no variation with the coordinate *y* is allowed. Thus, in the 3D equations (4.17) the partial derivatives with respect to *y* are neglected, i.e., $\partial/\partial y(\cdot) = 0$.

The equations are transformed to the terrain-following coordinate system (sigma-coordinates). Doing so makes it possible to naturally increase the vertical resolution over the shallower regions. The equations are solved over a domain bounded below by the topography and a rigid lid above. The flow is

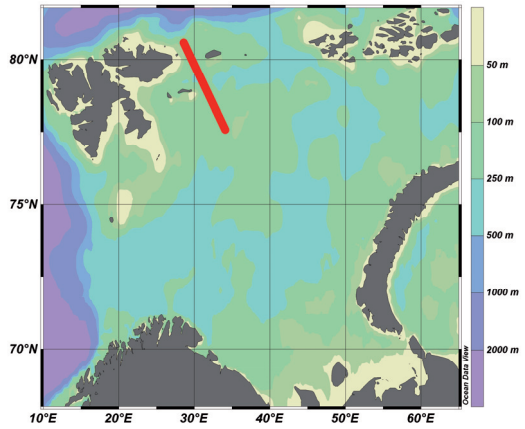

Fig. 4.24. Area map with the cross-section between the points 34.11° E, 77.57° N and 28.61° E, 80.58° N

forced by a semidiurnal tidal inflow at the left boundary of the form $V_T \sin(\omega t)$ where ω is the M_2 tidal frequency with a period $T = 12.4$ h. At the right boundary an outflow condition is used. The water column is initially resting and has a horizontally uniform density. The horizontal grid size is 90 m and the vertical sigma-coordinate resolution consists of 80 grid points. The time step is tied to the Courant–Friedrichs–Levy condition and varies from 2 to 5 s.

The modelling efforts were performed for a cross-section in the Barents Sea close to the Franz Victoria Trough (Fig. 4.24). The whole wave path is located to the North of the critical latitude (74.5ºN). The bathymetry along this cross-section was taken from the GEBCO database (solid line in Fig. 4.25). It is splined for the purpose of modelling by 8 Fourier components for a better description of the middle portion of the domain as

$$H(x) = a_0 + \sum_{m=1}^{8} \left[a_m \cos(m\kappa x) + b_m \sin(m\kappa x) \right], \tag{4.18}$$

where $\kappa = 0.03398$ 1/m and a_m and b_m are the Fourier coefficients (dotted line in Fig. 4.25). The double humped sills along the modeling path remind of the double ridge structure in Luzon Strait where tidally generated IWs are widely observed.

The typical vertical density profile in this area is taken from the GDEM climatology for July. It is fitted by the exponential function

$$\rho = 1000 + q_1 \exp(r_1 z) + q_2 \exp(r_2 z), \tag{4.19}$$

with $q_1 = 27.93$, $r_1 = 1.64 \times 10^{-4}$ [1/m], $q_2 = -1.2$, $r_2 = -0.02844$ [1/m], and the buoyancy frequency $N(z)$ (Fig. 4.26) is calculated.

The considered region is characterized by strong tidal currents and underwater mountain ridges. The map of the mean tidal velocities in the Arctic Ocean (with the 8 tidal components) calculated with the help of the Arctic Ocean Tidal Inverse Model (AOTIM) is presented in (Padman and Erofeeva, 2004). Four major tidal components M_2, S_2, K_1 and O_1 contain up to 79%, 10%, 5% and 1% of the total (8-components) potential energy of the tide,

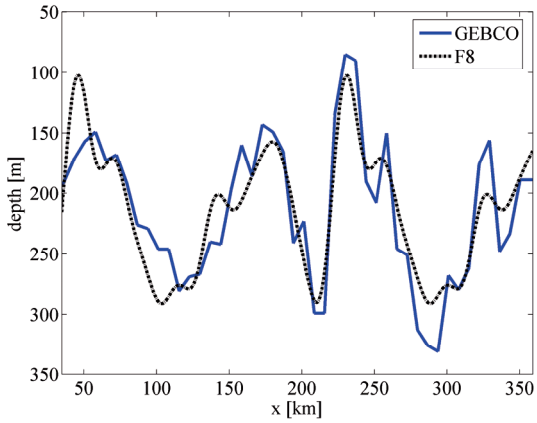

Fig. 4.25. Bottom relief of the area cross-section shown in Fig. 4.24 (solid line denotes data from the GEBCO, dotted line is the approximation).

respectively. Thus, the semi-diurnal tide M_2 dominates in the tidal velocities in this region of the Arctic Ocean.

The largest mean values of the tidal velocities approach 1 m/s in the southern Barents Sea near the entrance to the White Sea and around Bear Island in the western Barents Sea south of Svalbard. The maximal velocities exceed the mentioned values of the mean velocities as much as twice, at least. The barotropic tidal wave is presented in the model in Paper II only by the semidiurnal tide M_2. As the mean tidal current in the study area is about 0.5 m/s, the maximal barotropic tidal velocity constitutes 1 m/s, and we use this value for V_T to set up the model.

The calculated density fields and total (barotropic and baroclinic) horizontal velocity values are shown in Fig. 4.27 for various tidal phases together with the normalized density $(\rho - \rho_0)/1000$. Vlasenko et al. (2005) mentioned that full periodicity of the process is formed after 2–3 tidal periods T_{M2} for M_2.

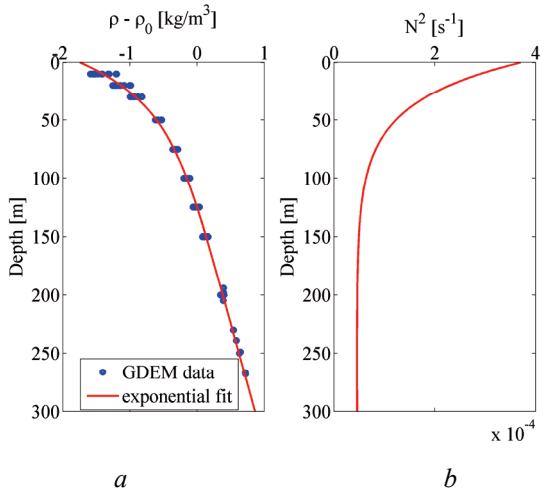

Fig. 4.26. The typical vertical density profile (a) and the Brunt–Väisälä frequency (b) in the studied area taken from the GDEM database for July

The time moment $3T_{M2}$ corresponds to the end of the ebb phase and the beginning of the flood phase. The velocity of the tide at $3T_{M2}$ is zero and there are large displacements of isopycnals over the left side of the largest hill. Intensive IWs are generated on the slopes of the highest central hill (located between 200 and 300 km with the crest at 230 km). Their amplitudes decrease when they propagate out of this zone.

After a quarter of the tidal period $t = 3.25T_{M2}$, the maximum of the tidal phase comes; velocities reach their maximums, and the zone of generation moves to the right lee slope of the central hill. At the time instant $t = 3.5T_{M2}$ the phase of the tide finishes and the tide velocity vanishes; IWs are developed

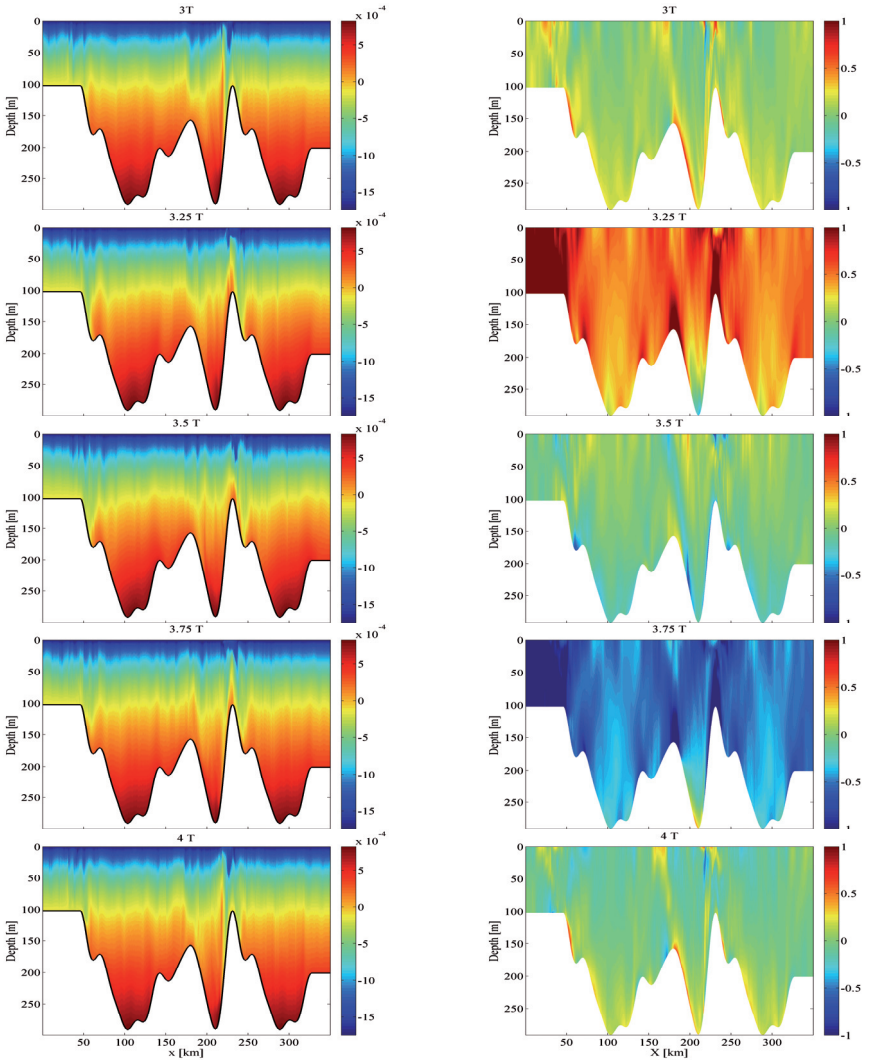

Fig. 4.27. Snapshots of the normalized density (left panel) and horizontal velocity [m/s] (right panel).

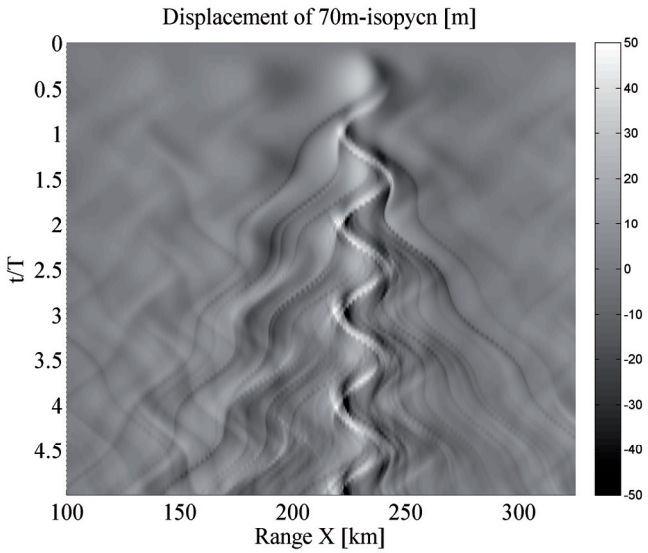

Fig. 4.28. The contour plot in the space–time domain for the displacement of the isopycnal located at the 70 m depth in the undisturbed state

well on the right side of the central hill. When the ebb is maximal (at $t = 3.75T_{M2}$) the zone of generation is also shifted to another (left) lee side of the hill and the waves gain the largest amplitude at $t = 4T_{M2}$ when the velocity of the tide vanishes.

Thus the generated IWs are mainly unsteady lee waves that are generated by the tide and ebb currents near the lee slope of the hill with the phase shift of about a quarter of the tidal period between the maximal tide velocity and maximal isopycnal displacement. The wave velocities are evident at the time moments $3T_{M2}$, $3.5T_{M2}$ and $4T_{M2}$, when the tidal current is zero. Their values do not exceed 0.4 m/s. The process is well illustrated in the Hovmuller plot (or *x*–*t* diagram) for the displacement of the isopycnal located at the 70 m depth in the undisturbed state (Fig. 4.28). The more intensive IWs with amplitudes of 50 m and total heights (crest-to-trough height) of about 80 m appear regularly in the strip of about 40 km in width and the central position approximately at 230 km. Their length may be evaluated using displacements in Fig. 4.29: about 6–12 km. The typical periods of the modelled waves are 0.2–0.35 T_{M2}.

Vlasenko et al. (2005) suggest a classification of the processes of IW generation based on the magnitude of the Froude number $Fr = u_{\max}/c$. Here $u_{\max}$ is the maximal velocity of the barotropic tidal flow in the *x*-cross-section ($u_{\max} = V_T H(x_0)/H(x)$) and c is the phase speed of the lowest-mode long IWs. This speed is numerically calculated from the eigenvalue problem for Eq. (1.9). In 'supercritical' regime $Fr > 1$ the generation of strong nonlinear internal lee waves by tide is possible at any latitude whereas there is no IW generation when $Fr << 1$ in the area to the north of the critical latitude. Therefore, waves shown in Figs. 4.27, 4.28 and 4.29 can be interpreted as internal lee waves.

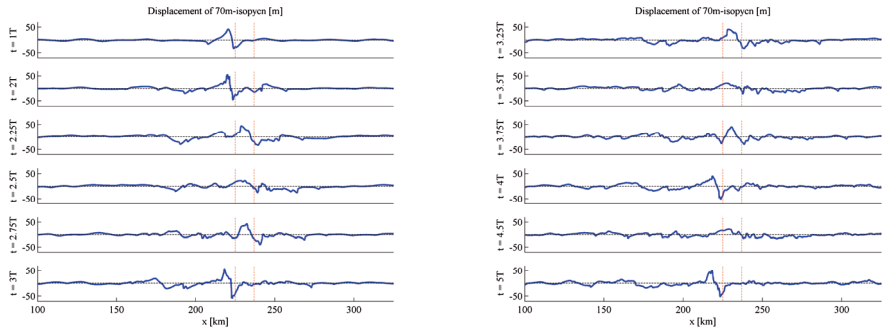

Fig. 4.29. Displacement of the 70 m isopycnal for different times

The spatial variation of the Froude number along the studied section is shown in Fig. 4.30 together with other characteristic quantities: linear phase speed of IWs, maximal tidal velocity and depth of the defined area of the sea. The zone where $Fr > 1$ lies between the points 225 km and 237 km. The most intensive IWs appeared in numerical runs exactly within this interval.

Concluding remarks

The presented examples confirm that largely different forcing mechanisms may generate large-amplitude, horizontally propagating IWs in coastal seas and straits. Typically these waves occur in regions of variable bottom topography, with the consequence that they are often modelled by nonlinear evolution equations of KdV-type with variable coefficients or by contemporary numerical models of full equations of hydrodynamics. The above material

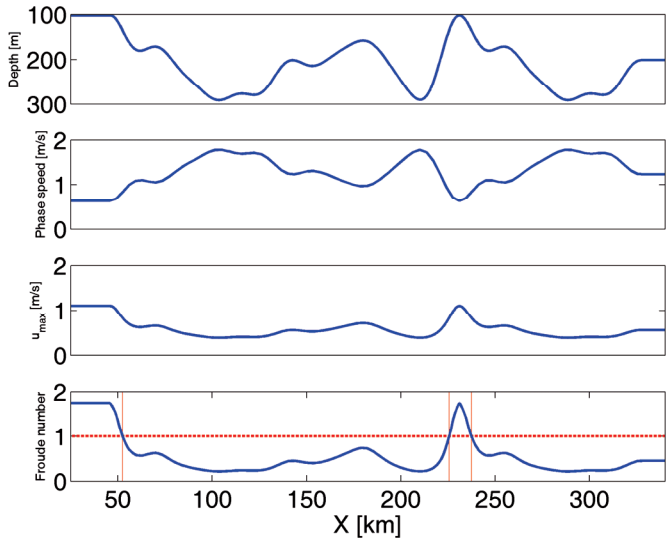

Fig. 4.30. The Froude number and auxiliary characteristic parameters against the distance along the section.

demonstrates how these models are used to describe the propagation, deformation and disintegration of SIWs in horizontally inhomogeneous shallow domains.

The highly complicated process of SIW propagation and transformations in the zones with critical points has been studied in detail for several cross-sections of the coastal shelf of the South China Sea and in the Baltic Sea. The properties of the background hydrophysical fields have been extracted from the GDEM database of stratification and the GEBCO bathymetry database.

The theory predicts that various scenarios of SIW structure transformation are possible. Several such scenarios have been illustrated in detail for two contrasting cross-sections of the coastal shelf of the South China Sea.One cross-section was taken across the shelf where the ASIAEX 2001 experiment took place, and we have simulated the transformation of a SIW generated in Luzon Strait, propagating across the deep part of the sea to the opposite shelf, where a change in its polarity takes place. The other cross-section was taken across a region where the cubic nonlinear coefficient is positive everywhere. In this case an initial solitary wave of moderate amplitude transforms into two solitary waves. The first wave is a 'sech'-like solitary wave, and the two waves interact near the location where the quadratic nonlinear coefficient changes sign, with transformation into a breather. This demonstrates the possibility of internal breather generation from an initial solitary wave in a realistic ocean situation. It is the second example of such a transformation after a simulation for the North West Australian Shelf (Grimshaw et al., 2007).

The influence of the Earth's rotation on IWs and the applicability of the Gardner–Ostrovsky model equation are discussed in the context of the possibility of the generation of strong nonlinear unsteady lee IWs by barotropic tide in the Barents Sea above the critical latitude. A numerical simulation using 2D incompressible Euler equations on a rotating *f*-plane showed that the modelled waves had the same amplitudes as the observed ones, 40 m, and the similar wavelengths, 6–12 km. They preserved significant amplitudes of isopycnal displacements at a distance of 20 km from the zone of generation. They appeared twice per semidiurnal tide period and persisted about 6.2 h, slowly propagating out of the peak of the underwater hill. More intensive waves were generated in the ebb phase and when the ebb velocity vanished. The largest observed height between the crest and trough (about 80 m) appeared at the end of the ebb phase each 12.4 h.

Conclusions

Summary

The presented research focuses on weakly nonlinear models that approximately describe the generation, propagation and transformation of relatively short-period internal waves in stratified horizontally inhomogeneous environment in the framework of long wave approximation. This framework allows using the Gardner equation and its generalizations for an adequate description of the features of internal wave trains and solitons on the ocean shelves. Both horizontal variability of the stratification and the impact of uneven seabed on the motion can be described using a variable-coefficient version of the Gardner equation. Its coefficients may be found, for example, from the available hydrological atlases of sea stratification. Exact solutions of the integrable version of this equation not only help to verify the numerical models and interpret the obtained results but also make it possible to get a realistic description of the propagation of large-amplitude solitary internal waves over the ocean shelves. The waves may have different shapes and polarities depending on the details of stratification.

Several coefficients of the Gardner equation vanish for a specific (but relatively often occurring in the Baltic Sea) three-layer symmetric stratification. For more adequate description of nonlinear wave dynamics in such situations it is necessary to extend the asymptotic analysis of the leading processes of wave propagation. It is shown that an extended modified Korteweg–de Vries equation (so-called 2+4KdV equation) that includes two nonlinear terms (of the third and fifth order) applies to such situations. As the obtained equation is apparently not integrable, the existence of soliton solutions is unlikely. It still possesses a variety of analytical solitary wave solutions characterized by limited amplitude, which is also calculated analytically. These solutions broaden with an increase in their energy and obtain a table-like shape for large amplitudes.

The interaction of solitary solutions of this equation with various polarities, in particular, of wide table-lake solitary waves, has been analysed numerically. The propagation of single solutions in an otherwise calm environment resembles the propagation of solitons. The collisions of such solitary waves are, however, weakly inelastic. The amplitude of radiated wavelike “tails” generated in this case depends on the amplitudes and polarities of the interacting components. The intensity of radiation is the largest for interactions of solitons with the same polarity and increases with the amplitudes of interacting waves. A principally new type of interaction is the collision of a wide table-like solution with solutions resembling the KdV soliton of the opposite polarity. This situation is impossible for the known equations of the KdV hierarchy. In this case, the large table-like solitary wave acquires a negative phase shift after the interaction.

Spatial and seasonal variability of the properties of the variable-coefficient Gardner model is analyzed for the Baltic Sea. The maps of its coefficients are built using the GDEM hydrological atlas. Seasonal variations of the underlying hydrological fields are mainly reflected in the variability of coefficients of quadratic and cubic nonlinearity, while the linear parameters (long IW phase speed and the coefficient at the dispersion term) have insignificant seasonal changes. The established kinematic and nonlinear parameters can be used for express evaluations of possible polarities and shapes of solitary internal waves, their limiting amplitudes, propagation speeds, etc. They also can help to set-up and initialize more complex full nonlinear multidimensional models for internal gravity waves. Normalized near-surface and near-bottom currents, which are the largest for the lowest mode of internal waves, are also mapped and analyzed for the entire Baltic Sea. They can be important for estimations of the impact of internal waves on bottom boundary layer, pollutant transport, visibility of internal waves by means of remote sensing, etc.

Surface wave climate is analyzed for the Darss Sill region, SW Baltic Sea. The results of two datasets from numerical calculations are compared to 20-year observational data. The local wave climate reveals several well-known features of semi-sheltered basins of the Baltic Sea: relatively modest long-term wave heights, the most frequent wave periods 2–4 s and heights around 0.5 m. The amplitude of the modelled annual highest waves has sawtooth-like behaviour in time, with a gradual increase for 1958–1990 from about 4 m to about 5 m, a drastic decrease in 1991–1992 and an increase since then again. The measured annual average and maximum wave heights have changed insignificantly for 1991–2010 but the threshold for the top 1% of waves has considerably decreased. This analysis is particularly important in the context of the establishing of potential sources of internal waves in this basin. In particular, high-frequency hydrodynamic activity in the Baltic Sea could partially replace the tidal generation of internal waves.

The processes of the propagation and transformation of solitary internal waves are further analysed in the framework of the generalized variable-coefficient Gardner equation for the hydrological conditions of cross-sections containing critical points in the South China Sea and the Baltic Sea. Different scenarios of wave metamorphoses are illustrated, such as adiabatic adjustment, wave amplification, transformation of a wide solitary wave into a sequence of narrow ones, change in their polarity, appearance of breather-like disturbances, and radiation of oscillatory dispersive tails of small amplitude.

A more adequate description of internal gravity waves can be obtained by means of direct solving of the primitive, fully three-dimensional equations of hydrodynamics under realistic density stratification. This approach was used to study the nonlinear baroclinic wave motions generated by M_2 barotropic tide in the Barents Sea. The possibility of generation of large-amplitude lee internal waves was shown for latitudes to the north of the critical latitude for linear internal waves.

Main conclusions proposed to be defended

1. A new nonlinear evolution equation (2+4 Korteweg–de Vries equation) is derived for the internal wave motion in a symmetric three-layer environment where all the leading-order nonlinear terms in the classical modified Korteweg–de Vries equation vanish simultaneously. Such situations may often happen in relatively shallow nontidal strongly stratified basins such as the Baltic Sea.
2. The 2+4 Korteweg–de Vries evolution equation for a symmetric three-layer environment expresses the specific balance of wave motion in which two nonlinear terms (cubic and quintic) are of the same magnitude as the dispersion term.
3. The 2+4 Korteweg–de Vries equation has solitary wave solutions, whose amplitude and propagation speed are limited. Larger-amplitude solitons have a table-like shape with very steep fronts. Numerical calculations confirm that their collision is only weakly inelastic.
4. The spatial and seasonal distributions of the kinematic and nonlinear parameters (incl. maps of the leading-order near-bottom and near-surface amplitude-scaled horizontal velocities) have been constructed governing the IW field in a frame of the Gardner equation on a $10' \times 10'$ grid for the Baltic Sea. The presented data and technique enable to systematically estimate the limiting amplitudes for solitary internal waves and to highlight the possible soliton branches.
5. Seasonal variations in the hydrophysical fields of the Baltic Sea are insignificant for the phase speed and the dispersion parameter of the Gardner equation. Relatively strong variations and even changes in the sign of the nonlinear terms are possible.
6. The properties of extreme surface waves in relatively shallow domains of the Baltic Sea are analysed on the example of the Darss Sill area. The largest measured significant wave height was 4.46 m in 1991–2010 but wave heights over 6 m apparently have occurred in this area within the last half-century.
7. The theoretically predicted variety of the processes of solitary internal wave propagation and transformations in the zones with critical points has been studied and illustrated for several cross-sections of the coastal shelf of the South China Sea and in the Baltic Sea. A change in polarity and transformation of an initial solitary wave of moderate amplitude into two interacting solitary waves demonstrate the possibility of internal breather generation from an initial solitary wave in a realistic ocean situation.
8. The possibility of the generation of strong nonlinear unsteady internal lee waves by barotropic tide above the critical latitude has been demonstrated numerically using 2D incompressible Euler equations on a rotating *f*-plane in the Barents Sea conditions. The largest crest-to-trough height (about 80 m) appears at the end of the ebb phase each 12.4 h.

Recommendations for further work

As typical for wave processes, propagation of IW provides a mechanism of the transfer of massive quantities of energy between different sea areas. This energy is mostly released in regions where the pycnocline is located so close to the sea surface or the bottom that the large-amplitude IW will break. In the Baltic Sea conditions, this location may vary considerably and frequently occurs in areas where upper layers of soft sediments are substantially polluted (Verta et al., 2007).

Water velocities in breaking IWs usually largely exceed the threshold for suspension of such sediment. The dimensions of resulting plume are basically determined by the above-considered limiting parameters of large-scale IW. The frequent upwellings (that have high chances to occur simultaneously with the presence of intense IW field) bring the pollution to the upper layers of the sea where surface currents redistribute it over a large sea area (Leppäranta and Myrberg, 2009).

The largest uncertainty of this multi-step process is currently connected with the insufficient knowledge about the IW fields in the Baltic Sea. Therefore, in connection with detailed studies into upwelling (Lehmann and Myrberg, 2008) and current-driven transport of different adverse impacts (Soomere et al., 2011), our study paves the way towards much better understanding the functioning of key features of the entire Baltic Sea (eco)system and has a large potential to contribute into mitigation and management marine-induced hazards, especially problems connected with coastal pollution and coastal zone management.

In essence, the performed research is a step on the way towards systematic incorporation of the information about IW fields into engineering applications. First of all, it is necessary to estimate the influence of IWs upon the sediment erosion processes on the sea bed in the locations of major installations on the seabed such as pipelines, oil rigs or deep-water wind energy devices. At the present time several such projects have been already realized and much more are planned for the future in the Baltic Sea. Estimations of IWs and their impact, as it can be judged by the literature, are virtually absent for such problems for the Baltic Sea. A feasible way forward requires integration of the presented models for IWs with engineering models of sediment dynamics. Given the ever increasing amount, resolution and quality of hydrological data and rapid development of computational facilities suggests that this can be done in the near future.

An important direction in the study of the IW field in the Baltic Sea is the investigation into the surface manifestations of IWs. Progress in this direction would considerable improve the methods of their detection by means of remote sensing, including satellite observations, and, consequently, lead to much more comprehensive understanding of the IW climatology and its spatio-temporal variations. The number of such observations is relatively small (for example, in comparison to other non-tidal seas such as the Black Sea or the Caspian Sea),

and it is necessary to estimate the threshold of visibility of IWs by means of remote sensing in the context of the Baltic Sea wave climate. A less explored reason for such an infrequent manifestation could be the specific multi-layer structure of the sea in which large velocities (and associated effects) are concentrated either at certain depths or at the sea bottom.

The study of the potential influence of the pronounced IW activity on regional biogeochemical and ecological problems (functioning and resilience of ecosystems, vertical mixing of oxygen and nutrients, various exchange processes through the sea surface, etc.) is equally important. Here possible applications of the developed model of IWs are also promising.

Surprisingly little is known about generation mechanisms of IWs in microtidal seas. Although the tidal range is very limited in the Baltic Sea, the tidal flows are still substantial in some parts of the sea and may excite quite energetic IWs waves under certain circumstances. The options of direct IW generation in strongly stratified sub-basins of the Baltic Sea are not explored at all. Frequent sources of IWs apparently are intense water exchange events through the straits connecting the Baltic Sea and the North Sea. Such episodic events can substantially influence the characteristics of the IW field in the Baltic Sea.

Finally, the ever improving computational facilities have made it possible to use 3D models of IWs in the regions with complex bathymetry, where the interaction of different systems of IWs is possible. The technique developed and equations derived in the thesis can be widely used to test 3D models. All these issues can help in developing engineering models of IWs, which will be able to solve regional problems arising in the preparation of large-scale engineering projects in the Baltic Sea.

References

Ablowitz, M.J., Clarkson, P.A. Solitons, Nonlinear Evolution Equations and Inverse Scattering. Cambridge: Cambridge University Press, 1991.

Ablowitz, M., Segur, H. Solitons and Inverse Scattering Transform. Philadelphia: SIAM, 2000.

Akylas, **T.R**., **Grimshaw**, **R.H.J.** Solitary internal waves with oscillatory tails. – J. Fluid Mech. 242; 1992, p.279–298.

Alenius, P., Myrberg, K., Nekrasov, A. The physical oceanography of the Gulf of Finland: a review. – Boreal Environ. Res. 3; 1998, p. 97 – 125.

Alenius, P., Nekrasov, A., Myrberg, K. Variability of the baroclinic Rossby radius in the Gulf of Finland. – Cont. Shelf Res. 23; 2003, p. 563–573.

Apel, J., Ostrovsky, L.A., Stepanyants, Y.A., Lynch, J.F. Internal solitons in the ocean and their effect on underwater sound. – J. Acoust. Soc. Am. 121; 2007, p. 695–722.

Augustin, J. Das Seegangsklima der Ostsee zwischen 1958-2002 auf Grundlage numerischer Daten (Sea state climate of the Baltic Sea 1958-2002 based on numerical data). Diploma Thesis. Institute for Coastal Research, GKSS Research Center Geesthacht (now Helmholtz-Zentrum Geesthacht), Geesthacht, Germany [in German]. 2005.

Babu, S.V., Rao, A.D. Mixing in the surface layers in association with internal waves during winter in the northwestern Bay of Bengal. – Nat. Hazards; 2010, doi: 10.1007/s11069-010-9607-5.

Benjamin, T.B. A unified theory of conjugate flows. – Philos. Trans. Roy. Soc. London A 269; 1971, p. 587.

Benney, D.J. Long nonlinear waves in fluid flows. – J. Math. Phys. 45; 1966, p. 52–63.

Benney D.J., Ko, D.R.S. The propagation of long large amplitude internal waves. – Stud. Appl. Math. 59; 1978, p. 187.

Boegman, L., Imberger, J., Ivey, G.N., Antenucci, **J.P.** High-frequency internal waves in large stratified lakes. – Limnol. Oceanogr. 48/2; 2003 p. 895–919.

Boegman, L., Ivey, G.N., Imberger, J. The degeneration of internal waves in lakes with sloping topography. – Limnol. Oceanogr. 50/5; 2005, p. 1620–1637.

Bogucki, D.J., Redekopp,L.G. A Mechanism for sediment resuspension by internal solitary waves. – Geophys. Res. Lett. 26; 1999, p. 1317–1320.

Buijsman, M.C., Kanarska, Y., McWilliams, J.C. On the generation and evolution of nonlinear internal waves in the South China Sea. – J. Geophys. Res. 115; 2010, Art. No. C02012, doi:10.1029/2009JC005275.

Cai, S, Long, X, Gan, Z. A method to estimate the forces exerted by internal solitons on cylindrical piles. – Ocean Eng. 30/5; 2003, p. 673–89.

Camassa, R., Rusas, P.-O., Saxen, A., Tiron, R. Fully nonlinear periodic internal waves in a two-fluid system of finite depth. – J. Fluid Mech. 652; 2010, p. 259.

Carr, M., Stastna, M., Davies, P.A. Internal solitary wave-induced flow over a corrugated bed. – Ocean Dyn. 60/4; 2010, p. 1007–1025.

Chakrabarti, S. (Ed.) Handbook of offshore engineering. London: Elsevier, 2005.

Chernysheva, E.S. On the modeling of long internal waves. In: Davidan, I.N. et al. (eds.), Problems of the Studies and Mathematical Modeling of the Baltic Sea Ecosystem. Modeling of the Ecosystem Components Issue No. 3. Leningrad: Gidrometeoizdat, 1987. p. 50–54.

Chin-Bing, S.A., Warn-Varnas, A., King, D.B., Lamb, K. Effects on acoustics caused by ocean solitons. – Part B. Acoustics. Nonlinear Analysis 71; 2009, p. e2194–e2204.

Choi, W., Camassa, R. Weakly nonlinear internal waves in a two-fluid system. – J. Fluid Mech. 313; 1996, p. 83–103.

Choi, W., Camassa, R. Fully nonlinear internal waves in a two-fluid system. – J. Fluid Mech. 396; 1999, p. 1–36.

Chow, **K**.**W**., **Grimshaw**, **R**.**H**.**J**., **Ding**, **E**. Interactions of breathers and solitons in the extended Korteweg–de Vries equation. – Wave Motion 43; 2005, p. 158–166.

Craig, P. Incorporation of damping into internal wave models. – Cont. Shelf Res.1; 1991, p. 563–577.

Craig, W., Guyenne, P., Kalisch, H. A new model for large amplitude long internal waves. – C.R. Mechanique 332; 2004, p. 525–530.

Djordjevic, V.D., Redekopp, L.G. The fission and disintegration of internal solitary waves moving over two-dimensional topography. – J. Phys. Oceanogr. 8; 1978, p. 1016–1024.

Drazin, P.G., Johnson, R.S. Solitons: an Introduction. Cambridge: Cambridge Univ. Press, 1996.

Du, T., Sun, L., Zhang, Y., Bao, X., Fang, X. An estimation of internal soliton forces on a pile in the ocean. – J. Ocean Univ. China 6/2; 2007, p. 101–116.

Du, T., Tseng, Y.-H., Yan, X.-H. Impacts of tidal currents and Kuroshio intrusion on the generation of nonlinear internal waves in Luzon Strait. – J. Geophys. Res. 113; 2008, Art. No. C08015 doi:10.1029/2007JC004294.

Dubriel-Jacotin, L. Sur les ondes type permanent dans les liquids heterogenes. – Atti della reale Academic Nationalite dei Lincei 15; 1932, p. 44–52.

Duda, T.F., Lynch, J.F., Irish, J.D., Beardsley, R.C., Ramp, S.R., Chiu, C.-S., Tang, T.Y., Yang, Y.-J. Internal tide and nonlinear internal wave behavior at the continental slope in the northern South China Sea. – IEEE J. Oceanic Eng. 29; 2004, p. 1105–1130.

Dunphy, M., Subich, C., Stastna, M. Spectral methods for internal waves: indistinuishable density profiles and double-humped solitary waves. – Nonlin. Process. Geophys. 18; 2011, p. 351–358.

Engelbrecht, J.K., Fridman, V.E., Pelinovsky, E.N. Nonlinear Evolution Equations (Pitman Research Notes in Mathematics Series, No. 180). London: Longman, 1988.

Erm, A., Elken, J., Pavelson, J., Kask, J., Voll, M., Kört, M., Roots, O., Liblik, T., Lagemaa, P., Buschmann, F., Observation of high-speed deep currents and resuspension of soft sediments in the central part of the Gulf of Finland. In: The 10th International Marine Geological Conference "The Baltic Sea Geology–10," 24–28 August 2010, VSEGEI, St. Petersburg, Russia. Press VSEGEI, Saint-Petersburg, 2010, p. 25–26.

Feser, F., Weisse, R., von Storch, H. Multi-decadal atmospheric modeling for Europe yields multi-purpose data. – EOS Transactions. 82; 2001, p. 305–310.

Fofonoff, N., Millard, R.Jr. Algoriths for computation of fundamental properties of seawater. – UNESCO Technical Paper in Marine Sience 44; 1983, p. 15–25.

Fornberg, B. A Practical Guide to Pseudospectral Methods. Cambridge/New York/Melbourne: Cambridge University Press, 1998. 231 p.

Funakoshi, M., Oikawa, M. Long internal waves of large amplitude in a two-layer fluid. – J. Phys. Soc. Japan 55; 1986, p. 128–144.

Funakoshi, M. Long internal waves in a two-layer fluid. – J. Phys. Soc. Japan 54; 1985, p. 2470–2476.

Gear, J., Grimshaw, R. A second order theory for solitary waves in shallow fluids. – Phys. Fluids 26; 1983, p. 14–29.

Golenko, N.N., Mel'nikov, V.A., Estimation of spatio-temporal parameters of the internal wave field in the Southwest Baltic Sea using data by towed probe. – In: Scientific reports of the Russian Geographic Union (Kaliningrad branch), Russian State Univ., Kaliningrad 5; 2007, p. C1–C4.

Gorshkov, K.A., Ostrovsky, L.A., Soustova, I.A., Irisov, V.G. Perturbation theory for kinks and its application for multisoliton interactions in hydrodynamics. – Phys. Rev. E 69; 2004, Art. No. 016614.

Grimshaw, R., Pelinovsky, E., Talipova, T. The modified Korteweg–de Vries equation in the theory of large-amplitude internal waves. – Nonlin. Process. Geophys. 4/4; 1997, p. 237–350.

Grimshaw, R., Pelinovsky, E., Talipova, T. Solitary wave transformation due to a change in polarity. – Stud. Appl. Math. 101; 1998, p. 357–388.

Grimshaw, R. Internal solitary waves. In: Environmental Stratified Flows, ed. by: Grimshaw, R. Boston: Kluwer, 2001.

Grimshaw, R., **Pelinovsky, E., Poloukhina, O.** Higher-order Korteweg–de Vries models for internal solitary waves in a stratified shear flow with a free surface. – Nonlin. Process. Geophys. 9; 2002a, p. 221–235.

Grimshaw, R., Pelinovsky, D., Pelinovsky, E., Slunyaev, **A.** The generation of large-amplitude solitons from an initial disturbance in the extended Korteweg–de Vries equation. – Chaos 12/4; 2002b, p. 1070–1076.

Grimshaw, R., Pelinovsky, E., Talipova, T. The modified Korteweg–de Vries equation in the theory of the large–amplitude internal waves. – Nonlinear Process. Geophys. 4/4; 1997, p. 237-250.

Grimshaw, R., Pelinovsky, E., Talipova, T. Solitary wave transformation in a medium with sign-variable quadratic nonlinearity and cubic nonlinearity. – Physica D 132/1-2; 1999, p. 40-62.

Grimshaw, R., **Pelinovsky, E., Talipova, T.** Modeling internal solitary waves in the coastal ocean. – Surveys Geophys. 28/2; 2007, p. 273–298.

Grimshaw, R., Helfrich, K. Long-time solutions of the Ostrovsky equation. Stud. Appl. Math. 121/1; 2008, p. 71–88.

Grimshaw, R., Slunyaev, A., Pelinovsky, E. Generation of solitons and breathers in the extended Korteweg–de Vries equation with positive cubic nonlinearity. – Chaos 20; 2010, Art. No. 013102-1-11.

Grimshaw, R., Helfrich, K., Scotti, A. Large amplitude internal waves in the coastal ocean. – Nonlin. Processes Geophys. 18; 2011, p. 653–655.

Grue, J., Jensen, A., Rusas, P.O., Sveen, J.K. Properties of large-amplitude internal waves. – J. Fluid Mech. 380; 1999, p. 257–278.

Guyenne, P. Large-amplitude internal solitary waves in a two-fluid model. – C.R. Mecanique 334/6; 2006, p. 341–346.

Hamdi, S., Morse, B., Halphen, B., Schiesser, W. Analytical solutions of long nonlinear internal waves: Part I. – Nat. Hazards. 57; 2011a, p. 597.

Hamdi, S., Morse, B., Halphen, B., Schiesser, W. Conservation laws and invariants of motion for nonlinear internal waves: Part II. – Nat. Hazards. 57; 2011b p. 609.

Helfrich, K.R., Melville, W.K. Long nonlinear internal waves. – Annu. Rev. Fluid Mech. 38; 2006, p. 395–425.

Holloway, P., Pelinovsky, E., Talipova, T., Barnes, B. A Nonlinear Model of Internal Tide Transformation on the Australian North West Shelf. – J. Phys. Oceanogr. 27/6; 1997, p. 871 – 896.

Holloway, P., Pelinovsky, E., Talipova, T. A generalized Korteweg–de Vries model of internal tide transformation in the coastal zone. – J. Geophys. Res. 104/C8; 1999, p. 18333–18350.

Holloway, P., Pelinovsky, E., Talipova, T. Internal tide transformation and oceanic internal solitary waves, in: Environmental Stratified Flows, ed. by: Grimshaw, R., Boston: Kluwer, 2001.

http://science.nasa.gov/science-news/science-at-nasa/2008/19mar_grits/ (last attended March 4th 2012).

Hutter, K. (Ed.) Nonlinear internal waves in lakes. Berlin Heidelberg: Springer-Verlag, 2012.

Ivanov, V.A., Pelinovsky, E.N., Stepanyants, Yu.A., Talipova, T.G. Statistical estimation of nonlinear internal long wave parameters from field measuments. – Izvestiya, Atmosph. Ocean Phys. 28/10-11; 1992, p. 794–799.

Ivanov, V.A., Pelinovsky, E.N., Talipova, T.G., Troitskaya, Yu.I. Statistical estimates of the parameters of nonlinear long internal waves off the South Crimea in the Black Sea. – Phys. Oceanogr. 6; 1998, p. 253–262.

Ivanov, V.A., Lisichenok, A.D. Internal waves in the shelf zone and near the shelf edge in the Black Sea. – Phys. Oceanogr. 6; 2002, p. 353–360.

Ivanov, V.A., Lisichenok, A.D., Nemirovsky, M.S. Excitation of short-period internal waves by wind pulsations. – Izvestiya, Atmosph. Ocean Phys. 23/2; 1987, p. 179–185.

Jaagus, J. Long-term changes in frequencies of wind directions on the western coast of Estonia. – Institute of Ecology, Tallinn University. Publications. 11; 2009, p. 11–24 [in Estonian].

Jackson, Ch.R. (Ed.) An atlas of internal solitary-like waves and their properties. 2nd ed. – Alexandria (Va): Global Ocean Associates, 2004. 560 pp. (http://www.internalwaveatlas.com)

Jeans, D.R.G. Solitary internal waves in the qcean: A literature review completed as part of the internal wave contribution to Morena, UCES, Marine Science Labs, University of North Wales, Rep. U-95, 1995.

Kakutani, T., Yamasaki, N. Solitary waves in a two–layer fluid. – J. Phys. Soc. Japan 45; 1978, p .674–679.

Kalnay, E., Kanamitsu, M., Kistler, R., Collins, W., Deaven, D., Gandin, L., Iredell, M., Saha, S., White, G., Woollen, J., Zhu, Y., Chelliah, M., Ebisuzaki, W., Higgins, W., Janowiak, J., Mo, K., Ropelewski, C., Wang, J., Leetmaa, A., Reynolds, R., Jenne, R., Joseph, D. The NCEP/NCAR reanalysis project. – Bull. Am. Meteorol. Soc. 77; 1996, p. 437–471.

Kistler, R., Kalnay, E., Collins, W., Saha, S., White, G., Wollen, J., Chelliah, M., Ebisuzaki, W., Kanamitsu, M., Kousky, V., van den Dool, H., Jenne, R., Fioriono, M. The NCEP/NCAR 50-year reanalysis: monthly means CD-ROM and documentation. – Bull. Am. Meteorol. Soc. 82; 2001, p. 247–267.

Klymak, J.M., Pinkel, R., Liu, Ch.-T., Liu, A.K., David, L. Prototypical solitons in the South China Sea. – Geophys. Res. Lett. 33; 2006, p. L11607, doi:10.1029/2006GL025932.

Knauss, J.A. Introduction to physical oceanography. London: Prentice Hall, 1996, 309 pp.

Kol'chitskii, N.N., Monin, A.S., Paka, V.T. On internal seiches in the deep Baltic Sea. – Doklady Akademii Nauk 346/2; 1996, p. 249–255.

Komen, G.J., Cavaleri, L., Donelan, M., Hasselmann, K., Hasselmann, S., Janssen, P.A.E.M. Dynamics and modelling of ocean waves. Cambridge: Cambridge University Press, 1994.

Koop, C.G., Butler, G. An investigation of internal solitary waves in a two–fluid system. – J. Fluid Mech. 112; 1981, p. 225–251.

Krauss, B. Interne Wellen. Berlin: Gebrurder Borntraeger, 1966.

Kurkina, O.E., Kurkin, A.A., Dorokhov, D.V., Gorbatsky, V.V., Morozov, E.G., Pankratov, A.S. Distribution, vertical structure and seasonal variability of horizontal currents near the Curonian Spit in south-eastern Baltic Sea in 2010. – Book of Abstracts of 8th Baltic Sea Science Congress (22–26, August 2011, St. Petersburg, Russia); 2011, p. 272.

Lamb, G.L. Jr. Elements of soliton theory. N.Y.: John Wiley & Sons. 1980.

Lamb, K. Numerical experiments of internal wave generation by strong tidal flow across a finite amplitude bank edge. – J. Geophys. Res. 99/C1; 1994, p. 843 – 864.

Lamb, K., Yan, L. The evolution of internal wave undular bores: comparisons of a fully nonlinear numerical model with weakly nonlinear theory. – J. Phys. Oceanogr. 26; 1996, p.2712–2734.

Lamb, K.G. Particle transport by nonbreaking, solitary internal waves. – J. Geophys. Res. 102/C8; 1997, p. 18641–18660.

Lamb, K. A numerical investigation of solitary internal waves with trapped cores formed via shoaling. – J. Fluid Mech. 451; 2002, p.109–144.

Lamb, K.G., Polukhina, O., Talipova, T., Pelinovsky, E., Xiao, W., Kurkin, A. Breather generation in fully nonlinear models of a stratified fluid. – Phys. Rev. E75/4; 2007, Art. No. 046306.

Lavrova, O.Yu., Mityagina, M.I., Sabinin, K.D. Manifestations of internal waves on the sea surface in the North-Eastern part of the Black sea. – Issledovanie Zemli iz Kosmosa (Study of the Earth from Space) 6; 2009, p. 49–55 [In Russian].

Lavrova, O.Yu., Karimova, S.S., Mityagina, M.I., Bocharova, T.Yu. On-line satellite monitoring of the aquatories of the Black, Baltic and Caspian Seas in 2009 – 2010. – In: Modern Problems of Remote Sensing of the Earth from Space. Collected papers 7/1; 2010, p. 168–185 [In Russian].

Lavrova, O.Yu., Mityagina, M.I., Sabinin, K.D., Serebryany, A.N. Satellite Observations of Surface Manifestations of Internal Waves in the Caspian Sea. – Izvestiya, Atmosph. Ocean Phys. 47/9; 2011, p. 1119–1126.

LeBlond, P.H., Mysak, L.A. Waves in the ocean. Amsterdam: Elsevier. 1978.

Lehmann, A., Myrberg, K. Upwelling in the Baltic Sea – A review. – J. Marine Syst. 74/S; 2008, p. S3–S12.

Lehmann, A., Getzlaff, K., Harlass, J. Detailed assessment of climate variability in the Baltic Sea area for the period 1958 to 2009. – Clim. Res. 46; 2011, p. 185–196.

Leppäranta, M. Myrberg, K. Physical oceanography of the Baltic Sea. Praxis, Berlin, Heidelberg, New York: Springer. 2009.

Lilover, M.-J. Tidal currents as estimated from ADCP measurements in „practically non-tidal" Baltic Sea. – In: Proceedings of the IEEE/OES Baltic 2012 International Symposium "Ocean: Past, Present and Future. Climate Change Research, Ocean Observation & Advanced Technologies for Regional Sustainability," May 8–11, Klaipėda, Lithuania, IEEE; 2012, p. 4.

Liu, A.K., Holbrock, J.R., Apel, J.R. Nonlinear internal wave evolution in the Sulu Sea. – J. Phys. Oceanogr. 15; 1985, p. 1613–1624.

Liu, A.K. Analysis of nonlinear internal waves in the New York Bight. – J. Geophys. Res. 93; 1988, p.12317–12329.

Liu, A.K., Chang, Y.S., Hsu, M.-K., Liang, N.K. Evolution of nonlinear internal waves in the East and South China Seas. – J. Geophys. Res. 103; 1998, p. 7995–8008.

Liu, A.K., Ramp, S.R., Zhao, Y., Tang, T.Y. A case study of internal solitary wave propagation during ASIAEX 2001. – IEEE J. Oceanic Eng. 29; 2004, p. 1144–1156.

Liu, Ch.-T., Pinkel, R., Klymak, J., Hsu, M.-K., Chen, H.-W., Villanoy, C. Nonlinear internal waves from the Luzon Strait. – EOS Transactions. 87; 2006, p. 449–451.

Llewellyn Smith, S.G., Young, W.R. Conversion of the barotropic tide. – J. Phys. Oceanogr. 32; 2002, p. 1554–1566.

Long, R.R.. Some aspects of the flow of stratified fluids. I. A theoretical investigation. – Tellus 42; 1953, p. 42–58

Maderich, V., Brovchenko, I., Terletska, K., Hutter, K. Numerical simulations of the nonhydrostatic transformation of basin-scale internal gravity waves and wave-enhanced meromixis in lakes. – In: Nonlinear internal waves in lakes, ed. by K. Hutter, Berlin, Heidelberg: Springer-Verlag, 2012, p. 195–278.

Maderich, V., Talipova, T., Grimshaw, R., Pelinovsky, E., Choi, B.H., Brovchenko, I., Terletska, K., Kim, D.C. The transformation of an interfacial solitary wave of elevation at a bottom step. – Nonlin. Process. Geophys. 16; 2009, p.33–42.

Maderich, V., Talipova, T., Grimshaw,R., Terletska, E., Brovchenko, I., Pelinovsky, E., Choi, B.H. Interaction of a large amplitude interfacial solitary wave of depression with a bottom step. – Phys. Fluids 22; 2010, Art. No. 076602.

Makarenko, N.I. On the non-uniqueness of conjugate flows. – J. Appl. Mech. Techn. Phys. 45; 2004, p. 68.

Makarenko, N.I., Maltseva, Zh.L., Kazakov, A.Yu. Conjugate flows and amplitude bounds for internal solitary waves. – Nonlin. Process. Geophys. 16; 2009, p. 169.

Meier, H.E.M. Modeling the pathways and ages of inflowing salt- and freshwater in the Baltic Sea. – Estuar. Coast. Shelf Sci. 74; 2007, p. 717–734.

Meier, H.E.M., Döscher, R., Faxén, T. A multiprocessor coupled ice-ocean model for the Baltic Sea: application to salt inflow. – J. Geophys. Res. 108/C8; 2003, Art. No. 3273.

Mercier, M.J., Vasseur, R., Dauxois, T. Resurrecting dead-water phenomenon. – Nonlin. Process. Geophys. 18; 2011, p. 193–208.

Michallet, H., Barthelemy, F. Experimental study of interfacial solitary waves. – J. Fluid Mech. 366; 1998, p. 159.

Miles, J.W. On internal solitary waves. – Tellus 31; 1979, p. 456.

Miles, J.W. On internal solitary waves II. – Tellus 33; 1981, p. 397.

Mirie, R.M., Pennel, S.A. Internal solitary waves in a two-fluid system. – Phys. Fluids A 1; 1989, p. 986.

Miropolsky, Yu.Z. Dynamics of internal gravity waves in the ocean. Springer-Verlag, Berlin, 2001.

Mityagina, M.I., Lavrova, O.Yu. Satellite observations of surface manifestations of internal waves in non-tidal seas. – In: Modern problems of remote sensing of the Earth from space. Collected papers 7/1; 2010, p. 260–272 [In Russian].

Mityagina, M.I., Lavrova, O.Yu. Satellite observations of vortex and wave processes in coastal zone of north-eastern part of the Black Sea. – Issledovanie Zemli iz Kosmosa (Study of the Earth from Space) 5; 2009, p. 72–79 [In Russian].

Miyata, M. Long internal waves of large amplitude. – In: Nonlinear Water Waves, ed. by K. Horikawa and H. Maruo, 1988, p. 399–406.

Miyata, M. A note on broad and narrow solitary waves. IPRC Report 00-01 SOEST 00-05. Honolulu, Hawaii, 2000.

Morozov, E.G., Pisarev, S.V. Internal tides at the arctic latitudes (numerical experiments). – Oceanology 42; 2002, p. 153–161.

Muller, P., Briscoe, M. Diapycnal mixing and internal waves. – Oceanography 13/2; 2000, p. 98–103.

Nakamura, T., Awaji, T., Hatayama, T., Akimoto, K., Takizawa, T., Koho, T., Kawasaki, Y., Fukasava, M. The generation of large-amplitude unsteady lee waves by subinertial tidal flow: a possible vertical mixing mechanism in the Kuril Straits. – J. Phys. Oceanogr. 30; 2000, p. 1601–1621.

Nansen, F. Fram in the Polar Sea. Moscow: Drofa. 2007 [In Russian].

Nayfeh, A.H. Perturbation Methods. Wiley, Weinheim, 2004.

Novikov, S.P., Zakharov, V.E., Manakov, S.V., Pitaevsky, L.V. Soliton theory. Plenum, New York, 1984.

Orr, M.H., Mignerey, P.C. Nonlinear internal waves in the South China Sea: Observation of the conversion of depression internal waves to elevation internal waves. – J. Geophys. Res. 108/C3; 2003, p. 3064.

Osborne, A.R. Nonlinear ocean waves and the Inverse Scattering Transform. Elsevier, San Diego, 2010.

Osborne, A.R., Burch, T.L., Scarlet, R.I. The influence of internal waves on deep-water drilling. – J Petroleum Technol. 30/10; 1978, p. 1497–1504.

Osiński, R., Rak, D., Walczowski, W., Piechura, J. Baroclinic Rossby radius of deformation in the southern Baltic Sea. – Oceanologia 52/3; 2010, p. 417–429.

Ostrovsky, L.A. Nonlinear internal waves in a rotating ocean. – Oceanology 18; 1978, p.119–125 [English translation of the Russian journal Okeanologiya].

Ostrovsky, L.A., Stepanyants, Yu.A. Do internal solitons exist in the ocean? – Rev. Geophys. 27/3; 1989, p. 293–310.

Ostrovsky, L., Stepanyants, Yu. Internal solitons in laboratory experiments: comparison with theoretical models. – Chaos 15; 2005, Art. No. 037111.

Padman, L., Erofeeva, S. A barotropic inverse tidal model for the Arctic Ocean. – Geophys. Res. Lett. 31; 2004, Art. No. L02303.

Pelinovsky, **D**.**E**., **Grimshaw**, **R.H.J.** Structural transformation of eigenvalues for a perturbed algebraic soliton potential. – Phys. Lett. A 229; 1997, p. 165–172.

Pelinovskii, E.N., Polukhina, O.E., Lamb, K. Nonlinear internal waves in the ocean stratified in density and current. – Oceanology 40/6; 2000, p. 757–766.

Pelinovsky, E.N., Shavratsky, S.Kh., Raevsky, M.A. The Korteweg–de Vries equation for nonstationary internal waves in an inhomogeneous ocean. – Izvestiya, Atmosph. Ocean Phys. 13/3; 1977, p. 226–228.

Pelinovsky, E., Stepanyants, Yu., Talipova, T. Modelling of the propagation of nonlinear internal waves in horizontally inhomogeneous ocean. – Izvestiya, Atmosph. Ocean Phys. 30/1; 1994, p. 79–85.

Pelinovsky, E., Talipova, T., Ivanov, V. Estimations of nonlinear properties of internal wave Field off the Israel Coast. – Nonlin. Process. Geophys. 2/2; 1995, p. 80–88.

Pelinovsky, E., Polukhina, O., Slunyaev, A., Talipova, T. Internal solitary waves. In: Solitary Waves in Fluids, ed by R. Grimshaw, Southampton, Boston: WIT Press. 2007.

Pelinovsky, E.N., Talipova, T.G. Non-reflected wave propagation in strongly inhomogeneous media. – Fundam. Appl. Hydrophys. 3/9; 2010, p. 4–13 [in Russian].

Pinet, P.R. Invitation to oceanography. Jones and Barlett Learning, Sudbury 2003.

Pinet, .R. Oceanography, an introduction to the planet Oceanus. West Publishing Company, St. Paul 1992.

Pisarev, S.V. Low-frequency internal waves near the shelf edge of the Arctic Basin. – Oceanology 36; 1996, p. 771–778.

Polukhin, N., Talipova, T., Pelinovsky, E., Lavrenov, I. Kinematic characteristics of the high-frequency internal wave field in the Arctic. – Oceanology 43; 2003, p.333–343.

Poloukhin, N.V., Pelinovsky, E.N., Talipova, T.G., Muyakshin, S.I. On the effect of shear currents on the vertical structure and kinematic parameters of internal waves. – Oceanology 44; 2004, p. 22–29.

Pullin, D.I., Grimshaw, R.H.J. Finite-amplitude solitary waves at the interface between two homogeneous fluids. – Phys. Fluids 31; 1998, p. 3550.

Räämet, A., Soomere, T. The wave climate and its seasonal variability in the northeastern Baltic Proper. – Estonian J. Earth Sci. 59; 2010, p. 100–113.

Ramp, S.R., Tang, T.Y., Duda, T.F., Lynch, J.F., Liu, A.K., Chiu, C.-S., Bahr, F.L., Kim, H.-R., Yang, Y.-J. Internal solitons in the northeastern South China Sea, Part I: sources and deep water propagation. – IEEE J. Oceanic Eng. 29; 2004, p. 1157–1181.

Reeder, D.B., Ma, B.B., Yang, Y.J. Very large subaqueous sand dunes on the upper continental slope in the South China Sea generated by episodic, shoaling deep-water internal solitary waves. – Marine Geol. 279/12; 2011, p. 12–18.

Rouvinskaya, E.A., Kurkina, O.E., Kurkin, A.A. Improved nonlinear evolution equation for internal gravity waves in a three-layer symmetric fluid. – Transactions of R.E.Alekseev Nizhny Novgorod State Technical University. 4; 2010, p. 30–39 [In Russian].

Rouvinskaya, E., Kurkina, O., Kurkin, A. Investigation of the structure of large-amplitude solitary internal waves in a three-layer fluid. – Transactions of Moscow State Regional University, Series: “Physics –Mathematics”. 2; 2011, p. 61–74 [In Russian].

Rusas, P.-O., Grue, J. Solitary waves and conjugate flows in a three–layer fluid. – European J. Mech. B/Fluids 21; 2002, p. 185–206.

Sabinin, K., Serebryany, A. Intense short-period internal waves in the ocean. – J. Marine Res. 63; 2005, p. 227–261.

Sanchez-Garrido, J.C., Vlasenko, V. Long-term evolution of strongly nonlinear internal solitary waves in a rotating channel. – Nonlin. Processes Geophys., 16; 2009, p. 587–598, doi:10.5194/npg-16-587-2009.

Sandstrom, H., Elliott, J.A. Internal tide and solitons on the Scotian Shelf: A nutrient pump at work. – J. Geophys. Res. 89/C4; 1984, p. 6415–6426.

Slyunyaev, A.V., Pelinovskii, E.N. Dynamics of large-amplitude solitons. – JETP 89; 1999, p. 173.

Slyunyaev, **A.V.** Dynamics of localized waves with large amplitude in a weakly dispersive medium with a quadratic and positive cubic nonlinearity. – JETP 92; 2001, p. 529–534.

Schlitzer, R. Ocean Data View [Electronic data and program], Alfred Wegener Institute for Polar and Marine Research, Bremerhaven, Germany, 2004.

Scotti, A., Beardsley, R.C., Butman, B., Pineda, J. Shoaling of nonlinear internal waves in Massachusetts Bay. – J. Geophys. Res. 113; 2008, p.C08031, doi:10.1029/2008JC004726.

Song, Z.J., Teng, B., Gou, Y., Lu, L., Shi, Z.M., Xiao, Y., Qu, Y. Comparisons of internal solitary wave and surface wave actions on marine structures and their responses. – Appl. Ocean Res. 33; 2011, p. 120–129.

Soomere, T. Coupling coefficients and kinetic equation for Rossby waves. – Nonlin. Process. Geophys. 10; 2003, p. 385–396.

Soomere, T. Wind wave statistics in Tallinn Bay. – Boreal Environ. Res. 10; 2005, p. 103–118.

Soomere, T., Behrens, A., Tuomi, L., Nielsen, J.W. Wave conditions in the Baltic Proper and in the Gulf of Finland during windstorm Gudrun – Nat. Hazards Earth Syst. Sci. 8; 2008, p. 37–46.

Soomere, T. Solitons interactions. – In: Encyclopedia of complexity and systems science, ed. by R.A. Meyers, Springer, vol. 9; 2009, p. 8479.

Soomere, T., Zaitseva-Pärnaste, I., Räämet, A., Kurennoy, D. Spatio-temporal variations of wave fields in the Gulf of Finland. – Fund. Appl. Hydrophys. 4/10; 2010, p. 90–101 [in Russian].

Soomere, T., Weisse, R., Behrens, A. Wave climatology in the Arkona Basin, the Baltic Sea. – Ocean Sci. 8/2; 2012, p. 287–300.

Soomere, T., Delpeche, N., Viikmäe, B., Quak, E., Meier, H.E.M., Döös, K. Patterns of current-induced transport in the surface layer of the Gulf of Finland. – Boreal Environ. Res. 16/1; 2011, p. 1–21.

Sridevi, B., Murty, T.V.R., Sadhuram, Y., Murty, V.S.N. Impact of internal waves on the acoustic field at a coastal station off Paradeep, east coast of India. – Nat. Hazards; 2010, DOI 10.1007/s11069-010-9567-9.

Stastna, M., Lamb, K.G. Sediment resuspension mechanisms associated with internal wave in coastal waters. – J. Geophys. Res. 113; 2008, p. C10016.

Stober, U., Moum, J.N. On the potential for automated realtime detection of nonlinear internal waves from seafloor pressure measurements. – Appl. Ocean Res. 33; 2011, p. 275–285.

Talipova, T., Pelinovsky, E., Kõuts, T. Kinematics characteristics of the internal wave field in the Gotland Deep. – Oceanology 38/1; 1998, p. 37–46.

Talipova, T., Pelinovsky, E., Lamb, K., Grimshaw, R., Holloway, P. Cubic nonlinearity effects in the propagation of intense internal waves. – Doklady Earth Sciences 365; 1999, p. 241.

Talipova, T., Polukhin, N. Averaged characteristics of the internal wave propagation parameters in the World Ocean. – Izvestia of Russian Academy of Engineering Sciences, Applied Mathematics and Informatics 2; 2001, p. 139–155.

Talipova, T.G., Pelinovsky, E.N., Kharif, Ch. Modulation instability of long internal waves with moderate amplitudes in a stratified horizontally inhomogeneous ocean. – JETP Letters 94/3; 2011, p. 182–186.

Teague, W.J., Carron, M.J., Hogan, P.J. A comparison between the Generalized Digital Environmental Model and Levitus climatologies. – J. Geophys. Res. 95; 1990, p. 7167–7183.

Verta, M., Salo, S., Korhonen, M., Assmuth, T., Kiviranta, H., Koistinen, J., Ruokojärvi, P., Isosaari, P., Bergqvist, P.-A., Tysklind, M., Cato, I., Vikelsøe, J., Larsen, M.M. Dioxin concentrations in sediments of the Baltic Sea – A survey of existing data. – Chemosphere 67; 2007, p. 1762–1775.

Vidal, J., Casamitjana, X., Colomer, J., Serra, T. The internal wave field in Sau reservoir: Observation and modeling of a third vertical mode. – Limnol. Oceanogr. 50/4; 2005, p. 1326–1333.

Vlasenko, V., Brandt, P., Rubino, A. Structure of large–amplitude internal solitary waves. – J. Phys. Oceanogr. 30; 2000, p. 2172–2185.

Vlasenko, V.I., Hutter, K. Transformation and disintegration of strongly nonlinear internal waves by topography in stratified lakes. – Ann. Geophys. 20; 2002, p. 2087–2103.

Vlasenko, V.I., Ivanov, V.A., Krasin, I.G., Lisichenok, A.D. The generation of intensive short-period internal waves in the frontal zone of a coastal upwelling. – Phys. Oceanogr. 9/3; 1998, p. 155–168.

Vlasenko, V., Stashchuk, N., Hutter, K. Baroclinic tides: Theoretical modeling and observational evidence. Cambridge: Cambridge University Press. 2005.

Vlasenko, V., Stashchuk, N., Hutter, K., Sabinin, K. Nonlinear internal waves forced by tides near the critical latitude. – Deep-Sea Res. 50/1; 2003, p. 317–338.

Vlasenko, V., Stashchuk, N., Guo, C., Chen, X. Multimodal structure of baroclinic tides in the South China Sea. – Nonlin. Processes Geophys. 17; 2010, p.529–543.

Warn-Varnas, A., Chin-Bing, S.A., King, D.B., Hawkins, J., Lamb K. Effects on acoustics caused by ocean solitons, Part A. Oceanography. – Nonlinear Analysis 71; 2009, p. e1807–e1817.

Warn-Varnas, A., Hawkins, J., Lamb, K.G., Piacsek, S., Chin-Bing, S., King, D., Burgos, G. Solitary wave generation dynamics at Luzon Strait. – Ocean Model. 31; 2010, p.9–27.

Weisse, R., Günther, H. Wave climate and long-term changes for the Southern North Sea obtained from a high-resolution hindcast 1958–2002. – Ocean Dyn. 57; 2007, p. 161–172.

Weisse, R., von Storch, H., Callies, U., Chrastansky, A., Feser, F., Grabemann, I., Günther, H., Plüss, A., Stoye, T., Tellkamp, J., Winterfeldt, J., Woth, K. Regional meteorological marine reanalyses and climate change projections: results for Northern Europe and potential for coastal and offshore applications. – Bull. Am. Meteor. Soc. 90; 2009, p. 849–860.

Wood, D.J., Grue, J. Modelling of high amplitude internal waves integrating the primitive (Navier–Stokes) equations. – Appl. Ocean Res. 24/6; 2002, p. 331–340.

Yang, Y.J., Tang, T.Y., Chang, M.-H., Liu, A.K., Hsu, M.-K., Ramp, S.R. Convex and concave types of second baroclinic mode internal solitary waves. – Nonlin. Process. Geophys. 17; 2010, p. 605.

Zahibo, N., Slunyaev, A., Talipova, T., Pelinovsky, E., Kurkin, A., Polukhina, O. Strongly nonlinear steepening of long interfacial waves. – Nonlin. Process. Geophys. 14; 2007, p. 1–10.

Zhao, Z., Alford, M.H. Source and propagation of internal solitary waves in the northeastern South China Sea. – J. Geophys. Res. 111; 2006, Art. No. C11012.

Zhao, Z., Klemas, V.V., Zheng, Q., Li, X., Yan, X.-H. Satellite observation of internal solitary waves converting polarity. – Geophys. Res. Lett. 30/19; 2003, Art. No. 1988.

Zhao, Z., Klemas, V.V., Zheng, Q., Li, X., Yan, X.-H. Estimating parameters of a two-layer stratified ocean from polarity conversion of internal solitary waves observed in satellite SAR images. – Remote Sens. Environ. 92; 2004, p. 276–287.

Zhou, X., Grimshaw, R. The effect of variable currents on internal solitary waves. – Dynamics Atmos. Oceans. 14; 1989, p. 17–39.

Papers constituting the thesis

I. **Grimshaw, R., Talipova, T., Pelinovsky, E., Kurkina, O.** Internal solitary waves: propagation, deformation and disintegration. – Nonlin. Process. Geophys. 17; 2010, p. 633–649.

II. **Kurkina. O., Talipova, T.** Huge internal waves in the vicinity of the Spitsbergen Island (Barents Sea). – Natural Hazards Earth Syst. Sci. 11; 2011, p. 981–986.

III. **Kurkina, O., Pelinovsky, E., Talipova, T., Soomere, T.** Mapping the internal wave field in the Baltic Sea in the context of sediment transport in shallow water. – J. Coast. Res. Special Issue 64(II); 2011, p. 2042–2047.

IV. **Kurkina, O.E., Kurkin, A.A., Soomere, T., Pelinovsky, E.N., Rouvinskaya, E.A.** Higher-order (2+4) Korteweg–de Vries–like equation for interfacial waves in a symmetric three-layer fluid. – Phys. Fluids 23 /11; 2011, Art. No. 116602, 13 pp.

V. **Kurkina, O.E., Kurkin, A.A., Rouvinskaya, E.A., Pelinovsky, E.N., Soomere, T.** Dynamics of solitons in non-integrable version of the modified Korteweg–de Vries equation. – JETP Letters 95 /2; 2012, p. 91–95.

VI. **Soomere, T., Kurkina, O.** Statistics of extreme wave conditions in the south-western Baltic Sea. – Fund. Appl. Hydrophys. 4 /4; 2011, p. 43–57 [In Russian].

Abstract

Nonlinear dynamics of long internal gravity waves is studied for model examples of stratified water as well as for realistic shallow sea conditions. A higher-order (2+4) Korteweg–de Vries–like equation for interfacial waves is derived for a symmetric three-layer stratification. Its coefficients are determined analytically as functions of the properties of the layers. Solitary wave solutions are derived for this equation. The derived equation apparently is non-integrable. Numerical investigation of the properties and propagation of its solutions with different polarities reveals several features characteristic to solitons but their interaction is still weakly inelastic.

Average kinematic and nonlinear parameters of long high-frequency internal waves in a frame of Gardner equation are calculated for the Baltic Sea hydrological conditions. Possible nonlinear wave regimes, polarities and limiting amplitudes of solitary internal waves are analysed. The leading-order weakly-nonlinear near-bed and near-surface amplitude-scaled velocities of horizontal currents induced by internal waves have been mapped. Spatial and seasonal distributions of the listed parameters and effects of stratification and water depth on the IW propagation are discussed for the entire Baltic Sea. Statistics of extreme surface wave conditions has been derived for the south-western part of the Baltic Sea.

Various regimes of propagation and transformation of long nonlinear internal waves along cross-sections with contrasting properties in different regions of the World Ocean are illustrated in detail by means of mathematical modeling for the South China Sea, the Baltic Sea and the Barents Sea. Weakly nonlinear model based on the variable-coefficient Gardner equation for long internal waves in non-rotating basins was used for the South China Sea and the Baltic Sea. Using the concept of the critical points, where the coefficient of the quadratic, or of the cubic, nonlinear term is zero, it is demonstrated how a solitary wave may undergo a dramatic transformation, involving a polarity change and a disintegration into a wave train. For the non-tidal seas, such as the Baltic Sea, such a transformation can be inverted to reveal the possibility of a reverse metamorphosis and wave train focusing into a SIW. A full nonlinear numerical model for simulating the generation and propagation of internal waves based on the two-dimensional (vertical section) inviscid, incompressible Boussinesq equations on a rotating *f*-plane was used for the Barents Sea. The possibility of generation of strong nonlinear unsteady lee internal waves by the barotropic tide in the Barents Sea above the critical latitude has been demonstrated.

Resümee

Töös on analüüsitud pikkade mittelineaarsete siselainete dünaamikat nii mõnedel praktilist huvi pakkuvatel erijuhtudel kui ka veemasside realistlike stratifikatsioonide jaoks. On tuletatud uus võrrand, nn. (2+4) Korteweg–de Vriesi võrrand – Gardneri võrrandi üldistus – lainelevi jaoks kolmekihilises sümmeetriliselt stratifitseeritud meres. Selline veemasside struktuur esineb sageli Läänemeres, kuid olemasolevad võrrandid ei võimalda analüüsida lainelevi iseärasusi taolises keskkonnas. Tuletatud võrrandi kõigi liikmete koefitsiendid on leitud analüütiliselt veekihtide parameetrite alusel. On näidatud, et tuletatud võrrandil eksisteerivad erilahendid üksiklainete näol ning analüüsitud nende omadusi. Kuna kõnesolev võrrand tõenäoliselt pole integreeruv, ei ole alust oodata, et selle lahendite seas oleks solitone. Saadud lahendite numbrilise analüüsi alusel on näidatud, et üksiklainete interaktsioon pole perfektselt elastne, kuid sellel on siiski on mitmeid Gardneri võrrandi solitonlahendite interaktsiooni omadusi. Interaktsiooni käigus säilub komponentide identiteet ja kuju ning kiiratakse vaid väike kogus energiat.

On leitud pikkade suhteliselt väikese perioodiga siselainete levikut kirjeldava Gardneri võrrandi kinemaatiliste ja mittelineaarsuse määra iseloomustavate parameetrite keskmised väärtused Läänemere erinevate piirkondade jaoks. Saadud ruumiliste jaotuste alusel on analüüsitud võimalikke mittelineaarsete lainete leviku režiime, häirituste polaarsust ja maksimaalseid amplituude. Nende alusel on leitud põhjalähedaste kiiruste dimensioonitud amplituudid. Kõnesolevate suuruste väärtused on kaardistatud kogu Läänemere jaoks lahutusvõimega 10’ (ligikaudu 10–20 km). On analüüsitud nende väärtuste sesoonset muutlikkust juuli- ja jaanuarikuule vastavate kaartide võrdluse alusel ning vastava muutlikkuse võimalikku mõju siselainete leviku tingimustele Läänemeres. Lisaks on leitud Läänemere edelaosas (mis on üks tõenäolisemaid siselainete tekkimise piirkondi) esinevate kõrgeimate tormilainete statistika.

Pikkade mittelineaarsete siselainete erinevate levikurežiime ning lainete transformeerumise mehhanismide paljusust maailmamere erinevates osades on analüüsitud arvutisimulatsioonide abil Lõuna-Hiina mere, Läänmere ja Barentsi mere radikaalselt erinevates tingimustes. Mittekonstantsete kordajatega Gardneri võrrandil baseeruva nõrgalt mittelineaarse mudeli abil on demonstreritud, et kriitiliste punktide lähistel (kus selle võrrandi ruut- või kuupliige on null) võivad siselained dramaatiliselt ümber kujuneda. Võimalik on laine polaarsuse muutumine, aga ka üksiklaine konverteerumine lainete jadaks. Praktiliselt tõusu-mõõnavabade merede puhul (nt. Läänemeres) on võimalik pöördsituatsioon, kus siselainete jada fokuseerub võimsaks üksiklaineks. Barentsi mere jaoks rakendati pöörleva *f*-tasandi lähendust ja mittelineaarset Boussinesq’i võrrandit siselainete tekkimise ja leviku reprodutseerimiseks teatavas kahemõõtmelises läbilõikes. Demonstreeriti, et mittelineaarsete siselainete tekkimine on lineaarsete lainete jaoks kriitilisest laiusest põhja pool siiski võimalik.

Appendix A: Curriculum Vitae

1. Personal data

Name	Oxana Kurkina (before 2010 Polukhina/Poloukina)
Date and place of birth	20.10.1977, Gorky (now Nizhny Novgorod)
Citizenship	Russian Federation

2. Contact information

Address	Akadeemia tee 21, 12618, Tallinn
Phone	(+372) 620 4260
E-mail	oxana@cens.ioc.ee

3. Education

Educational Institution	Graduation year	Education (field of study/degree)
Nizhny Novgorod State Technical University	2002	Mechanics of fluids, gases and plasma; Candidat of Mathematical and Physical Sciences
Nizhny Novgorod State University	1999	Applied Mathematics; Diploma (MSc equivalent)

4. Language skills

Language	Level
Russian	native language
English	fluent
French	basic

5. Further training

Period	Educational or other institution
October 2006 October 2005 May 2004	University of Waterloo (Waterloo, Canada)
May 2006 – June 2006	Ocean University of China (Qingdao, China)
July 2005	Advanced school “Waves in Geophysics” (International Centre for Mechanical Sciences, Udine, Italy)
July – October 1999	Universite de Toulon et du Var (Toulon, France)

6. Professional employment

Period	Organisation	Position
2007 – to date	National Research University Higher School of Economics (Nizhny Novgorod, Russia)	Associated professor
2007 – to date	Nizhny Novgorod State Technical University	Senior researcher
2003 – to date	Institute of Applied Physics, Russian Academy of Sciences	Researcher
2003 – 2007	Nizhny Novgorod State Technical University	Associated professor
January – November 2003	Nizhny Novgorod State Technical University	Assistant Professor
1999 – 2003	Institute of Applied Physics, Russian Academy of Sciences	Junior Researcher

7. Scientific work

Peer-reviewed publications

Articles in journals indexed by ISI Web of Science (1.1)

O.E. Kurkina, A.A. Kurkin, E.A. Rouvinskaya, E.N. Pelinovsky, T. Soomere, Dynamics of solitons in non-integrable version of the modified Korteweg–de Vries equation. *JETP Letters*, **95**, No 2, 91–95 (2012).

O.E. Kurkina, A.A. Kurkin, T. Soomere, E.N. Pelinovsky, E.A. Rouvinskaya, Higher-order (2+4) Korteweg–de Vries–like equation for interfacial waves in a symmetric three-layer fluid. *Phys. Fluids*., **23**, No 11, 116602-1–13 (2011).

O. Kurkina, T. Talipova, E. Pelinovsky, T. Soomere, Mapping the internal wave field in the Baltic Sea in the context of sediment transport in shallow water. *Journal of Coastal Research*, Special Issue **64**, Part II, 2042–2047 (2011).

O. Kurkina, T. Talipova, Huge internal waves in the vicinity of the Spitsbergen Island (Barents Sea). *Natural Hazards and Earth System Sciences*, **11**, 981–986 (2011).

R. Grimshaw, T. Talipova, E. Pelinovsky, O. Kurkina, Internal solitary waves: propagation, deformation and disintegration. *Nonlinear Processes in Geophysics*, **17**, 633–649 (2010).

E. Pelinovsky, O. Polukhina, A. Kurkin, Rogue edge waves in the ocean. *The European Physical Journal. Special Topics*, **185**, 35–44 (2010).

O.E. Polukhina, N.M. Samarina, Cylindrical divergence of solitary internal waves in the context of the generalized Gardner equation. *Izvestiya, Atmospheric and Oceanic Physics*, **43**, No 6, 755–761 (2007).

N. Zahibo, A. Slunyaev, E. Pelinovsky, T. Talipova, A. Kurkin, O. Polukhina, Strongly nonlinear steepening of long interfacial waves. *Nonlinear Processes in Geophysics*, **14**, 1–10 (2007).

K.G. Lamb, O. Polukhina, T. Talipova, E. Pelinovsky, W. Xiao, A. Kurkin, Breather generation in fully nonlinear models of a stratified fluid. *Physical Review E*, **75**, 046306-1–6 (2007).

O.E. Polukhina, A.A. Kurkin, N.V. Polukhin, Interpretation of edge waves observations on Shikotan island. *Oceanology*, **46**. No 5, 645–649 (2006).

A.A. Kurkin, E.N. Pelinovsky, O.E. Poloukhina, Amplitude variations of edge waves on a shelf slowly varying in the alongshore direction. *Izvestiya, Atmospheric and Oceanic Physics*, **42**, No 3, 353–361 (2006).

A.B. Ezersky, O.E. Polukhina, J. Brossard, F. Marin, I. Mutabazi, Spatiotemporal properties of solitons excited on the surface of shallow water in a hydrodynamic resonator. *Phys. Fluids*, **18**, 067104-1–12 (2006).

V.A. Dubinina, A.A. Kurkin, E.N. Pelinovsky, O.E. Poloukhina, Resonance three-wave interactions of Stokes edge waves. *Izvestiya, Atmospheric and Oceanic Physics*, **42**, No 2, 277–284 (2006).

O.E. Poloukina, A.A. Kurkin, Improved theory of nonlinear topographic Rossby waves. *Oceanology*, **45**, No 5, 607–616 (2005).

V.A. Dubinina, A.A. Kurkin, O.E. Poloukhina, Nonlinear dynamics of edge waves over a linearly sloping bottom. *Izvestiya, Atmospheric and Oceanic Physics*, **41**, No 2, 242–246 (2005).

A.A. Kurkin, O.E. Poloukhina, Nonlinear focusing of anomalous Rossby waves in the ocean: numerical experiments. *Izvestiya, Atmospheric and Oceanic Physics*, **41**, No 1, 93–101 (2005).

V.A. Dubinina, A.A. Kurkin, E.N. Pelinovsky, O.E. Poloukhina, Weakly nonlinear periodic Stokes edge waves. *Izvestiya, Atmospheric and Oceanic Physics*, **40**, No 4, 464–469 (2004).

V.A. Dubinina, A.A. Kurkin, O.E. Polukhina, Focusing of edge waves over the Sea Shelf. *Izvestiya, Atmospheric and Oceanic Physics*, **39**, No 6, 758–767 (2003).

R. Grimshaw, E. Pelinovsky, O. Poloukhina, Higher order Korteweg–de Vries models for internal solitary waves in a stratified shear flow with a free surface. *Nonlinear Processes in Geophysics*, **9**, 221–235 (2002).

E.N. Pelinovskii, O.E. Polukhina, K. Lamb, Nonlinear internal waves in the ocean stratified in density and current. *Oceanology*, **40**, No 6, 757–766 (2000).

Peer-reviewed articles in other international research journals (1.2)

T. Soomere, O. Kurkina, Statistics of extreme wave conditions in the south-western Baltic Sea. *Fundamental and Applied Hydrophysics*, **4**, No 4, 43–57 (2011).

D. Tyugin, O. Kurkina, A. Kurkin, Software package for modeling of internal gravity waves in the World ocean. *Fundamental and Applied Hydrophysics*, **4**, No 2, 32–44 (2011).

E. Rouvinskaya, O. Kurkina, A. Kurkin, Investigation of the structure of large-amplitude solitary internal waves in a three-layer fluid. *Transactions of Moscow State Regional University, Series: "Physics –Mathematics"*, **2**, 61–74 (2011).

E. Rouvinskaya, O. Kurkina, A. Kurkin, Modeling of "internal weather" in an ecosystem of a stratified sea shelf. *Ecological Systems and Devices*, **6**, 8–16 (2011).

E. Averbukh, O. Kurkina, A. Kurkin, Modeling of surfactant film dynamics in a field of linear propagating edge waves on a sea shelf. *Transactions of Moscow State Regional University, Series: "Natural sciences"*, **2**, 109–121 (2011).

D. Tyugin, O. Kurkina, A. Kurkin, The digital atlas of kinematic and nonlinear parameters of internal gravity waves in the World Ocean. *Sensors & Systems*, **12**, 39–52 (2011).

E.A. Ruvinskaya, O.E. Kurkina, A.A. Kurkin, Improved nonlinear evolution equation for internal gravity waves in a three-layer symmetric fluid. *Transactions of R.E.Alekseev Nizhny Novgorod State Technical University*, No 4, 30–39 (2010).

V.A. Dubinina, A.A. Kurkin, O.E. Poloukhina, On the nonlinear interactions in edge wave triads on a sea shelf. *Physical Ocenography*, No 3, 3–19 (2008).

I. Bezruk, N. Zelenova, O. Polukhina, The study of nonlinear regimes in a hydrodynamic resonator on a boundary of two fluids. *Izvestiya, Russian Academy of Engineering Sciences, Applied Mathematics and Mechanics*, **20**, 113–118 (2007).

N. Zelenova, I. Bezruk, O. Polukhina, Nonlinear dynamics of intensive impulses on an interface of two fluid layers of almost equal depth bounded by rigid walls in the framework of improved Boussinesq-type two-wave model. *Izvestiya, Russian Academy of Engineering Sciences, Applied Mathematics and Mechanics*, **20**, 119–125 (2007).

A.A. Kurkin, E.N. Pelinovsky, O.E. Poloukhina, Amplitude variations of edge waves on a shelf slowly varying in the alongshore direction. *Izvestiya, Atmospheric and Oceanic Physics*, **42**, No 3, 353–361 (2006).

O.E. Polukhina, A.V. Slunyaev, Improved evolutionary model on a base of Gardner equation for internal waves in stratified fluid. *Izvestiya, Russian Academy of Engineering Sciences, Applied Mathematics and Mechanics*, **18**, 82–90 (2006).

E. Pelinovsky, A. Lechuga, A. Kurkin, O. Poloukhina, V. Dubinina, Ondas de orilla gigantes. *J. Ingenieria Civil*, No 140, 93–98 (2005).

N.V. Polukhin, T.G. Talipova, A.A. Kurkin, O.E. Poloukina, X. Zhaoting, Kinematic parameters of internal waves for Yallow, Japan and East-China Seas. *Izvestiya, Russian Academy of Engineering Sciences, Applied Mathematics and Mechanics*, **14**, 47–59 (2005).

A.B. Ezersky, O.E. Polukhina, J. Brossard, F. Marin, I. Mutabazi, Dynamics of surface wave solitons in shallow water resonators: Theory and experiment. *Applied Nonlinear Dynamics*, **12**, No 1-2, 138 –158 (2004).

A.B. Ezersky, O.E. Polukhina, E.N. Pelinovsky, Excitation of internal wave solitons in resonators. *Izvestiya, Russian Academy of Engineering Sciences, Applied Mathematics and Mechanics*, **6**, 90–97 (2004).

O.E. Polukhina, A.A. Kurkin, Nonlinear continental shelf waves. *Izvestiya, Russian Academy of Engineering Sciences, Applied Mathematics and Mechanics*, **4**, 17–25 (2003).

A.A. Krasiltschikov, O.E. Polukhina, T.G. Talipova, A.A. Kurkin, Solitary internal waves and their surface manifestations on the Laptev Sea Shelf. *Izvestiya, Russian Academy of Engineering Sciences, Applied Mathematics and Mechanics*, **4**, 156–170 (2003).

O.E. Polukhina, T.G. Talipova, Numerical modeling of surfactant dynamics in the field of nonstationary inhomogeneous currents and waves. *Izvestiya, Russian Academy of Engineering Sciences, Applied Mathematics and Mechanics*, **3**, 3–11 (2002).

O.E. Poloukhina, Surface waves in stratified ocean with shear velocity. *Izvestiya, Russian Academy of Engineering Sciences, Applied Mathematics and Mechanics*, **2**, 126–138 (2001).

N.V. Poloukhin, O.E. Poloukhina, V. Rey, Sediment transport under surface wave action. *Izvestiya, Russian Academy of Engineering Sciences, Applied Mathematics and Mechanics*, **1**, 181–193 (2000).

Contributions to books published by internationally renowned publishers (3.1)

E. Pelinovsky, O. Polukhina, A. Slunyaev, T. Talipova, Internal solitary waves. In “Solitary Waves in Fluids,” WIT Press. Southampton, Boston. 2007. P. 85–110.

E. Pelinovsky, A. Kurkin, O. Poloukhina, Unsteady dynamics of edge waves above a sloping beach. In Proceedings of the “Long Wave Symposium 2003” (Thessaloniki, Greece), 2003, P. 161–168.

A. Ezersky, O. Poloukhina, J. Brossard, F. Marin, I. Mutabazi, Modelisation des ondes solitaires excitees dans un canal en eau peu profonde. In Proceedings of “16-eme Congres Francais de Mecanique”, Nice, 1–5 Septembre 2003. P. 1–6.

V.A. Dubinina, A.A. Kurkin, O.E. Poloukhina, Nonlinear properties of long edge waves above a cylindrical shelf. In Proceedings of The Sixth (2004)

ISOPE Pacific/Asia Offshore Mechanics Symposium, Vladivostok, Russia, September 12–16, 2004. P. 157–162.

E. Pelinovsky, A. Lechuga, A. Kurkin, O. Poloukhina, V. Dubinina, Freak edge waves. In Proceedings of the 5th International Symposium on Ocean Waves, Measurement and Analysis "Waves-2005", 3–7 July 2005, Madrid, Spain. P. 1–9.

O. Poloukhina, A. Kurkin, E. Pelinovsky, V. Dubinina, Edge waves on uniform shelf: focusing, instability and interactions, In Proceedings of 8th conference on Dynamical systems – theory and applications. Lodz, Poland. 2005. P. 149–156.

E.A. Vladykina, O.E. Polukhina, A.A. Kurkin, Internal gravity waves in the ocean with two pycnoclines: Models and dynamics. In Proceedings of the 9th international conference on the Mediterranean coastal environment, MEDCOAST 2009, E. Ozhan (editor), 10–14 November 2009, Sochi, Russia. P. 949–960.

Conference presentations

IUTAM Symposium "Waves in fluids: effects of non-linearity, rotation, stratification and dissipation", Moscow, Russia: "Modeling of internal gravity waves and their surface manifestations in the Baltic Sea", "Improved version of software package for modeling of internal gravity waves in the World Ocean" (2012).

EGU General Assembly, Vienna, Austria: "Second-order theory for long nonlinear continental shelf waves on a beach with a general depth distribution", "High-order nonlinear evolution models for topographic Rossby waves", "Internal soliton generation in closed basins", "Nonlinear interactions of edge waves above a uniform beach", "Nonlinear internal wave generation by barotropic tide in the Arctic Basin", "Generation of intense solitary waves in lakes with external periodic forcing", "Solitons and breathers in the Euler equations for stratified waters", "Cylindrical divergence of internal solitary waves in the framework of Gardner equation", "Large amplitude long nonlinear internal gravity waves in stratified basins: models and dynamics", "Nonlinear dynamics of internal gravity waves in a three-layer fluid", "Estimations of large-amplitude internal waves in the Arctic Seas", "Large-amplitude internal solitons and breathers in the Luson Straight", "Influence of hydrological data sources upon the geographical and seasonal distribution of kinematic and nonlinear parameters of long internal gravity waves", "Rogue edge waves in the ocean", "Extended modified Korteweg–de Vries equation for internal gravity waves in a symmetric three-layer fluid", "Modeling of intensive internal wave generation over the critical latitude in the Barents Sea: effects of bottom slopes", "Modulation instability and hazardous internal waves in South China and Baltic Seas", "GIS for Studying Internal Gravity Waves", "Prognostic characteristics of internal waves for the Baltic Sea", "Nonlinear dynamics of intensive internal waves in bounded stratified basins", "Dynamics of surfactants in the field of edge and internal waves in coastal areas", "Higher-order weakly nonlinear theory for internal waves in three-layer fluid" (2005, 2006, 2007, 2010, 2011, 2012).

11th Internatonal Coastal Symposium "ICS 2011", Szczecin, Poland: "Mapping the internal wave field in the Baltic Sea in the context of sediment transport in shallow water" (2011).

8th Baltic Sea Science Congress, St. Petersburg, Russia: "Distribution, vertical structure and seasonal variability of horizontal currents near the Curonian Spit in southeastern Baltic Sea in 2010" (2011).

XXXIV Summer School – Conference "Advanced Problems in Mechanics," St. Petersburg, Russia: "Dynamics of two-dimensional long internal gravity waves in a three-layer fluid" (2006).

XIX International Conference of Young Scientists "Study of Natural Catastrophes on Sakhalin and Kuril Islands" devoted to the 60-anniversary of the Institute of Marine Geology and Geophysics FEB RAS, Yuzhno-Sakhalinsk, Russia: "Extreme wave regimes in different classes of ocean waves", "Prognosis of internal wave characteristics on a base of improved mathematical models and global hydrological atlases", "Modeling of edge and shelf waves in the ocean with cylindrical bottom relief" (2006).

XXXIII Summer School – Conference "Advanced Problems in Mechanics," St. Petersburg, Russia: "Anomalous continental shelf waves", "Unsteady dynamics of edge waves above a shelf slowly varied along shore", "Influence of alongshore currents on the process of edge wave focusing", "Nonlinear three-wave interaction of edge waves over cylindrical shelf" (2005).

International Conference "Fluxes and Structures in Fluids," Moscow, Russia: "Nonlinear dynamics of multimodal edge waves propagating above a cylindrical shelf" (2005).

The 5th International Symposium on Ocean Waves, Measurement and Analysis "Waves-2005", Madrid, Spain: "Freak Edge Waves" (2005).

The 8th conference on Dynamical systems – theory and applications, Lodz, Poland: "Edge waves on uniform shelf: focusing, instability and interactions" (2005).

XXXII summer school-conference "Advanced Problems in Mechanics," St.Petersburg, Russia: "Modelling of transformation of nonlinear edge wave on a shelf of the sea" (2004).

XXI International Congress of Theoretical and Applied Mechanics, Warsaw, Poland: "Extended Nonlinear Theory for Topographic Rossby Waves" (2004).

AGU Joint Assembly, Montreal, Canada: "Extreme Edge Waves Above a Cylindrical Shelf" (2004).

EGU General Assembly, Nice, France: "Nonlinear Instability of Edge Waves", "Second-order theory for nonlinear topographic Rossby waves", (2004).

EGS-AGU-EUG Joint Assembly, Nice, France: "The extended Gardner equation for internal waves in a stratified ocean", "Exitation of surface wave solitons in shallow water resonator: experiment and theory", "Focusing of large-amplitude edge and Rossby waves", "Dynamics of surface pollution induced by internal solitons in the Arctic Ocean" (2003).

International Conference "Fluxes and structures in fluids," St.Petersburg, Russia: "Anomalous high trapped waves above a concave exponential beach", "Nonlinear theory for long shelf waves", "Generation of tsunami by underwater land-slides" (2003).

XXXI summer school-conference "Advanced Problems in Mechanics," St.Petersburg, Russia: "Coastal trapped waves in a rotating ocean" (2003).

Long Waves Symposium, Thessaloniki, Greece: "Unsteady dynamics of edge waves above a sloping beach" (2003).

International Symposium "Topical Problems of Nonlinear Wave Physics," Nizhny Novgorod, Russia: "Exitation of surface wave solitons and soliton bound states in a shallow water resonator", "Weakly nonlinear periodic Stokes edge waves", "Generation of tsunami by underwater landslides in Black Sea", "The Gardner equation as the model for long internal waves", "Second-order theory for long shelf waves", "Modeling of transformation of the internal solitons on the ocean shelves and their mathematical manifestation on the surface" (2003).

8. Defended theses

Generalized Korteweg–de Vries equation in the theory of nonlinear internal waves in stratified flows. Candidate of Science's degree, 2002.

Development of physical and mathematical model of large-amplitude internal waves. Master's degree equivalent, 1999.

9. Main areas of scientific work/Current research topics

Nonlinear dynamics, nonlinear waves, nonlinear evolution equations, asymptotic methods, waves in fluids, internal waves, ocean waves, dynamics of coastal zone, numerical simulations, mathematical models.

10. Other research projects

Leader of grant projects

Russian Foundation for Basic Research: No 01-05-06208 "Support for young scientists" (2001), 02-05-06043 "Support for young scientists" (2002), 03-05-06116 "Support for young scientists" (2003), 05-05-64333 "Strongly nonlinear long internal waves in stratified ocean" (2005–2007).

Grant of President of Russian Federation for Young Scientists MK-1358.2005.1 "Strongly nonlinear internal waves in stratified flows: models and dynamics" (2005–2006), MK-846.2009.1 "Dynamics of large-amplitude localized internal gravity waves in stratified horizontally inhomogeneous fluid" (2009–2010).

11. Honours and awards

Laureate of the Scientific Council Award of Nizhny Novgorod State Technical University n.a. R.E. Alekseev, 2005.

Scholarship for young scientists of Academician G.A. Razuvaev, 2002.

Scholarship for students of George Soros Foundation, ISSEP, 1997

Appendix B: Elulookirjeldus

1. Isikuandmed

Ees- ja perekonnanimi	Oxana Kurkina (kuni 2010 Polukhina/Poloukina)
Sünniag ja .koht	20.10.1977, Gorki (praegu Nižni Novgorod)
Kodakondsus	Venemaa

2. Kontaktandmed

Address	Akadeemia tee 21, 12618, Tallinn
Phone	(+372) 620 4260
E-mail	oxana@cens.ioc.ee

3. Hariduskäik

Õppeasutus	Lõpetamise aeg	Haridus (eriala/kraad)
Nižni Novgorodi Riiklik Tehnikaülikool	2002	Vedelike, gaaside ja plasmafüüsika Füüsika-matemaatikakandidaat
Nižni Novgorodi Riiklik Ülikool	1999	Rakendusmatemaatika (matemaatik; võrdsustatud magistrikraadiga)

4. Keelteoskus

Keel	Tase
Vene	Emakeel
Inglise	Kesktase
Prantsuse	algtase

5. Täiendusõpe

Õppimise aeg	Täiendusõppe läbiviija
Oktoober 2006	Waterloo Ülikool (Waterloo, Kanada)
Oktoober 2005	
Mai 2004	
Mai – juuni 2006	Hiina Ookeanide Ülikool (Qingdao, Hiina)
Juuli 2005	Suvekool “Lained geofüüsikas” (International Centre for Mechanical Sciences, Udine, Italy)
Juuli – oktoober 1999	Universite de Toulon et du Var (Toulon, France)

6. Teenistuskäik

Töötamise aeg	Tööandja	Ametikoht
2007 – tänaseni	Rahvuslik Majanduse Kõrgkool, Nižni Novgorod	Dotsent
2007 – tänaseni	Nižni Novgorodi Riiklik Tehnikaülikool	Vanemteadur

2003 – tänaseni	Venemaa Teaduste Akadeemia Rakendusfüüsika Instituut	Teadur
2003 – 2007	Nižni Novgorodi Riiklik Tehnikaülikool	Dotsent
Jaanuar – november 2003	Nižni Novgorodi Riiklik Tehnikaülikool	Assistent
1999 – 2003	Venemaa Teaduste Akadeemia Rakendusfüüsika Instituut	Nooremteadur

7. Teadustegevus

Teadusartiklite ja peetud konverentsiettekannete loetelu on toodud ingliskeelse elulookirjelduse juures.

8. Kaitstud lõputööd ja väitekirjad

Üldistatud Korteweg–de Vries'i võrrand mittelineaarsete siselainete jaoks stratifitseeritud voolamistes (Generalized Korteweg–de Vries equation in the theory of nonlinear internal waves in stratified flows); väitekiri füüsika-matemaatikakandidaadi teadusliku kraadi saamiseks 2002.

Suure amplituudiga siselainete matemaatiline ja füüsikaline modelleerimine (Development of physical and mathematical model of large-amplitude internal waves); 5-aastase kõrgkooliõppe diplomitöö 1999.

9. Teadustöö põhisuunad

Mittelineaarne dünaamika, mittelineaarsed lained, mittelineaarsed evolutsioonivõrrandid, asümptootilised meetodid, lained pidevas keskkonnas, siselained, merelained, rannikuvööndi dünaamika, numbriline modelleerimine, lainete matemaatilised mudelid

10. Teadusprojektide juhtimine

Venemaa Teadusfond (Russian Foundation for Basic Research); grantid "Noorteadlaste toetamine" 01-05-06208 (2001), 02-05-06043, (2002), 03-05-06116 (2003), grant 05-05-64333 "Tugevalt mittelineaarsed pikad siselained stratifitseeritud ookeanis" (2005–2007).

Venemaa Presidendi grant noorteadlastele MK-1358.2005.1 "Tugevalt mittelineaarsed siselained stratifitseeritud voolamistes: mudelid ja dünaamika" (2005–2006), MK-846.2009.1 "Suure amplituudiga lokaliseeritud siselainete dünaamika horisontaalsuunas mittehomogeenses keskkonnas" (2009–2010).

11. Tunnustused

R.E. Alekseevi nimelise preemia laureaat, Nižni Novgorodi Riikliku Ülikooli nõukogu (2005).

Akadeemik G.A. Razuvaev'i nimeline stipendium noorteadlastele (2002).

George Soros'i fondi stipendium, ISSEP (1997)

Paper I

Grimshaw, R., Talipova, T., Pelinovsky, E., Kurkina, O. Internal solitary waves: propagation, deformation and disintegration. – Nonlinear Processes in Geophysics 17; 2010, p. 633–649.

Nonlin. Processes Geophys., 17, 633–649, 2010
www.nonlin-processes-geophys.net/17/633/2010/
doi:10.5194/npg-17-633-2010

Nonlinear Processes in Geophysics

Internal solitary waves: propagation, deformation and disintegration

R. Grimshaw[1], **E. Pelinovsky**[2], **T. Talipova**[2], **and O. Kurkina**[3,4]

[1]Department of Mathematical Sciences, Loughborough University, Leicestershire, UK
[2]Institute of Applied Physics, Nizhny Novgorod, Russia
[3]State University, Higher School of Economics, Nizhny Novgorod, Russia
[4]Institute of Cybernetics, Tallinn University of Technology, Tallinn, Estonia

Received: 1 September 2010 – Revised: 5 November 2010 – Accepted: 5 November 2010 – Published: 17 November 2010

Abstract. In coastal seas and straits, the interaction of barotropic tidal currents with the continental shelf, seamounts or sills is often observed to generate large-amplitude, horizontally propagating internal solitary waves. Typically these waves occur in regions of variable bottom topography, with the consequence that they are often modeled by nonlinear evolution equations of the Korteweg-de Vries type with variable coefficients. We shall review how these models are used to describe the propagation, deformation and disintegration of internal solitary waves as they propagate over the continental shelf and slope.

1 Introduction

Solitary waves are nonlinear localized waves of permanent form, first observed by Russell (1844) as a free surface solitary wave in a canal, and then in a series of experiments. Later, analytical studies by Boussinesq (1871) and Rayleigh (1876) for small-amplitude water waves confirmed Russell's observations. Then Korteweg and de Vries (1895) derived their well-known equation, which contains the "sech"^{2} solitary wave as one of its main solutions. But it was not until the second half of the twentieth century that it was realised that the Korteweg-de Vries (KdV) equation, was, on the one hand, a notable integrable equation, and on the other hand a universal model for weakly nonlinear long waves in a wide variety of physical contexts. The KdV equation, together with various extensions, describes a balance between nonlinear wave-steepening and linear wave dispersion.

Correspondence to: R. Grimshaw
(r.h.j.grimshaw@lboro.ac.uk)

Of principal concern in this paper are the large-amplitude internal solitary waves which propagate in the shallow water of coastal oceans. It is now widely accepted that the basic paradigm for internal waves in shallow seas is based on the KdV equation, first derived in this context by Benney (1966) and Benjamin (1966) and subsequently by many others; for recent reviews see, for instance, Grimshaw (2001), Holloway et al. (2001), Ostrovsky and Stepanyants (2005), Helfrich and Melville (2006), Apel et al. (2007), Grimshaw et al. (2007), or the book by Vlasenko et al. (2005). However, in the coastal ocean, the waves are propagating in a region of variable depth and also through regions of horizontally varying hydrology. In this situation, the appropriate model equation is the variable-coefficient KdV equation

$$A_t + cA_x - \frac{cQ_x}{Q}A + \mu A\,A_x + \delta A_{xxx} = 0\,, \tag{1}$$

Here $A(x,t)$ is the amplitude of the wave, and x, t are space and time variables, respectively. The coefficient $c(x)$ is the relevant linear long wave speed, while $Q(x)$ is the linear modification factor, defined so that $Q^{-2}A^2$ is the wave action flux for linear long waves. The coefficients $\mu(x)$ and $\delta(x)$ of the nonlinear and dispersive terms respectively, are determined by the properties of the basic state. All these coefficients are slowly-varying functions of x. The variable-coefficient KdV equation for water waves was developed by Ostrovsky and Pelinovsky (1970) and later systematically derived by Johnson (1973b), while Grimshaw (1981) gave a detailed derivation for internal waves (see also Zhou and Grimshaw, 1989 and Grimshaw, 2001). The first two terms in (1) are the dominant terms, and hence we can make the transformation

$$A = QU\,, \qquad \xi = \int^x \frac{dx}{c}\,, \qquad s = \xi - t\,. \tag{2}$$

Published by Copernicus Publications on behalf of the European Geosciences Union and the American Geophysical Union.

Substitution into (1) yields, to the same leading order of approximation where (1) holds,

$$U_\xi + \alpha U\, U_s + \lambda U_{sss} = 0 \tag{3}$$

$$\alpha = \frac{Q\mu}{c}\,, \qquad \lambda = \frac{\delta}{c^3}\,. \tag{4}$$

The coefficients α, λ are functions of ξ alone. Note that ξ measures travel time along the spatial path of the wave, while s is a temporal variable measuring the wave phase.

However because internal solitary waves are often of large amplitudes, it is sometimes useful to include a cubic nonlinear term in (1) and (3), which then become, respectively (see the review by Grimshaw, 2001),

$$A_t + cA_x - \frac{cQ_x}{Q}A + \mu A\, A_x + \mu_1 A^2 A_x + \delta A_{xxx} = 0\,, \tag{5}$$

$$U_\xi + \alpha U\, U_s + \beta U^2 U_s + \lambda U_{sss} = 0\,, \tag{6}$$

$$\text{where} \quad \beta = \frac{Q^2\mu_1}{c}\,. \tag{7}$$

Equations (3) and (6), sometimes with various modifications such as with an additional dissipative term, or with a term taking account of the Earth's rotation, have been applied to the study of internal solitary wave wave transformation in the coastal zone by many authors (for instance Cai et al., 2002; Djordjevic and Redekopp, 1978; Grimshaw et al., 2004, 2006, 2007; Holloway et al., 1997, 1999; Hsu et al., 2000; Liu et al., 1988, 1998, 2004; Orr and Mignerey, 2003; Shroyer et al., 2009 and Small, 2001a, b, 2003).

In Sect. 2, we shall present a more detailed description of the derivation of these model equations. Then in Sect. 3, we shall describe the slowly-varying solitary wave solutions of the evKdV equation (6) and in particular examine the behaviour at certain critical points where either α or β vanish. Then in Sect. 4 we shall indicate how these theoretical results can be applied for realistic oceanic conditions, such as those found in the South China Sea.

2 Evolution equations

2.1 Constant depth

The KdV equation is obtained by a weakly nonlinear long wave expansion from the fully nonlinear equations (see Grimshaw, 2001 or Grimshaw et al., 2007). We shall consider only a two-dimensional configuration, see Fig. 1, but initially we assume that the fluid has constant depth h. In the basic state the fluid has density $\rho_0(z)$, a horizontal shear flow $u_0(z)$ in the x-direction, and a pressure field $p_0(z)$ such that $p_{0z} = -g\rho_0$. The density stratification is described by the buoyancy frequency $N(z)$, where

$$N^2(z) = -\frac{g\rho_{0z}}{\rho_0}\,. \tag{8}$$

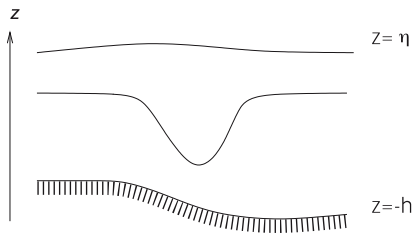

Fig. 1. Coordinate system.

Then, relative to this basic state, the outcome is, to leading order in the small parameter ϵ characterizing the long wave approximation,

$$\zeta \sim \epsilon^2 A(X,T)\phi(z) + \ldots\,, \quad X = \epsilon(x-ct)\,, \quad T = \epsilon^3 t\,. \tag{9}$$

Here ζ is the vertical particle displacement relative to the basic state and the modal function $\phi(z)$ satisfies the system

$$\left\{\rho_0(c-u_0)^2\phi_z\right\}_z + \rho_0 N^2\phi = 0\,, \quad \text{for} \quad -h < z < 0\,, \tag{10}$$

$$\phi = 0 \quad \text{at} \quad z = -h\,, \quad (c-u_0)^2\phi_z = g\phi \quad \text{at} \quad z = 0\,, \tag{11}$$

Equation (10) is the long-wave limit of the Taylor-Goldstein equation, and with the boundary conditions (11), determines the modal function and the linear long wave speed c.

Typically, this boundary-value problem (10, 11) defines an infinite sequence of regular modes, $\phi_n^{\pm}(z)$, $n = 0, 1, 2, \ldots$, with corresponding speeds $c_n^{\pm}$, where "$\pm$" indicates waves with $c_n^+ > u_M = \max u_0$ and $c_n^- < u_M = \min u_0$, respectively. Note that it is useful to let $n = 0$ denote the surface gravity waves for which c scales with $\sqrt{gh}$, and then $n = 1, 2, 3, \ldots$ denotes the internal gravity waves for which c scales with Nh. In general, the boundary-value problem (10, 11) is solved numerically. Typically, the surface mode ϕ_0 has no extrema in the interior of the fluid and takes its maximum value at the surface $z = 0$, while the internal modes $\phi_n^{\pm}(z)$, $n = 1, 2, 3, \ldots$, have n extremal points in the interior of the fluid, and vanish near $z = 0$ (and, of course, also at $z = -h$). Since the modal equations are homogeneous, a normalization condition can be imposed. Here we choose $\phi(z_m) = 1$ where $|\phi(z)|$ achieves a maximum value at $z = z_m$ with respect to z. In this case the amplitude $\epsilon^2 A$ is uniquely defined as the amplitude of ζ (to leading order in ϵ) at z_m.

It can then be shown that, within the context of linear long wave theory, any localised initial disturbance will evolve into a set of outwardly propagating modes, each propagating with the relevant linear long wave speed. Assuming that the speeds $c_n^{\pm}$ of each mode are distinct, it is sufficient for large times to consider just a single mode, as expressed by (9) Then, as time increases, the hitherto neglected nonlinear terms come into play and cause wave steepening. However, this is opposed by the terms representing linear

wave dispersion, also neglected in the linear long wave theory. A balance between these effects emerges as time increases, technically obtained as a compatibility condition at the second order in the expansion. The outcome is the Korteweg-de Vries (KdV) equation for the wave amplitude

$$A_T + \mu A\, A_X + \delta A_{XXX} = 0\,. \tag{12}$$

The coefficients μ and δ are given by

$$I\mu = 3\int_{-h}^{0} \rho_0 (c-u_0)^2 \phi_z^3 dz\,, \tag{13}$$

$$I\delta = \int_{-h}^{0} \rho_0 (c-u_0)^2 \phi^2 dz\,, \tag{14}$$

$$I = 2\int_{-h}^{0} \rho_0 (c-u_0) \phi_z^2 dz\,. \tag{15}$$

Note that after reverting to the original variables x and t, and using (9) Eq. (12) is equivalent to (1) for the case when all coefficients are constant and $Q_x = 0$. The KdV equation (12) is integrable and the long-time evolution from a localized initial condition is a finite number of solitary waves (solitons) and dispersing radiation.

A particularly important special case arises when the nonlinear coefficient μ defined by the expression (13) is close to zero. In this situation, a cubic nonlinear term is needed, and this can be achieved with a rescaling. The optimal choice is to assume that μ is $0(\epsilon)$, and then replace A with A/ϵ in (9); in effect the amplitude parameter is ϵ in place of ϵ^2. The outcome is that the KdV equation (12) is replaced by the extended KdV equation, widely known as the Gardner equation,

$$A_T + \mu A\, A_X + \mu_1 A^2 A_X + \delta A_{XXX} = 0\,,. \tag{16}$$

Again, after reverting to the original variables in (9) Eq. (16) is equivalent to (5) (with $Q_x = 0$). Expressions for the coefficient μ_1 are available, see Grimshaw et al. (2002) and the references therein. Like the KdV equation, (16) is integrable and has solitary wave solutions. There are two independent forms of the eKdV equation (16), depending on the sign of $\delta\mu_1$.

The solitary wave family of the eKdV equation (16) is given by

$$A = \frac{H}{1 + B\cosh K(X - VT)}\,, \tag{17}$$

$$\text{where} \quad V = \frac{\mu H}{6} = \delta K^2\,,\; B^2 = 1 + \frac{6\delta\mu_1 K^2}{\mu^2}\,, \tag{18}$$

characterized by a single parameter B. The wave amplitude is $a = H/(1+B)$. For $\delta\mu_1 < 0$, $0 < B < 1$, and the family ranges from small-amplitude waves of KdV-type ("sech^2"-profile) ($B \to 1$) to a limiting flat-topped wave of amplitude $-\mu/\mu_1$ ($B \to 0$), the so-called "table-top" wave, see the upper panel in Fig. 2. For $\delta\mu_1 > 0$ there are two branches; one branch has $1 < B < \infty$ and ranges from small-amplitude KdV-type waves ($B \to 1$), to large waves with a "sech"-profile ($B \to \infty$). The other branch with $-\infty < B < -1$, has the opposite polarity and ranges from large waves with a "sech"-profile when $B \to -\infty$, to a limiting algebraic wave of amplitude $-2\mu/\mu_1$ when $B \to -1$, see the lower panel in Fig. 2 Solitary waves with smaller amplitudes cannot exist, and from the point of view of the associated spectral problem are replaced by breathers, that is, pulsating solitary waves, see, for instance, Pelinovsky and Grimshaw (1997), Grimshaw et al. (1999, 2010), Clarke et al. (2000), Lamb et al. (2007). When $\mu_1 \to 0$, $B \to 1$ and the family reduces to the well-known KdV solitary wave family

$$A = a\,\mathrm{sech}^2(K(X - VT))\,, \quad V = \frac{\mu a}{3} = 4\delta K^2\,. \tag{19}$$

Here we have replaced a, K with $2a$, $2K$ to conform with the usual KdV notation.

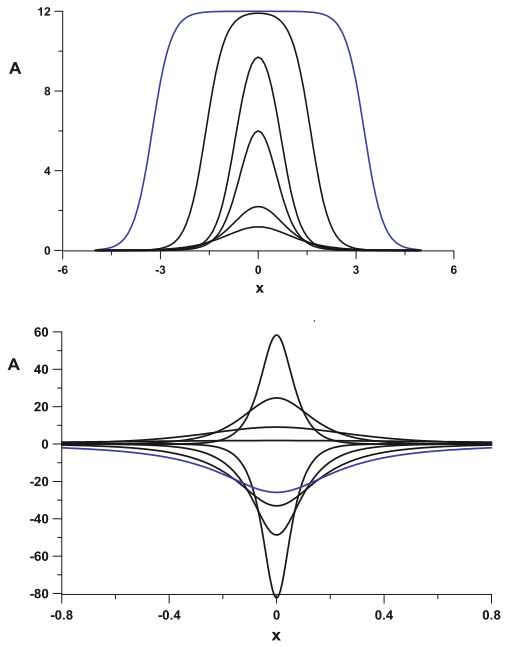

Fig. 2. Solitary wave family (17). The upper panel is for $\mu_1 < 0$ and the lower panel is for $\mu_1 > 0$; in both panels $\mu > 0$, $\delta > 0$.

2.2 Variable background

The derivation sketched above was for the case of constant depth, and when the basic state hydrology is independent of x. But in the ocean, the depth varies and the basic state hydrology may also vary in the propagation direction. These effects can be incorporated into the theory by supposing

that the basic state is a function of the slow variable $\chi = \epsilon^3 x$. That is, $h = h(\chi)$, $u_0 = u_0(\chi, z)$ with a corresponding vertical velocity field $\epsilon^3 w_0(z,\chi)$, a density field $\rho_0(z,\chi)$ a corresponding pressure field $p_0(\chi, z)$ and a free surface displacement $\eta_0(\chi)$. This basic state is assumed to satisfy the full equation set possibly with body forces in the momentum equations. With this scaling, the slow background variability enters the asymptotic analysis at the same order as the weakly nonlinear and weakly dispersive effects. As noted in the Introduction, it is now necessary to replace the variables x, t with ξ, s (2), where it is also convenient to replace the slow variable χ with ξ. An asymptotic analysis analogous to that described above then produces the vKdV equation (1) (Grimshaw, 1981; Zhou and Grimshaw, 1989). The modal system is again defined by (10, 11), but now $c = c(\xi)$ and $\phi = \phi(z,\xi)$, where the ξ-dependence is parametric. The analysis then proceeds as in the constant depth case, but with extra terms corresponding to the slow variability in the basic state, while the compatibility condition then yields the vKdV equation (1) now with variable coefficients $\mu = \mu(\xi), \delta = \delta(\xi)$, but which are again defined by (13, 14, 15) (but the upper limit in the integrals is now $z = \eta_0$ replacing $z = 0$). For the present case of internal waves, we find that the linear modification factor is given by, see Zhou and Grimshaw (1989),

$$Q^2 = \frac{1}{Ic^2}\,, \tag{20}$$

where I is defined by (15). Note also that the expression for Q can also be simply determined by requiring that $Q^{-2}A^2$ should be the wave action flux in the linear long wave limit. The variable-coefficient extended KdV equation (5) is obtained in a similar manner.

We shall conclude this section with some illustrative examples. First consider the case of *surface waves*. We put the density $\rho =$ constant so that then $N^2 = 0$ (8). Then, for the case when there is no background flow so that $u_0 = 0$, $\eta_0 = 0$, we obtain the well-known expressions

$$\phi = \frac{z+h}{h} \quad \text{for} \quad -h < z < 0\,, \quad c = (gh)^{1/2}\,. \tag{21}$$

$$\text{and so} \quad \mu = \frac{3c}{2h}\,, \quad \delta = \frac{ch^2}{6}\,, \quad Q^2 = \frac{1}{2gc}\,. \tag{22}$$

Similarly, for *interfacial waves* in a two-layer fluid, let the density be a constant ρ_1 in an upper layer of height h_1 and $\rho_2 > \rho_1$ in the lower layer of height $h_2 = h - h_1$. That is

$$\rho_0(z) = \rho_1 H(z+h_1) + \rho_2 H(-z-h_1)\,,$$

$$\text{so that} \quad \rho_0 N^2 = g(\rho_2 - \rho_1)\delta(z+h_1)\,.$$

Here $H(z)$ is the Heaviside function and $\delta(z)$ is the Dirac δ-function. Again we assume that there is no background flow ($u_0 = 0$, $\eta_0 = 0$). and we replace the free boundary with a rigid boundary so that the upper boundary condition for $\phi(z)$ becomes just $\phi(0) = 0$. This is a good approximation for oceanic internal solitary waves. Then we find that

$$\phi = \frac{z+h}{h_2} \quad \text{for} \quad -h < z < h_1, \quad \phi = -\frac{z}{h_1} \quad \text{for} \quad -h_1 < z < 0,$$

$$c^2 = \frac{g(\rho_2 - \rho_1)h_1 h_2}{\rho_1 h_2 + \rho_1 h_2}\,. \tag{23}$$

Substitution into (13, 14, 15) yields

$$\mu = \frac{3c\left(\rho_2 h_1^2 - \rho_1 h_2^2\right)}{2h_1 h_2(\rho_2 h_1 + \rho_1 h_2)}\,, \quad \delta = \frac{ch_1 h_2(\rho_2 h_2 + \rho_1 h_1)}{6(\rho_2 h_1 + \rho_1 h_2)}\,,$$

$$Q^2 = \frac{1}{2g(\rho_2 - \rho_1)c}. \tag{24}$$

Note that for the usual oceanic situation when $\rho_2 - \rho_1 \ll \rho_2$, the nonlinear coefficient μ for these interfacial waves is negative when $h_1 < h_2$ (that is, the interface is closer to the free surface than the bottom), and is positive in the reverse case. The case when $h_1 \approx h_2$ leads to the necessity to use the extended KdV equation (16), where the coefficient μ_1 is given by

$$\mu_1 = -\frac{3c}{8h_1^2 h_2^2(\rho_1 h_2 + \rho_2 h_1)^2} \left\{\left(\rho_1 h_2^2 - \rho_2 h_1^2\right)^2 + 8\rho_1\rho_2 h_1 h_2 (h_1 + h_2)^2\right\}. \tag{25}$$

Note that $\mu_1 < 0$, and so the eKdV equation (16) for a two-layer fluid always has $\delta\mu_1 < 0$.

However, in a three-layer fluid there are parameter regimes where one or two modes may have $\mu_1 > 0$ (Grimshaw et al., 2002), and there are many cases for real oceanic conditions with smooth stratification and background shear when the parameter $\mu_1 > 0$, see Grimshaw et al. (2004, 2007).

3 Deformation of internal solitary waves

3.1 Slowly varying solitary wave

In general the evKdV equation (6) with variable coefficients $\alpha = \alpha(\xi)$, $\beta = \beta(\xi)\lambda = \lambda(\xi)$ must be solved numerically. However, it is first instructive to consider the slowly-varying solitary wave. This is described in detail in review article by Grimshaw et al. (2007), but for convenience we shall present a brief summary here. The slowly-varying solitary wave is an asymptotic solution based on the assumption that the background state varies slowly relative to a typical wavelength. Formally, we suppose that

$$\alpha = \alpha(\sigma), \quad \beta = \beta(\sigma), \quad \lambda = \lambda(\sigma), \quad \sigma = \kappa\xi\,, \quad \kappa \ll 1. \tag{26}$$

We then invoke a multi-scale asymptotic expansion of the form (see Grimshaw, 1979)

$$U = U_0(\psi, \sigma) + \kappa U_1(\psi, \sigma) + \ldots, \tag{27}$$

$$\psi = s - \frac{1}{\kappa}\int^{\sigma} V(\sigma)d\sigma\,. \tag{28}$$

Here ψ is a temporal variable in a frame moving with the speed V. U is defined over the domain $-\infty < \psi < \infty$, and we will require that U remain bounded in the limits $\psi \to \pm\infty$. Since we can assume that $\lambda > 0$ small-amplitude waves will propagate in the negative s-direction, and so we can suppose that $U \to 0$ as $\psi \to \infty$. However, it will transpire that we cannot impose this boundary condition as $\psi \to -\infty$. This procedure is well-known for the vKdV equation (see Johnson, 1973a for the case of water waves, and Grimshaw, 1979 for the general case) and is readily extended to the evKdV equation (see the recent reviews by Grimshaw, 2007 and Grimshaw et al., 2007).

Substitution of (27) into (3) yields,

$$-VU_{0\psi} + \alpha U_0 U_{0\psi} + \beta U_0^2 U_\psi + \lambda U_{0\psi\psi\psi} = 0\,, \tag{29}$$

$$-VU_{1\psi} + \alpha(U_0U_1)_\psi + \beta\left(U_0^2U_1\right)_\psi + \lambda U_{1\psi\psi\psi} = -U_{0\sigma}\,. \tag{30}$$

Equation (29) has the solitary wave solution

$$U_0 = \frac{D}{1 + B\cosh K\psi}\,, \tag{31}$$

$$\text{where}\quad V = \frac{\alpha D}{6} = \lambda K^2\,,\quad B^2 = 1 + \frac{6\lambda\beta K^2}{\alpha^2}\,. \tag{32}$$

When the coefficients are constants, this is just the eKdV solitary wave (17). Here it is a slowly-varying solitary wave as the parameter $B = B(\sigma)$ and hence $a = D/(1+B) = a(\sigma)$, $V = V(\sigma)$, $K = K(\sigma)$. The main aim of the analysis is then to determine how these parameters vary, and this is determined at the next order of the expansion.

We now seek a solution of (30) for $U_1 \to 0$, $\psi \to \infty$ and for which U_1 is bounded as $\psi \to -\infty$. In order to determine the conditions that need to be imposed on the right-hand side of (30) to ensure that such a solution can be obtained, we need to consider the adjoint equation to the homogeneous operator on the left-hand side of (30), which is for the dependent variable $\tilde{U}_1$,

$$-V\tilde{U}_{1\psi} + \alpha U_0\tilde{U}_{1\psi} + \beta U_0^2\tilde{U}_{1\psi} + \lambda\tilde{U}_{1\psi\psi\psi} = 0\,. \tag{33}$$

The required compatibility conditions are then that the right-hand side of (30) should be orthogonal to all linearly independent solutions of the adjoint Eq. (33) which decay at infinity. Two linearly independent solutions of the adjoint Eq. (33) are 1, U_0. While both of these are bounded, only the second solution satisfies the condition that $U_1 \to 0$ as $\psi \to \infty$. The third solution is unbounded as $\psi \to \pm\infty$. Hence only one compatibility condition can be imposed, namely that the right-hand side of (30) is orthogonal to U_0, which leads to

$$P_{0\sigma} = 0 \quad \text{where} \quad P_0 = \int_{-\infty}^{\infty} U_0^2\,d\psi\,. \tag{34}$$

Thus P_0 is a constant, and as the solitary wave (19) has just one free parameter B, this condition suffices to determine its variation.

However, the evKdV equation (6) has two conservation laws

$$\frac{\partial M}{\partial\xi} = 0,\quad M = \int_{-\infty}^{\infty} U\,ds\,, \tag{35}$$

$$\frac{\partial P}{\partial\xi} = 0,\quad P = \int_{-\infty}^{\infty} U^2\,ds\,, \tag{36}$$

for "mass" and "momentum" respectively. In physical terms, (35) is an approximation to the conservation of physical mass, while (36) expresses conservation of wave action flux at the leading order. The condition (34) is easily recognized as the leading order expression for conservation of momentum (36). But since this completely defines the slowly-varying solitary wave, we now see that this cannot simultaneously conserve mass. This is also apparent when one examines the solution of (30) for U_1, from which it is readily shown that although $U_1 \to 0$ as $\psi \to \infty$, $U_1 \to D_1$ as $\psi \to -\infty$ where

$$VD_1 = -M_{0\sigma}\,,\quad \text{where}\quad M_0 = \int_{\infty}^{\infty} U_0\,d\psi\,. \tag{37}$$

This non-uniformity in the slowly-varying solitary wave has been recognized for some time, see, for instance, Knickerbocker and Newell (1978, 1980), Grimshaw (1979) or Grimshaw and Mitsudera (1993) and the references therein. The remedy is the construction of a trailing shelf $U^{(s)}$ of small amplitude $O(\kappa)$ but long length-scale $O(1/\kappa)$, which thus has $O(1)$ mass, but $O(\kappa)$ momentum. It resides behind the solitary wave, and to leading order is given by

$$U^{(s)} = \kappa U^{(s)}(T),\ \text{for}\ T = \kappa\xi < \Psi(\sigma) = \int^{\sigma} V(\sigma)d\sigma\,. \tag{38}$$

Here $T = \Psi(\sigma)$ defines the location of the solitary wave. $U^{(s)}(T)$ is independent of σ, and is determined so that the shelf amplitude is just $\kappa D_1(\sigma)$ at the location of the solitary wave, that is $U^{(s)}(\Psi(\sigma)) = D_1(\sigma)$ (37). At higher orders in κ the shelf itself will evolve and may generate secondary solitary waves, see El and Grimshaw (2002) and Grimshaw and Pudjaprasetya (2004). The slowly-varying solitary wave and the trailing shelf together satisfy conservation of mass.

Substitution of the solitary wave (31) into the expression (34) for P_0 yields

$$P_0 = \frac{D^2}{K}\int_{-\infty}^{\infty} \frac{du}{(1 + B\cosh u)^2}\,, \tag{39}$$

$$\text{or}\qquad G(B) = P_0\left|\frac{\beta^3}{\lambda\alpha^2}\right|^{1/2}, \tag{40}$$

$$\text{where}\quad G(B) = \left|B^2 - 1\right|^{3/2}\int_{-\infty}^{\infty} \frac{du}{(1 + B\cosh u)^2}\,. \tag{41}$$

The expression (40) determines the variation of the parameter B since P_0 is a constant, determined by the initial conditions. The integral term in $G(B)$ can be explicitly evaluated,

$$B^2 > 1: \quad G(B) = 2(B^2-1)^{1/2} \mp 4\arctan\sqrt{\frac{B-1}{B+1}}, \tag{42}$$

$$0 < B < 1: \quad G(B) = 4\,\mathrm{arctanh}\sqrt{\frac{1-B}{1+B}} - 2\left(1-B^2\right)^{1/2}. \tag{43}$$

The alternative signs in (42) correspond to the cases $B > 1$ or $B < -1$. Next, the trailing shelf is found from (37, 38) where

$$B^2 > 1: \quad M_0 = \pm|\frac{6\lambda}{\beta}|^{1/2} 4\arctan\sqrt{\frac{B-1}{B+1}}\,, \tag{44}$$

$$0 < B < 1: \quad M_0 = \pm|\frac{6\lambda}{\beta}|^{1/2} 4\,\mathrm{arctanh}\sqrt{\frac{1-B}{1+B}}\,. \tag{45}$$

Here the alternative signs in (44) and (45) correspond to the cases $\alpha B > 0$ or $\alpha B < 0$.

The expression (40) provides an explicit formula for the dependence of B on the basic state parameters $\alpha, \beta, \lambda, \nu$. It is readily shown that $G(B)$ (42) is a monotonically increasing function of $|B|$ for $1 < |B| < \infty$, and is a monotonically decreasing function of B for $0 < B < 1$ (43). Thus as $|\beta^3/\lambda\alpha^2| \to \infty$, then so does $G(B)$. If $\beta < 0$ so that $0 < B < 1$, $B \to 0$ and the wave approaches the limiting "table-top" shape. On the other hand if $\beta > 0$ and $1 < |B| < \infty$ then $|B| \to \infty$ and the wave shape approaches the "sech"-profile, The behaviour of the wave amplitude in these limits depends on the behaviour of each of the parameters α, β, λ. But since we can usually expect β to be finite and $\lambda(>0)$ to be non-zero, we see that these limiting shapes are usually achieved at the critical point where $\alpha \to 0$. This case is discussed below in Sect. 3.2. On the other hand, if $|\beta^3/\lambda\alpha^2| \to 0$, then so does $G(B)$. In this case $B \to 1$, $G(B) \sim |B-1|^{3/2}$ (see (42, 43)) and the wave profile reduces to the KdV "sech^2"-shape, provided that either $\beta < 0$ when $0 < B < 1$, or if $\beta > 0$, then the wave belongs to the branch defined by $1 < B < \infty$. These scenarios are usually achieved at the alternative critical point where $\beta = 0$, discussed below in Sect. 3.2.

3.2 Passage through a critical point

The adiabatic deformation of a solitary wave discussed above in Sect. 3.1 shows that the critical points where $\alpha = 0$, or where $\beta = 0$, are sites where we may anticipate a change in the wave structure. First we recall the vKdV model (3) where $\beta = 0$. In this case the adiabatic law (40) collapses to $a^3 \propto \alpha/\lambda$ where a is the solitary wave amplitude (19), and the expression (37) collapses to $D_1 = a_\sigma/2\lambda K^3$. Suppose that $\alpha = 0$ at $\sigma = 0$, where, without loss of generality, we can assume that α passes from a negative to a positive value as σ increases through zero. Initially the solitary wave is located in $\sigma < 0$ and has negative polarity, corresponding to the usual oceanic situation. Then, near the transition point, the amplitude of the wave decreases to zero as $a \sim -|\alpha|^{1/3}$, while $K \sim |\alpha|^{2/3}$; the momentum of the solitary wave is of course conserved (to leading order), but the mass of the solitary wave increases (in absolute value) as $1/|\alpha|^{1/3}$, its speed decreases as $|\alpha|^{4/3}$, and the amplitude $D_1 > 0$ of the trailing shelf just behind the solitary wave grows as $|\alpha|^{-8/3}$; the total mass of the trailing shelf is positive and grows as $1/|\alpha|^{1/3}$, in balance with the negative mass of the solitary wave, while the total mass remains a negative constant. Since the tail grows to be comparable with the wave itself, the adiabatic approximation breaks down as the critical point is approached. Nevertheless, we can infer that the the solitary wave itself is destroyed as the wave passes through the critical point $\alpha = 0$. The structure of the solution beyond this critical point has been examined numerically by Knickerbocker and Newell (1980) and revisited by Grimshaw et al. (1998a), who showed that the shelf passes through the critical point as a positive disturbance, which then being in an environment with $\alpha > 0$, can generate a train of solitary waves of positive polarity, riding on a negative pedestal, see Fig. 3.

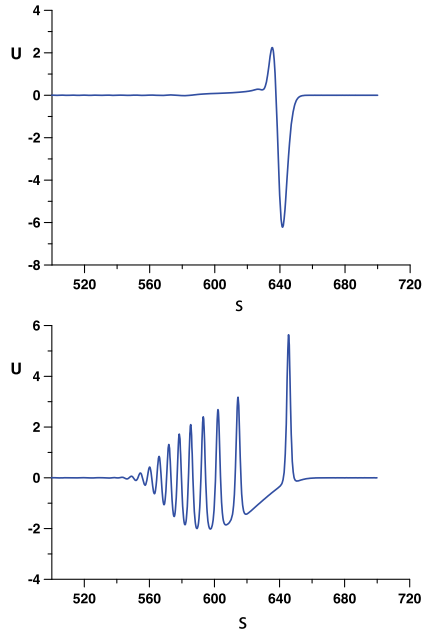

Fig. 3. Numerical simulation of the vKdV equation (3) with $\delta = 1$ and as α varies from -1 to $+1$. The upper panel is when $\alpha = 0$ and the lower panel is when $\alpha = 1$. The simulation shows a strong deformation of the initial solitary wave of depression at $\alpha = 0$, followed at $\alpha = 1$ by the emergence of a number of solitary waves of elevation riding on a negative pedestal.

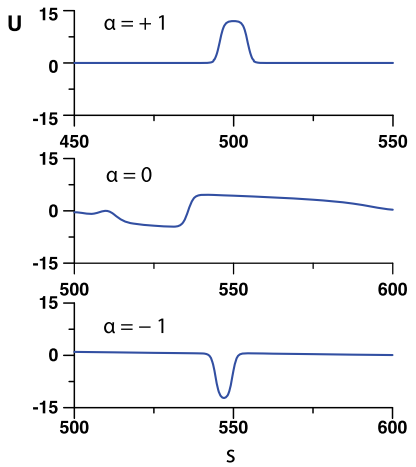

Fig. 4. Numerical simulation of the evKdV equation (6) with $\delta = 1$, $\beta = -0.083$ and as α varies from 1 to -1. The upper panel shows the initial condition of a "table-top" solitary wave of elevation at $\alpha = -1$, the middle panel shows a strong deformation at $\alpha = 0$, and the lower panel shows the leading wave at $\alpha = -1$. This wave is a "table-top" wave of depression riding on a small positive pedestal.

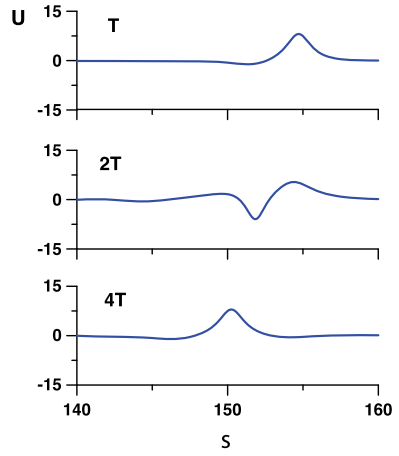

Fig. 5. Numerical simulation of the evKdV equation (6) for the case when $\delta = 1$, $\beta = 0.3$, $\nu = 0$ and α varies from 1 to -1. The initial wave (not shown) is a solitary wave of elevation belonging to the branch for which $B > 0$. It then passes adiabatically through the critical point, changing the sign of B to $B < 0$, and arrives at the location $\alpha = -1$ where $\xi = T$ with only a small deformation. However, at this stage its amplitude is below that allowed for a steady solitary wave, and so it deforms into a breather, shown in the middle panel for $\xi = 2T$ and the lower panel for $\xi = 4T$.

We next take account of the cubic nonlinear term in (6) and suppose again that α passes through zero at $\sigma = 0$ but that $\beta \neq 0$ at the critical point. First, let us suppose that $\beta < 0$, $0 < B < 1$. Then as $\alpha \to 0$, we see from (40) and (43) that $G(B) \sim 1/|\alpha|$, and $B \to 0$ with $B \sim 2\exp(-G/2)$. Thus the approach to the limiting "table-top" wave is quite rapid. From (31) $K \sim |\alpha|$ in this limit, and the amplitude approaches the limiting value $a \sim -\alpha/\beta$. Thus the wave amplitude decreases to zero, and, interestingly, this is a more rapid destruction of the solitary wave than for the case when $\beta = 0$. The mass M_0 (45) of the solitary wave grows as $|\alpha|^{-1}$ and so the amplitude D_1 of the trailing shelf (37) grows as $1/|\alpha|^4$. The overall scenario after α has passed through zero is similar to that described above for the vKdV equation (3) and has been discussed in detail by Grimshaw et al. (1999); see Fig. 4 for a case when a "table-top" solitary wave is converted to another such wave of opposite polarity, riding on a pedestal.

Next, let us suppose that $\beta > 0$ so that $1 < |B| < \infty$ There are two sub-cases to consider, $B > 0$ or $B < 0$, when the the solitary wave has the same or opposite polarity to α. Then as $\alpha \to 0, |B| \to \infty$ as $|B| \sim 1/|\alpha|$. It follows from (31) that then $K \sim 1$, $D \sim 1/|\alpha|, a \sim 1$, $M_0 \sim 1$. It follows that the wave adopts the "sech"-profile, but has *finite* amplitude, and so can pass through the critical point $\alpha = 0$ without destruction. But the wave changes branches from $B > 0$ to $B < 0$ as $|B| \to \infty$, or vice versa. An interesting situation then arises when the wave belongs to the branch with $-\infty < B < -1$ and the amplitude is reducing. If the limiting amplitude of $-2\alpha/\beta$ is reached, then there can be no further reduction in amplitude for a solitary wave, and instead a breather will form. An example of this outcome is shown in Fig. 5, where the wave has entered this regime after passing through the critical point.

Finally, consider the case when $\beta \to 0$, $\alpha \neq 0$. This case has been studied by Nakoulima et al. (2004) using both an asymptotic analysis similar to that used here, and numerical simulations. As already noted above, in this case $B \to 1$, $G(B) \sim |B-1|^{3/2}$ (42, 43), and it then follows from (40) that $G \sim |\beta|^{3/2}$ and so $|B-1| \sim |\beta|$. There are three sub-cases to consider. First, suppose that initially $\beta < 0$ and so $0 < B < 1$. As $|\beta| \to 0$, $1 - B \sim |\beta|$ and the wave profile becomes the familiar KdV "sech^2"-shape. It is readily shown from (31) that then K, a, M_0, $D_1 \sim 1$ and so the wave can pass through the critical point $\beta = 0$ without destruction. However, after passage through the critical point, the wave has moved to a different solitary branch (see Fig. 2), and this may change its ultimate fate. A typical scenario is shown in Fig. 6, which shows the transformation of a "table-top" solitary wave (upper panel in Fig. 2) to a KdV "sech^2"-KdV solitary wave at the critical point, and further evolution as a solitary wave of the upper branch in the lower panel of Fig. 2. Second, suppose that initially $\beta > 0$ and $1 < B < \infty$. Now $B - 1 \sim \beta$ and again the wave profile becomes the familiar KdV "sech^2"-shape, while K, a, M_0, $D_1 \sim 1$,

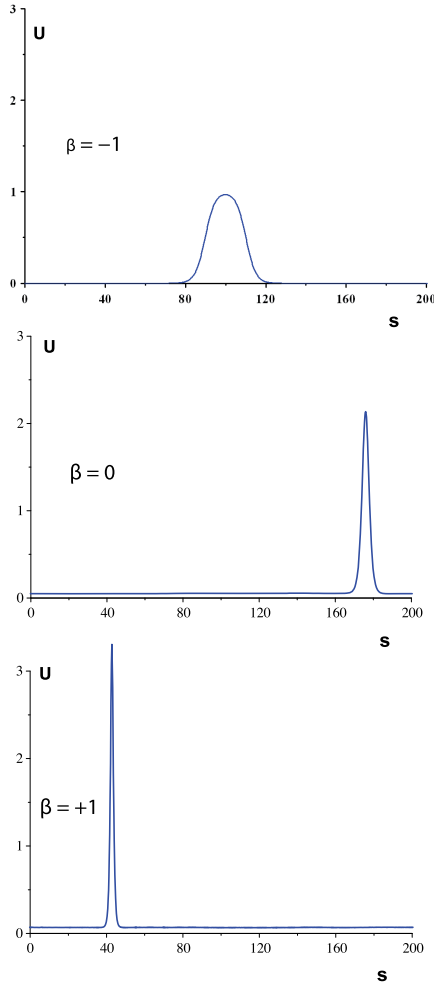

Fig. 6. Numerical simulation of the evKdV equation (6) with $\alpha = 1$, $\lambda = 1$ and β varies from -1 to 1, showing the transformation of a "table-top" solitary wave to a KdV "sech^2"-KdV solitary wave at the critical point, and further evolution as a solitary wave tending to a "sech"-profile.

allowing the wave to pass through the critical point $\beta = 0$ without destruction, but moving now from the upper branch in the lower panel of Fig. 2 to the "table-top" branch in the upper panel of Fig. 2. Third, suppose that initially $\beta > 0$ and $-1 > B > -\infty$. In this case it an be shown from (42) that $G(B)$ decreases from ∞ to a finite value of 2π as B increases from $-\infty$ to -1. Consequently the limit $\beta \to 0$ in (40) cannot be achieved. Instead as β decreases the limit $B = -1$ is reached, when the wave becomes an algebraic solitary wave, and a further decrease in β generates a breather.

4 Application to internal solitary waves in the South China Sea

In a typical oceanic situation, where there is a relatively sharp near-surface pycnocline, an internal solitary wave of depression is generated in the deep water and propagates shorewards until it reaches a critical point. For a simple two-layer model, this is where the pycnocline is close to the mid-depth, see (24). The theory described above then predicts that this wave will be destroyed in the vicinity of this critical point and replaced in the shallow water shorewards of the critical point by one or more internal solitary waves of elevation riding on a negative pedestal. This basic scenario has been observed in several places in the ocean, For instance, this phenomena has been reported by Salusti et al. (1989) in the Eastern Mediterranean, by Holloway et al. (1997, 1999) and Grimshaw et al. (2004) in the North West Shelf of Australia, by Hsu et al. (2000) in the East China Sea, during the ASIAEX experiment in the South China Sea by Duda et al. (2004), Liu et al. (1998, 2004), Orr and Mignerey (2003), Ramp et al. (2004), Yang et al. (2004), Zhao et al. (2003, 2004) and Zheng et al. (2003), and on the New Jersey shelf by Shroyer et al. (2009). Further, numerical simulations of the full Euler equations predict polarity reversal in Lake Constance (Vlasenko and Hutter, 2002), in the Andaman Sea (Vlasenko and Staschuk, 2007) and in the Saint Lawrence estuary (Bourgault et al., 2007). But elsewhere in the ocean, where there are no such critical points, the shoreward propagating small-amplitude internal solitary waves are expected to deform adiabatically (at least within the framework of the vKdV equation). Examples of this behaviour occur on the Malin Shelf off the North West coast of Scotland (Small, 2003; Grimshaw et al., 2004; Small and Hornby, 2005), in the Laptev Sea in the Arctic (Grimshaw et al., 2004) and in the COPE experiment on the Oregon shelf (Vlasenko et al., 2005).

The South China Sea (SCS) is well known as a location where internal solitary waves have been commonly observed, and has been intensively studied both experimentally and through numerical simulations, see for instance the reports based on the 2001 ASIAEX experiments by Duda et al. (2004), Ramp et al. (2004) and Liu et al. (2004). Typically, large amplitude internal waves are generated by the barotropic tidal currents, possibly combined with the Kuroshio current extension, interacting with the topography in Luzon Strait, see Liu et al. (1998), Cai et al. (2002), Ramp et al. (2004, 2006). Solitary-like waves with amplitudes up to 80 m (in a depth of 300 m) have been observed at the two underwater mountain ridges in Luzon Strait, see the bathymetry in Fig. 7 and the wave field in Fig. 8, taken from Liu et al. (2006). These waves cross the deep basin and then shoal on the continental shelf in water of depth 400–200 m, see for example the reports of the ASIAEX experiment by Duda et al. (2004), Ramp et al. (2004) and Liu et al. (2004). Wave amplitudes can reach to 100 m

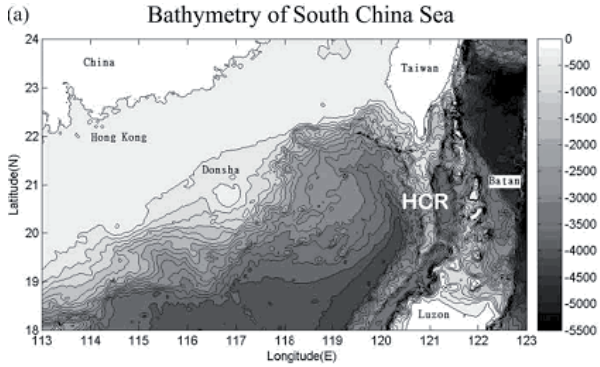

Fig. 7. Bathymetry of the northern part of the South China Sea, from Liu et al. (2006).

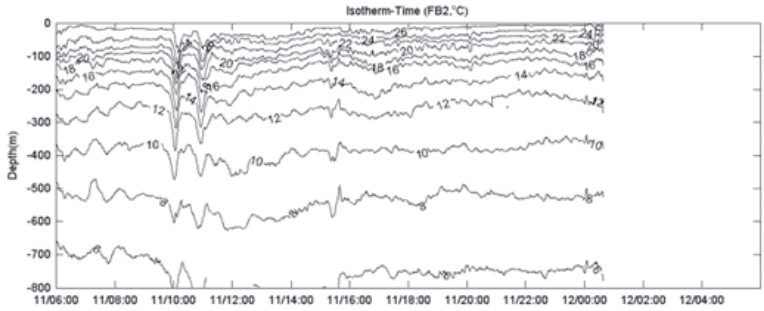

Fig. 8. Displacement of the isotherms as measured in the South China Sea, from Liu et al. (2006).

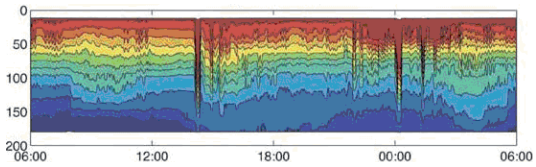

Fig. 9. Time series of internal waves in the South China Sea, from Duda et al. (2004).

and their shapes compare well with theoretical solitary wave shapes, see Klymak et al. (2006) and Fig. 9 from Liu et al. (2006). Numerical modeling of internal solitary wave transformation on the continental slope and shelf of the SCS has often been based on the vKdV and evKdV models, using mainly two-layer representations of the density stratification, and the results have been used to interpret the observed solitary wave evolution and especially the observed polarity changes, see Orr and Mingerey (2003), Zhao et al. (2003, 2004), Liu et al. (1998, 2004). There are also a few numerical simulations using the full Euler equations for stratified flow, see Buijsman et al. (2008), Du et al. (2008), Scotti et al. (2008), Warn-Varnas et al. (2010) and Vlasenko et al. (2010) for instance.

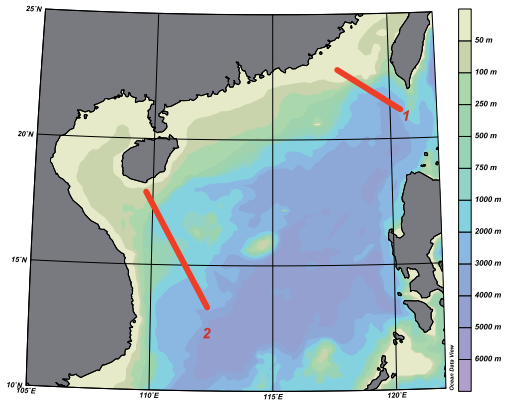

Fig. 10. Bathymetry of the South China Sea, with the chosen cross-sections.

We shall supplement these studies by a set of numerical simulations of the evKdV equation (6) for two typical cross-sections of the SCS, shown in Fig. 10. The first cross-section is close to the conditions for ASIAEX 2001, where the internal solitary waves are generated by westward tidal

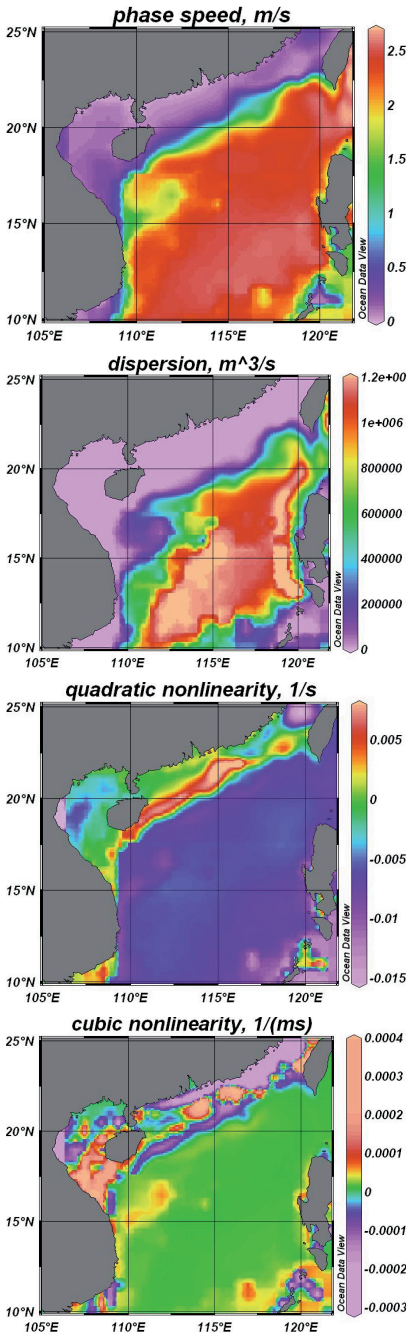

Fig. 11. Contour maps of the coefficients of the evKdV equation for the South China Sea. The plots are those for the phase speed c, the dispersion coefficient δ, the quadratic coefficient μ, and the cubic coefficient μ_1.

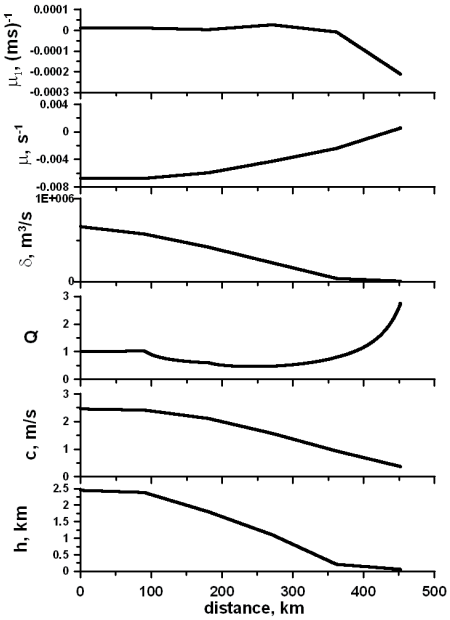

Fig. 12. Coefficients of the evKdV equation (5) along cross-section 1.

currents in Luzon Strait, see Liu et al. (2006) and Zhao and Alford (2006) for instance. The second cross-section is chosen to have a positive cubic nonlinear coefficient along the whole wave path. Contour maps of the linear long wave speed, the coefficients of the quadratic and cubic nonlinear terms and the coefficient of the linear dispersive term in the evKdV equation (5) are shown on Fig. 11. They are based on the vertical density profiles from the database GDEM for January (GDEM), while the bathymetry is taken from GEBCO. The speed c and the dispersion coefficient δ correlate well with the depth h as expected, see Talipova and Polukhin (2001) and Polukhin et al. (2003). The quadratic nonlinear coefficient μ is negative in the deep part of the SCS, and changes its sign to positive everywhere on the continental slope, as expected in the SCS, see Orr and Mignerey (2003) and Zhao et al. (2003, 2004) for instance. The cubic nonlinear coefficient, μ_1 is very small and positive in the deep part of the sea, but its sign changes in some parts of the continental slope to negative, while in other places it stays positive and grows in absolute value. To understand the role of quadratic and cubic nonlinearity in internal wave dynamics three values should be compared, c, μA, $\mu_1 A^2$. In the deep part of the SCS $c = 2.5\,\mathrm{m\,s^{-1}}$ and even if the internal wave amplitude is taken as 80 m (usually much less in deep water) $\mu A = 0.48\,\mathrm{m\,s^{-1}}$ and $\mu_1 A^2 = 0.13\,\mathrm{m\,s^{-1}}$; hence nonlinear effects are small in the deep part of the SCS. But on the continental slope c is less than $0.5\,\mathrm{m\,s^{-1}}$ and for the same

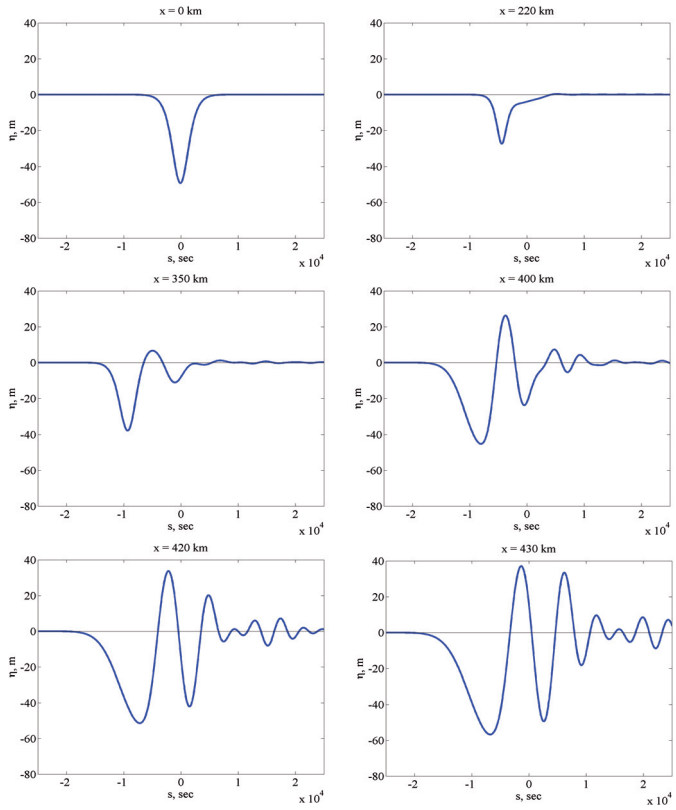

Fig. 13. Transformation of an internal solitary wave along cross-section 1.

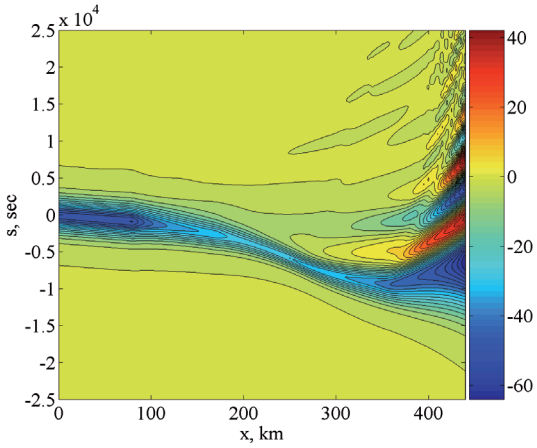

Fig. 14. Contour plot in the space-time domain of an internal solitary wave transformation along cross-section 1.

internal wave amplitude of about 80 m, $\mu A = 0.48\,\mathrm{m\,s^{-1}}$, comparable with c, and $\mu_1 A^2 = 1.28\,\mathrm{m\,s^{-1}}$, much large than the quadratic nonlinear term. Thus in the the shelf zones the waves are strongly nonlinear. Indeed the ratio of the nonlinear terms to the speed of propagation is about 3.5. Nevertheless, the eKdV (Gardner) model may be used as demonstrated by Maderich et al. (2009, 2010). However, it is pertinent to note that several other higher-order KdV-type models have been proposed, see the recent review by Apel et al. (2007) for instance.

4.1 Numerical results for cross-section 1

The wave path is close to the conditions of the ASIAEX 2001 experiment on the shelf (Ramp et al., 2004) and is here extended to the Luzon Strait to the site where the westward propagating solitary waves were observed see (Liu et al., 2006; Zhao and Alford, 2006 for instance). The model coefficients are shown on Fig. 12. The depth decreases from 2.5 km to 200 m, the linear long wave speed c varies from

$2.5\,\mathrm{m\,s^{-1}}$ to $0.2\,\mathrm{m\,s^{-1}}$, the linear modification factor Q is equal to 1 initially, then decreases to 0.5 at the location $x = 250$ km, before increasing to 2.5 on the shelf. Corresponding to the change of depth, the dispersion coefficient δ decreases along the cross-section. The nonlinear quadratic coefficient μ is negative for most of the wave path, but changes sign once only at a depth about 100 m. The cubic nonlinear coefficient μ_1 is positive in the deep water and becomes negative at a depth of about 400 m. Hence here there are two critical points, both on the shelf. The amplitude of the initial solitary wave (17) is chosen as 49 m at $x = 0$ in Fig. 14. This is less than that mentioned by Liu et al. (2006) where the amplitude of an observed solitary wave was estimated as 140 m, but it is large enough for our purposes.

The solitary wave evolution is shown in Fig. 13. The leading wave amplitude has decreased by a factor of two at $x = 220$ km from 49 m to 25 m. Over this same distance, the cubic nonlinear coefficient is almost constant, the quadratic nonlinear coefficient has decreased, the dispersive coefficient has decreased, while the linear modification factor has decreased by a factor of one-half; together these have the effect that the initial wave has started to deform with formation of a trailing tail. At the location $x = 350$ km the linear modification factor is decreasing, the cubic nonlinear coefficient changes sign and quadratic nonlinear coefficient tends to zero. The leading solitary wave now has an amplitude of about 35 m and is wider than at the location $x = 220$ km. At $x = 400$ km the quadratic nonlinear coefficient changes sign, and we see the typical destruction of the negative solitary wave, and the consequent generation of several positive solitary waves. The space-time contour plot of this internal wave transformation is shown in Fig. 14.

4.2 Numerical results for cross-section 2

On this cross-section, the initial point lies in deep water of depth $h = 3$ km, and the last point lies near Hainan Island. Here, the cubic nonlinear coefficient is positive everywhere, while the quadratic nonlinear coefficient changes sign on the shelf. The model coefficients are shown in Fig. 15. The depth decreases from 3 km to 200 m non-monotonically, producing the analogous tendencies for the dispersion coefficient δ, and the linear long wave speed c. The linear modification factor Q is initially close to one, and then decreases before increasing after the location $x = 700$ km. The quadratic coefficient μ grows after $x = 400$ km in absolute value and after $x = 580$ km tends to zero, changing sign at the location $x = 700$ km. The cubic coefficient μ_1 is positive everywhere, but grows by an order of magnitude.

This is a scenario when we might expect the formation of a breather from a solitary wave at the location of where the quadratic coefficient changes sign, provided the leading wave amplitude is large enough. Here we did two runs with initial solitary wave amplitudes of 23 m and 41 m. The solitary wave transformation for the first run is shown in Fig. 16. Due to the increase of the cubic nonlinear coefficient the initial solitary wave becomes narrower and a trailing tail emerges, developing oscillations after $x = 600$ km. This process occurs without a significant change in the leading wave amplitude because the modification factor increases slowly. At the location $x = 700$ km a "sech"-like solitary wave has appeared. Then, at the location $x = 730$ km the quadratic nonlinear coefficient changes sign, but the leading wave amplitude is then not large enough for transformation into a "sech"-like solitary wave of negative polarity, but with a positive quadratic coefficient. Instead, the wave disintegrates and at the location $x = 760$ km, we see the formation of secondary solitary waves of opposite polarity. The space-time contour plot of this run is shown in Fig. 17.

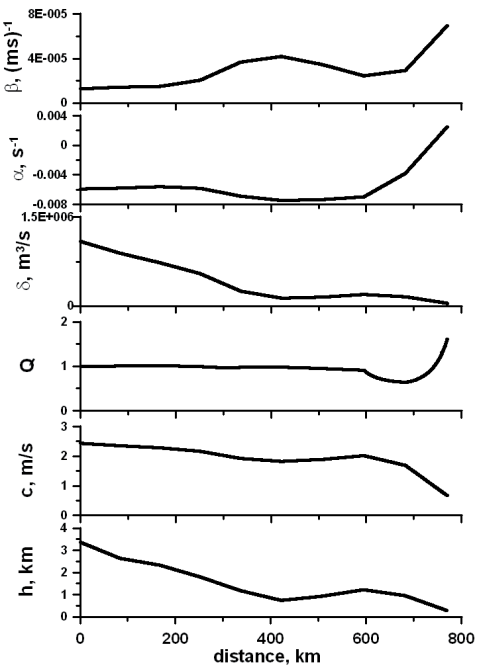

Fig. 15. Coefficients of the evKdV equation (5) along cross-section 2.

The second run has an initial amplitude of 41 m. The solitary wave transformation is shown in Fig. 18. Again a "sech"-like solitary wave forms by the location $x = 500$ km, and its amplitude grows to 60 m. At the location $x = 600$ m a second solitary waves begins to form, and due to the increase of the linear modification factor Q, the amplitude of leading wave decreases to about 45 m. Then as the quadratic nonlinear coefficient tends to zero, the cubic nonlinear coefficient grows rapidly, and the leading solitary wave begin to destruct around the location $x = 700$ km, until at the location $x = 720$ km there is a strong indication that an internal breather has formed in association with an

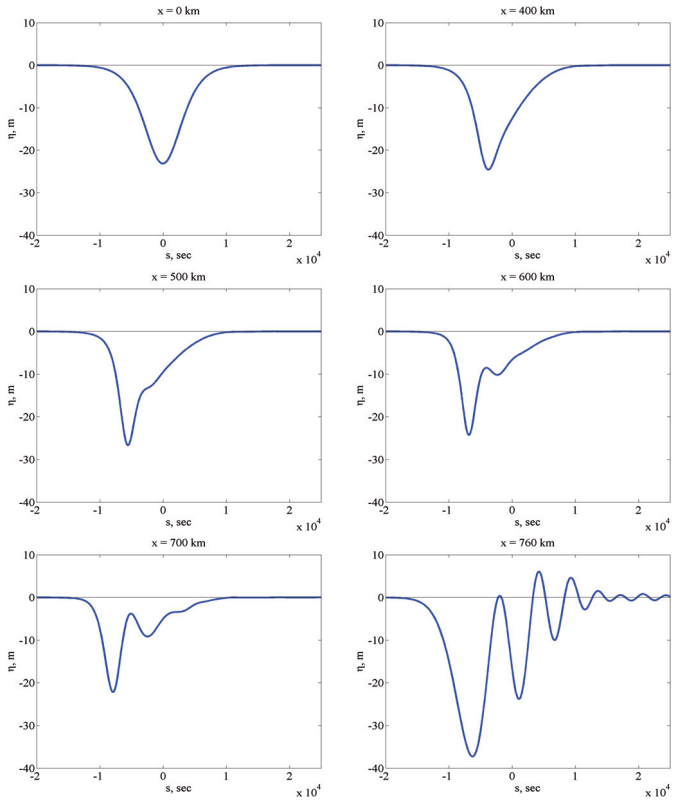

Fig. 16. Transformation of an internal solitary wave along cross-section 2, initial amplitude 23 m.

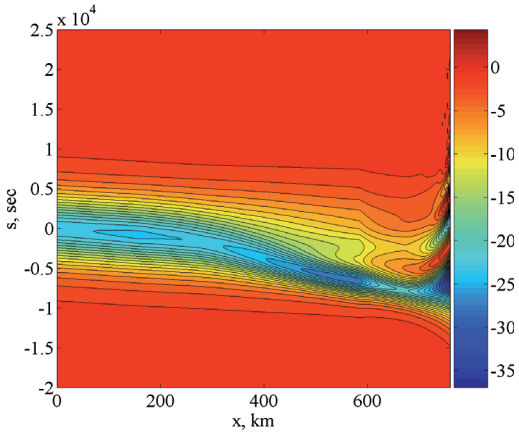

Fig. 17. Transformation of an internal solitary wave along cross-section 2, initial amplitude 23 m.

oscillatory trailing wave train. The division of the initial solitary wave into two is clearly shown in the space-time contour plots in Fig. 19, from the location $x = 400$ km to the location $x = 650$ km, with breather formation after $x = 700$ km.

5 Discussion

As we have mentioned in the Introduction, the vKdV equation (3) and its extension to allow for cubic nonlinearity, the evKdV equation (6) have been widely used to model the propagation of large amplitude internal solitary waves in coastal seas. In this review article we have presented a brief outline of the derivation of these models by an asymptotic expansion from the full Euler equations. Then we have described how an examination of the slowly-varying solitary wave solutions lead to the concept that the critical point where the coefficient of the quadratic, or of he cubic, nonlinear term is zero defines a location of special interest where a solitary wave may undergo a dramatic transformation, often involving a polarity change

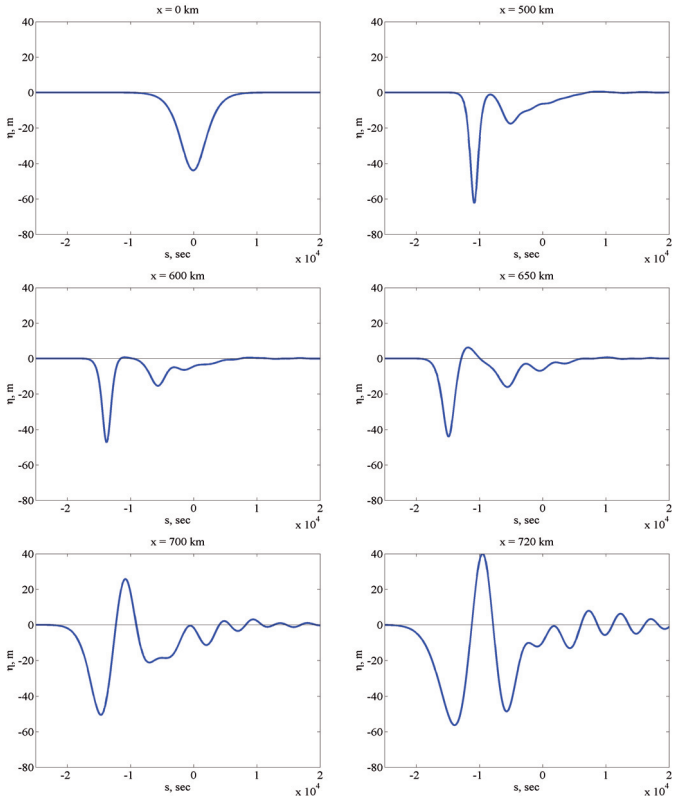

Fig. 18. Transformation of an internal solitary wave along cross-section 2, initial amplitude 41 m.

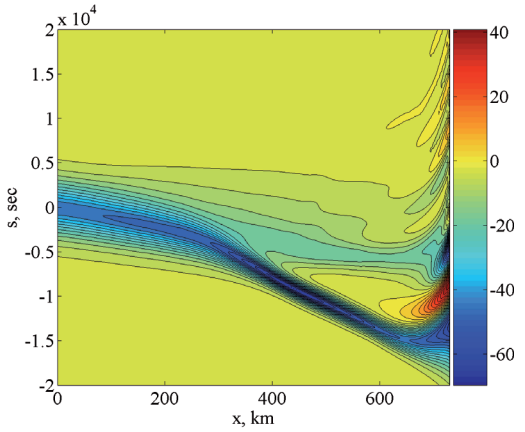

Fig. 19. Contour plot in the space-time domain of an internal solitary wave transformation along cross-section 2, initial amplitude 41 m.

and a disintegration into a wave train. We have illustrated this in detail for two contrasting cross-sections of the coastal shelf of the South China Sea. Each cross-section is based on the GDEM database of sea stratification, and the bathymetry database GEBCO. The first cross-section is taken across the shelf where the ASIAEX 2001 experiment took place, and we have simulated the transformation of an internal solitary wave generated in the Luzon Strait, propagating across the cross deep part of the sea to the opposite shelf, where a change in its polarity takes place, The second cross-section is taken across a region where the cubic nonlinear coefficient is positive everywhere. In this case an initial solitary wave of moderate amplitude transforms into two solitary waves. Th first wave is a ”sech”-like solitary wave, and the two waves interact near the location where the quadratic nonlinear coefficient changes sign, with transformation into a breather This demonstrates the possibility of internal breather generation from an initial solitary wave in a realistic ocean situation. It is the the second example of such a transformation, the first being a simulation for the North West Australian Shelf, see Grimshaw et al. (2007).

There are several important issues relating to internal solitary waves, which we have not considered here, notably stability, transverse structure, the effect of the background earth rotation and the effect of friction. An extension of the evKdV model (6) which takes into account of the last three factors could be

$$\left\{A_t + cA_x - \frac{cQ_x}{Q}A + \mu A\,A_x + \mu_1 A^2 A_x + \delta A_{xxx} + \nu|A|A\right\}_x + \frac{c}{2}\left(A_{yy} - \frac{f^2}{c^2}A\right) = 0. \quad (46)$$

The transverse term A_{yy} is just that which converts the KdV equation into its well-known two-dimensional extension, the KP equation, while the rotation term contains the Coriolis parameter f and was originally introduced by Ostrovsky (1978) and later by Grimshaw (1985) with the transverse term added as well. It is known that the effect of background rotation is to cause a solitary wave to decay through the radiation of inertia-gravity waves, see the review by Helfrich and Melville (2006) and the recent studies by Grimshaw and Helfrich (2008) and Sánchez-Garrido and Vlasenko (2009). In practice, the time-scale for this decay is one or two inertial periods. In (46) we have chosen Chezy friction, as this is the one most commonly used, although other forms of friction such as boundary-layer friction or Burgers-type friction have been proposed. The friction coefficient is given by

$$I\nu = \rho_0 C_D (c-u_0)^2 |\phi_z|^3, \quad \text{at } z = -h, \quad (47)$$

where C_D is the usual drag coefficient, while the modal functions and the integral I are defined by (10, 11, 15). Clearly friction will cause the solitary wave to decay, but as oceanic internal solitary waves are observed to be long-lived, this decay is evidently quite slow. There have been several recent observational studies of the decay of shoaling internal solitary waves from which we infer that the time scale is around an inertial period, and the decay process itself is complicated by the generation of localized shear instability, see for instance Moum et al. (2007) and Shroyer et al. (2010). We also note the interesting theoretical prediction by Grimshaw et al. (2003) that a decaying solitary wave with the parameter $B < -1$ (which requires that $\delta\mu_1 > 0$) may transform into a breather. Finally, we comment that although solitary waves are stable in the framework of the KdV or eKdV equations, in practice they can be unstable due to localized shear instability. This is a high-wavenumber phenomenon, which is not captured in the present long-wave asymptotic models. There have been several laboratory studies of shear instabiity of internal solitary waves, see Fructus et al. (2009) for a recent study, and several analogous ocean observations, see Moum et al. (2003, 2007).

Acknowledgements. This work was partially supported by grants RFBR 09-05-90408, 09-05-20024 (TT), and by RFBR 10-05-00199, Russian Grant for young scientists MK-846.2009.1 (O.K).

Edited by: V. I. Vlasenko
Reviewed by: Y. A. Stepanyants and two other anonymous referees

References

Apel, J., Ostrovsky, L. A., Stepanyants, Y. A., and Lynch, J. F.: Internal solitons in the ocean and their effect on underwater sound, J. Acoust. Soc. Am., 121, 695–722, 2007.

Benjamin, T. B.: Internal waves of finite amplitude and permanent form, J. Fluid Mech., 25, 241–270, 1966.

Benney, D. J.: Long non-linear waves in fluid flows, J. Math. Phys., 45, 52–63, 1966.

Bourgault, D., Blokhina, M. D., Mirchak, R., and Kelly, D. E.: Evolution of a shoaling internal solitary wave train, Geophys. Res. Lett., 34, L03601, doi:10.1029/2006GL028462, 2007.

Boussinesq, M. J.: Théorie de l'intumescence liquide appellée onde solitaire ou de translation, se propageant dans un canal rectangulaire, Comptes Rendus Acad. Sci., Paris, 72, 755–759, 1871 (in French).

Buijsman, M. C., Kanarska, Y., and McWilliams, J. C.: On the generation and evolution of nonlinear internal waves in the South China Sea, J. Geophys. Res., 115, C02012, doi:10.1029/2009JC005275, 2010.

Cai, S., Long, X., and Gan, Z.: A numerical study of the generation and propagation of internal solitary waves in the Luzon Strait, Oceanol. Acta, 25, 51–60, 2002.

Clarke, S., Grimshaw, R., Miller, P., Pelinovsky, E., and Talipova, T.: On the generation of solitons and breathers in the modified Korteweg-de Vries equation, Chaos, 10, 383–392, 2000.

Djordjevic, V. and Redekopp, L.: The fission and disintegration of internal solitary waves moving over two-dimensional topography, J. Phys. Oceanogr., 8, 1016–1024, 1978.

Du, T., Tseng, Y.-H., and Yan, X.-H.: Impacts of tidal currents and Kuroshio intrusion on the generation of nonlinear internal waves in Luzon Strait, J. Geophys. Res., 113, C08015, doi:10.1029/2007JC004294, 2008.

Duda, T. F., Lynch, J. F., Irish, J. D., Beardsley, R. C., Ramp, S. R., Chiu, C.-S., Tang, T. Y., and Yang, Y.-J.: Internal tide and nonlinear internal wave behavior at the continental slope in the northern south China Sea, IEEE J. Oceanic Eng., 29, 1105–1130, 2004.

El, G. A. and Grimshaw, R.: Generation of undular bores in the shelves of slowly-varying solitary waves, Chaos, 12, 1015–1026, 2002.

Fructus, D., Carr, M., Grue, J., Jensen, A., and Davies, P. A.: Shear induced breaking of large amplitude internal solitary waves, J. Fluid Mech., 620, 1–29, 2009.

Grimshaw, R.: Slowly varying solitary waves. I: Korteweg-de Vries equation, Proc. Roy. Soc. A, 368, 359–375, 1979.

Grimshaw, R.: Evolution equations for long nonlinear internal waves in stratified shear flows, Stud. Appl. Math., 65, 159–188, 1981.

Grimshaw, R.: Evolution equations for weakly nonlinear, long internal waves in a rotating fluid, Stud. Appl. Math., 73, 1–33, 1985.

Grimshaw, R.: Internal solitary waves. In: Environmental Stratified Flows, edited by: Grimshaw, R., Kluwer, Boston, Chapter 1, 1–28, 2001.

Grimshaw, R.: Internal solitary waves in a variable medium, Gesellschaft fur Angewandte Mathematik, 30, 96–109, 2007.

Grimshaw, R. and Mitsudera, H.: Slowly-varying solitary wave solutions of the perturbed Korteweg-de Vries equation revisited, Stud. Appl. Math., 90, 75–86, 1993.

Grimshaw, R., Pelinovsky, E., and Talipova, T.: Solitary wave transformation due to a change in polarity, Stud. Appl. Math., 101, 357–388, 1998a.

Grimshaw, R., Pelinovsky, E., and Talipova, T.: Solitary wave transformation in a medium with sign-variable quadratic nonlinearity and cubic nonlinearity, Physica D, 132, 40–62, 1999.

Grimshaw, R., Pelinovsky, E., and Poloukhina, O.: Higher-order Korteweg-de Vries models for internal solitary waves in a stratified shear flow with a free surface, Nonlin. Processes Geophys., 9, 221–235, doi:10.5194/npg-9-221-2002, 2002.

Grimshaw, R, Pelinovsky, E and Talipova, T.: Damping of large-amplitude solitary waves, Wave Motion, 37, 351–364, 2003.

Grimshaw, R. H. J. and Pudjaprasetya, S. R.: Generation of secondary solitary waves in the variable-coefficient Korteweg-de Vries equation, Stud. Appl. Math., 112, 271–279, 2004.

Grimshaw, R., Pelinovsky, E., Talipova, T., and Kurkin, A.: Simulation of the transformation of internal solitary waves on oceanic shelves J. Phys. Oceanogr., 34, 2774–2779, 2004.

Grimshaw, R., Pelinovsky, E., Stepanyants, Y., and Talipova, T.: Modelling internal solitary waves on the Australian North West Shelf, Mar. Freshwater Res., 57, 265–272, 2006.

Grimshaw, R., Pelinovsky, E., and Talipova, T.: Modeling internal solitary waves in the coastal ocean, Surv. Geophys., 28, 273–298, 2007.

Grimshaw, R. and Helfrich, K. R.: Long-time solutions of the Ostrovsky equation, Stud. Appl. Math., 121, 71–88, 2008.

Grimshaw, R., Slunyaev, A., and Pelinovsky, E.: Generation of solitons and breathers in the extended Korteweg-de Vries equation with positive cubic nonlinearity, Chaos, 20, 013102, doi:10.1063/1.3279480, 2010.

Helfrich, K. R. and Melville, W. K.: Long nonlinear internal waves, Annu. Rev. Fluid Mech., 38, 395–425, 2006.

Holloway, P., Pelinovsky, E., Talipova, T., and Barnes, B.: A nonlinear model of the internal tide transformation on the Australian North West Shelf, J. Phys. Oceanogr., 27, 871–896, 1997.

Holloway, P., Pelinovsky, E., and Talipova, T.: A generalised Korteweg-de Vries model of internal tide transformation in the coastal zone, J. Geophys. Res., 104, 18333–18350, 1999.

Holloway, P., Pelinovsky, E., and Talipova, T.: Internal tide transformation and oceanic internal solitary waves, in: Environmental Stratified Flows, edited by: Grimshaw, R., Kluwer, Boston, Chapter 2, 29–60, 2001.

Hsu, M.-K., Liu, A. K., and Liu, C.: A study of internal waves in the China Seas and Yellow Sea using SAR, Cont. Shelf Res., 20, 389–410, 2000.

Johnson, R. S.: On an asymptotic solution of the Korteweg-de Vries equation with slowly varying coefficients, J. Fluid Mech., 60, 813–824, 1973a.

Johnson, R. S.: On the development of a solitary wave moving over an uneven bottom, Proc. Camb. Philos. Soc., 73, 183–203, 1973b.

Klymak, J. M., Pinkel, R., Liu, Ch.-T., Liu, A. K., and David, L.: Prototypical solitons in the South China Sea, Geophys. Res. Lett., 33, L11607, doi:10.1029/2006GL025932, 2006.

Knickerbocker, C. J. and Newell, A. C.: Internal solitary waves near a turning point, Phys. Lett. A, 75, 326–330, 1978.

Knickerbocker, C. J. and Newell, A. C.: Shelves and the Korteweg-de Vries equation, J. Fluid Mech., 98, 803–818, 1980.

Korteweg, D. J. and de Vries, H.: On the change of form of long waves advancing in a rectangular canal, and on a new type of long stationary waves, Philos. Mag., 39, 422–443, 1895.

Lamb, K. G., Polukhina, O., Talipova, T., Pelinovsky, E., Xiao, W., and Kurkin, A.: Breather generation in fully nonlinear models of a stratified fluid, Phys. Rev. E, 75, 046306, doi:10.1103/PhysRevE.75.046306, 2007.

Liu, A. K., Chang, Y. S., Hsu, M.-K., and Liang, N. K.: Evolution of nonlinear internal waves in the East and South China Seas, J. Geophys. Res., 103, 7995–8008, 1998.

Liu, A. K., Ramp, S. R., Zhao, Y., and Tswen Yung Tang, T. Y.: A case study of internal solitary wave propagation during ASIAEX 2001, IEEE J. Oceanic Eng., 29, 1144–1156, 2004.

Liu, Ch.-T., Pinkel, R., Klymak, J., Hsu, M.-K., Chen, H.-W., and Villanoy, C.: Nonlinear internal waves from the Luzon Strait, EOS T. Am. Geophys. Un., 87, 449–451, 2006.

Maderich, V., Talipova, T., Grimshaw, R., Pelinovsky, E., Choi, B. H., Brovchenko, I., Terletska, K., and Kim, D. C.: The transformation of an interfacial solitary wave of elevation at a bottom step, Nonlin. Processes Geophys., 16, 33–42, doi:10.5194/npg-16-33-2009, 2009.

Maderich, V., Talipova, T., Grimshaw, R., Terletska, E., Brovchenko, I., Pelinovsky, E., and Choi, B. H.: Interaction of a large amplitude interfacial solitary wave of depression with a bottom step, Phys. Fluids, 22, 076602, doi:10.1063/1.3455984, 2010.

Moum, J. N., Farmer, D. M., Smyth, W. D., Armi, L., and Vagle, S.: Structure and generation of turbulence at interfaces strained by internal solitary waves propagating shoreward over the continental shelf, J. Phys. Oceanogr., 33, 2093–2112, 2003.

Moum, J. N., Farmer, D. M., Shroyer, E. L., Smyth, W. D., and Armi, L.: Dissipative losses in nonlinear internal waves propagating across the continental shelf, J. Phys. Oceanpgr., 37, 1989–1995, 2007.

Nakoulima, O., Zahibo, N., Pelinovsky, E., Talipova, T., Slunyaev, A., and Kurkin, A.: Analytical and numerical studies of the variable-coefficient Gardner equation, Appl. Math. Comput., 152, 449–471, 2004.

Orr, M. H. and Mignerey, P. C.: Nonlinear internal waves in the South China Sea: Observation of the conversion of depression internal waves to elevation internal waves, J. Geophys. Res., 108(C3), 3064, doi:10.1029/2001JC001163, 2003.

Ostrovsky, L.: Nonlinear internal waves in a rotating ocean, Oceanogology, 18, 119–125, 1978.

Ostrovsky, L. A. and Pelinovsky, E. N.: Wave transformation on the surface of a fluid of variable depth, Akad. Nauk SSSR, Izv. Atmos. Ocean Phys., 6, 552–555, 1970.

Ostrovsky, L. A. and Stepanyants, Y. A.: Internal solitons in laboratory experiments: Comparison with theoretical models, Chaos, 15, 037111, doi:10.1063/1.2107087, 28 pp., 2005.

Pelinovsky, D. and Grimshaw, R. H. J.: Structural transformation of eigenvalues for a perturbed algebraic soliton potential, Phys. Lett. A, 229, 165–172, 1997.

Polukhin, N., Talipova, T., Pelinovsky, E., and Lavrenov, I.: Kinematic characteristics of the high-frequency internal wave field in the Arctic, Oceanology, 43, 333–343, 2003.

Ramp, S. R., Tang, T. Y., Duda, T. F., Lynch, J. F., Liu, A. K., Chiu, C.-S., Bahr, F. L., Kim, H.-R., and Yang, Y.-J.: Internal solitons in the northeastern South China Sea, Part I: sources and deep water propagation, IEEE J. Oceanic Eng., 29, 1157–1181, 2004.

Rayleigh, J. W. S.: On waves, Philos. Mag., 1, 257–279, 1876.

Russell, J. S.: Report on Waves, 14th meeting of the British Association for the Advancement of Science, 311–390, 1844.

Salusti, F., Lascaratos, A., and Nittis, K.: Changes of polarity in marine internal waves: Field evidence in eastern Mediterranean Sea, Ocean Model., 82, 10–11, 1989.

Sánchez-Garrido, J. C. and Vlasenko, V.: Long-term evolution of strongly nonlinear internal solitary waves in a rotating channel, Nonlin. Processes Geophys., 16, 587–598, doi:10.5194/npg-16-587-2009, 2009.

Scotti, A., Beardsley, R. C., Butman, B., and Pineda, J.: Shoaling of nonlinear internal waves in Massachusetts Bay, J. Geophys. Res., 113, C08031, doi:10.1029/2008JC004726, 2008.

Shroyer, E. L., Moum, J. N., and Nash, J. D.: Observations of polarity reversal in shoaling nonlinear internal waves, J. Phys. Oceanogr., 39, 691–701, 2009.

Shroyer, E. L., Moum, J. N., and Nash, J. D.: Energy transformations and dissipation of nonlinear internal waves over New Jersey's continental shelf, Nonlin. Processes Geophys., 17, 345–360, doi:10.5194/npg-17-345-2010, 2010.

Small, J.: A nonlinear model of the shoaling and refraction of interfacial solitary waves in the ocean. Part I: Development of the model and investigations of the shoaling effect, J. Phys. Oceanogr., 31, 3163–3183, 2001a.

Small, J.: A nonlinear model of the shoaling and refraction of interfacial solitary waves in the ocean. Part II: Oblique refraction across a continental slope and propagation over a seamount, J. Phys. Oceanogr., 31, 3184–3199, 2001b.

Small, J. Refraction and shoaling of nonlinear internal waves at the Malin Shelf Break, J. Phys. Oceanogr., 33, 2657–2674, 2003.

Small, R. J. and Hornby, R. P.: A comparison of weakly and fully non-linear models of the shoaling of a solitary internal wave, Ocean Model, 8, 395–416, 2005.

Talipova, T. and Polukhin, N.: Averaged characteristics of the internal wave propagation parameters in the World Ocean, Izvestia of Russian Academy of Engineering Sciences, Series: Applied Mathematics and Informatics, 2, 139–155, 2001.

Vlasenko, V. I. and Hutter, K.: Transformation and disintegration of strongly nonlinear internal waves by topography in stratified lakes, Ann. Geophys., 20, 2087–2103, doi:10.5194/angeo-20-2087-2002, 2002.

Vlasenko, V. I., Stashchuk, N. M., and Hutter, K.: Baroclinic Tides: Theoretical Modelling and Observational Evidence, Cambridge University Press, Cambridge, 2005.

Vlasenko, V. I., Ostrovsky, L. A., and Hutter, K.: Adiabatic behaviour of strongly nonlinear internal solitary waves in slope-shelf areas, J. Geophys. Res., 110, C04006, doi:10.1029/2004JC002705, 2005.

Vlasenko, V. and Stashchuk, N.: Three-dimensional shoaling of large amplitude internal waves, J. Geophys. Res., 112, C11018, doi:10.1029/2007JC004107, 2007

Vlasenko, V., Stashchuk, N., Guo, C., and Chen, X.: Multimodal structure of baroclinic tides in the South China Sea, Nonlin. Processes Geophys., 17, 529–543, doi:10.5194/npg-17-529-2010, 2010.

Warn-Varnas, A., Hawkins, J., Lamb, K. G., Piacsek, S., Chin-Bing, S., King, D., and Burgos, G.: Solitary wave generation dynamics at Luzon Strait, Ocean Model., 31, 9–27, 2010.

Yang, Y.-J., Tang, T. Y., Chang, M. H., Liu, A. K., Hsu, M.-K., and Ramp, S. R.: Solitons northeast of Tung-Sha Island during the ASIAEX pilot studies, IEEE J. Oceanic Eng., 29, 1182–1199, 2004.

Zhao, Z., Klemas, V. V., Zheng, Q., Li, X., and Yan, X.-H.: Satellite observation of internal solitary waves converting polarity, Geophys. Res. Lett., 30(19), 1988, doi:10.1029/2003GL018286, 2003.

Zhao, Z., Klemas, V. V., Zheng, Q., Li, X., and Yan, X.-H.: Estimating parameters of a two-layer stratified ocean from polarity conversion of internal solitary waves observed in satellite SAR images, Remote Sens. Environ., 92, 276–287, 2004.

Zhao, Z. and Alford, M. H.: Source and propagation of internal solitary waves in the northeastern South China Sea, J. Geophys. Res., 111, C11012, doi:10.1029/2006JC003644, 2006.

Zheng, Q., Klemas, V., Yan, X.-H., and Pan, J.: Nonlinear evolution of ocean internal solitons propagating along an inhomogeneous thermocline, J. Geophys. Res., 106, 14083–14094, 2001.

Zheng, Q., Klemas, V., Zheng, Q., and Yan, X.-H.: Satellite observation of internal solitary waves converting polarity, Geophys. Res. Lett., 30(19), 4–1, 2003.

Zhou, X. and Grimshaw, R.: The effect of variable currents on internal solitary waves, Dynam. Atmos. Oceans., 14, 17–39, 1989.

Paper II

Kurkina O., Talipova, T. Huge internal waves in the vicinity of the Spitsbergen Island (Barents Sea). – Natural Hazards and Earth System Sciences 11; 2011, p. 981–986.

Nat. Hazards Earth Syst. Sci., 11, 981–986, 2011
www.nat-hazards-earth-syst-sci.net/11/981/2011/
doi:10.5194/nhess-11-981-2011

Natural Hazards and Earth System Sciences

Huge internal waves in the vicinity of the Spitsbergen Island (Barents Sea)

O. E. Kurkina[1,2,3] **and T. G. Talipova**[4]

[1]Institute of Cybernetics, Tallinn University of Technology, Tallinn, Estonia
[2]State University The Higher School of Economics, Nizhny Novgorod Branch, Nizhny Novgorod, Russia
[3]Nizhny Novgorod State Technical University, Nizhny Novgorod, Russia
[4]Institute of Applied Physics of Russian Academy of Sciences, Nizhny Novgorod, Russia

Received: 21 September 2010 – Revised: 6 January 2011 – Accepted: 7 January 2011 – Published: 25 March 2011

Abstract. The generation of huge amplitude internal waves by the barotropic tide in the Barents Sea at high latitudes is examined using the numerical model of the Euler 2-D equations for incompressible stratified fluid. The area considered is located between the Spitsbergen (Svalbard) Island and the Franz-Victoria Trough with a cross-section of 350 km length. There are two underwater hills about 100–150 m high on the background depth of about 300 m. It is shown that intensive nonlinear internal waves with amplitudes up to 50 m and lengths of about 6–12 km are generated in this zone. The total height of such waves is huge and they must be considered as a significant factor of the environment in this basin.

1 Introduction

Internal waves in the shelf zones are generated mainly by tidal forcing. Very often they have huge amplitudes reaching sometimes a hundred meters and are observed over and over again everywhere in coastal zones of the World oceans (Morozov, 1985; Ostrovsky and Stepanyants, 1989; Helfrich and Melville, 2006; Vlasenko et al., 2005; Apel et al., 2007; Duda et al., 2004). Intensive internal waves generated over the shelf edge and continental slope are an important source of strong currents, vertical mixing (Babu and Rao, 2010), bottom erosion (Bogucki and Redekopp, 1999). They strongly impact on acoustic fields and significantly reduce the distance of acoustic pulse propagation (Apel et al., 2007; Warn-Varnas et al., 2009; Sridevi et al., 2010), and may be dangerous for underwater vehicles and underwater parts of oil platforms and pipelines. The prediction of underwater weather is becoming a branch of hydrometeorology now and the analysis of the baroclinic disturbances periodically generated by barotropic tide over topography is the first and principal step in this problem. Detection of zones where internal waves have amplitudes large enough can be done with help of numerical modeling methods.

The modeling of tidal internal waves on various shelves of the World oceans is carried out now using numerical models of different levels (see, for example, Helfrich and Melville, 2006; Vlasenko et al., 2005; Holloway et al., 1999; Warn-Varnas et al., 2005, 2010). We are focusing here on the Barents Sea, and moreover, on internal waves generated over the critical latitude (74.5° N) for the semidiurnal (M_2) tide. The critical latitude is determined as the latitude φ where the tidal frequency equals the local inertial frequency $f = 2\Omega_E \sin\varphi$, $\Omega_E = 0.00007292\,\mathrm{s}^{-1}$ is the frequency of the Earth's rotation. The linear theory of baroclinic tide generation predicts that there is no baroclinic wave generation over this latitude (LeBlond and Mysak, 1978). Nevertheless observations show existence of internal waves of very large amplitudes here.

We reproduce briefly the description of results (Morozov and Pisarev, 2002; Pisarev, 1996): *"Special measurements of internal waves with distributed temperature sensors were carried out from drifting ice in 1983 in Saint Anna Trough and in 1986–1989 in Franz Victoria Trough. The latitude of the measurements was 80°–81° N and the depths were within bounds of 200–500 m. In addition to the other phenomena, very short and localized semidiurnal internal waves were found. Their lengths were within 2–6 km. They were propagating from the slope of the trough and their amplitudes reached 40 m. When the measuring instruments drifted from the slopes of the trough to a distance of 20–40 km toward flat bottom regions, the amplitude of these waves significantly decreased. Under certain stipulations, these semidiurnal waves were classified as internal tides."*.

Correspondence to: O. E. Kurkina
(oksana.kurkina@mail.ru)

Published by Copernicus Publications on behalf of the European Geosciences Union.

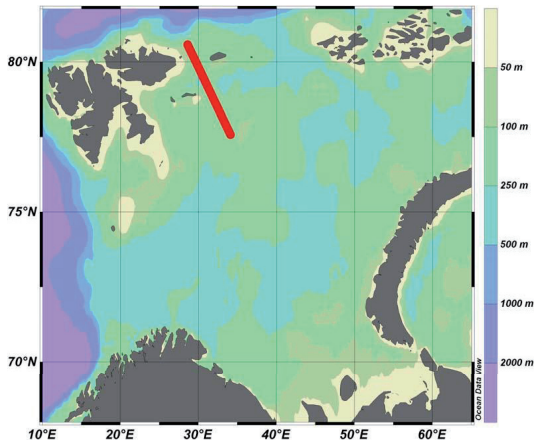

Fig. 1. Area map with the cross-section (red strip) between the points 34.11° E, 77.57° N and 28.61° E, 80.58° N.

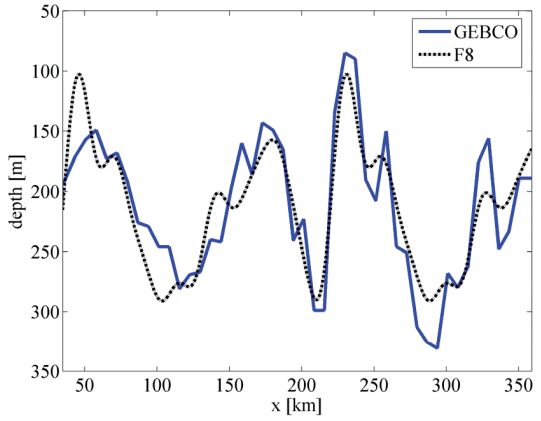

Fig. 2. Bottom relief of the area cross-section shown in Fig. 1 (blue line is GEBCO, dotted line is the spline).

The possibility of the generation of internal tidal waves by topography above the critical latitude was shown by Nakamura et al. (2000), with the use of the fully nonlinear nonhydrostatic model. These waves are generated and trapped by the barotropic tidal flux at the lee side of the sill. They were called unsteady lee waves and their amplitudes depend on the amplitude of the tidal flow speed and steepness of the bottom topography. Vlasenko et al. (2003) were the first who modeled the nonlinear generation of internal waves near and over the critical latitude in the Barents Sea near Bear Island and found propagated short nonlinear internal waves with amplitudes about 20 m.

The aim of this paper is to explain the nature of large amplitude internal waves observed over the critical latitude

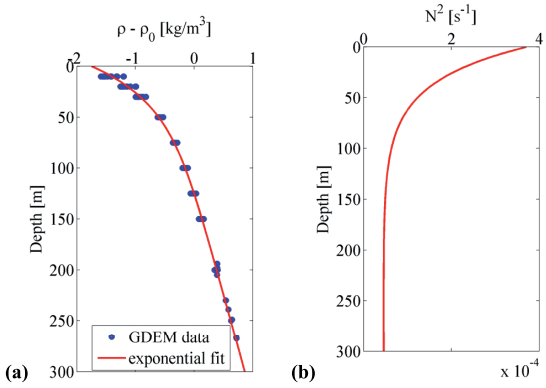

Fig. 3. The typical vertical density profile **(a)** in the studied area and the Brunt-Väisälä frequency **(b)** taken from the Database GDEM for July.

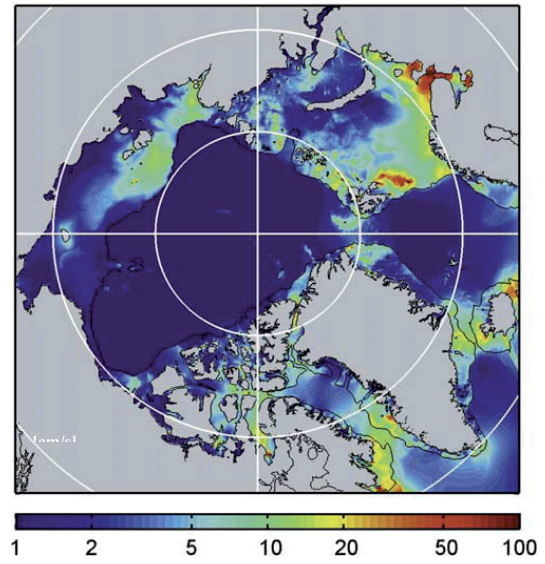

Fig. 4. The mean tidal current speed ($cm\,s^{-1}$) based on the simulation of 14 days of hourly total tidal speed from the 8-constituent inverse solution AOTIM.

(mainly in the Franz Victoria Trough), using the numerical results within the framework of fully nonlinear Euler equations for stratified water, their features and to carry out the forecast of dangerous underwater events for this region. The paper is organized as following: the numerical model is briefly described in Sect. 2, model input is discussed in Sect. 3 and in Sect. 4 the results of the numerical modeling are presented. They are discussed in Sect. 5.

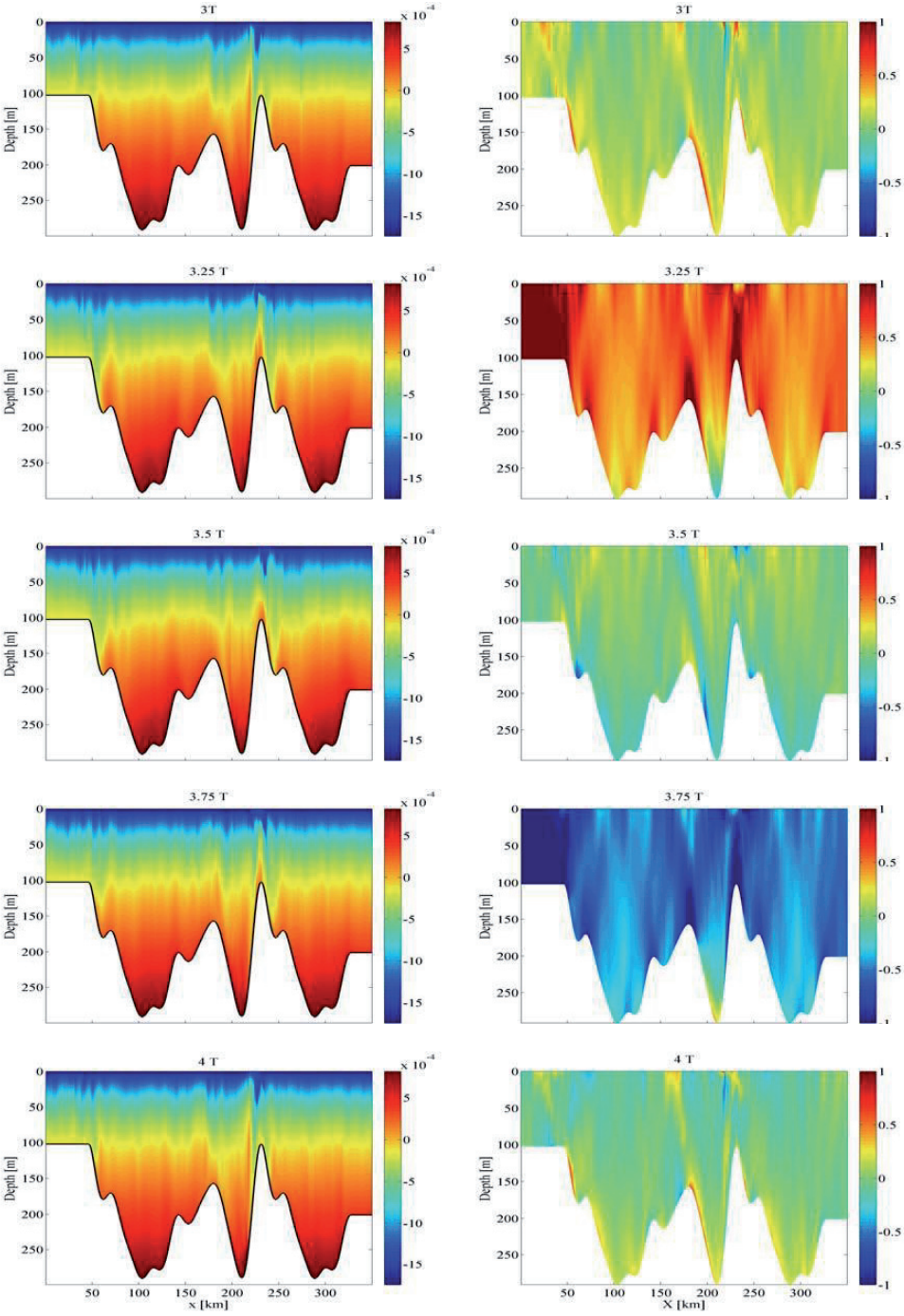

Fig. 5. Snapshots of the normalized density (left panel) and horizontal velocity (in m s^{-1}) (right panel).

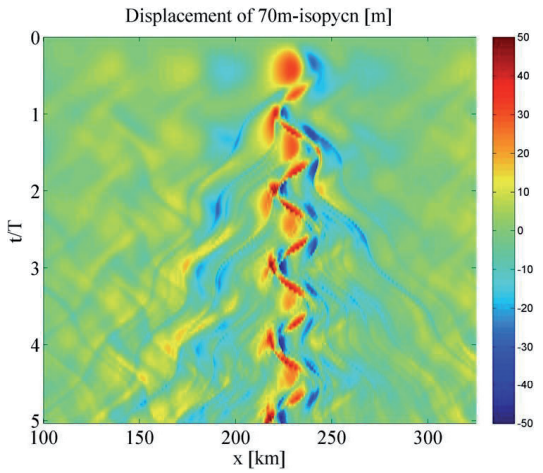

Fig. 6. The Hovmuller plot for the displacement of the isopycn located at 70 m depth in the undisturbed state.

2 Numerical model

The Lamb (1994) model is taken for simulating the generation and propagation of internal waves in the Barents Sea. The model equations are the two-dimensional (vertical section) inviscid, incompressible Boussinesq equations on a rotating f-plane. The coordinates are defined as follows: x is along a section, y is perpendicular to section, and z is the depth. The equations of the model are

$$\boldsymbol{V}_t + (\boldsymbol{V}\nabla)\boldsymbol{V} - f\boldsymbol{V}\times\boldsymbol{k} = -\nabla P - \boldsymbol{k}\rho g \quad (1)$$

$$\rho_t + \boldsymbol{V}\nabla\rho = 0 \quad (2)$$

$$\nabla\boldsymbol{V} = 0 \quad (3)$$

where $\boldsymbol{V}(u,v,w)$ is the velocity vector, ∇ is the three-dimensional vector gradient operator, subscript t denotes the time derivative, ρ is the density, P is the pressure, g is the gravitational acceleration, f is the Coriolis parameter taken as $1.425\times10^{-4}\,\mathrm{s}^{-1}$ for the latitude of 78.5 degrees, and $\boldsymbol{k}$ is the unit vector along the z-direction. The normal to the section velocity is included in the model, but no variation with coordinate y is allowed. So, in the three-dimensional Eqs. (2)–(4) the partial derivatives with respect to y are neglected, i.e., $\frac{\partial}{\partial y}() = 0$.

The equations are transformed to the following terrain coordinate system (sigma-coordinates) which leads to higher vertical resolution over the bank regions. The equations are solved over a domain bounded by the topography below and a rigid lid above. The flow is forced by specifying a semidiurnal tidal inflow at the left boundary of the form $V_T\sin(\omega t)$ where ω is the M_2 tidal frequency assumed to have a 12.4-h period (T). The value V_T is discussed below. On the right boundary an outflow condition is used. The initial conditions comprise the undisturbed equilibrium state with uniform horizontal density.. The horizontal grid size is 90 m, and the vertical sigma-coordinate resolution consists of 80 grid points. The time step is tied to the Courant-Levi condition and varies from 2 s to 5 s.

3 Input for the modeling

For the modeling we chose the cross-section close to the Franz Victoria Trough in the Barents Sea shown on Fig. 1. It starts from point 34.11° E, 77.57° N and finishes at point 28.61° E, 80.58° N. A whole wave path lays over the critical latitude (74.5° N). The bathymetry along this cross-section taken from GEBCO is marked in Fig. 2 by the blue line. It is splined for the purpose of modeling by 8 Fourier components for a better description of the middle portion of the domain as

$$H(x) = a_0 + \sum_{m=1}^{8}(a_m\cos(m\kappa x) + b_m\sin(m\kappa x)) \quad (4)$$

where $\kappa = 0.03398\,\mathrm{m}^{-1}$ and a_m and b_m are the Fourier coefficients. The approximation is shown in Fig. 2 by the dotted line. Typical vertical density profile in this area is taken from GDEM climatology for July. It is fitted by the exponential functions

$$\rho = 1000 + q_1\exp(r_1 z) + q_2\exp(r_2 z) \quad (5)$$

($q_1 = 27.93$; $r_1 = 1.64\times10^{-4}$; $q_2 = -1.2$; $r_2 = -2.844\times10^{-2}$) and the Brunt-Väisälä frequency $N(z)$ is calculated, both $\rho(z) - \rho_0$ (ρ_0 is $1027.48\,\mathrm{kg\,m}^{-3}$) and $N(z)$ are shown in Fig. 3.

The region in question is characterized by strong tidal currents and underwater mount ridges. The map of the mean tidal velocities in the Arctic Ocean (with the 8 tidal components) calculated with the help of the Arctic Ocean Tidal Inverse Model (AOTIM) is presented in Padman and Erofeeva (2004) and represented in Fig. 4. A logarithmic color scale is used to resolve speed variability in both weak and energetic regions. It is mentioned that four tidal components M_2, S_2, K_1 и O_1 contain up to 79%, 10%, 5% и 1% of total (8-components) potential energy of the tide, respectively. So the semi-diurnal tide M_2 dominates in the variability of tidal velocities in Arctic Ocean.

The largest mean values of the tidal velocities approaches $100\,\mathrm{cm\,s}^{-1}$ in the southern Barents Sea near the entrance to the White Sea and around Bear Island in the western Barents Sea south of Svalbard. The maximal velocities exceed the mentioned values of the mean velocities as much as twice, at least.

The barotropic tidal wave is presented only by the semidiurnal tide, and taking into account that the mean tidal current in the studied area is about $50\,\mathrm{cm\,s}^{-1}$, the maximal barotropic tidal velocity constitutes $1\,\mathrm{m\,s}^{-1}$, and we use this value for V_T to setup the model.

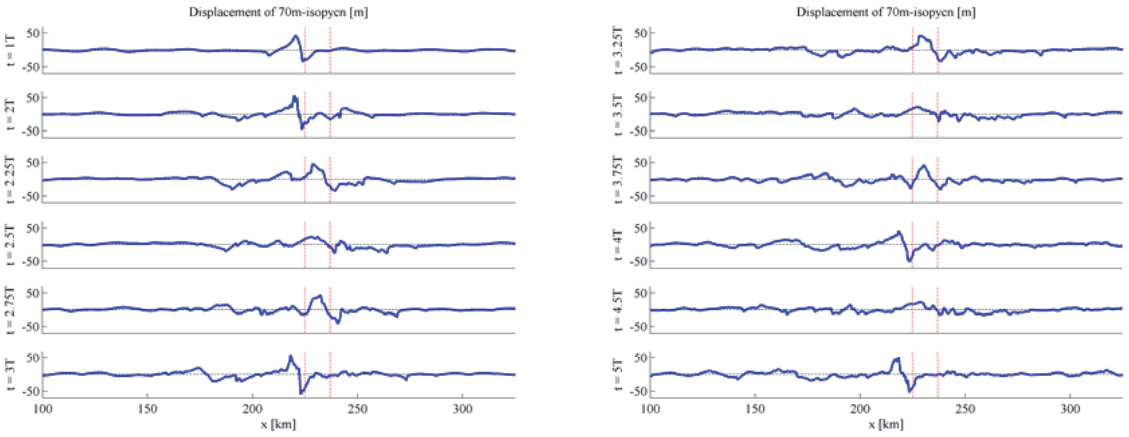

Fig. 7. Displacement of 70 m isopycn for different times.

4 Results of the modeling

The calculated density fields (left) and total (barotropic and baroclinic) horizontal velocity values (right) are shown in Fig. 5 for various tidal phases. Normalized density $(\rho - \rho_0)/1000$ is given, where ρ is sea water density [kg m^{-3}]. In the book by Valsenko et al. (2005) it was mentioned that the full periodicity of the process is formed after 2–3 T (T is tidal period for M_2).

The time moment 3 T corresponds to the ending of the ebb phase and starting of the flood phase. The velocity of the tide at this moment is zero and there are large displacements of isopycnes over the left side of the largest hill. The more intensive internal waves are generated on the slopes of the highest central hill (between 200 and 300 km with the crest at 230 km); their amplitudes decreases when they propagate out of this zone.

After a quarter of the tidal period ($t = 3.25T$), the maximum of the tidal phase comes; velocities reach their maximums, the zone of generation moves to the right lee slope of the central hill. At the time moment $t = 3.5T$ the phase of the tide finishes and the tide velocity vanishes; internal waves are developed well on the right side of the central hill. When the ebb is maximal (at $t = 3.75T$) the zone of generation is also shifted to another (left) lee side of the hill and the waves become maximal at time $t = 4T$ when the velocity of the tide vanishes. So, the internal waves generated are mainly the unsteady lee waves generated by the tide and ebb currents near the lee slope of the hill with the phase shift of about quarter of the tidal period between the maximal tide velocity and maximal isopycnal displacement. The wave velocities are evident at the time moments 3 T, 3.5 T and 4 T, when the tidal current is zero, and their values do not exceed 0.4 m s^{-1}. The process is well illustrated in the Hovmuller plot (or $x - t$ diagram) for displacement of the isopycn located at 70 m depth in the undisturbed state (Fig. 6). The more intensive internal waves with amplitudes of 50 m and total heights (crest-to-trough height) of about 80 m appear regularly in the strip of about 40 km width and central position approximately at 230 km. Their length may be evaluated using displacements presented in Fig. 7; they are about 6–12 km long. The typical periods of the modeled waves are 0.2–0.35 T.

In the book by Vlasenko et al. (2005), the classification of the processes of internal wave generation is suggested. The classification is based on the magnitude of the Froude number, $Fr = u_{\max}/C_{\mathrm{ph}}$, where $u_{\max}$ is maximal velocity of the barotropic tidal flow in the x-cross-section ($u_{\max} = V_T H(x_0)/H(x)$) and C_{ph} is the phase speed of long internal waves. It is calculated from the eigenvalue problem numerically (Grimshaw et al., 2002; Holloway et al., 1997). It was stated that when $Fr > 1$, a generation of strong nonlinear internal lee waves by tide is possible at any latitude, whereas there is no internal wave generation when $Fr \ll 1$ above the critical latitude. So the conclusion that the waves shown in Figs. 5, 6, and 7 are the internal lee waves should be drawn.

Spatial variation of the Froude number along the studied section is shown in Fig. 8 together with other characteristic quantities: phase speed of internal waves, maximal tidal velocity, and depth of the defined area of the Sea. The zone where the Froude number is greater than 1 lies between the points 225 km and 237 km; there the intensive internal waves were discovered.

5 Conclusions

The possibility of generation of strong nonlinear unsteady lee internal waves by the barotropic tide in the Barents Sea above the critical latitude has been demonstrated through numerical simulation. The chosen area for the modeling was

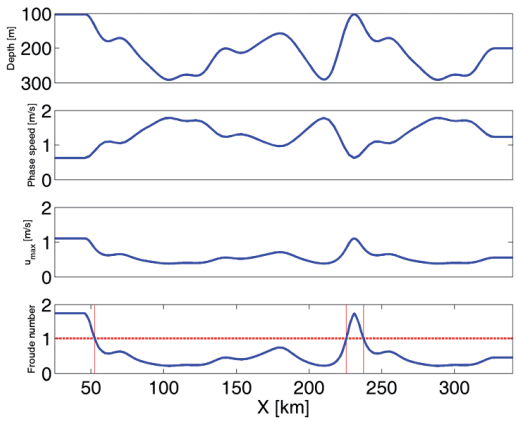

Fig. 8. The Froude number and other characteristic quantities against the distance at the defined area of the Sea.

close to the Franz Victoria Trough; the parameters of the calculated internal waves in the chosen region agree qualitatively to those observed in the Trough. The modeled waves had the same amplitudes as the observed ones, 40 m, and the close wavelengths, 6–12 km. They preserved significant amplitudes of isopycn displacements at a distance of 20 km from the zone of generation. They appeared two times per semidiurnal tide period and live about 6.2 h slowly propagating out of the peak of the underwater hill. More intensive waves were generated in the ebb phase and at the end of the ebb phase, when the ebb velocity vanished. The largest observed drop between the crest and trough was about 80 m; it appeared at the end of the ebb phase each 12.4 h.

Acknowledgements. This work was supported by grants RFBR 10-05-00199 and Grant of President of RF for young researchers MK-846.2009.1 (O.K.) and RFBR 09-05-00204 and 09-05-90408 (T.T.).

Edited by: E. Pelinovsky
Reviewed by: two anonymous referees

References

Apel, J., Ostrovsky, L. A., Stepanyants, Y. A., and Lynch, J. F.: Internal solitons in the ocean and their effect on underwater sound, J. Acoust. Soc. Am., 121, 695–722, 2007.

Babu, S. V. and Rao, A. D.: Mixing in the surface layers in association with internal waves during winter in the northwestern Bay of Bengal, Nat. Hazards, in press, doi:10.1007/s11069-010-9607-5, 2010.

Bogucki, D. J. and Redekopp, L. G.: A Mechanism for sediment resuspension by internal solitary waves, Geophys. Res. Lett., 26, 1317–1320, 1999.

Duda, T. F., Lynch, J. F., Irish, J. D., Beardsley, R. C., Ramp, S. R., Chiu, C.-S., Tang, T. Y., and Yang, Y.-J.: Internal tide and nonlinear internal wave behavior at the continental slope in the northern south China Sea, IEEE J. Oceanic Eng., 29, 1105–1130, 2004.

Grimshaw, R., Pelinovsky, E., and Poloukhina, O.: Higher-order Korteweg-de Vries models for internal solitary waves in a stratified shear flow with a free surface, Nonlin. Processes Geophys., 9, 221–235, doi:10.5194/npg-9-221-2002, 2002.

Helfrich, K. R. and Melville, W. K.: Long nonlinear internal waves, Annu. Rev. Fluid Mech., 38, 395–425, 2006.

Holloway, P., Pelinovsky, E., Talipova, T., and Barnes, B.: A nonlinear model of internal tide transformation on the Australian North West Shelf, J. Phys. Oceanogr., 27(6), 871–896, 1997.

Holloway, P., Pelinovsky, E., and Talipova, T.: A generalized Korteweg-de Vries model of internal tide transformation in the coastal zone, J. Geophys. Res., 104(C8), 18333–18350, 1999.

Lamb, K.: Numerical experiments of internal wave generation by strong tidal flow across a finite amplitude bank edge, J. Geophys. Res., 99(C1), 848–864, 1994.

LeBlond, P. H. and Mysak, L. A.: Waves in the Ocean, Elsevier, Amsterdam, 602 p., 1978.

Morozov, E. G.: Ocean Internal Waves, Nauka, Moscow, 1985 (in Russian).

Morozov, E. G. and Pisarev, S. V.: Internal Tides at the Arctic Latitudes (Numerical Experiments), Oceanology, 42, 153–161, 2002.

Nakamura, T., Awaji, T., Hatayama, T., Akimoto, K., Takizawa, T., Koho, T., Kawasaki, Y., and Fukasava, M.: The generation of large-amplitude unsteady lee waves by subinertial tidal flow: a possible vertical mixing mechanism in the Kuril Straits, J. Phys. Oceanogr., 30, 1601–1621, 2000.

Ostrovsky, L. and Stepanyants, Yu.: Do internal solitons exist in the ocean?, Rev. Geophys., 27, 293–310, 1989.

Padman, L. and Erofeeva, S.: A barotropic inverse tidal model for the Arctic Ocean, Geophys. Res. Lett., 31, L02303, doi:10.1029/2003GL019003, 2004.

Pisarev, S. V.: Low-Frequency Internal Waves Near the Shelf Edge of the Arctic Basin, Oceanology, 36, 771–778, 1996.

Sridevi, B., Murty, T. V. R., Sadhuram, Y., and Murty, V. S. N.: Impact of internal waves on the acoustic field at a coastal station off Paradeep, east coast of India, Nat. Hazards, in press, doi:10.1007/s11069-010-9567-9, 2010.

Vlasenko, V., Stashchuk, N., Hutter, K., and Sabinin, K.: Nonlinear internal waves forced by tides near the critical latitude, Deep-Sea Res. Pt. I, 50, 317–338, 2003.

Vlasenko, V., Stashchuk, N., and Hitter, K.: Baroclinic tides, Cambridge Univ. Press, Cambridge, 2005.

Warn-Varnas, A. C., Chin-Bing, S. A., King, D. B., Hawkins, J. A., Lamb, K. G., and Teixeira, M.: Yellow Sea ocean-acoustic solitary wave modeling studies, J. Geophys. Res., 110, C08001, doi:10.1029/2004JC002801, 2005.

Warn-Varnas, A., Chin-Bing, S. A., King, D. B., Hawkins, J., and Lamb, K.: Effects on acoustics caused by ocean solitons, Parts A,B, Nonlinear Anal.-Theor., 71, e1807–e1817, e2194–e2204, 2009.

Warn-Varnas, A., Hawkins, J., Lamb, K. G., Piacsek, S., Chin-Bing, S., King, D., and Burgos, G.: Solitary wave generation dynamics at Luzon Strait, Ocean Model., 31, 9–27, 2010.

Paper III

Kurkina, O., Pelinovsky, E., Talipova, T., Soomere, T. Mapping the internal wave field in the Baltic Sea in the context of sediment transport in shallow water. – Journal of Coastal Research, Special Issue 64, Part II; 2011, p. 2042–2047.

Journal of Coastal Research	SI 64	2042 - 2047	ICS2011 (Proceedings)	Poland	ISSN 0749-0208

Mapping the internal wave field in the Baltic Sea in the context of sediment transport in shallow water

O. Kurkina†‡∞, T. Talipova§, E. Pelinovsky‡∞§ and T. Soomere†

† Institute of Cybernetics at Tallinn University of Technology, Tallinn, EE-12618, Estonia, soomere@cs.ioc.ee

‡ State University, Higher School of Economics, Nizhny Novgorod Branch, Nizhny Novgorod, Russia, Oksana.Kurkina@mail.ru

∞ Nizhny Novgorod State Technical University, Nizhny Novgorod, Russia pelinovsky@hydro.appl.sci-nnov.ru

§ Institute of Applied Physics of Russian Academy of Sciences, Nizhny Novgorod, Russia tgtalipova@mail.ru

ABSTRACT

Kurkina, O.; Pelinovsky, E.; Talipova, T., and Soomere, T., 2011. Mapping the internal wave field in the Baltic Sea in the context of sediment transport in shallow water. Journal of Coastal Research, SI 64 (Proceedings of the 11th International Coastal Symposium), 2042 – 2047. Szczecin, Poland, ISSN 0749-0208

The geographical and seasonal distributions of kinematic and nonlinear parameters of long internal waves obtained on a base of GDEM climatology in the Baltic Sea region are examined. The considered parameters (phase speed of long internal wave, dispersion, quadratic and cubic nonlinearity parameters) of the weakly-nonlinear Korteweg-de Vries-type models (in particular, Gardner model), can be used for evaluations of the possible polarities, shapes of solitary internal waves, their limiting amplitudes and propagation speeds. The key outcome is an express estimate of the expected internal wave parameters for different regions of the Baltic Sea. The central kinematic characteristic is the near-bottom velocity in internal waves in areas where the density jump layers are located in the vicinity of seabed. In such areas internal waves are the major driver of sediment resuspension and erosion processes and may be also responsible for destroying the laminated structure of sedimentation regime (that frequently occurs in certain areas of the Baltic Sea).

ADDITIONAL INDEX WORDS: *density stratification, internal soliton, Korteweg-de Vries equation, Gardner equation*

INTRODUCTION

Large-amplitude internal waves (IW) are often very energetic events in stratified and coastal marine environments. They have a significant role in particle transport and mixing of water masses, as well as affecting acoustic propagation. Understanding the impact of large IW is of key importance in the coastal marine environment. The regional aspect is essential in IW studies as the vertical stratification of the ocean is highly inhomogeneous in the horizontal direction. Here the attention is drawn t the Baltic Sea which is strongly influenced by wind forcing and buoyancy, that causes mesoscale variability of hydrological fields with horizontal scales of 5–20 km. The Baltic Sea is known as non tidal region and generation of IW is mainly accounts for the strong winds. The cyclones propagating with the winds of 10–15 m/s here cause the generation of IW with amplitudes of 11–15 m, while the current velocities in the upper layer are about 11–15 cm/s, and in the lower layer, they are about 5–8 cm/s (Chernysheva, 1987). The characteristics of IW measured in the Baltic Sea are given in (Kol'chitskii *et al.*, 1996; Golenko and Mel'nikov, 2007). In particular, IW with periods of 0.1–1 h, observed in the central part of the Gotland Deep, formed internal wave trains with duration of several hours and current amplitudes of about 3 cm/s. IW in the inertial frequency range can induce wave currents with velocities reaching 20 cm/s.

The horizontal variability of hydrological fields becomes evident in the weakly nonlinear internal wave theory (Talipova et al., 1998; Holloway et al, 1999; Pelinovsky et al, 2007) as spatial variability of the coefficients of the corresponding nonlinear evolution equations. These coefficients, such as propagation speed, quadratic and cubic nonlinearities and dispersion, represent the kinematic characteristics of internal wave field. Horizontal variability of vertical stratification is especially evident in the sea shelf zones and shallow-water basins of estuary type.

When IW are modeled numerically, an important problem is to specify the hydrological conditions determining density variations with depth to initialize the numerical models. An adequate way is to use gridded temperature-salinity data from international hydrological atlases. This approach allows reproducing the internal "weather" of the considered basin, because hydrological atlases represent the long-term mean density stratifications.

The aim of this study is to examine the geographical and seasonal distributions of kinematic parameters of long IW obtained on a base of GDEM (Generalized Digital Environmental Model) climatology in the Baltic Sea region. This data set reflects the global climatology of the temperature and salinity of the global oceans.

The first such estimations for the Baltic Sea are given in (Talipova et al., 1998) for the region of the Gotland Basin. The considered kinematic parameters can be used for express-evaluations of the possible polarities, shapes of solitary IW, their limiting amplitudes, propagation speeds, etc. They also can help to set-up and initialize more complex models for internal gravity waves (IGW, MIT GCM, POM).

We present overview of spatial variability of the listed parameters and several interesting features of the underlying hydrophysical fields such as the depth of the maximal value in the Brunt-Vaisala frequency (BVF) profile and the maximal values of the BVF over such profiles for different months. The averaged values of coefficients of the Gardner equation allow producing the estimations of nonlinear IW shapes and limiting amplitudes before numerical simulations.

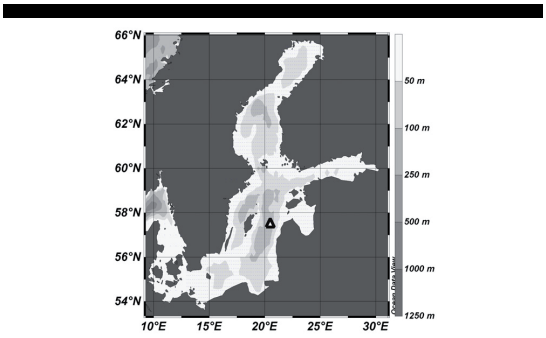

Figure 1. Bathymetry of the Baltic Sea. The triangle shows the location of measurements presented in Fig. 12.

The key outcome of our calculations is an express estimate of the expected internal wave parameters for different regions of the

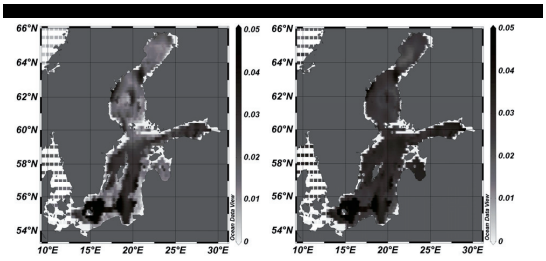

Figure 2. Maximal value in the BVF profile [s^{-1}] (left panel: January, right panel: July).

Baltic Sea. The central IW field characteristic is the near-bottom velocity in IW in areas where the density jump layers are located in the vicinity of seabed. In such areas IW are the major driver of sediment resuspension and erosion processes and may be also responsible for destroying the laminated structure of sedimentation regime (that frequently occurs in certain areas of

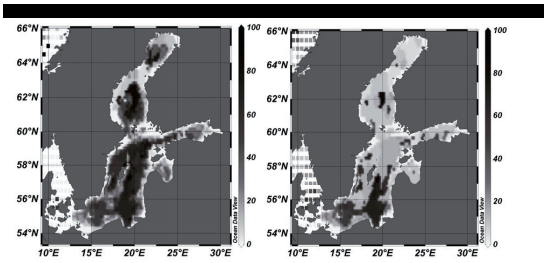

Figure 3. Depth [m] of maximal value in the Brunt-Vaisala frequency profile (left panel: January, right panel: July).

the Baltic Sea). As the pycnocline is in many cases located at a depth of only a few meters in some areas of the Baltic Sea during spring and summer (Leppäranta and Myrberg, 2009), the impact of IW on sedimentation processes frequently extends to the coastal

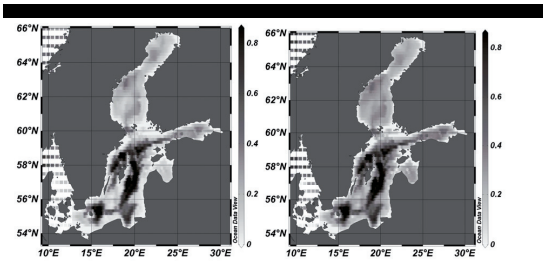

Figure 4. Long linear IW speed [m s^{-1}] (left panel: January, right panel: July).

zone and overlaps with the nearshore affected by surface waves. Such situation often happens in partially sheltered sub-basins of the Baltic Sea (Figure 1) such as the Gulf of Finland where the role of high near-bottom velocities, eventually created by high-amplitude IW, has been systematically underestimated in engineering applications (Erm *et al*., 2010).

INTERNAL WAVES IN STRATIFIED BASINS

The weakly nonlinear theory of long IW in a vertical section of stratified basin assumes, that the internal wave field (in particular, the vertical isopycnal displacement $\zeta(z,x,t)$) can be expressed as a series (up to the 2nd in nonlinearity) (Pelinovsky *et al*., 2007):

$$\zeta(z,x,t) = \eta(x,t)\Phi(z) + \eta^2(x,t)F(z) \tag{1}$$

where x is horizontal axis, z is vertical axis directed upward, t is time, $\eta(x,t)$ describes the transformation of a wave along the axis of propagation and its evolution in time. Function $\Phi(z)$ (the vertical mode) describes vertical structure of long internal wave, and $F(z)$ is the first nonlinear correction to $\Phi(z)$. $\Phi(z)$ is a solution of an eigenvalue problem, which can be written in the form (in Boussinesq approximation usually valid for natural sea stratifications):

$$\frac{d^2\Phi}{dz^2} + \frac{N^2(z)}{c^2}\Phi = 0, \quad \Phi(0) = \Phi(H) = 0 \tag{2}$$

here eigenvalue c is the phase speed of long linear internal wave, H is the total water depth, $N(z)$ is the Brunt-Väisälä frequency (BVF) determined by the expression:

$$N^2(z) = -\frac{g}{\rho(z)}\frac{d\rho(z)}{dz}, \tag{3}$$

g is gravity acceleration and $\rho(z)$ is undisturbed density profile. It is well known, that problem (2) has an infinite number of eigenvalues $c_1>c_2>c_3>\ldots$ and corresponding eigenfunctions Φ_1, Φ_2, Φ_3,... We consider only the first (lowest) mode, when the function Φ has a single zero at $z=0$ and $z=H$. This mode is usually the most energetic in the internal wave spectrum. It is convenient to normalize the solution so that the maximum of $\Phi(z)$ is $\Phi_{\max} = \Phi(z_{\max}) = 1$.

In this case the leading order solution $\eta(x, t)$ coincides with the isopycnal surface displacement at $z_{\max}$:

$$\varsigma(x, z_{\max}, t) = \eta(x,t) \tag{4}$$

Function $F(z)$ can be found as a solution of the inhomogeneous boundary problem:

$$\frac{d^2F}{dz^2} + \frac{N^2}{c^2}F = -\frac{\alpha}{c}\frac{d^2\Phi}{dz^2} + \frac{3}{2}\frac{d}{dy}\left[\left(\frac{d\Phi}{dz}\right)^2\right], \tag{5}$$

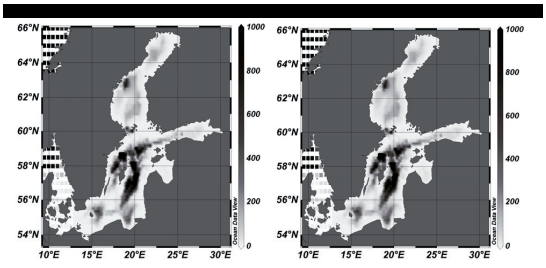

Figure 5. Long linear IW dispersion parameter [$m^3 \cdot s^{-1}$] (left panel: January, right panel: July).

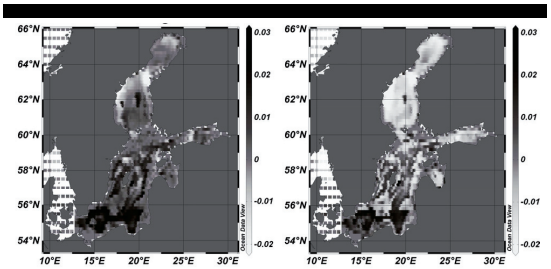

Figure 6. Quadratic nonlinearity parameter [s^{-1}] (left panel: January, right panel: July).

$$F(0) = F(H) = 0\,,$$

where the auxiliary normalization condition $F(z_{max})=0$ is used to determine the solution uniquely.

In this model, the function $\eta(x,t)$ satisfies the nonlinear evolution equation (extended Korteweg-de Vries (KdV) or Gardner equation):

$$\frac{\partial \eta}{\partial t} + \left(c + \alpha\eta + \alpha_1\eta^2\right)\frac{\partial \eta}{\partial x} + \beta\frac{\partial^3 \eta}{\partial x^3} = 0\,. \qquad (6)$$

This equation contains cubic nonlinearity, the presence of which provides better predictions of wave form, especially in the coastal zone. The coefficients of this equation are determined through the $\Phi(z)$ and $F(z)$:

$$\beta = \frac{c}{2D}\int_0^H \Phi^2 dz\,,\ \alpha = \frac{3c}{2D}\int_0^H \left(\frac{d\Phi}{dz}\right)^3 dz\,,\ D = \int_0^H \left(\frac{d\Phi}{dz}\right)^2 dz \qquad (7)$$

$$\alpha_1 = \frac{1}{2D}\int_0^H dz\left\{9c\frac{dF}{dz}\left(\frac{d\Phi}{dz}\right)^2 - 6c\left(\frac{d\Phi}{dz}\right)^4 + 5\alpha\left(\frac{d\Phi}{dz}\right)^3 - \right.$$

$$\left. - 4\alpha\frac{dF}{dz}\frac{d\Phi}{dz} - \frac{\alpha^2}{c}\left(\frac{d\Phi}{dz}\right)^2\right\} \qquad (8)$$

In the present paper we construct and discuss the geographical charts for parameters c, β, α and α_1 of the Gardner equation (6) in the Baltic Sea region, using climatological oceanographic data and calculating Brunt-Väisälä frequency (3) from temperature and salinity profiles.

KINEMATIC CHARACTERISTICS OF THE INTERNAL WAVE FIELD IN THE BALTIC SEA

We use long-term mean temperature and salinity profiles from GDEM-V3.0 (Teague et al., 1990) to calculate density stratifications for the Baltic Sea. With these profiles speed of propagation, dispersive and both nonlinear parameters of the Gardner equation are computed and presented in the form of charts with a resolution of 10'×10' along latitudes and longitude. We also discuss spatial and seasonal (July and January) variations of these parameters. GDEMs at 10 minute resolution have been developed for selected regions where data is sufficient to support the higher resolution; particularly, such data are available for the Baltic Sea.

Visualization of results was done using the software Ocean Data View (Schlitzer, 2010).

The bathymetry of the Baltic Sea (Figure 1) and charts representing the magnitude of seasonal variability of the density stratification (in terms of maxima of BVF (Figure 2) and the depth where the maximum of BVF occurs (Figure 3)) can help in the interpretation of obtained results and in explaining the features of the geographical distribution of kinematic parameters of the IW field. Figures 2 and 3 demonstrate that stratification data strongly depend on the particular season. Note the increase in the maximal BVF values during summer simultaneously with a decrease of their depths. So, in general one can expect an increase in the impact of IW upon the sediment transport in shallow-water regions of the Baltic Sea in late summer and autumn.

Seasonal variations in the linear parameters c, β (Figures 4 and 5) are not very significant. Also the main features of their geographical distribution do not change from season to season. The maximal value of c is about 90 cm/s. These parameters apparently are mostly determined by the bathymetry. However the nonlinear parameters α, α_1 (Figures 6 and 7) are more sensitive to the fine structure of the density stratification. Their seasonal variability is significant, and they can even change their signs from season to season. The quadratic nonlinearity parameter changes from –0.02 to 0.03 s^{-1} and for July (Figure 6, right panel) it is mainly positive in the southern part of the Baltic Sea (the Arcona Basin, the Bornholm Basin and the Slupsk Furrow), in the central part (the Gotland Basin) there are the spots of different signs of α, and the Gulf of Finland and the Bothnian Sea are characterized by the negative value of this parameter. In winter season (Figure 6, left panel) the zone of positive values broadens including the central part of the Baltic Sea and most of the Gulf of Finland. The cubic nonlinear parameter (Figure 7), which changes from –0.003 to 0.004 $m^{-1}s^{-1}$, shows the spotty character of the zones with positive and negative values with the predominance of negative values in winter (Figure 7, left panel) the positive values in the Bothnian Sea in summer (Figure 7, right panel).

SHAPES OF NONLINEAR INTERNAL WAVES

Let us consider the single-soliton solution of Eq. (6):

$$\eta(x,t) = \frac{A}{1 + B\mathrm{ch}(\gamma(x - Vt))}, \qquad (9)$$

where the soliton velocity $V = c + \beta\gamma^2$ is expressed through the inverse width of soliton, γ, and the soliton amplitude, a, or the extremum of the function (9), is

$$a = \frac{A}{1+B}\,,\ \text{and}\quad A = \frac{6\beta\gamma^2}{\alpha},\qquad B^2 = 1 + \frac{6\alpha_1\beta\gamma^2}{\alpha^2}\,. \qquad (10)$$

Let us consider in detail now the possible combinations of the signs of the nonlinear coefficients in the Gardner equation.

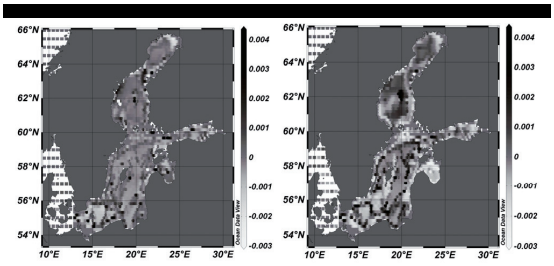

Figure 7. Cubic nonlinearity parameter [$m^{-1} \cdot s^{-1}$] (left panel: January, right panel: July).

Korteweg-de Vries soliton

When the cubic nonlinearity vanishes ($\alpha_1 = 0$), the solution (9) is reduced to the classical Korteweg-de Vries (KdV) soliton:

$$\eta(x,t) = a\,\mathrm{sech}^2\left[\sqrt{\frac{\alpha a}{12\beta}}\left(x - \left[c + \frac{\alpha a}{3}\right]t\right)\right]. \qquad (11)$$

It has only one polarity defined by the sign of quadratic nonlinearity α.

Gardner soliton

When the cubic nonlinear coefficient α_1 is negative, soliton

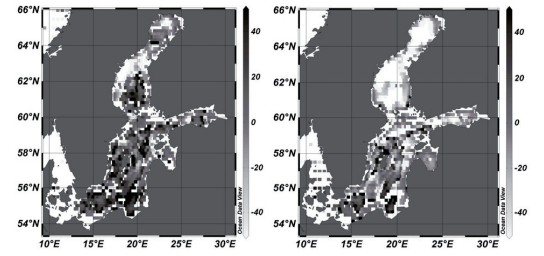

Figure 8. Limiting amplitudes [m] of "top-table" solitary waves (for negative cubic nonlinearity values, left panel: January, right panel: July).

solutions of single polarity, with $\alpha\eta > 0$, exist with amplitudes between zero and a limiting value

$$a_{\lim} = \frac{\alpha}{|\alpha_1|}. \qquad (12)$$

The soliton shapes for different combinations of signs of nonlinear parameters are discussed in details in (Pelinovsky et al, 2007). The increase in the soliton amplitude to the limiting value (12) ($B \to 0$) leads to the unlimited increase of its width. The solitary wave becomes "wide", or "table-shaped." It has a flat crest, and its slopes are shock-like waves, or kinks.

If $\alpha_1 > 0$, soliton families of either polarity exist. One of these families with $\alpha\eta > 0$ has $1 < B < \infty$, and the amplitude is not bounded. For large amplitudes ($B \to \infty$) the solution has the shape of the soliton of the modified KdV equation:

$$\eta(x,t) = a\,\mathrm{sech}\left[\sqrt{\frac{\alpha_1 a^2}{6\beta}}\left(x - \left[c + \frac{\alpha_1 a^2}{6}\right]t\right)\right]. \qquad (13)$$

Another family of solitons (with $\alpha\eta < 0$) corresponds to negative B ($-\infty < B < -1$). At $B \to -\infty$ such solitons are transformed into the modified KdV soliton (13). Waves of this family have a minimum amplitude $a_{\mathrm{alg}} = -2\alpha/\alpha_1$.

At near-critical amplitudes ($B \to -1$) soliton (9) tends to so-called "algebraic" soliton:

$$\eta(x) = \frac{a_{\mathrm{alg}}}{1 + \alpha^2 (x - ct)^2 / 6\beta}, \quad V = c. \qquad (14)$$

Note that its speed is equal to linear long wave speed. In the gap between the zero and a_{alg} there are no any solitons.

Figures 8 and 9 illustrate geographical distributions of amplitudes a_{lim} (12) for the points with negative cubic nonlinearity and a_{alg} (15) for the points with positive cubic nonlinearity values in the Baltic Sea. The range for the values of these amplitudes is about ±40 m.

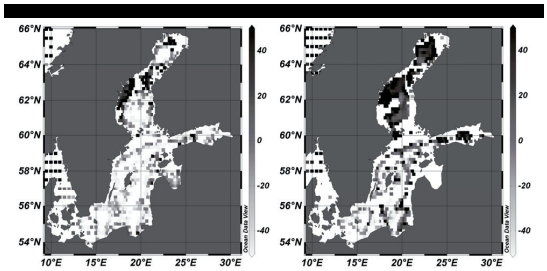

Figure 9. Amplitudes [m] of algebraic solitons (left panel: January, right panel: July).

HORIZONTAL VELOCITY

With the use of Eq. (1) the components of velocities of fluid particles (u, w) in the vertical section (x, z) can be expressed as follows:

$$u(x,z,t) = c\,\eta(x,t)\frac{d\Phi}{dz} + \left(\frac{\alpha}{2}\frac{d\Phi}{dz} + c\frac{dF}{dz}\right)\eta^2, \qquad (15)$$

$$w(x,z,t) = -c\frac{\partial \eta}{\partial x}\Phi(z) - \left(\alpha\Phi(z) + 2cF(z)\right)\eta\frac{\partial \eta}{\partial x}, \qquad (16)$$

The horizontal velocity component u gives the greatest contribution into the local current speed. This is typical for long waves and this characteristic of internal wave field must be considered in the analysis of near-bottom processes connected with sediment transport.

The first terms in Eqs. (15) and (16) correspond to the leading order of the asymptotic expansion. The remaining additives reflect the first nonlinear correction in the asymptotic series. Thus, for the forecast of the local current speed one has to determine the isopycnal displacement $\eta(x, t)$ at the level of $z_{\max}$ (see (4)), the vertical IW mode $\Phi(z)$ and its nonlinear correction $F(z)$. The amplitude of $\eta(x, t)$ is not known a priori, it depends upon a large number of background conditions of internal wave generation, and can be found by means of the detailed simulation.

For the analysis of the geographical features of the near-bottom velocity distribution it is convenient to consider a normalized quantity u/η (Figure10). To the leading order, it is independent of

η. The largest values of near-bottom velocities can be expected along all the coasts, especially in the eastern part of the Gulf of Finland and in the south-western part of the Baltic Sea (the Arcona basin and the Bornholm Basin) with the tendency to increase in the warm season.

The contribution from second-order terms in the horizontal velocity (Eq. (19)) can be estimated for the model of a three-layer stratification – a situation that frequently occurs in the Baltic Sea. The water masses in its central part often consist of a mixed upper layer, well-defined seasonal thermocline at a depth about 20–40 m, an intermediate layer and main halocline at a depth about 80–100 m. In many cases the total depth is 120–140 m and density changes between the layers are more or less equal (Soomere, 2003). We model this sort of three-layer density profile using the formula

$$\rho = \rho_0 - \Delta_{\rho_1} \tanh\frac{z - z_1}{d_1} - \Delta_{\rho_2} \tanh\frac{z - z_2}{d_2} \qquad (17)$$

where the parameters are chosen to reproduce the profiles presented in (Soomere, 2003): ρ_0 = 1007 [kg/m^3], $\Delta_{\rho 1} = \Delta_{\rho 2}$ = 2 [kg/m^3], d_1 = 3 [m], d_2 = 10 [m], z_1 = –20 [m], z_2 = –80 [m], total depth is 130 m. Figure 11a presents the BVF profile and corresponding lowest vertical mode $\Phi(z)$ and the nonlinear correction $F(z)$ profiles. Such background conditions give positive signs of both nonlinear parameters (α, α_1), and the solitons of both polarities can exist. The isopycnal displacements and horizontal velocity contours induced by the passage of the lowest-mode solitons (9) of positive and negative polarities with approximately equal amplitudes ($a \cong$ 13.4 m) are demonstrated by Figure 11b-e (for the leading order of the Eqs. (1) and (15)) and by Figure 12 (where the nonlinear correction terms are taken into account in Eqs. (1) and (15)). These figures show quasi-three-layer structure of horizontal velocity fields with thin transition layers of thicknesses d_1 and d_2. Notice that the velocity is positive when the fluid particles move in the direction of soliton propagation (to the right), and negative in the opposite case. The fields of horizontal velocities in elevation and depression solitons are positive and negative, respectively, in the lower near-bottom layer, and have the reversed in the middle and upper layer. Near-bottom and near-surface velocities reach the greatest values whereas the velocity in the mid-layer is not significant. The influence of the nonlinear correction manifests itself firstly in the shape of the lines of zero horizontal velocity: they are curved oppositely to the soliton polarity while for the leading order wave field they are horizontal. Also the wavefield accounting for the nonlinear correction has smaller maximal absolute values of negative velocities (near-surface for the soliton of elevation, and near-bottom for the soliton of depression) and larger maximal values of positive velocities.

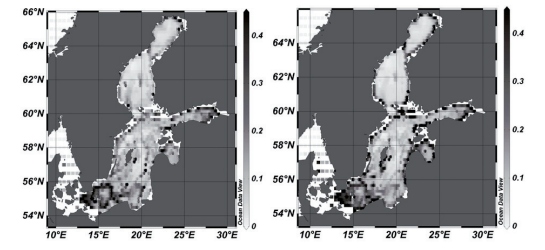

Figure 10. The value of leading-order near-bottom velocity in internal wave field divided by η (x, t) in [1/s] (left panel: January, right panel: July).

DISCUSSION AND CONCLUSIONS

In essence, the performed research is a step on the way towards systematic incorporation of the information about internal wave fields into engineering applications. As typical for wave processes, propagation of IW provides a mechanism of the transfer of massive quantities of energy between different sea areas. This energy is mostly released in regions where the pycnocline is located so close to the sea surface or the bottom that the large-amplitude IW will break. In the Baltic Sea conditions, this location may vary considerably and frequently occurs in areas where upper layers of soft sediments are substantially polluted (Verta *et al.*, 2007).

Water velocities in breaking IW usually largely exceed the

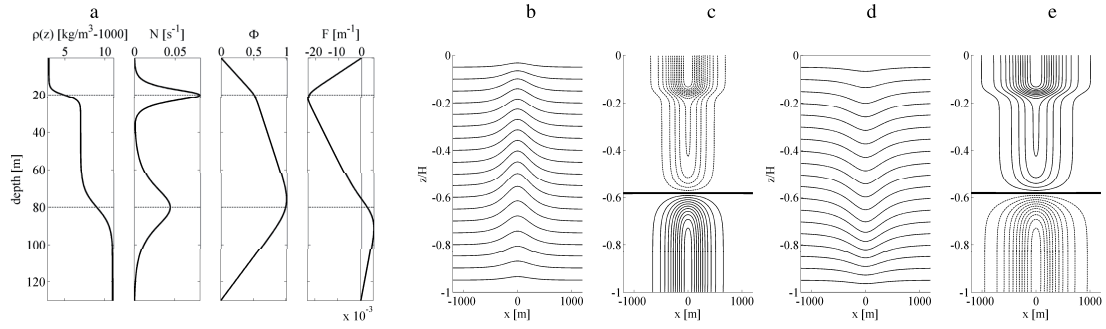

Figure 11. (a) Model of almost three-layer density stratification and corresponding profiles of Brunt-Väisälä frequency $N(z)$, lowest vertical mode $\Phi(z)$ and its nonlinear correction $F(z)$; leading order of isopycnal displacements (b, d) and horizontal velocity (c,e) contours while the soliton of positive/negative polarity propagates. In panels b, d contours are given with H/20 interval; in panels d, e solid/dashed lines correspond to positive/negative horizontal velocities, thick lines are the lines of zero horizontal velocity, the interval between contours is 0.025c.

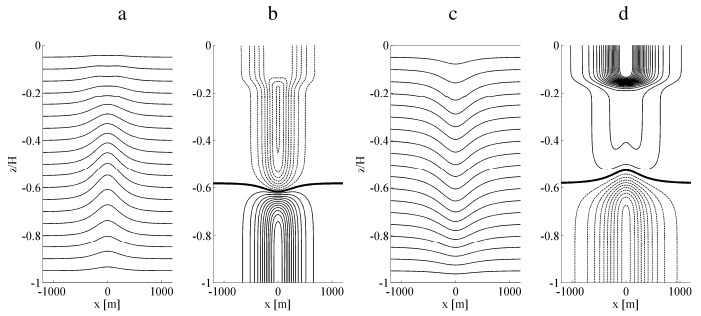

Figure 12. Isopycnal displacements (a, c) and horizontal velocity (b,d) contours while the soliton of positive/negative polarity propagates. In panels a, c contours are given with *H*/20 interval; in panels c, d solid/dashed lines correspond to positive/negative horizontal velocities, thick lines are the lines of zero horizontal velocity, the interval between contours is 0.025*c*.

threshold for suspension of such sediment. The dimensions of resulting plume are basically determined by the above-considered limiting parameters of large-scale IW. The frequently occurring process of upwelling (that has high chances to occur simultaneously with the presence of intense internal wave field) brings the pollution to the upper layers of the sea where surface currents redistribute it over a large sea area (Leppäranta and Myrberg, 2009).

The largest uncertainty of this multi-step process is currently connected with insufficient knowledge about the internal wave fields in the Baltic Sea. Therefore, in connection with detailed studies into upwelling (Lehmann and Myrberg, 2008) and current-drive transport of different adverse impacts (Soomere *et al*., 2011), our study paves the way towards much better understanding the functioning of key features of the entire Baltic Sea (eco)system and has a large potential to contribute into mitigation and management marine-induced hazards, especially problems connected with coastal pollution and coastal zone management.

LITERATURE CITED

Erm, A.; Elken, J.; Pavelson, J.; Kask, J.; Voll, M.; Kört, M.; Roots, O.; Liblik, T.; Lagemaa, P., and Buschmann, F., 2010. Observation of high-speed deep currents and resuspension of soft sediments in the central part of the Gulf of Finland. In: *The 10th International Marine Geological Conference "The Baltic Sea Geology–10,"* 24–28 August 2010, VSEGEI, St. Petersburg, Russia. Press VSEGEI, Saint-Petersburg, pp. 25–26.

Chernysheva, E.S., 1987. On the modeling of long internal waves. In: Davidan, I.N. et al. (eds.), *Problems of the Studies and Mathematical Modeling of the Baltic Sea Ecosystem. Modeling of the Ecosystem Components* Issue No. 3, Leningrad, Gidrometeoizdat, pp. 50–54.

Golenko, N.N. and Mel'nikov, V.A., 2007. Estimation of spatio-temporal parameters of the internal wave field in the Southwest Baltic Sea using data by towed probe. *Scientific reports of the Russian Geographic Union (Kaliningrad branch), Russian State Univ., Kaliningrad*, Volume 5, pp. C1–C4.

Holloway, P.; Pelinovsky, E., and Talipova, T., 1999. A generalized Korteweg-de Vries model of internal tide transformation in the coastal zone. *Journal of Geophysical Research*, 104 (C8), 18333–18350.

Leppäranta, M. and Myrberg, K., 2009. *Physical oceanography of the Baltic Sea*. Springer Praxis, Berlin Heidelberg New York, 378 p.

Lehmann, A. and Myrberg, K., 2008. Upwelling in the Baltic Sea – A review. *Journal of Marine Systems*, 74 (S), S3–S12.

Kol'chitskii, N.N.; Monin, A.S., and Paka, V.T., 1996. On internal seiches in the deep Baltic Sea. *Doklady Akademii Nauk*, 346 (2), 249–255.

Pelinovsky, E.; Polukhina, O.; Slunyaev, A., and Talipova, T., 2007. Internal solitary waves. *In* Grimshaw, R. (ed.), *Solitary Waves in Fluids*. WIT Press, Southampton, Boston, pp. 85–110.

Schlitzer, R., 2010. Ocean Data View, http://odv.awi.de.

Soomere, T., 2003. Coupling coefficients and kinetic equation for Rossby waves. *Nonlinear Processes in Geophysics*, 10, 385–396.

Soomere, T.; Delpeche, N.; Viikmäe, B.; Quak, E.; Meier, H.E.M., and Döös, K., 2011. Patterns of current-induced transport in the surface layer of the Gulf of Finland. *Boreal Environment Research*, 16 (1), 1–21.

Talipova, T.; Pelinovsky, E., and Kõuts, T., 1998. Kinematics characteristics of the internal wave field in the Gotland Deep. *Oceanology*, 38 (1), 37–46.

Teague, W.J.; Carron, M.J., and Hogan, P.J., 1990. A comparison between the Generalized Digital Environmental Model and Levitus climatologies. *Journal of Geophysical Research*, 95, 7167–7183.

Verta, M.; Salo, S.; Korhonen, M.; Assmuth, T.; Kiviranta, H.; Koistinen, J.; Ruokojärvi, P.; Isosaari, P.; Bergqvist, P.-A.; Tysklind, M.; Cato, I.; Vikelsøe, J., and Larsen, M.M., 2007, Dioxin concentrations in sediments of the Baltic Sea – A survey of existing data. *Chemosphere*, 67, 1762–1775.

ACKNOWLEDGEMENT

The research is partially supported by Russian Foundations for Basic Research grants (10-05-00199 and 09-05-00204), Estonian Science Foundation Grants (7413 and 8870), and the targeted financing by the Estonian Ministry of Education and Science (grants SF0140077s08 and SF0140007s11). OK acknowledges as well RF President grant for young researchers MD-99.2010.5 and Federal Target Program "Research and scientific-pedagogical cadres of Innovative Russia" for 2009-2013, as part of the event 1.2.1 (Contracts 518 and 851).

Paper IV

Kurkina, O., Kurkin, A., Soomere, T., Pelinovsky, E., Rouvinskaya, E. Higher-order (2+4) Korteweg-de Vries–like equation for interfacial waves in a symmetric three-layer fluid. – Physics of Fluids 23 /11; 2011, Art. No. 116602, p. 1–13.

Higher-order (2 + 4) Korteweg-de Vries-like equation for interfacial waves in a symmetric three-layer fluid

O. E. Kurkina,[1,2,3] A. A. Kurkin,[3] T. Soomere,[1] E. N. Pelinovsky,[2,3,4] and E. A. Rouvinskaya[2,4]
[1]*Wave Engineering Laboratory, Institute of Cybernetics, Tallinn University of Technology, Tallinn, Estonia*
[2]*Department of Mathematics, National Research University Higher School of Economics, Nizhny Novgorod Branch, Nizhny Novgorod, Russia*
[3]*Department of Applied Mathematics, Nizhny Novgorod State Technical University, Nizhny Novgorod, Russia*
[4]*Department of Nonlinear Geophysical Processes, Institute of Applied Physics of Russian Academy of Sciences, Nizhny Novgorod, Russia*

(Received 25 March 2011; accepted 26 September 2011; published online 18 November 2011)

We address a specific but possible situation in natural water bodies when the three-layer stratification has a symmetric nature, with equal depths of the uppermost and the lowermost layers. In such case, the coefficients at the leading nonlinear terms of the modified Korteweg-de Vries (mKdV) equation vanish simultaneously. It is shown that in such cases there exists a specific balance between the leading nonlinear and dispersive terms. An extension to the mKdV equation is derived by means of combination of a sequence of asymptotic methods. The resulting equation contains a cubic and a quintic nonlinearity of the same magnitude and possesses solitary wave solutions of different polarity. The properties of smaller solutions resemble those for the solutions of the mKdV equation, whereas the height of the taller solutions is limited and they become table-like. It is demonstrated numerically that the collisions of solitary wave solutions to the resulting equation are weakly inelastic: the basic properties of the counterparts experience very limited changes but the interactions are certainly accompanied by a certain level of radiation of small-amplitude waves. © *2011 American Institute of Physics*. [doi:10.1063/1.3657816]

I. INTRODUCTION

Internal gravity waves serve as one of the most important constituent of nonlinear wave motions in stratified environment.[1] Internal waves often play the decisive role in various processes in geophysical and other similar media where they may serve as major agents carrying energy from remote areas to specific domains in the ocean. For example, energy release into local turbulent motions and subsequent mixing caused by internal waves apparently is an important source of the potential energy that is needed to bring deep, dense bottom water to the surface.[2–4] Their impact on the functioning of the ocean has been relatively well understood in shelf regions where high-amplitude, nonlinear, or breaking internal waves frequently contribute to localized highly energetic motions that not only are able to substantially affect offshore engineering activities[5] but also cause resuspension and transport of bottom sediments[6] or release of nutrients and pollution into the water column. Extensive patches of turbulence associated with propagation and breaking of such waves are hypothesized to be an important source of vertical mixing of water masses and, consequently, a key mechanism supporting penetration of various substances (including adverse impacts) from bottom layers up to the ocean surface. Changes to the properties of water at some depths may substantially modify acoustic properties of the environment.

The most interesting phenomena in this respect are internal solitons—localized, long-living disturbances that can carry wave energy and momentum far from the place of their generation, survive collisions with similar entities along their journey, and release the energy in certain specific conditions. The existence such phenomena has been recognized for a long time and their generic representatives have received a lot of attention.[7,8] Still there are major gaps in our understanding of the conditions of existence, properties, appearance, and dynamics of long-living solitonic internal waves and wave packets. Most of the relevant research has addressed their properties in a greatly simplified environment; usually in the framework of different versions of the two-layer fluid and/or solitonic solutions of integrable evolution equations. The simplest equation of this class is the well-known Korteweg-de Vries (KdV) equation that describes the motion of weakly nonlinear internal waves in the long-wave limit.[9] Later on, a variety of its extensions have been introduced, for example, the modified Korteweg-de Vries (mKdV) equation[10,11] and Gardner equation (sometimes called the KdV equation with combined nonlinearity[12–14] as it accounts for both quadratic and cubic nonlinearity).

The need for systematically accounting for higher nonlinearities stems from the nature of these equations. While the coefficients of similar equations in some other environments can be expressed in terms of simple combinations of governing scales for the particular problem,[15,16] the coefficients of nonlinear evolution equations for internal waves are defined by the particular vertical distribution of water density, properties of shear flow, and boundary conditions at the water surface.[17–20] A specific property of such equations is that some coefficients at the nonlinear terms may vanish for certain symmetric situations.[10,21] In such cases, it is necessary to account for higher-order nonlinearities to adequately describe

the motion. This process not only leads to the necessity of inclusion of some additional terms in the governing equations but also naturally highlights a variety of qualitatively new phenomena in the dynamics of localized, solitonic (non-radiating) internal waves – solutions to such equations.[12–14,22,23]

In this paper, we shall analyze properties of internal solitons in the framework of the widely used concept of layered fluid. Models of wave motion for such environments are attractive for both theoretical research and applications because of their ability to mirror the basic properties of the actual internal wave systems using model equations of stratified media containing small number parameters and in many cases allowing for extensive analytical studies of the properties of solutions. As mentioned above, the simplest system basically representing the key properties of internal waves is the two-layer model. Various properties of internal waves in this approximation have been addressed in numerous analytical and numerical studies as well as by means of *in situ* observations and laboratory experiments.[17,21,24–33] These studies cover a wide range of different regimes of wave motion, from ideally linear systems and weakly nonlinear models up to fully nonlinear phenomena.

The two-layer model and the family of the KdV equation and its generalizations have been used as a simple but instructive model to demonstrate the richness of internal wave phenomena compared to long weakly nonlinear surface waves. Namely, for internal waves, the coefficient at the quadratic nonlinearity in the KdV equation vanishes for the naturally occurring symmetric situation when the layers have equal thicknesses in Boussinesq approximation. The leading nonlinear term in almost symmetric situations is the cubic one and the Gardner equation (or its generalizations) has to be used to describe the wave motion.[21,24,25,34–37] The inclusion of only one (cubic) nonlinear term gives rise to several principally new phenomena that do not occur in the KdV environment. For example, if the coefficient at the cubic term is negative (this is the case for the two-layer fluid), the amplitude of solitons has an upper limit. While the increase in the energy for the KdV soliton is associated with a higher and narrower wave profile, the similar process for the relevant class of solutions of the Gardner equation results in a widening of the wave profile and formation of a plateau-like entity with steep front and back and very gently sloping upper part. Such appearance of large-amplitude solitary waves has been repeatedly observed in both laboratory and field conditions.[11,38,39]

The two-layer fluid is, in fact, quite a simplified representation of the natural stratified flows. For example, in many areas of the World Ocean, the vertical stratification has a clearly pronounced three-layer structure, with well-defined seasonal thermocline at a depth of $\sim$100 m and the main thermocline at much larger depths.[40,41] Several basins such as the Baltic Sea host more or less continuously three-layer vertical structure.[42] In order to reveal the basic features of the internal wave field in such environments it is necessary to introduce a three-layer model. Such models are considerably more complex than the two-layer systems; however, they allow for much more analytical progress compared to the fully stratified situation.

In this paper, we address a generalization of the mKdV equation for the three-layer stratification. This procedure is basically straightforward, albeit cumbersome and technically complicated. The resulting equation admits solitary wave solutions for a certain range of parameters. The focus of the study is almost symmetric situations in which the lower-order nonlinear terms vanish, and the higher-order contributions govern the behavior of wave phenomena in the system. A simple symmetric situation corresponds to the equal thicknesses of the uppermost and the lowermost layers provided the density differences between the layers are also equal. This situation can naturally occur in shallow strongly stratified seas as the Baltic Sea where the interplay of fresh water discharge to the surface and irregular salt water intrusion in the bottom layers frequently give rise to two density jumps of comparable size and sharpness and an almost symmetric three-layer structure and may lead to vanishing of several interactions between baroclinic Rossby waves.[42,43] The key development through the research into such an environment (that is impossible in the two-layer medium) is the possibility of having the cubic nonlinearity with a positive coefficient. Moreover, this coefficient may change its sign in different domains and may even vanish under certain conditions.[10] As a result, the dynamics of internal waves in such environments is much richer in content and reveals several features that cannot become evident in two-layer flows. In particular, the possibility of simultaneous vanishing of the coefficients at both the quadratic and cubic nonlinear terms makes it possible to naturally generalize the mKdV equation towards accounting for the quadric nonlinearity and towards even more detailed analytical description of the properties of internal wave dynamics in layered fluids.

Almost zero values of the coefficients of quadratic and cubic nonlinear terms of the mKdV equation and its generalizations (see Eq. (6) below for an example), albeit not very usual in the World Ocean, can still be found for real sea stratifications in certain regions. The maps of the geographical points where the coefficient α of quadratic nonlinearity is small ($|\alpha| < 1 \times 10^{-4}$, while the usual values of this parameter are of order of 1×10^{-2}), and at the same time the coefficient α_1 of cubic nonlinearity is also small and non-negative ($0 \leq \alpha_1 \leq 1 \times 10^{-5}$, usual values of order of 1×10^{-3}) (Fig. 1) reveals that such situations occur during some months in selected shelf seas and in the North Atlantic. Hydrological data to calculate the numerical values of the nonlinear parameters on a base of integral expressions for continuous stratification[44] were taken from the climatological atlas GDEM V3.0.[45] Horizontal shear flow was not accounted for. The maps in Figs. 1 and 2 are drawn using OCEAN DATA VIEW software.[46]

Three-layer density stratification (and its symmetric examples as well) frequently appears in the Baltic Sea. The density structure of the central part often consists of a mixed upper layer, well-defined seasonal thermocline, an intermediate layer, and main halocline (Fig. 2). Importantly, the density changes between the layers are more or less equal.[42] There is evidence that this stratification will be more frequent in the Baltic Sea for some climate change scenarios.

The paper is organized as follows. Section II presents the basic equations of motion for the three-layer model.

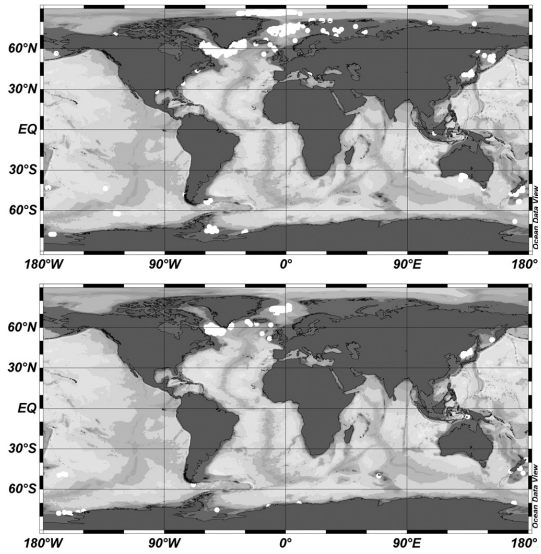

FIG. 1. Maps of the geographical locations (white points) where the coefficient of quadratic nonlinearity is small and the coefficient of cubic nonlinearity is small and non-negative ($|\alpha| < 1 \times 10^{-4}$, $0 \le \alpha_1 < 1 \times 10^{-5}$): upper panel – January, lower panel – July.

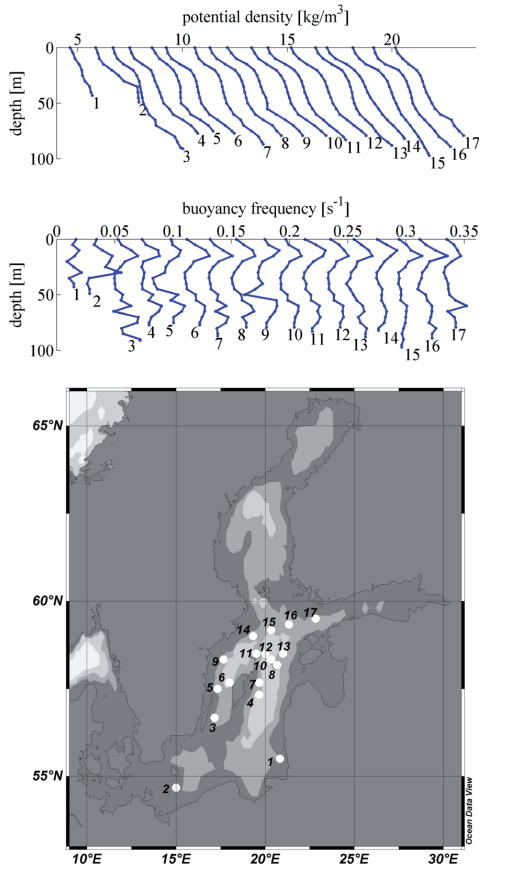

FIG. 2. (Color online) Upper panel: vertical density profiles in the Baltic Sea (based on GDEM V3.0 climatology for July). The profile number M is shifted to the right by M–1 density units. Middle panel: corresponding vertical buoyancy frequency profiles. The profile number M is shifted to the right by $0.02(M–1)$ s^{-1}. Lower panel: map of the geographical locations (white points) of the profiles above.

Asymptotic analysis of the equations for the interfaces of the three-layer model is provided in Sec. III up to the 4th order with respect to the small parameters in the system. Section IV focuses on the modifications of the derivation of the mKdV equation towards expressing the balance between nonlinear and dispersive terms in the case when the coefficients of the leading nonlinear terms vanish. The basic properties of solitary solutions to the resulting equation are discussed in Sec. V and their nonlinear interactions in Sec. VI. Section VII presents discussion and conclusions and Appendix—the analytical expression of the coefficients of the derived equations and parameters of numerical simulations.

II. NONLINEAR EQUATIONS OF MOTION

Let us consider a model situation of irrotational motions in a three-layer inviscid fluid of total thickness H overlying a flat horizontal bottom in the approximation of a rigid lid on the surface of the fluid (Fig. 3). We consider the symmetric case in which the thicknesses h of the surface and bottom layer are equal and assume that the density differences between the layers are also equal; then densities in the layers are $\rho_1 = \rho$, $\rho_2 = \rho + \Delta\rho$, $\rho_3 = \rho_2 + \Delta\rho = \rho + 2\Delta\rho$, where ρ is the density in the bottom layer. As usual, we employ the Boussinesq approximation and assume that densities in the layer differ insignificantly ($\Delta\rho/\rho \ll 1$). In this case, the equations of the motion are Laplace equations for the velocity potential in each layer

$$\nabla^2\Phi_i = 0, \quad i = 1, 2, 3. \tag{1}$$

The vertical velocities at the bottom and at the fixed upper boundary obviously vanish

$$\Phi_{1z}(z = 0) = 0, \quad \Phi_{3z}(z = H) = 0, \tag{2}$$

where the subscript x, y, or z denotes a partial derivative. The classical kinematic and dynamic boundary conditions at the interfaces between the layers complete the setup of the problem

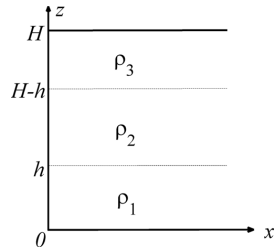

FIG. 3. Definition sketch of the three-layer fluid.

$$\left.\begin{aligned} \eta_t + \Phi_{1_x}\eta_x - \Phi_{1_z} &= 0 \\ \eta_t + \Phi_{2_x}\eta_x - \Phi_{2_z} &= 0 \\ \rho_1\left(\Phi_{1t} + \frac{1}{2}(\nabla\Phi_1)^2 + g\eta\right) &= \rho_2\left(\Phi_{2t} + \frac{1}{2}(\nabla\Phi_2)^2 + g\eta\right) \end{aligned}\right\} z = h + \eta(x,t),$$

$$\left.\begin{aligned} \zeta_t + \Phi_{2_x}\zeta_x - \Phi_{2_z} &= 0 \\ \zeta_t + \Phi_{3_x}\zeta_x - \Phi_{3_z} &= 0 \\ \rho_2\left(\Phi_{2t} + \frac{1}{2}(\nabla\Phi_2)^2 + g\zeta\right) &= \rho_3\left(\Phi_{3t} + \frac{1}{2}(\nabla\Phi_3)^2 + g\zeta\right) \end{aligned}\right\} z = H - h + \zeta(x,t). \tag{3}$$

Here, the unknown functions $\eta(x, t)$ and $\zeta(x, t)$ denote the instantaneous position of the interface between the bottom and the middle layer and between the upper and middle layer, respectively.

III. ASYMPTOTIC EXPANSION

In order to derive an evolution equation for wavelike motions of relatively small amplitude in the described environment, it is convenient to introduce characteristic scales of both the environment and the waves, and to perform the analysis in nondimensional form. The system of motions has one obvious length scale—the fluid depth H. Wave motions provide two more natural scales—the typical horizontal scale of motions L and amplitude a (understood here as the typical magnitude of deviation of the interfaces from their undisturbed location). Following the underlying assumptions usually made in derivation of the KdV equation and its generalizations, we focus on long waves, that is, on the situation $L \gg H$ where the typical wave length considerably exceeds the depth of the fluid. In this case, small parameter $\bar{\mu} = H/L$ naturally enters the system. Long-living wave motions usually exist in the system if the amplitude of such motions is small compared to the fluid depth, equivalently, when the parameter of nonlinearity $\varepsilon = a/H \ll 1$. Finally, the parameter characterizing the role of dispersion in wave propagation $\mu = \bar{\mu}^2$ becomes evident in the process of nondimensionalisation.

As long-living wave motions and solitary waves usually exist when the magnitude of the terms representing nonlinear and dispersive is balanced, we assume that $\varepsilon \sim \mu$. This implies that $\bar{\mu} \sim \sqrt{\varepsilon}$.

The asymptotic analysis is straightforward under assumption that all the above-discussed parameters are small. As it is quite cumbersome and largely follows that in Ref. 24, we omit the details and depict only the major steps. All unknown functions are expanded into Taylor series in the vicinity of one of the interfaces. The constituents of the resulting series are then expanded into power series with respect to powers of $\varepsilon = a/H \ll 1$. In order to use the technique of multiple time and spatial scales,[43,47,48] we introduce the "slow" time and "stretched" coordinate along the x-axis

$$\xi = \varepsilon^{1/2}(x - ct), \quad \tau = \varepsilon^{3/2}t, \tag{4}$$

where c is the phase speed. Substitution of these expansions and expressions (4) into nondimensionalised Eqs. (3) leads to an infinite system of equations. This system can be solved recursively until any desired order. Details of the relevant derivation are available in Ref. 49.

The system of equations for the leading order ($\sim\varepsilon^0$) terms has a relatively simple form and describes the field of linear internal waves in the three-layer environment in question. One of the two wave modes that exist in this system has a completely symmetric nature and results in synchronous in-phase movements of both the interfaces $\eta(x, t) = \zeta(x, t)$. The other mode is antisymmetric: the motions of the interfaces are synchronous but have opposite signs $\eta(x, t) = -\zeta(x, t)$.

Below, we shall consider only the nonlinear motions of the symmetric mode corresponding to the following expression for the phase speed (similar to that of the classical interfacial waves in two-layer medium):

$$c^2 = \frac{gh\Delta\rho}{\rho}. \tag{5}$$

The outcome of the asymptotic procedure at the first order ($\sim\varepsilon^1$) is, as expected, the well-known KdV equation that describes the motion of both the interfaces.

Combining of lower-order equations leads to the following generalization of the KdV equation for the interfaces (presented here in the original coordinates for ζ):

$$\begin{aligned} &\zeta_t + c\zeta_x + \alpha\zeta\zeta_x + \beta\zeta_{xxx} + \alpha_1\zeta^2\zeta_x + \beta_1\zeta_{5x} + \gamma_1\zeta\zeta_{xxx} + \gamma_2^*\zeta_x\zeta_{xx} \\ &\quad + \alpha_2^*\zeta^3\zeta_x + \beta_2\zeta_{7x} + \gamma_{21}\zeta_{xx}\zeta_{xxx} + \gamma_{22}\zeta_x\zeta_{xxxx} + \gamma_{23}\zeta\zeta_{5x} \\ &\quad + \gamma_{31}\zeta_x^3 + \gamma_{32}\zeta\zeta_x\zeta_{xx} + \gamma_{33}\zeta^2\zeta_{xxx} + \alpha_3\zeta^4\zeta_x + \beta_3\zeta_{9x} \\ &\quad + \gamma_{41}^*\zeta_x\zeta_{6x} + \gamma_{42}^*\zeta_{xx}\zeta_{5x} + \gamma_{42}^*\zeta_{xxx}\zeta_{xxxx} + \gamma_{51}\zeta\zeta_{xx}\zeta_{xxx} \\ &\quad + \gamma_{52}\int\zeta_x\zeta_{xx}\zeta_{xxx}dx + \gamma_{53}\zeta\zeta_x\zeta_{xxxx} + \gamma_{54}\zeta^2\zeta_{5x} + \gamma_{55}\zeta_\tau^2\zeta_{xxx} \\ &\quad + \gamma_{56}\zeta_x\zeta_{xx}^2 + \gamma_{61}^*\zeta\zeta_x^3 + \gamma_{62}^*\zeta^2\zeta_x\zeta_{xx} + \gamma_{63}^*\zeta^3\zeta_{xxx} = 0. \end{aligned} \tag{6}$$

The coefficients of Eq. (6) are given in Appendix. The equation for η has a similar structure and differs from Eq. (6) only by signs of a few additives marked by *.

An interesting, important, and rich in content particular case occurs when the coefficients α at quadratic terms and the coefficient reflecting the role of nonlinear dispersion γ_1 vanish simultaneously. This always happens for the symmetric distribution of layers in the three-layer medium for an arbitrary ratio of the layers' thicknesses. This case, as mentioned above, is not very common, but eventually occurs in natural conditions in some domains of micro-tidal estuaries and shelf seas and thus needs more detailed analysis.

IV. MODIFIED KdV EQUATION (mKdV)

In essence, the vanishing of the coefficient α at quadratic terms in the resulting evolution equations means that some other terms largely govern the motion and that the straightforward asymptotic expansion introduced above becomes invalid. It is easy to see that, formally, the reason for the failure is that the assumption of equivalence of the contributions of nonlinearity and dispersion ($\varepsilon \sim \mu$) to the formation of motion patterns is no more valid. In such situations, it is first necessary to establish which from the higher-order terms provides the largest contribution to the motion. As the presence of solitonic solutions in the system in question normally is associated with a specific balance of nonlinear and dispersive terms, it is natural to keep this balance also in the higher-order modifications to the KdV equation. The appearance of Eqs. (6) suggests that such a balance in symmetric stratified media is possible if $\varepsilon^2 \sim \mu$. This property actually means that the higher-order nonlinear terms provide a relatively large contribution to the governing equation compared with the dispersive terms.

Introducing variables $\eta = \varepsilon\tilde{\eta}$, $\zeta = \varepsilon\tilde{\zeta}$, $\tilde{x} = \bar{\mu}x$, $\tilde{t} = \bar{\mu}t$, Eq. (6) can be presented as follows (for simplicity we omit tildes):

$$\begin{aligned}
&\zeta_t + c\zeta_x + \varepsilon\alpha\zeta\zeta_x + \mu\beta\zeta_{xxx} + \varepsilon^2\alpha_1\zeta^2\zeta_x + \mu^2\beta_1\zeta_{5x} \\
&\quad + \varepsilon\mu\left(\gamma_1\zeta\zeta_{xxx} + \gamma_2^*\zeta_x\zeta_{xx}\right) + \varepsilon^3\alpha_2^*\zeta^3\zeta_x + \mu^3\beta_2\zeta_{7x} \\
&\quad + \varepsilon\mu^2(\gamma_{21}\zeta_{xx}\zeta_{xxx} + \gamma_{22}\zeta_x\zeta_{xxxx} + \gamma_{23}\zeta\zeta_{5x}) \\
&\quad + \varepsilon^2\mu\left(\gamma_{31}\zeta_x^3 + \gamma_{32}\zeta\zeta_x\zeta_{xx} + \gamma_{33}\zeta^2\zeta_{xxx}\right) + \varepsilon^4\alpha_3\zeta^4\zeta_x + \mu^4\beta_3\zeta_{9x} \\
&\quad + \varepsilon\mu^3\left(\gamma_{41}^*\zeta_x\zeta_{6x} + \gamma_{42}^*\zeta_{xx}\zeta_{5x} + \gamma_{43}^*\zeta_{xxx}\zeta_{xxxx}\right) \\
&\quad + \varepsilon^2\mu^2\left(\gamma_{51}\zeta\zeta_{xx}\zeta_{xxx} + \gamma_{52}\int\zeta_x\zeta_{xx}\zeta_{xxx}dx + \gamma_{53}\zeta\zeta_x\zeta_{xxxx}\right. \\
&\quad \left. + \gamma_{54}\zeta^2\zeta_{5x} + \gamma_{55}\zeta_x^2\zeta_{xxx} + \gamma_{56}\zeta_x\zeta_{xx}^2\right) \\
&\quad + \varepsilon^3\mu\left(\gamma_{61}^*\zeta\zeta_x^3 + \gamma_{62}^*\zeta^2\zeta_x\zeta_{xx} + \gamma_{63}^*\zeta^3\zeta_{xxx}\right) = 0. \qquad (7)
\end{aligned}$$

Making Making use of assumption $\varepsilon^2 = \mu$ leads to the following equation:

$$\begin{aligned}
&\zeta_t + c\zeta_x + \alpha_1\zeta^2\zeta_x + \beta\zeta_{xxx} + \varepsilon\left(\alpha_2^*\zeta^3\zeta_x + \gamma_2^*\zeta_x\zeta_{xx}\right) \\
&\quad + \varepsilon^2\left(\alpha_3\zeta^4\zeta_x + \gamma_{31}\zeta_x^3 + \gamma_{32}\zeta\zeta_x\zeta_{xx} + \gamma_{33}\zeta^2\zeta_{xxx} + \beta_1\zeta_{5x}\right) \\
&\quad + O\left(\varepsilon^3\right) = 0, \qquad (8)
\end{aligned}$$

where the analytical expressions for the coefficients are presented in Appendix and, as above, in the equation for $\eta(x, t)$ the signs of coefficients α_2^* and γ_2^* are reversed. The lowest order terms in Eq. (8) form well-known modified KdV equation (mKdV) that are complemented with terms describing the contribution of higher-order ($O(\varepsilon)$ and $O(\varepsilon^2)$) nonlinearities, nonlinear dispersion and also linear dispersion $\beta_1\zeta_{5x}$.

It is interesting and instructive to analyze the dependence of the coefficients of Eq. (8) on the ratio of the layers' thicknesses in our case of symmetric stratification. Figure 4 demonstrates that the coefficient α_1 at the cubic nonlinear term and the coefficient α_2 at the highest-order quadratic nonlinearity vanish simultaneously at $h/H = 9/26 \equiv h_{cr}/H$. For both coefficients, this is the zero-crossing point at which their sign is reversed. Only the coefficient α_3 at the quintic nonlinearity is always negative. The coefficients β, β_1 reflecting the contribution from linear dispersive terms as well as the coefficient γ_2 characterizing nonlinear dispersion are always positive. Finally, the coefficients at nonlinear dispersive terms γ_{31}, γ_{32}, and γ_{33} have one zero-crossing point, whereas these points coincide neither with each other nor with the point h_{cr}/H.

The performed analysis shows that although the higher-order terms of the mKdV are usually small in comparison with the leading-order nonlinear and dispersive terms, in the symmetric stratification the coefficients at the two leading nonlinear terms vanish simultaneously. Although this situation evidently does not happen very often, its presence is likely in some domains in natural conditions[43] and it is, therefore, important to analyze the behavior of internal waves in conditions when the contribution from these two terms is negligible and the motion is governed by higher order additives.

It is convenient to start the detailed analysis of this case from expansion of the coefficients of Eq. (8) into Taylor series in the vicinity of the zero-crossing point for the coefficients of the leading-order nonlinearities h_{cr} ($\Delta = (h - h_{cr})/H$)

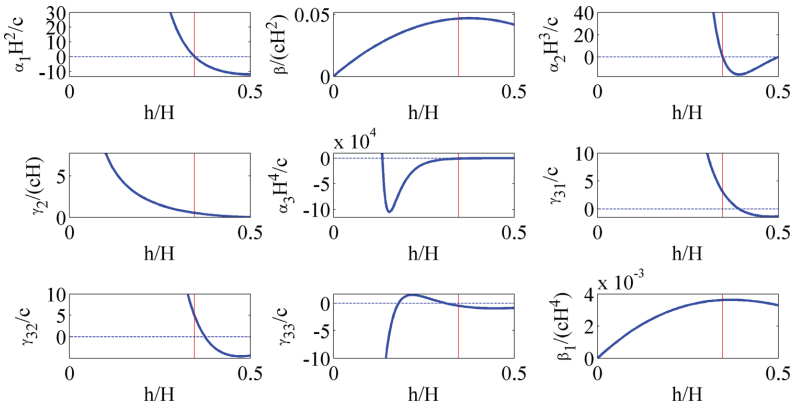

FIG. 4. (Color online) The dependence of coefficients of Eq. (8) on the ratio of the thicknesses of the layers in the case of symmetric stratification. Horizontal dotted lines indicate the zero-crossing points of the relevant coefficients and the vertical dotted lines—the point h_{cr}/H.

$$\alpha_1 = -\frac{c}{H^2}\frac{57122}{243}\Delta + \mathrm{O}(\Delta^2) = \tilde{\alpha}_1\Delta + \mathrm{O}(\Delta^2),$$
$$\beta = cH^2\left(\frac{63}{1352} + \frac{1}{52}\Delta\right) + \mathrm{O}(\Delta^2) = \tilde{\beta} + \mathrm{O}(\Delta),$$
$$\alpha_2^* = \frac{c}{H^3}\frac{5940688}{6561}\Delta + \mathrm{O}(\Delta^2) = \tilde{\alpha}_2\Delta + \mathrm{O}(\Delta^2),$$
$$\frac{\gamma_2^*}{cH} = \frac{7}{13} - \frac{115}{18}\Delta + \mathrm{O}(\Delta^2),$$
$$\frac{\alpha_3 H^4}{c} = -\frac{47411260}{59049} + \frac{12084101978}{531441}\Delta + \mathrm{O}(\Delta^2),$$
$$\frac{\gamma_{31}}{c} = \frac{1483}{486} - \frac{298285}{2916}\Delta + \mathrm{O}(\Delta^2),$$
$$\frac{\gamma_{32}}{c} = \frac{2341}{486} - \frac{641017}{2916}\Delta + \mathrm{O}(\Delta^2),$$
$$\frac{\gamma_{33}}{c} = -\frac{109}{243} - \frac{30589}{2916}\Delta + \mathrm{O}(\Delta^2),$$
$$\frac{\beta_1}{cH^4} = \frac{66291}{18279040} + \frac{1099}{1054560}\Delta + \mathrm{O}(\Delta^2).$$

The extension of the mKdV equation towards inclusion of the higher-order terms for small values of Δ (equivalently, in the vicinity of the point h_{cr}) is as follows:

$$\zeta_t + c\zeta_x + \tilde{\alpha}_1\Delta\zeta^2\zeta_x + \tilde{\beta}\zeta_{xxx} + \varepsilon\left(\tilde{\alpha}_2^*\Delta\zeta^3\zeta_x + \tilde{\gamma}_2^*\zeta_x\zeta_{xx}\right) + \varepsilon^2\left(\tilde{\alpha}_3\zeta^4\zeta_x + \tilde{\gamma}_{31}\zeta_x^3 + \tilde{\gamma}_{32}\zeta\zeta_x\zeta_{xx} + \tilde{\gamma}_{33}\zeta^2\zeta_{xxx} + \tilde{\beta}_1\zeta_{5x}\right) + O\left(\varepsilon^3\right) = 0. \tag{9}$$

It is easy to see that in this particular case of the symmetric three-layer stratification a balance between nonlinear and dispersive effects exists when the small parameters Δ and ε are related as follows $\Delta \sim \varepsilon^2$. After performing rescaling $\hat{x} = \bar{\mu}x$, $\hat{t} = \bar{\mu}t$ and removing the "hats," we have

$$\zeta_t + \varepsilon^2\left(\tilde{\alpha}_1\zeta^2\zeta_x + \tilde{\alpha}_3\zeta^4\zeta_x\right) + \mu\tilde{\beta}\zeta_{xxx} + \varepsilon\mu\tilde{\gamma}_2^*\zeta_x\zeta_{xx} + \varepsilon^2\mu\left(\tilde{\gamma}_{31}\zeta_x^3 + \tilde{\gamma}_{32}\zeta\zeta_x\zeta_{xx} + \tilde{\gamma}_{33}\zeta^2\zeta_{xxx}\right) + \mu^2\tilde{\beta}_1\zeta_{5x} + O\left(\varepsilon^3, \mu^3, \varepsilon\mu^2\right) = 0,$$

where, as above, the equation for $\eta(x, t)$ only differs from the above one by the reversed sign of the coefficient $\tilde{\gamma}_2^*$.

Summarizing the above considerations, in this particular case the balance between the leading (nonzero) dispersive and nonlinear terms occurs when $\varepsilon^2 = \mu$. In the coordinate system consisting of slow time and stretched x-axis $\hat{x} = x - ct$, $\hat{t} = \varepsilon^2 t$, the relevant equation for any of the interfaces is (the "hats" omitted)

$$\zeta_t + \tilde{\alpha}_1\zeta^2\zeta_x + \tilde{\alpha}_3\zeta^4\zeta_x + \tilde{\beta}\zeta_{xxx} = 0. \tag{10}$$

Equation (10) provides a description of motions and phenomena occurring in situations when the leading-order nonlinear and dispersive terms of the mKdV equation are negligible. In this case, the resulting equation contains two leading nonlinear terms of the same magnitude: the cubic and quintic nonlinearities. Both the terms consist of the product of a power (2nd or 4th) of the unknown function and its first-order spatial derivative. The resulting equation differs from the classical Gardner equation (that is frequently used for motions in situations containing zero-crossing of the coefficient at the quadratic nonlinearity, for example, in two-layer media with almost equal layers) by the presence of the quintic nonlinearity. This equation, obviously, belongs to the family of generalized Gardner equations[50,51] used to describe different properties of internal waves. Following the nomenclature of different extensions of the KdV equation, Eq. (10) may be called $2+4$ Korteweg-de Vries-like equation, abbreviated $2+4$ KdV.

The above has shown that auxiliary equations derived in the process of the asymptotic analysis had different appearances for different interfaces. Remarkably, Eq. (10) is universal in the sense that it is identical for both the upper and the lower interfaces. This feature is not completely unexpected as the classical mKdV equation is also universal for both the interfaces. Therefore, we can analyze only one equation (10) without the loss of generality. We shall do this for the upper interface $\zeta(x, t)$.

As equations $\zeta_t + \zeta^n\zeta_x + \zeta_{xxx} = 0$ with $n > 2$ are non-integrable (in particular, with respect to the Zakharov-Shabat method[52,53]), it is likely that Eq. (10) is also non-integrable. The question about its integrability is, however, out of the scope of the current study.

Differently from Eq. (8), Eq. (10) has two conservation laws of mass and energy

$$M = \int_{-\infty}^{\infty}\zeta dx, \quad E = \int_{-\infty}^{\infty}\zeta^2 dx. \tag{11}$$

The decisive parameters for wave motion in media described by Eq. (10) are the signs of the coefficients at its nonlinear terms. As mentioned above, the coefficient α_1 at the cubic nonlinearity is sign-variable in the vicinity of h_{cr}/H. The coefficient α_3 at the quintic nonlinearity is negative in this region but may change its sign at $h/H < (423 - 3\sqrt{6641})/1324 \approx 0.1348$. The analysis of the stratification corresponding to these values of the layers' thicknesses is out of the scope of this paper, mostly because it corresponds to quite large values of Δ but Eq. (10) is valid in the neighborhood of $\Delta = 0$.

An important feature of Eq. (10) is that it has solitary wave solutions. The relevant analysis of their existence and appearance (including the impact of the quintic nonlinearity on their shape compared to that of the classical mKdV equation) is presented in the following sections. It is well-known that solitons of the extensions of KdV equations of the form $\zeta_t + \zeta^n\zeta_x + \zeta_{xxx} = 0$ with $n \geq 4$ are unstable,[53] and that for such equations both smooth and localized initial conditions develop singularities within finite time (or at finite distances). To our knowledge, neither integrability of Eq. (10) nor stability of solitary wave solutions for Eq. (10) (or its analogues with combined (cubic and quintic) nonlinearity) has been addressed in literature. But all our numerical simulations of the initial problem for Eq. (10) with smooth and localized initial conditions showed a stable wave dynamics, with no evidence of instabilities or collapses even in interactions. Therefore, it seems plausible that the cubic nonlinearity plays a stabilizing

role. This conjecture, however, requires a more detailed study, which is out of scope of this paper.

V. SOLITARY WAVE SOLUTIONS

Let us consider steady-state (in a properly chosen moving coordinate system) localized solutions $\zeta_s(x - Vt)$ to Eq. (10). Such solutions can be expressed in implicit form in terms of the integral

$$Y - Y_0 = \sqrt{\beta}\int_{v_0}^{v_S}\left(V\zeta^2 - \frac{\alpha_1}{6}\zeta^4 - \varepsilon\frac{\alpha_3}{15}\zeta^6\right)^{-1/2}d\zeta, \qquad (12)$$

where V is the propagation speed of the disturbance and $Y = x - Vt$. The substitution $A = \zeta^2$ would reduce Eq. (12) to a similar expression for the Gardner equation, and the solitary wave solutions can be derived. For $\alpha_1 > 0$ these solutions can be expressed explicitly

$$\zeta(Y) = \pm\sqrt{\frac{60V}{5\alpha_1 + \sqrt{25\alpha_1^2 + 240\alpha_3 V}\cosh\left(2Y\sqrt{\frac{V}{\beta}}\right)}}. \qquad (13)$$

It is easy to demonstrate that Eq. (13) describes localized solutions to Eq. (10). The maximum amplitude a of the excursions of the interface is obviously

$$a = \sqrt{\frac{60V}{5\alpha_1 + \sqrt{25\alpha_1^2 + 240\alpha_3 V}}}. \qquad (14)$$

Similarly to the solutions of the Gardner equation, the propagation speed of such solutions depends on their amplitude a

$$V = \frac{\alpha_1}{6}a^2 + \frac{\alpha_3}{15}a^4.$$

The natural limit for the wave speed stems from the request that expressions under the square root in Eqs. (13) and (14) must be non-negative for physically meaningful solutions. This condition means that the wave speed V has an upper limit

$$V_{\lim} = -\frac{5\alpha_1^2}{48\alpha_3}. \qquad (15)$$

Consequently, the amplitude of solutions is also limited by the following value:

$$a_{\lim} = \frac{1}{2}\sqrt{\frac{5\alpha_1}{-\alpha_3}}. \qquad (16)$$

The limiting amplitude in Eq. (16) can be expressed using the relative thickness of the lower and upper layers (equivalently, using the ratio $l = h/H$):

$$\frac{a_{\lim}}{H} = \frac{2}{3}l^2\sqrt{15}\sqrt{\frac{9 - 26l}{1324l^3 - 1508l^2 + 513l - 45}}. \qquad (17)$$

The limiting amplitude reaches its maximum values $a_{\lim} \approx 0.0864\,H$ at $h/H \approx 0.286$. This corresponds to the highest possible location $h + a_{\lim} \approx 0.397\,H$ of the lower interface,

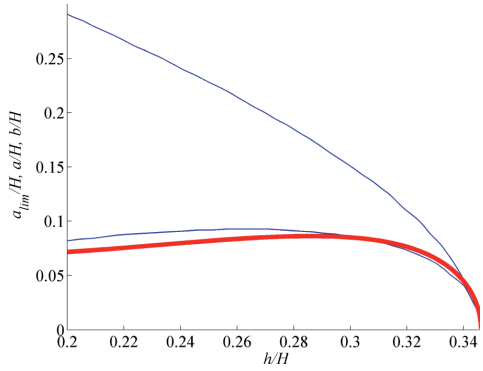

FIG. 5. (Color online) Nondimensional values of limiting amplitudes of solitary wave solutions to Eq. (10) (thick line) and nondimensional amplitudes of deviations of interfaces in three-layer symmetric flows with conjugate flows (thin lines, $a(b)$ in Ref. 60). The upper and lower thin lines show the deviation of the lower and the upper interfaces, respectively, for the positive disturbances. The situation is reversed for the negative solitary waves.

whereas the relevant $h \approx 0.3243\,H$ insignificantly differs from h_{cr}.

The dependence of the limiting amplitude $a_{\lim}$ on the relative thickness of layers h/H has quite a complicated appearance (Fig. 5). This amplitude increases slowly with the increase in h/H and reveals a very gently sloping maximum at $h/H \approx 0.286$. Further increase in h/H is first accompanied with a gentle decrease in $a_{\lim}$ that is replaced by almost explosive decrease in the limiting amplitude near the zero-crossing point $h/H = 9/26$.

For relatively low solitary wave speeds (equivalently, relatively low amplitudes), the profiles of solitary solutions to Eq. (10) resemble similar solutions to the mKdV equation (Fig. 6; see the expressions for the relevant parameters in

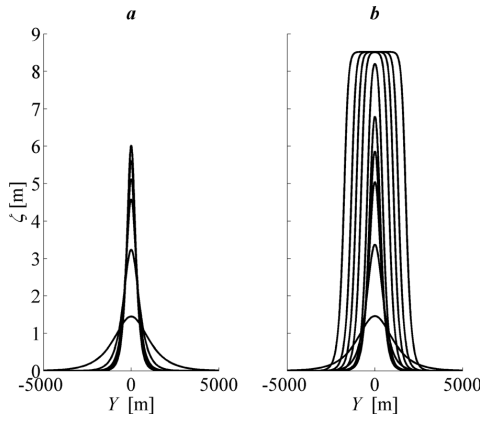

FIG. 6. The shape of solitary wave solutions to the classical mKdV equation (a) and for Eq. (10) (b), for solitary wave speeds of $V = 0.001$, 0.005, 0.01, 0.0125, 0.015, 0.0172, 0.017294, 0.01729412, 0.01729412063, 0.01729412063364 (m/s). The smaller speeds correspond to the lower-amplitude waves. The parameters for the calculations are indicated in Appendix. Note that several lines for large-amplitude waves in panel (a) are not separable from each other.

Appendix). For larger wave speeds (larger amplitudes), the two sets of solutions considerable differ from each other. The key difference is that large-amplitude solutions to Eq. (10) form a table-like wide signal that may, theoretically, infinitely widen in the process $V \to V_{\lim}$ whereas their amplitude asymptotically tends to $a_{\lim}$. Both positive and negative solitary wave solutions are possible for each combination of the signs of the coefficients of Eq. (10).

Similar table-like solutions are characteristic for some other equations containing higher-order nonlinear terms, for example, they exist for the Gardner equation that describes motions in the two-layer fluid and where the cubic nonlinearity is of the leading order. The existence of such wide table-like solitons and the possibility of their propagation in combinations with other solitons have been demonstrated for several other classes of nonlinear wave models.[27,38,54,55]

The solutions in question have several features similar to Gardner solitons; in particular, their amplitude is limited and the increase in the amplitude is accompanied by virtually unlimited widening of the wave profile. The set of Gardner solitons has much more rich in content variety of properties compared to the KdV and mKdV solitons. For example, this set allows for propagation of smaller solitons along the wide table-like crest of large solitons the amplitude of which is close to the limiting one, or the possibility of formation of two trains of solitons of different polarity during the process of dispersion of disturbances with amplitudes exceeding the limiting amplitude. Moreover, the development of the system of solitons is very much different for rectangular and smooth initial pulses of otherwise equivalent properties. It is natural to expect that the set of solutions to Eq. (10) also possesses a larger variety of different features compared to the ensembles of KdV or mKdV solitons.

The described table-like appearance of solutions for the relatively large-amplitude and rapidly moving disturbances with steep fronts may have substantial consequences in practical applications. The propagation of such disturbances is similar to the motion of smooth bores that possess considerable danger for objects on their way. Such horizontal motions (smooth bores, sometimes called conjugate flows) are frequent in vertically inhomogeneous fluids.[56–58] The performed analysis shows that such flows can naturally occur in three-layer fluids for some combinations of the layers' thicknesses and density variations.

Numerical simulations of flows in media with continuous vertical stratification with two pycnoclines and with a simplified three-layer model have been performed by several authors.[59–61] A comparison of the results of the theory of conjugate fluxes in symmetric three-layer environment with the values of the limiting amplitude based on Eqs. (16) and (17) is presented in Fig. 5. For the situations in which the thicknesses of the upper and lower layers are close to h_{cr}, the amplitudes of deviations of the interfaces from their undisturbed locations are relatively small and almost equal for all the presented cases, for conjugate fluxes in the nonlinear model and for the above derived estimate of $a_{\lim}$ in the weakly nonlinear model. If the thicknesses of the layers are considerably different from h_{cr}, the amplitudes of deviations of the upper and lower interfaces become substantially different. It is remarkable that the estimate of the deviation $a_{\lim}$ in the weakly nonlinear framework practically coincides with one of those for the fully nonlinear case for a wide range of h/H. The similarity occurs for the deviation of the interface that bends into the thinner outer (the uppermost or the lowermost) layer.

For the range of layers' depths $h > h_{cr}$ ($\Delta > 0$), a solution exists neither for our weakly nonlinear approach nor in the theory of conjugate flows.

VI. INTERACTIONS OF SOLITARY SOLUTIONS OF THE 2 + 4 KdV EQUATION

Generally speaking, interactions and collisions of solitary solutions to non-integrable evolution equations are inelastic. It is, therefore, not unexpected that solitary solutions to Eq. (10) interact inelastically with each other and with the background wave fields. As a demonstration of this feature, we present an example of numerically simulated collision of two solitonic solutions corresponding to the values of coefficients given in Appendix.

The numerical code used in integration of Eq. (10) employs an implicit pseudo-spectral method[62] that conserves the integrals presented in Eq. (11). The spatial domain was chosen based on the analytically estimated propagation speed

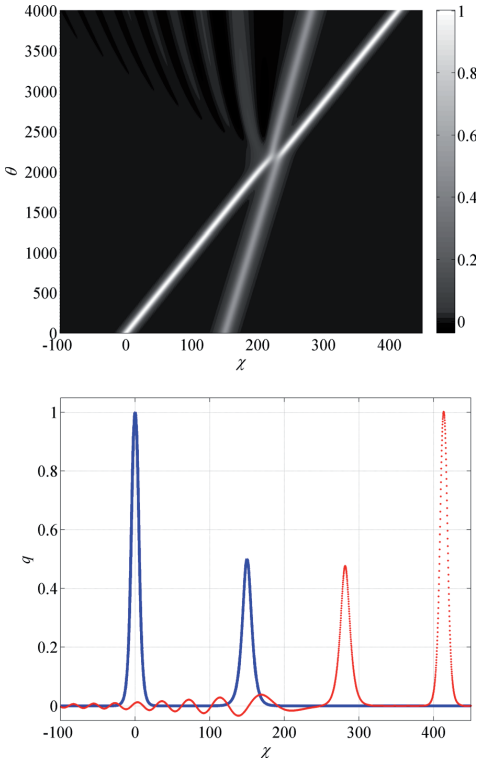

FIG. 7. (Color online) Interaction of solitary wave solutions of elevation to Eq. (10) in nondimensional coordinates: space-time plot (above); cross-section of the wave field at $\theta = 0$ (solid lines), and after the collision ($\theta = 4000$, dotted line, below).

of solitons and interaction time and was extended as occasion required. The numerical code was tested against exact analytical multisoliton solutions to the classical mKdV equation and by means of long-term tracking of propagation of exact solitary solutions to Eq. (10) in the absence of other disturbances. In particular, the results of the latter test did not change when the spatial step was decreased by a factor of two. For simplicity, we use the nondimensional form of Eq. (10)

$$q_\theta + q^2 q_\chi - q^4 q_\chi + q_{\chi\chi\chi} = 0, \tag{18}$$

where

$$\theta = \left|\frac{\alpha_1^3}{\alpha_3}\right|^{3/4} (\beta)^{-1/2} t, \quad \chi = \left|\frac{\alpha_1^3}{\alpha_3}\right|^{1/4} (\beta)^{-1/2} x, \quad q = \left|\frac{\alpha_1}{\alpha_3}\right|^{1/2} \varsigma. \tag{19}$$

The step in the x-direction was set to 0.2 and the step in time to 0.1. The performed tests indicated that the numerical inaccuracies for this choice of parameters is of the order of 10^{-6} whereas the value of the small parameter $\mu > 0.04$.

The initial state was composed from two solitary waves with nondimensional amplitudes of 1 and ± 0.5. The nondimensional limiting amplitude for the parameters in use is $\sqrt{5}/2 \approx 1.118$. The corresponding dimensional amplitudes would have been 7.62 m and ± 3.81 m, respectively. Before integrating this constellation, evolution of each of the counterparts was integrated until $\theta = 4000$. During this interval, the total error of the numerical solution (caused, e.g., by small distortions of the amplitude of the numerical solution owing to its discrete representation and by radiation of wave energy) did not exceed 1×10^{-6}.

The initial state for studies of interaction of these solitary waves was composed simply as a linear superposition of the counterparts. The smaller wave was placed ahead of the larger one, at a distance (counted as the distance between the relevant maxima) of 150 nondimensional units of length. The simulation was performed until $\theta = 4000$, that is, quite a long time after the interaction of the highest parts of the waves was terminated (Fig. 7).

The evolution of solitary waves of elevation resembled the typical scenarios for soliton interactions of similar type in the classical KdV and mKdV frameworks in which the taller wave overtakes the smaller one.[63,64] In such interactions, the counterparts usually lose their identity and merge into a composite structure at a certain instant. After a while,

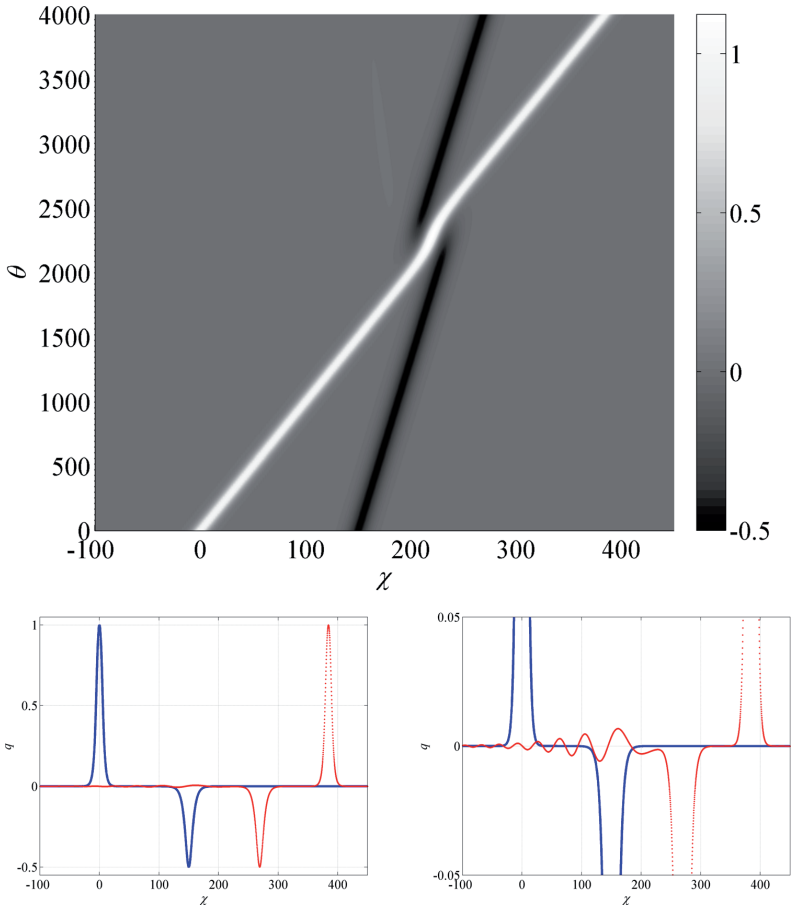

FIG. 8. (Color online) Interaction of solitary waves of different polarity in the framework of Eq. (10) in nondimensional coordinates: space-time plot (above); cross-section of the wave field at $\theta = 0$ (solid lines), and after the collision ($\theta = 4000$, dotted line, below). The right bottom panel is a zoomed version of the left bottom panel.

the counterparts emerge again whereas one cannot say whether the counterparts propagate through each other as waves do or collide as particles do. The interaction process is accompanied, as in the case of KdV solitons, by a clear decrease of the amplitude of the composite structure during the merging phase and by a substantial phase shift.

Differently from processes governed by integrable equations, the collision was accompanied by generation of very long and almost stationary localized depression area. The entire process was also accompanied by a modest radiation of wave energy from the interaction region. The amplitude of wavelike disturbances was about 4×10^{-2}, that is, by several orders of magnitude larger than the level of numerical errors ($<1 \times 10^{-6}$). This level of wave generation signifies the effects of dispersion on the evolution of the system. Note that the amplitude of the disturbances matches the magnitude of the relevant dispersive terms $O(\mu) = O(\Delta)$ that also is about 4×10^{-2}.

The collision of solitary waves of different polarities has a similar appearance. Both the counterparts largely survive the collision but the phase shift for the wave of depression is more pronounced (Fig. 8). The amplitude of radiated waves is, however, much smaller than in the above case and does not exceed 1×10^{-2}. Test simulations with a twice higher spatial resolution led to practically identical results. Therefore, the described side effects such as wave radiation in both cases and the formation of a long depression area in the collision of waves of elevation evidently are an inherent part of interactions of solitary waves in the framework of Eq. (10).

Consequently, collisions of solitary wave solutions of Eq. (10) basically have inelastic nature although both the intensity of wave radiation and changes to the amplitudes of the solitons are fairly minor. For example, the collision of waves of elevation led to the increase in the amplitude of the taller soliton from 1 to 1.002 and an accompanying decrease in the smaller solution from 0.5 to 0.477. The collision of waves of different polarity led to much smaller changes: the post-collision amplitudes of the waves were 1.001 and -0.499, respectively. Note that this effect also does not exceed the order of $O(\mu)$. The effects caused by interactions of different solitary waves with similar entities and with the wave background could, of course, be much larger during longer time intervals and/or caused by multiple collisions. As expected for non-integrable equations, such interactions should finally lead to damping of solitary waves to a level of magnitude at which they are either practically linear or are governed by a different balance of nonlinear and dispersive terms.

VII. CONCLUSIONS AND DISCUSSION

Although contemporary numerical methods and fully nonlinear approaches such as the method of conjugate flows allow for extensive studies into properties of highly nonlinear internal waves, many specific features can still be recognized, analyzed, and understood using classical methods for analytical studies into internal waves in ideal layered fluids and in the weakly nonlinear framework. Such fully analytical methods make it possible to exactly establish qualitative appearance of disturbances of different shapes and amplitudes, and, more importantly, to understand the specific features of the behavior of waves corresponding to situation where a substantial change in the overall regime of wave propagation is possible.

The performed analytical investigation of different regimes of wave propagation in a relatively simple but frequently occurring in nature symmetric three-layer environment reveals several interesting feature of wave shapes that are usually hidden in the analysis of non-symmetric situations. The key development is the derivation of a new nonlinear evolution equation that describes the wave motion in situations where all the leading-order nonlinear terms in the classical modified Korteweg-de Vries (mKdV) equation vanish simultaneously. Such situations may happen quite frequently in relatively shallow non-tidal strongly stratified basins such as the Baltic Sea. In this case, the evolution equation governing wave motion contains two nonlinear terms (cubic and quintic nonlinearities) of the same magnitude. This equation is obtained using the basically standard asymptotic procedure that is widely used in similar problems and is of the second order of accuracy as the mKdV equation for the non-symmetric situation.

The resulting equation differs from the mKdV equation in two important aspects. First, it reflects a different balance between the (higher-order) nonlinear terms and the dispersive terms compared to that exploited in the mKdV equation. More importantly, this equation contains two nonlinear terms of the same magnitude—the cubic and quintic nonlinearities, the latter one distinguishing the resulting equation from the mKdV equation. The resulting equation has solitary wave solutions. As this equation probably is not integrable, the possible solitonic nature of these solutions, the persistence of these solutions in interactions and the existence of multisoliton solutions is a subject of further research.

The presence of the quintic nonlinearity does not substantially modify the shape of the solitons of relatively small amplitude but leads to radical changes in the appearance of larger-amplitude solitary waves. Their amplitude and propagation speed are limited. Larger-amplitude solitons have a table-like shape with very steep fronts. The motion of such solitary waves may be accompanied by high water speeds and strong hydrodynamic loads in the areas where the structure of medium is favorable for their existence. It is likely that the classical solitary solutions to the mKdV equation are transformed into such structures when they approach sea areas where the coefficients at the lower-order nonlinear terms vanish.

ACKNOWLEDGMENTS

The research is partially supported by Russian Foundations for Basic Research grants (10-05-00199, 09-05-00204, 11-02-00483, and 11-05-00216), Estonian Science Foundation (Grant No. 7413), the BONUS+ BalticWay project and the targeted financing by the Estonian Ministry of Education and Science (Grant No. SF0140007s11). O.K., A.K., and E.R. acknowledge as well RF President grant for young researchers MD-99.2010.5.

APPENDIX: COEFFICIENTS OF THE EXTENDED KdV EQUATION

The coefficients of, Eq. (6), expressed in nondimensional form in terms of $l = h/H$ are as follows:

$$c^2 = \frac{gh\Delta\rho}{\rho}; \quad \alpha = 0;$$

$$\frac{\beta}{cH^2} = -l\frac{4l-3}{12}; \quad \frac{\alpha_1}{c}H^2 = -\frac{3(26l-9)}{8l^3};$$

$$\frac{\beta_1}{cH^4} = l\frac{16l^3-45l+30}{1440}; \quad \gamma_1 = 0;$$

$$\frac{\gamma_2^*}{cH} = \frac{3(8l^2-10l+3)}{8l}; \quad \frac{\alpha_2^*}{c}H^3 = \frac{9(52l^2-44l+9)}{16l^5};$$

$$\frac{\beta_2}{cH^6} = -\frac{c\left(320l^5-1008l^4+1260l^3-945l^2+630l-252\right)l}{120\,960};$$

$$\frac{\gamma_{21}}{cH^3} = -\frac{256l^4-200l^3-198l^2+231l-57}{96l};$$

$$\frac{\gamma_{22}}{cH^3} = -\frac{352l^4-704l^3+486l^2-123H^3l+6}{192l};$$

$$\gamma_{23} = 0; \quad \frac{\gamma_{31}}{c} = \frac{40l^3+726l^2-819l+207}{96l^3};$$

$$\frac{\gamma_{32}}{c} = \frac{1912l^3-678l^2-927l+342}{96l^3};$$

$$\frac{\gamma_{33}}{c} = \frac{952l^3-1110l^2+369l-36}{96l^3};$$

$$\frac{\alpha_3}{c}H^4 = -\frac{9(1324l^3-1508l^2+513l-45)}{128l^7};$$

$$\frac{\beta_3}{cH^8} = -\frac{\left(17152l^7-76800l^6+151200l^5-171360l^4+121275l^3+56700l^2+21420l-6120\right)l}{29030400};$$

$$\frac{\gamma_{41}^*}{cH^5} = \frac{11264l^6-33376l^5+37824l^4-19350l^3+4335l^2-684l+180}{34560l};$$

$$\frac{\gamma_{42}^*}{cH^5} = \frac{5504l^6-4192l^5+40152l^4-55030l^3+31005l^2-7218l+444}{11520l};$$

$$\frac{\gamma_{43}^*}{cH^5} = \frac{4864l^6-14240l^5+7968l^4-13578l^3+21219l^2-10809l+1926}{6912l};$$

$$\frac{\gamma_{51}}{cH^2} = -\frac{16544l^5-18784l^4+16842l^3-25377l^2+18504l-3996}{2304l^3};$$

$$\frac{\gamma_{52}}{cH^2} = -\frac{3(32l^3-64l^2+42l-9)}{256l};$$

$$\frac{\gamma_{53}}{cH^2} = -\frac{56864l^5+93936l^4-330570l^3+26485l^2-76320l+6804}{11520l^3};$$

$$\frac{\gamma_{54}}{cH^2} = -\frac{48672l^5-94256l^4+64590l^3-18255l^2+2430l-216}{11520l^3};$$

$$\frac{\gamma_{55}}{cH^2} = \frac{189280l^5-646880l^4+743190l^3-334395l^2+33030l+6804}{11520l^3};$$

$$\frac{\gamma_{56}}{cH^2} = \frac{121120l^5-275560l^4+152040l^3+70800l^2-91035l+20844}{5760l^3};$$

$$\frac{\gamma_{61}^*}{c}H = -\frac{1424l^4 + 332l^3 - 3444l^2 + 2271l - 405}{64l^5};$$

$$\frac{\gamma_{62}^*}{c}H = -\frac{10928l^4 - 11476l^3 - 192l^2 + 2787l - 594}{128l^5};$$

$$\frac{\gamma_{63}^*}{c}H = -\frac{1904l^4 - 3172l^3 + 1848l^2 - 441l + 36}{64l^5}.$$

The coefficients for the first-order terms and for the quadratic nonlinearity for the symmetric three-layer medium have been obtained in Ref. 22 and presented here only for completeness.

In calculations, we use the following parameters of the medium: total depth $H = 100$ м, depth of the uppermost and lowermost layers $h = 30$ m and the relative change in the density $\Delta\rho/\rho = 1 \times 10^{-2}$. The corresponding values of the linear wave speed and the coefficients of Eq. (10) are as follows:

Parameter	Value
c (m/s)	1.72
α (s^{-1})	0.0
β (m^3/s)	771.98
α_1 $(m{\cdot}s)^{-1}$	0.002859
α_3 $(m^3{\cdot}s)^{-1}$	−0.00004924
a_{lim} (m)	8.5194
V_{lim} (m/s)	0.01729

[1]Yu. Z. Miropol'sky, *Dynamics of Internal Gravity Waves in the Ocean* (Kluwer, Dordrecht, The Netherlands, 2001), 424 p.
[2]J. R. Ledwell, E. T. Montgomery, K. L. Polzin, L. C. St. Laurent, R. W. Schmitt, and J. M. Toole, "Evidence for enhanced mixing over rough topography in the abyssal ocean," Nature (London) **403**, 179 (2000).
[3]R. Ferrari and C. Wunsch, "Ocean circulation kinetic energy: Reservoirs, sources, and sinks," Annu. Rev. Fluid Mech. **41**, 253 (2009).
[4]C. Wunsch and R. Ferrari, "Vertical mixing, energy and the general circulation of the oceans," Annu. Rev. Fluid Mech. **36**, 281 (2004).
[5]A. R. Osborne and T. L Burch, "Internal solitons in the Andaman Sea," Science **208**, 451 (1980).
[6]D. B. Reeder, B. B. Ma, and Y. Jang Yang, "Very large subaqueous sand dunes on the upper continental slope in the South China Sea generated by episodic, shoaling deep-water internal solitary waves," Marine Geol. **279**, 12 (2011).
[7]L. Ostrovsky and Y. Stepanyants, "Do internal solitons exist in the ocean?," Rev. Geophys. **27**, 293, doi:10.1029/RG027i003p00293 (1989).
[8]J. R. Apel, L. A. Ostrovsky, Y. A. Stepanyants, and J. F. Lynch, "Internal solitons in the ocean and their effect on underwater sound," J. Acoust. Soc. Am. **121**, 695 (2007).
[9]D. J. Benney, "Long non-linear waves in fluid flows," J. Math. Phys. **45**, 52 (1966).
[10]R. Grimshaw, E. Pelinovsky, and T. Talipova, "The modified Korteweg-de Vries equation in the theory of the large–amplitude internal waves," Nonlinear Processes Geophys. **4**, 237, doi:10.5194/npg-4-237-1997 (1997).
[11]T. Talipova, E. Pelinovsky, K. Lamb, R. Grimshaw, and P. Holloway, "Cubic nonlinearity effects in the propagation of intense internal waves," Dokl. Earth Sci. **365**, 241 (1999).
[12]A. V. Slyunyaev and E. N. Pelinovsky, "Dynamics of large-amplitude solitons," J. Exp. Theor. Phys. **89**, 173 (1999).
[13]A. V. Slyunyaev, "Dynamics of localized waves with large amplitude in a weakly dispersive medium with a quadratic and positive cubic nonlinearity," J. Exp. Theor. Phys. **92**, 529 (2001).
[14]R. Grimshaw, D. Pelinovsky, E. Pelinovsky, and A. Slunyaev, "The generation of large amplitude solitons from an initial disturbance in the extended Korteweg-de Vries equation," Chaos **12**, 1070 (2002).
[15]K. A. Gorshkov, L. A. Ostrovsky, I. A. Soustova, and V. G. Irisov, "Perturbation theory for kinks and its application for multisoliton interactions in hydrodynamics," Phys. Rev. E **69**, 016614 (2004).
[16]M. J. Ablowitz and P. A. Clarkson, *Solitons, Nonlinear Evolution Equations and Inverse Scattering* (Cambridge University Press, Cambridge, 1991), 532 p.
[17]M. Funakoshi, "Long internal waves in a two-layer fluid," J. Phys. Soc. Jpn. **54**, 2470 (1985).
[18]K. Lamb and L. Yan, "The evolution of internal wave undular bores: Comparisons of a fully nonlinear numerical model with weakly nonlinear theory," J. Phys. Oceanogr. **26**, 2712 (1996).
[19]E. N. Pelinovsky, O. E. Polukhina, and K. Lamb, "Nonlinear internal waves in the ocean stratified in density and current," Oceanology **40**, 757 (2000).
[20]R. Grimshaw, E. Pelinovsky, and O. Poloukhina, "Higher-order Korteweg-de Vries models for internal solitary waves in a stratified shear flow with a free surface," Nonlinear Processes Geophys. **9**, 221 (2002).
[21]T. Kakutani and N. Yamasaki, "Solitary waves on two-layer fluid," J. Phys. Soc. Jpn. **45**, 674 (1978).
[22]R. Grimshaw, E. Pelinovsky, and T. Talipova, "Solitary wave transformation in a medium with sign-variable quadratic nonlinearity and cubic nonlinearity," Physica D **132**, 40 (1999).
[23]R. Grimshaw, A. Slunyaev, and E. Pelinovsky, "Generation of solitons and breathers in the extended Korteweg-de Vries equation with positive cubic nonlinearity," Chaos **20**, 013102 (2010).
[24]C. G. Koop and G. Butler, "An investigation of internal solitary waves in two-fluid system," J. Fluid Mech. **112**, 225 (1981).
[25]M. Funakoshi and M. Oikawa, "Long internal waves of large amplitude in a two-layer fluid," J. Phys. Soc. Jpn. **55**, 128 (1986).
[26]D. I. Pullin and R. H. J. Grimshaw, "Finite-amplitude solitary waves at the interface between two homogeneous fluids," Phys. Fluids **31**, 3550 (1998).
[27]R. M. Mirie and S. A. Pennel, "Internal solitary waves in a two-fluid system," Phys. Fluids A **1**, 986 (1989).
[28]W. Choi and R. Camassa, "Weakly nonlinear internal waves in a two-fluid system," J. Fluid Mech. **313**, 83 (1996).
[29]W. Choi and R. Camassa, "Fully nonlinear internal waves in a two-fluid system," J. Fluid Mech. **396**, 1 (1999).
[30]W. Craig, P. Guyenne, and H. Kalisch, "A new model for large amplitude long internal waves," C. R. Mec. **332**, 525 (2004).
[31]P. Guyenne, "Large-amplitude internal solitary waves in a two-fluid model," C. R. Mec. **334**, 341 (2006).
[32]N. Zahibo, A. Slunyaev, T. Talipova, E. Pelinovsky, A. Kurkin, and O. Polukhina, "Strongly nonlinear steepening of long interfacial waves," Nonlinear Processes Geophys. **14**, 1 (2007).
[33]R. Camassa, P.-O. Rusas, A. Saxen, and R. Tiron, "Fully nonlinear periodic internal waves in a two-fluid system of finite depth," J. Fluid Mech. **652**, 259 (2010).
[34]D. J. Benney and D. R. S. Ko, "The propagation of long large amplitude internal waves," Stud. Appl. Math. **59**, 187 (1978).
[35]J. W. Miles, "On internal solitary waves," Tellus **31**, 456 (1979).
[36]J. W. Miles, "On internal solitary waves II," Tellus **33**, 397 (1981).
[37]J. Gear and R. Grimshaw, "A second order theory for solitary waves in shallow fluids," Phys. Fluids **26**, 14 (1983).
[38]H. Michallet and F. Barthelemy, "Experimental study of interfacial solitary waves," J. Fluid Mech. **366**, 159 (1998).
[39]P. Holloway, T. Talipova, and E. Pelinovsky, "A generalised Korteweg-de Vries model of internal tide transformation in the coastal zone," J. Geophys. Res. **104**, 18333, doi:10.1029/1999JC900144 (1999).
[40]J. A. Knauss, *Introduction to Physical Oceanography* (Prentice Hall, New Jersey, 1996), 309 p.
[41]Y. J. Yang, Y. C. Fang, T. Y. Tang, and S. R. Ramp, "Convex and concave types of second baroclinic mode internal solitary waves," Nonlinear Processes Geophys. **17**, 605 (2010).
[42]M. Leppäranta and K. Myrberg, *Physical Oceanography of the Baltic Sea* (Springer Praxis, Berlin/Heidelberg/New York, 2009), 378 p.
[43]T. Soomere, "Coupling coefficients and kinetic equation for Rossby waves," Nonlinear Processes Geophys. **10**, 385 (2003).
[44]E. Pelinovsky, O. Polukhina, A. Slunyaev, and T. Talipova, "Solitary Waves in Fluids," in *Internal Solitary Waves* (WIT, Southampton, Boston, 2007), Chap. 4, edited by R. H. J. Grimshaw.
[45]W. J. Teague, M. J. Carron, and P. J. Hogan, "A comparison between the generalized digital environmental model and Levitus climatologies," J. Geophys. Res. **95**, 7167, doi:10.1029/JC095iC05p07167 (1990).
[46]R. Schlitzer, *Ocean Data View [Electronic Data and Program]* (Alfred Wegener Institute for Polar and Marine Research, Bremerhaven, Germany, 2004).

[47]A. Nayfeh, *Perturbation Methods* (Wiley, New York, 2000), 437 p.
[48]J. K. Engelbrecht, V. E. Fridman, and E. N. Pelinovsky, *Nonlinear Evolution Equations*, Pitman Research Notes in Mathematics Series, 180 (Longman, London, 1988), 122 p.
[49]E. A. Ruvinskaya, O. E. Kurkina, and A. A. Kurkin, "A modified nonlinear evolution equation for internal gravity waves in a three-layer symmetric fluid," (in Russian) Transactions of the Nizhny Novgorod R. E. Alekseev State Technical University, **4**(83), 30 (2010), ISSN 1816-210X. (October 2011, available at website http://www1.nntu.ru/trudy/2010/04/030-039.htm).
[50]S. Hamdi, B. Morse, B. Halphen, and W. Schiesser, "Analytical solutions of long nonlinear internal waves: Part I," Nat. Hazards **57**, 597 (2011).
[51]S. Hamdi, B. Morse, B. Halphen, and W. Schiesser, "Conservation laws and invariants of motion for nonlinear internal waves: Part II," Nat. Hazards **57**, 609 (2011).
[52]S. P. Novikov, V. E. Zakharov, S. V. Manakov, and L. V. Pitaevsky, *Soliton Theory* (Plenum, New York, 1984).
[53]M. Ablowitz and H. Segur, *Solitons and Inverse Scattering Transform* (SIAM, Philadelphia, 2000), 425 p.
[54]M. Miyata, "Long internal waves of large amplitude," in *Nonlinear Water Waves* edited by K. Horikawa and H. Maruo (Springer-Verlag, Berlin, 1988), p. 399.
[55]M. Miyata, "A note on broad and narrow solitary waves," IPRC Report 00-01 SOEST 00-05 (Honolulu, Hawaii, 2000), 47 p.
[56]T. B. Benjamin, "A unified theory of conjugate flows," Philos. Trans. R. Soc. London **269**, 587 (1971).
[57]N. I. Makarenko, "On the non-uniqueness of conjugate flows," J. Appl. Mech. Technol. Phys. **45**, 204, doi: 10.1023/B:JAMT.0000017583.02455.94 (2004).
[58]N. I. Makarenko, Zh. L. Maltseva, and A. Yu Kazakov, "Conjugate flows and amplitude bounds for internal solitary waves," Nonlinear Processes Geophys. **16**, 169 (2009).
[59]K. G. Lamb and B. Wan, "Conjugate flows and flat solitary waves for a continuously stratified fluid," Phys. Fluids **10**, 2061 (1998).
[60]K. G. Lamb, "Conjugate flows for a three-layer fluid," Phys. Fluids **12**, 2169 (2000).
[61]P.-O. Rusas and J. Grue, "Solitary waves and conjugate flows in a three-layer fluid," Euro. J. Mech. B/Fluids **21**, 185 (2002).
[62]B. Fornberg, *A Practical Guide to Pseudospectral Methods* (Cambridge University Press, Cambridge/New York/Melbourne 1998), 231 p.
[63]T. Soomere, "Solitons interactions," in *Encyclopedia of Complexity and Systems Science*, edited by R. A. Meyers (Springer, New York, 2009), Vol. 9, p. 8479.
[64]P. G. Drazin and R. S. Johnson, *Solitons: An Introduction* (Cambridge University Press, Cambridge/New York, 1989), 226 p.

Paper V

Kurkina, O.E., Kurkin, A.A., Rouvinskaya, E.A., Pelinovsky, E.N., Soomere, T. Dynamics of solitons in non-integrable version of the modified Korteweg–de Vries equation. – JETP Letters 95 /2; 2012, p. 91–95.

Paper VI

Soomere, T., Kurkina, O. Statistics of extreme wave conditions in the south-western Baltic Sea. – Fundamental and Applied Hydrophysics 4 /4; 2011, p. 43–57.

УДК 551.466.3:004.925.8(261.243)

© *Т. Соомере*[1], *О. Куркина*[1, 2, 3], 2011
[1] Институт кибернетики при Таллинском технологическом университете, Таллин, Эстония
[2] НИУ «Высшая школа экономики», Нижний Новгород
[3] ФГБОУ ВПО «Нижегородский государственный технический университет им. Р.Е. Алексеева»
Oksana.Kurkina@mail.ru

СТАТИСТИКА ЭКСТРЕМАЛЬНОГО ВОЛНЕНИЯ В ЮГО-ЗАПАДНОЙ ЧАСТИ БАЛТИЙСКОГО МОРЯ

Свойства экстремальных штормов в районе порога Дарс юго-западной части Балтийского моря проанализированы на основе записей волномерного буя за 20 лет (1991–2010) и результатов численных экспериментов. Долгосрочная средняя значительная высота волн H_S составляет ~0.7 м, а характерные периоды – 2–4 с. Наибольшая измеренная H_S составила 4.46 м. Наибольшее расхождение (разница до 2 с) установлено между характерными измеренными и модельными периодами волн. Временная динамика годовых наивысших волн имеет пилообразный характер с увеличением в 1958–1990 гг., начиная с 1993 г., и резким снижением в 1991–1992 гг. Измеренные среднегодовые и максимальные высоты волн незначительно изменялись в 1991–2010 гг., но порог в 1 % наиболее высоких волн существенно снизился.

Ключевые слова: ветровое волнение, экстремальные волны, математическое моделирование, функции распределения.

Волновой климат Балтийского моря характеризуется некоторыми специфическими особенностями, такими как его весьма нестационарный характер, локализация периода штормов в несколько осенних и зимних месяцев, значительная пространственная и временная изменчивость свойств волнения, преобладание сравнительно коротких и крутых волн, а также существование волн почти такой же высоты, как в значительно большем по размерам Средиземном море [1, 2]. Обычно большую крутизну волн в Балтийском море связывают с его небольшими глубинами (в среднем 54 м), однако в большинстве случаев увеличение крутизны есть результат коротких, но сильных штормов с ограниченной длиной разгона волн. Такие штормы генерируют очень крутые волны даже в глубоководных областях, и при этом ограниченная глубина слабо влияет на характер волн.

Потенциальную роль малой глубины некоторых акваторий Балтийского моря для безопасности судоходства и другой деятельности в море и прибрежных районах можно более четко определить в терминах генерации волн-убийц [3] с помощью механизмов, для которых мелководность является основополагающим фактором. Один из таких механизмов – нелинейное взаимодействие плоских волн на мелкой воде, распространяющихся под углом друг к другу [4], – действует лишь в условиях ограниченной глубины и высоких длинных волн. Возможность частого выполнения условий для этого механизма и побудила нас к исследованию волнового климата в районе порога Дарс, отличающегося интенсивным судоходством и имеющего глубину всего около 20 м.

Одно из возможных определений волн-убийц основано лишь на отношении высоты индивидуальной волны к фоновой значительной высоте волн (H_S – средняя высота одной трети наибольших волн). Такое определение позволяет изучать волны-убийцы в самых разных условиях: от волн с характерными высотами 10–20 см [5] до таких монстров, как «новогодняя волна», возникшая среди волн с типичной высотой в 10 м [6]. И

хотя исследования мелкомасштабных аналогов «волн-убийц» определенно вносят вклад в понимание таких явлений, большинство практических задач связано с объяснением внезапного появления неожиданно высоких волн среди волн с достаточно большой высотой. Наиболее опасны ситуации, когда действие определенных механизмов концентрации волновой энергии и соответствующего увеличения высот волн в целом в отдельных областях (например, рефракция на течении [7] или на неоднородностях дна) сочетается со специфическими динамическими факторами (например, нелинейное усиление длинных поверхностных волн на мелкой воде); это может приводить к возникновению необычайно высоких или крутых волновых пиков [4, 7]. Такие условия могут быть источниками риска в мелководных и прибрежных областях (где они могут приводить также к внезапному резкому росту придонных скоростей, появлению волн-убийц или усилению волн от проходящих судов на берегу [8]), особенно в местах с интенсивным движением водного транспорта.

Процесс генерации высоких локализованных гребней, описанный в [4], весьма чувствителен к условиям, в которых происходит взаимодействие волн: глубина моря, высота волн, углы пересечения должны быть связаны особым образом, чтобы возникла экстремальная волна [9]. Поэтому необходимым условием всестороннего понимания потенциальной опасности волн-убийц является адекватное знание свойств экстремального волнения в соответствующих областях. Этот вопрос рассматривался в классических волновых атласах, справочниках и практических руководствах преимущественно с точки зрения высоты волн. Анализ [4] показывает, что направление распространения волн и особенно множественность направлений в волновом поле является даже более важным параметром. В реальных условиях еще одним ключевым параметром будет длина (или период) волн: она должна быть достаточно большой, чтобы стали заметны эффекты взаимодействия нелинейных волн на мелкой воде. В связи с последним аспектом вероятность возникновения аномальных волн большой крутизны должна уменьшаться с ростом длины волны, но резкое (почти восьмикратное) увеличение крутизны волны, возникающей при нелинейных взаимодействиях, одновременно приводит к росту риска появления волн-убийц [9].

Перечисленные факторы наиболее важны для вытянутых сравнительно мелких бассейнов (где свойства волн зависят главным образом от направления ветра и меньше – от его скорости), особенно для полузакрытых морских акваторий. В них обычно преобладают относительно короткие локально возбуждаемые волны, но распространение длинных волн из соседствующих областей может приводить к ситуациям, благоприятным для возникновения волн-убийц. В этом смысле две полузакрытые области Балтийского моря, вероятно, наиболее подвержены воздействию высоких и длинных волн при некоторых редких штормах, приходящих из Центральной Балтики. В восточной части Финского залива обычно преобладают короткие волны с периодами 2–4 с, возбуждаемые господствующими юго-западными ветрами [10], но периодически очень длинные волны, зарождающиеся в центральной части Балтийского моря, могут проникать в этот бассейн [11]. Недавние исследования показали, что даже сравнительно малые изменения гидрометеорологических условий в Невской губе и на прилегающих участках побережья могут существенным образом повлиять на процессы, происходящие в прибрежной зоне [10, 12]. Подобная по свойствам область расположена между о.Рюген и побережьем Дании в юго-западной части Балтийского моря. Преобладающие в этом бассейне юго-западные и западные ветры обычно возбуждают относительно короткие и крутые волны, а более редкие северо-восточные ветры могут влечь за собой гораздо более длинные волны той же (или даже большей) высоты. Обе эти области довольно мелкие, с характерными глубинами менее 20 м, поэтому волны с периодами около 5–8 с уже могут развивать свойства, необходимые для нелинейных взаимодействий волн на мелкой воде.

Хотя существует несколько поколений атласов волнения для Балтийского моря [1, 13], в литературе очень мало сведений о статистике измеренных волн для мелководных частей этого бассейна. Теоретические оценки экстремальных ветровых и волновых условий Финского залива представлены в [14]. Некоторые результаты ретроспективного волнового прогноза среднего разрешения и соответствующая статистическая обработка в рамках исследований [15] для всего Балтийского моря описаны в [16]. В этих исследованиях, однако, уделялось мало внимания периодам волн.

Существует возможность пролить свет на комбинацию свойств экстремальных волн для юго-западной части Балтийского моря, где характеристики волнения над порогом Дарс измеряются с помощью волноизмерительного буя «Seawatch Directional Waverider» с 1991 г. [17]. Кроме того, для данного региона были выполнены расчеты с сеткой среднего разрешения (около трех морских миль) в рамках исследований всего Балтийского моря, основанных на ретроспективном моделировании элементов волнения [15, 18, 19].

Порог Дарс расположен между двумя полузакрытыми акваториями юго-западной части Балтийского моря и разделяет море Бельт и бассейн Аркона (рис. 1). Размеры этой области, объединяющей восточную часть моря Бельт (Мекленбургская бухта, включая Любекскую) и бассейн Аркона, приблизительно совпадают с размерами Финского залива: общая длина около 300 км, а ширина варьируется от 50 до 100 км. Так как протяженность области образования волн ограничена в большинстве направлений и составляет около 100 км, ожидаемые волновые условия в этой области соответствуют ограниченному разгону. Другими словами, характерные сочетания высот и периодов волнения должны определяться спектром JONSWAP [1], а характерная крутизна должна превышать крутизну полностью развитого волнения со спектром Пирсона–Московица (который адекватно описывает волновые поля на севере центральной части Балтийского моря [2]).

Рис. 1. Карта местоположения точки измерений в районе порога Дарс в юго-западной части Балтийского моря.

Главная цель настоящей статьи – выявление потенциальной возможности существования высоких и длинных волн в полузакрытых сравнительно мелких областях Балтийского моря на примере его юго-западной части. Еще одним важным моментом является выяснение адекватности современных моделей волнения в смысле воспроизведения ими эмпирической статистики характерных волновых состояний и реконструкции экстремальных волновых условий, возникающих несколько раз за десятилетие в таких областях моря.

Данные измерений и результаты моделирования волнения. Измерения параметров волнения выполнялись в точке с глубиной 20 м, расположенной на 54°41.9' с.ш., 12°42.0' в.д. (рис. 1) в районе порога Дарс с 29 января 1991 г. с помощью волноизмерительного буя «Seawatch Directional Waverider» фирмы Datawell. Значительная высота волн измеряется непосредственно буем по 1600-секундному временному ряду смещений водной поверхности. Основные параметры волнения, такие как значительная высота и средний период, доступны с начала измерений. Некоторые другие характеристики, как, например, пиковая частота, представлены в базе данных лишь частично и поэтому не использовались в настоящей работе.

Обзор этих экспериментальных данных и их климатологический анализ представлены в [17]. В массиве данных пропущено два периода общей длительностью в несколько месяцев: 7 декабря 1991 г. – 23 апреля 1992 г. (в связи с техническими неполадками) и 01 февраля – 01 мая 1996 г. (из-за образования ледового покрова). В целом за промежуток с 29 января 1991 по 31 декабря 2010 г., рассматриваемый в настоящей статье, в наборе данных имеется 190 305 записей, за 6198 дней – хотя бы одна запись, и за 1107 дней записей не было. Наименьший процент дней, в которые проводились измерения, приходится на январь и октябрь, а также апрель–май, когда есть записи лишь для 15 лет из 20 [17]. Объем зарегистрированных данных с 8–10 измерений в сутки в первые годы исследований увеличивается до 48 – 20 мая 1997 г., колеблется от нуля до 50 с апреля 1999 до марта 2003 г., после чего стабилизируется около уровня 48 измерений в сутки. Среднее число измерений в сутки составляет примерно 26.

Проведено сравнение измеренных параметров волнения с двумя наборами результатов численного моделирования волновых полей, рассчитанных с использованием модели волнения третьего поколения WAM [20]. Расчеты выполнялись для всего Балтийского моря с пространственным разрешением около трех морских миль (5.5 × 5.5 км) и с шагом по направлению, равным 15°. Один из расчетов (далее называемый AW) произведен для периода с 1958 по 2002 г. с использованием 28 частот в диапазоне от 0.05 до 0.66 Гц (1.5–20 с) [19, 21] и ветровых полей, реконструированных с помощью региональной модели атмосферы [22] на основе обработанных метеоданных NCEP/NCAR (National Center for Environmental Prediction and the National Center for Atmospheric Research) [23, 24]. Волны на морской границе задавались на основе ретроспективного прогноза для Северного моря [18]. Для сравнения с экспериментальными мы использовали данные модели для точки сетки с координатами 54°42' с.ш., 12°42' в.д.

Другой набор расчетов (далее называемый RS, см. также в [16]), выполненных только для Балтийского моря с использованием геострофического ветра, в предположении, что проникновением волн через Датские проливы можно пренебречь, соответствует периоду с 1970 по 2007 г. Для определения скорости ветра на стандартной высоте 10 м геострофическая скорость была умножена на 0.6 и направлена на 15° влево. Чтобы обеспечить правильные скорости нарастания волн при слабом ветре после штиля [25], в расчетах использовался расширенный диапазон частот до 2 Гц (периоды волн до 0.5 с, 42 значения частоты). Данные для сравнения были взяты в точке сетки с координатами 54°42' с.ш., 12°42' в.д. Основные интегральные параметры волнения, такие как значительная высота, среднее направление и различные периоды волн доступны с временным

разрешением в один час для каждой из моделей. Так как в расчетах использовалась информация о ветре со сравнительно низким разрешением (раз в 3 или 6 ч), то время возникновения отдельных наиболее высоких волн может отличаться для модельных и измеренных волн, но статистика волнения воспроизводится адекватно.

Волновой климат. Так как основные свойства волнового климата можно найти в источниках в открытом доступе [17], приведем здесь только самые важные оценки. Наиболее часто используемый параметр для поверхностных волн – долгосрочная средняя значительная высота по всем доступным данным – составляет 0.753 м для измерений (или 0.757 м, если рассчитывать ее по суточным средним высотам волн), 0.836 м – по результатам AW-моделирования и 0.80 м – по результатам RS-расчетов. Поскольку средняя высота не имеет долгосрочного тренда во всех наборах данных, эти различия означают, что оба модельных эксперимента вполне адекватны. Небольшая завышенность оценок высот волн в моделях, очевидно, проистекает из специфики выбора информации о ветре для расчетов. Сравнение результатов RS-моделирования с визуальными наблюдениями волн на побережье [15] говорит о том, что эти расчеты недооценивают высоты волн примерно на 15 % (см. напр., [16] и ссылки оттуда, содержащие обсуждение достоверности визуального наблюдения волнения на побережье Балтийского моря), поэтому можно думать, что использованные скорости ветра слегка занижены для открытой центральной части Балтийского моря. Хорошее совпадение долгосрочной средней высоты волн над порогом Дарс показывает, однако, что точность определения скорости ветра для RS-расчетов из модели геострофического ветра адекватна для юго-западной части Балтийского моря.

Амплитуда суточных изменений в измеренных высотах волн составляет 2.6 см., т.е. почти 3.5 % от долгосрочного среднего. В июне и июле, когда высокие волны появляются в дневное время, амплитуда намного больше, примерно на 11 и 14.5 %, соответственно. В ноябре и декабре суточные вариации противоположны – более высокие волны возникают в вечернее время. Такой уровень колебаний показывает, что долгосрочные оценки параметров волнения должны, вообще говоря, вычисляться на основании суточных средних значений. Это, однако, не касается оценок свойств экстремальных волн.

Медиана для всех измеренных высот волн составляет 0.64 м, а порог для 10, 5 и 1 % высоких волн равен 1.43, 1.68 и 2.22 м соответственно. Те же значения, рассчитанные на основе средних суточных высот волн, равны 0.68, 1.36, 1.58 и 2.02 м соответственно. Поэтому волновые условия, при которых $H_S > 2$ м, уже являются достаточно экстремальными для этого района и частота их возникновения примерно равна 1 %, что дает приблизительно 100 ч в год. Подобное пороговое значение для центральной части Балтийского моря равно 4 м [2]. Волны выше 3 м появляются с частотой около 0.15 %, т.е. в течение 13 ч в году. Волны, превышающие 4 м, за последние 20 лет регистрировались лишь во время трех штормов (подробности даны ниже). Наибольшая, достоверно зарегистрированная волна имела высоту 4.46 м и наблюдалась 03 ноября 1995 г.

Распределения частот возникновения волн различной высоты (рис. 2) качественно схожи для всех трех массивов данных. Они имеют общие черты с распределениями для открытых частей Балтийского моря [2]. Суточная средняя измеренная высота волнения характеризуется, как и ожидалось, заметно меньшей частотой наименьшей и наибольшей высоты волн по сравнению с данными всего набора, так как посуточное усреднение, видимо, сглаживает крайние значения. Наиболее часто встречаются волны в диапазоне высот 0.25–0.625 м. Различия в форме распределений на рис. 2 становится очевидной в терминах параметров соответствующих распределений Вейбулла (табл. 1). Эти различия могут приводить к заметной разнице в оценках вероятности возникновения неблагоприятных морских условий.

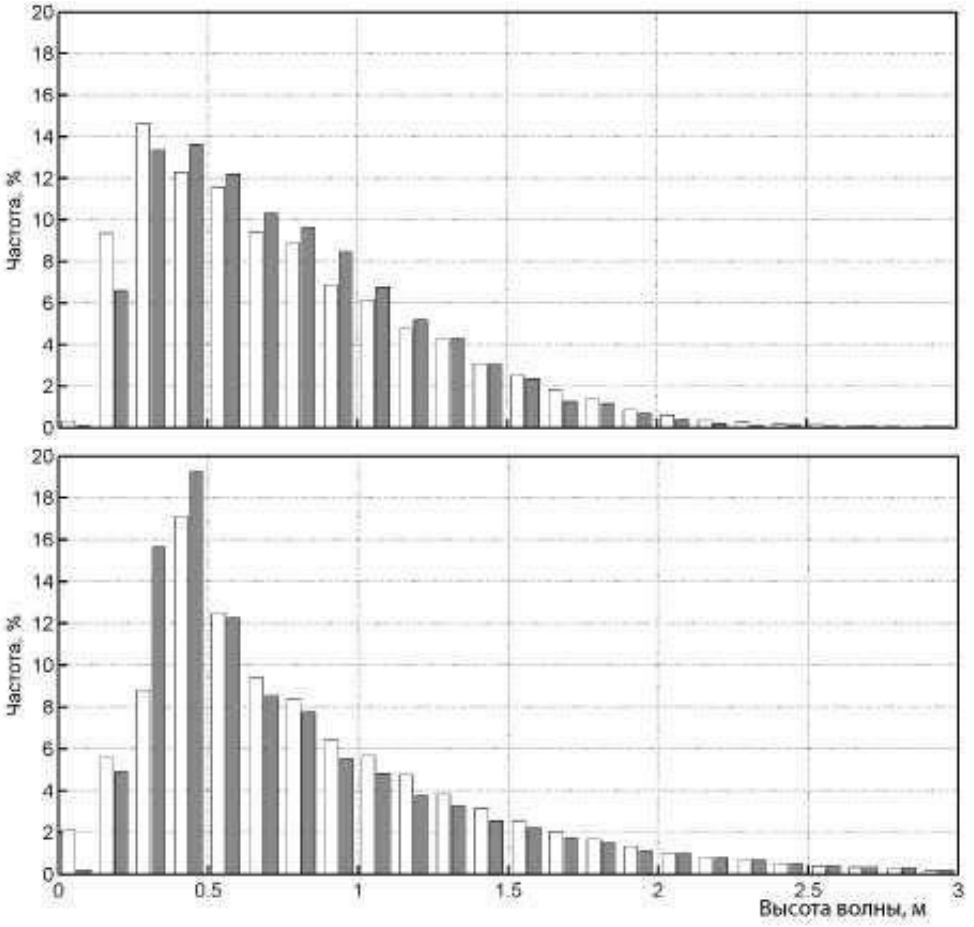

а

б

Рис. 2. Частота возникновения волн различной высоты в районе порога Дарс с шагом 0.125 м.

а – по всем измерениям (белые прямоугольники) и по суточным средним (темные прямоугольники);
б – результаты AW-моделирования (белые прямоугольники) и RS-расчетов (темные прямоугольники).

Распределения высот волнения в рамках обеих моделей очень близки, со значительной разницей лишь для волн высотой менее 0.5 м. Расчеты с использованием геострофического ветра завышают долю волн с высотами 0.25–0.5 м, но дают результаты, более близкие к измерениям для очень низких высот волнения (менее 0.125 м). Наиболее заметное различие распределений, рассчитанных по измерениям и модельным данным, проявляется в том, что обе модели переоценивают частоту волн с высотой в диапазоне 0.375–0.5 м и недооценивают в диапазоне 0.125–0.25 м. RS-расчеты также несколько завышают частоту волн с высотами 0.25–0.375 м. Общая вероятность волн высотой < 0.5 м почти одинакова для обеих моделей. Суженность распределения высоты волн при RS-моделировании, очевидно, обусловлена низким разрешением геострофических ветров, которые представляют усредненные свойства ветра над довольно обширными областями (примерно 1×1°) и поэтому имеют тенденцию сглаживать очень низкие и очень высокие локальные значения скорости ветра.

Необходимо отметить, что оба вида расчетов вполне корректно воспроизводят измеренные распределения частот возникновения волн с высотой > 0.5 м. Модели предсказывают чуть меньшую долю волн с высотой 0.625–1.125 м и чуть большую долю с высотой, превышающей 1 м, по сравнению с распределением измеренных волн, но эти различия невелики. Поэтому моделирование – как с использованием геострофического ветра, так и с ветровыми данными, полученными путем довольно сложного анализа NCEP/NCAR, – дает одинаковое в целом качество воспроизведения статистики высот в условиях умеренного волнения (здесь в диапазоне 0.5–3 м).

Распределения частоты повторяемости волн различной высоты сходны с двухпараметрическим распределением Вейбулла, поэтому такое распределение с интегральной функцией распределения вида

$$F(x,k,b)=1-\exp\left[-\left(\frac{x}{b}\right)^{k}\right]$$

может быть использовано для оценок порогов встречаемости высоких волн, подобно тому как это часто делается для скорости ветра. При заданных значениях параметров формы и масштаба, k и b, вероятность того, что высота волны h превысит заданный уровень H, находится как

$$P_{h>H}=\exp\left[-\left(\frac{H}{b}\right)^{k}\right].$$

Параметры k и b для волн из трех рассматриваемых массивов данных (табл. 1) различны между собой, а также сильно отличаются от распределения Рэлея с $k = 2$, которое часто используется для описания распределения скорости ветра в северо-восточной Европе. Интересно, что отклонения довольно велики для параметра k, отвечающего за форму, но ограничены для параметра масштабирования b. Поэтому в отличие от подобных распределений для скорости ветра на прибрежных станциях в северо-восточной части Балтийского моря [26], наибольшие различия в средних высотах волнения объясняются разными значениями параметра k. Эта особенность говорит о том, что «хвосты» соответствующих теоретических распределений могут существенно различаться. Эта гипотеза подтверждается данными табл. 2: теоретические оценки порога для очень высоких волн заметно отличаются для трех массивов данных. Более того, теоретические оценки пороговых значений существенно отличаются и от вычисленных на основе измеренных, и от полученных по результатам моделирования величин. Поэтому распределения рассчитанных и модельных высот волн в целом не подчиняются распределению Вейбулла, и оно не подходит для реконструкции параметров экстремальных волн по экспериментальным и численным данным, даже для районов моря с ограниченными условиями при разгоне волн. Очевидная причина несостоятельности такой теоретической модели кроется в том, что при определенных условиях в рассматриваемую акваторию могут приходить длинные и высокие волны, генерируемые в центральной части Балтийского моря (со свойствами, не описываемыми статистическими распределениями для локально образующихся волн).

Еще большие различия в статистических свойствах измеренных и прогнозируемых волн видны при анализе распределений средних периодов волн (рис. 3). Эти распределения асимметричны со сдвигом в более короткие волны и показывают, что наиболее часто встречаются волны с периодами около 3 с. Распределения для AW-моделирования и экспериментальных данных очень узки: 70 % волн имеют периоды в диапазоне 2.5–4 с. Отметим, что частая встречаемость волн с периодами 2–4 с вообще характерна для прибрежных акваторий Балтийского моря [2, 27]. Двухпиковая структура распределений для

обоих модельных наборов данных еще раз подтверждает высказанное предположение о том, что режим волнения в рассматриваемом месте – суперпозиция двух различных компонентов: локальный (прибрежный) режим волнения, возбуждаемого непосредственно в данном бассейне, плюс совокупность других волновых составляющих, происхождение которых связано с центральной частью Балтийского моря и относящихся к волновому режиму открытого моря.

Таблица 1

Параметры распределения Вейбулла для различных наборов данных

Характеристики	Высота волны		*k*	*b*	Порог для наиболее высоких волн, %						Годовой максимум	
					1		0.5		0.1			
	средняя	значительная			Данные	Оценка	Данные	Оценка	Данные	Оценка	Данные	Оценка
Измерения	0.64	0.75	1.59	0.84	2.22	2.18	2.51	2.39	3.19	2.82	3.37	3.50
AW-моделирование	0.68	0.84	1.41	0.83	2.74	2.32	3.06	2.55	3.86	3.05	4.01	3.66
RS-расчет	0.6	0.80	1.38	0.82	2.89	2.50	3.29	2.76	4.19	3.35	---	4.09

Примечание. Данные – вычисления на основе соответствующего набора, оценка – вычисления с использованием распределения Вейбулла. Пороговые значения для волн, появляющихся с вероятностью 1, 0.5 и 0.1 %, на основании распределения Вейбулла с прогнозируемыми параметрами. Годовой максимум высот волн рассчитан как среднее соответствующих годовых наивысших волн.

Очень редкая встречаемость волн с периодами ниже 2 с (0.02 %) в наблюдаемых волновых полях в основном, очевидно, связана с ограниченными возможностями волноизмерительного буя, который работает в диапазоне периодов волн 1.6–30 с. Аналогично обрезание диапазона периодов волн от 1.5 с и ниже в AW-вычислениях объясняется ограниченным интервалом частот в этой модели: наиболее короткие волны, учитываемые в расчетах, имеют период около 1.5 с. Это расхождение, видимо, приводит к усилению пика для волн с периодом ниже 3 с в рассматриваемом распределении. В RS-расчетах учитываются волны с периодом от 0.5 с. Поскольку наименьший период, куда приходится пик распределения для 1970–2007 гг., равен 1.03 с, то, по всей видимости, нет необходимости выбирать такой широкий диапазон периодов при прогнозировании волнения, но периоды в 0.7–0.8 с несомненно необходимы для правильного разрешения высокочастотной части волнового спектра в этом бассейне. Эти результаты также показывают, что в рассматриваемой акватории часто рождаются волны со средними периодами в диапазоне 1.5–2.2 с, которые не фиксируются в натурном эксперименте и не воспроизводятся при AW-моделировании.

Наиболее интересной особенностью распределения периодов на рис. 3 в контексте возникновения длинных и высоких волн является большое расхождение между частотой моделируемых и измеренных волн с периодами, превышающими 4 с. Распределение моделируемых периодов гораздо более отклонено в сторону больших значений, и периоды свыше 6 с встречаются с заметной частотой. Волны таких периодов не могут генерироваться локально из-за ограниченной длины разгона и, по всей видимости, приходят из центральной части Балтийского моря. В общем, моделируемое распределение может отражать суперпозицию двух волновых режимов: локально генерирующихся волн с характерными периодами около 3 с и достаточно часто появляющихся волновых систем с периодами > 4 с, зарождающихся в других районах Балтийского моря. Также стоит ска-

зать, что эта часть распределения периодов волн почти совпадает для обоих модельных наборов данных с настолько разными внешними воздействиями. Эта черта еще раз подтверждает, что прогнозное моделирование волнения с помощью простейших уточненных геострофических ветровых полей воспроизводит большую часть статистических свойств волновых полей в Балтийском море.

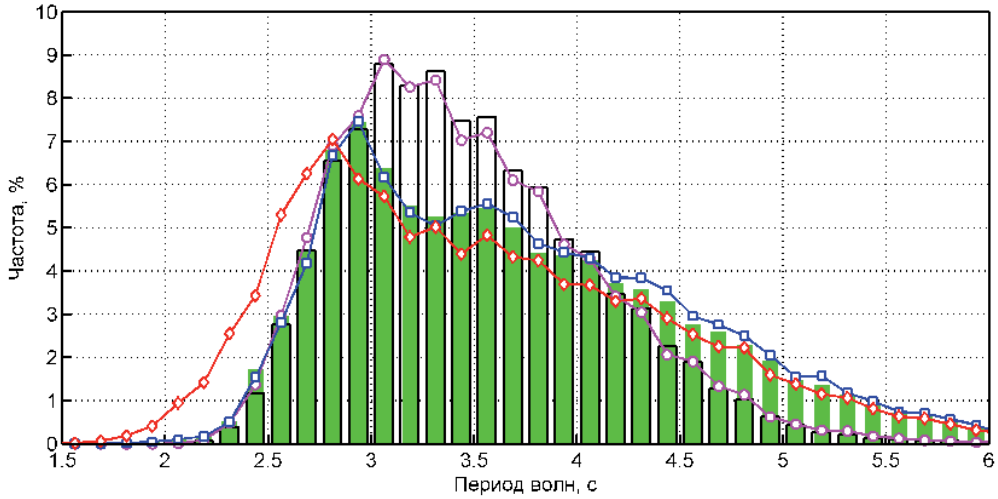

Рис. 3. Распределение средних периодов волн по данным измерений.
Результаты AW-моделирования: 1991–2010 гг. – светлые прямоугольники; 1957–2002 гг. – темные прямоугольники. Кружки и квадраты – значения для периода 1991–2002 гг., покрытого обоими наборами данных. Ромбы – данные RS-моделирования для 1970–2007 гг.

Сходство распределений периодов моделируемых волн за 1957–2002 гг. и за подынтервал 1991–2002 гг., когда доступны и измеренные, и модельные (AW) данные, говорит о том, что это распределение является устойчивым в течение многих десятилетий. Аналогичное заключение применимо и к экспериментальным данным за 1991–2010 и 1991–2002 гг. Это предположение совпадает с подобным заключением о том, что средние периоды волн в Балтийском море изменяются очень слабо [27]. Поэтому потенциальные изменения периодов волн в море не могут быть причиной различий в распределениях модельных и измеренных периодов волн. Пропуски в потоке данных с буя имеют общую продолжительность около 8 мес. и не могут являться источником такого большого различия в распределении периодов. Кроме проблем модели или неисправности буя при определенных условиях возможной причиной различий могут быть разные интерпретации волновых компонент, приходящих с различных направлений. Анализ в работе [17] позволяет сделать выводы о том, что данные с буя дают заниженные периоды для достаточно высоких (> 1.5 м) и длинных (период > 4.5 с) волн.

Экстремальные условия. Анализ совместных распределений высот и периодов волн [17] показывает, что в большинстве случаев с $H_S > 1$ м комбинации высот и средних периодов волн более или менее соответствуют волнению со спектром JONSWAP. Другими словами, типичные штормовые условия соответствуют большей крутизне волн, чем для развитого волнения со спектром Пирсона–Московица (ПМ). Поэтому штормовое волнение здесь обычно имеет довольно большую крутизну и тем самым опасно для судоходства и другой морской деятельности. Это свойство не было слишком неожидан-

ным, так как подобная черта в основном присуща волновым полям в Балтийском море, а поле волнения в рассматриваемой акватории имеет ограниченные условия для разгона.

В отличие экспериментальных данных значительного волнения, параметры которого хорошо описываются спектром ПМ, наиболее высокие моделируемые волны имеют периоды примерно на 2 с длиннее, чем аналогичное волнение со спектром ПМ.

Экспериментальные данные, как это обычно бывает, содержат несколько неправдоподобных записей высоких волн. Они были исключены из анализа. В табл. 2 дан обзор свойств волнения во время тринадцати наиболее серьезных штормов в рассматриваемой акватории, начиная с известного циклона «Гудрун» в январе 2005 г., во время которого возбуждались экстремально высокие волны [11], и был установлен рекорд нагона уровня воды в северо-восточной части Балтийского моря.

Наибольшие достоверные высоты волн зарегистрированы над порогом Дарс 3 ноября 1995 г., когда значительная высота волн достигала 4.46 м (рис. 4). Свойства AW-моделируемых волн в совершенстве воспроизводят распределение высоты волн во времени и только немного занижают ее общий максимум (3.93 м). Максимум шторма достигался при северо-восточном ветре. Акватория в районе порога Дарс почти полностью открыта по этому направлению (рис. 1). Максимальная скорость ветра составила 20.1 м/с. Отметим, что модельный период волн (7.7 с) был почти на 2 с больше в апогее шторма, чем измеренный период (6.2 с).

Шторм почти такой же силы произошел 14 ноября 1993 г., когда юго-западной ветер быстро достиг скорости около 21 м/с. Вновь в AW-расчетах почти точно воспроизведено изменение высоты волн со временем, но длительность сильного волнения слегка завышена. Волноизмеритель при этом, как обсуждалось выше, явно недооценивает периоды волн во время этого шторма.

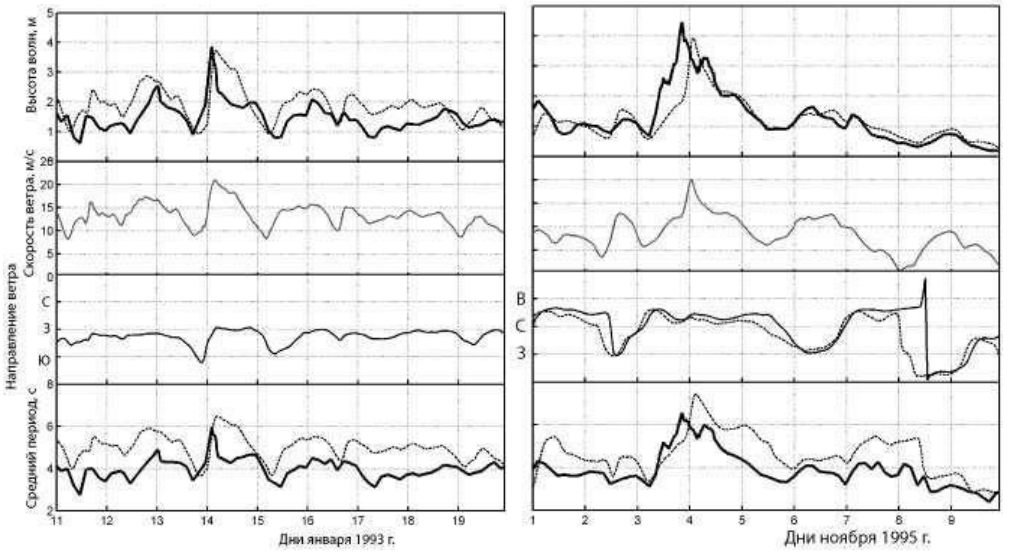

Рис. 4. Штормовое волнение над порогом Дарс в январе 1993 и ноябре 1995 гг.
Жирная линия – экспериментальные данные, пунктирная – AW-моделирование.

В рассматриваемом районе моря ветры могут быть и сильнее, чем указанные в табл. 2, поэтому естественно ожидать, что долгосрочный максимум высоты волн может быть существенно большим, чем максимальные значения, указанные в табл. 2. Это подтверждается AW-моделированием: предсказываемый общий максимум высоты волн в

районе порога Дарс за период с 1957 по 2002 г. составляет 6.23 м (26 января 1990 г.). Эти расчеты, однако, не учитывают возможного обрушения волн за счет взаимодействия с дном и могут в некоторой степени завышать высоту экстремальных волн. Тем не менее очень вероятно, что на данной акватории возможны одиночные, очень сильные штормы и что значительная высота волн вполне может превышать 5 м даже над порогом Дарс и быть существенно выше в бассейне Аркона.

Таблица 2

Максимальные характеристики волнения и ветра во время наиболее сильных штормов в месте измерений, 1991–2002 гг.

Дата	Данные измерений		AW-моделирование		Ветер	
	H_s, м	средний период T, с	H_s, м	средний период T, с	скорость	направление
14.01.1993	3.86	5.97	3.73	6.45	21.0	Ю до ЮЗ
03.11.1995	4.46	6.56	3.92	7.45	20.1	СВ
04.12.1999	3.86	5.71	3.87	6.65	21.1	ЮЗ до З
21.02.2002	3.76	6.06	3.68	6.65	21.1	СВ до С

Таблица 3

Максимальные измеренные характеристики волн во время наиболее сильных штормов в месте измерений, 2003–2010 гг.

Дата	Данные измерений		Направление прихода волны H_s
	H_s, м	T, с	
18.11.2004	3.54	5.56	ЮЗ до З
08.01.2005	3.47	5.63	ЮЗ
13.02.2005	> 3.52	–	–
23.02.2005	4.01	6.90	ВСВ
31.12.2006	3.63	5.80	Ю до З
27.06.2007	3.71	5.56	ЗЮЗ
22.03.2008	3.68	6.15	СВ
10/11.01.2010	4.01	6.90	ССВ
30.01.2010	3.65	6.02	ССВ

Вариации характеристик наиболее высоких волн. По данным табл. 2, десять из тринадцати наиболее сильных штормов (включая два из трех случаев, когда значительная высота волн достигала 4 м) зарегистрированы во втором десятилетии измерений. Однако число таких штормов недостаточно велико для того, чтобы делать достоверные выводы об ужесточении волнового климата в рассматриваемой области.

Анализ, проведенный в работе [17], показал, что не было зафиксировано статистически значимых изменений среднегодовых характеристик моделируемых и экспериментальных данных ни для одного из трех наборов данных. Измеренные высоты волн изменяются квазипериодически: самые высокие волны фиксировались около 1995, 2005 и 2010 гг., тогда как на рубеже веков отмечается снижение волновой активности. Такие вариации высот повторяют аналогичные закономерности, зарегистрированные по дан-

ным визуальных наблюдений на литовском побережье [28]. Формально тренд высот измеренного волнения понижается (на 18 мм за десятилетие). В отличие от ситуации в Финском заливе [16], порог для 10 % самых высоких волн, хотя и подвержен некоторым межгодовым вариациям, также не выявляет ни долгосрочного тренда, ни явно выраженной многолетней изменчивости. Среднегодовые значения этих характеристик близки друг к другу для всех трех исследуемых наборов данных. Их межгодовое поведение также очень сходно между собой и с годовой средней высотой волн, за исключением 1995 г., когда изменения происходили по-разному [17].

По сравнению с усредненными значениями годовая максимальная высота волны и годовые значения порогов для 1 % наиболее высоких волн демонстрируют, как и ожидалось, достаточно большую междугодичную изменчивость, и особенно высокие пики (соответствующие отдельным сильным штормам) (рис. 5). Интересно отметить, что порог для 1 % самых высоких волн имеет различный тренд для моделируемых и измеренных волн. Его значения по результатам AW-моделирования почти не меняются в течение 1958–2002 гг., тогда как значения, оцененные по измерениям, уменьшаются со сравнительно высокой скоростью – на 72 мм за десятилетие. Скорость этого снижения была бы еще большей, если бы не заметный пик 2010 г. (рис. 5). В рамках численной модели пороги, по данным и AW-, и RS-расчетов, совпадают между собой и с порогами, полученными на основании измерений для начала 1990-х годов. Измеренные значения отклоняются от модельных к концу 1990-х годов, становясь примерно на 1 м (т.е. почти на 50 %) ниже, чем оценки модели. Причины такого расхождения не вполне ясны, но несомненно требуют дальнейшего исследования свойств волнения в этом районе и во всем Балтийском море.

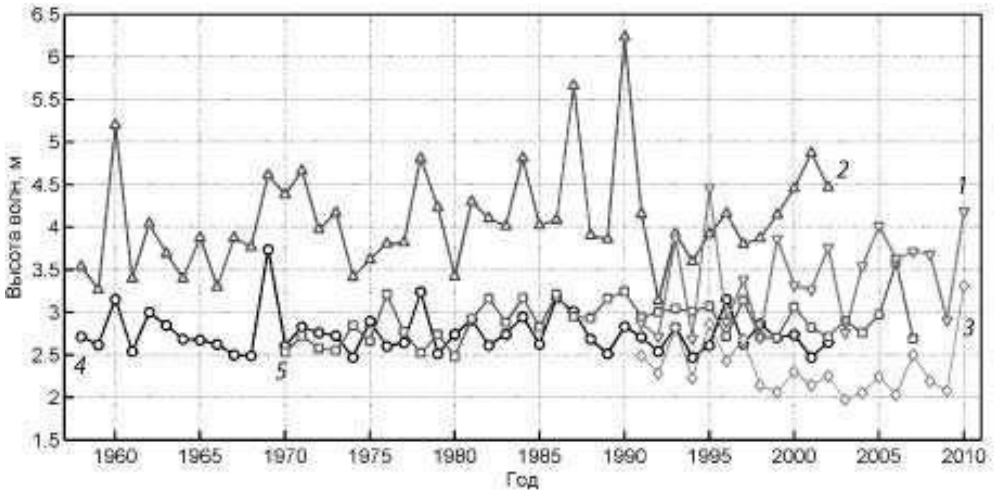

Рис. 5. Характеристики наиболее высоких волн.
1 – годовые максимумы высот, измеренных, *2* – моделируемых волн; *3* – годовые пороги для 1 % наиболее высоких волн: *3* – измерения, *4* – AW-расчеты, *5* – RS-расчеты.

Многолетняя динамика максимальных годовых средних высот волн в AW-расчетах характеризуется пилообразной структурой. Величина этого параметра постепенно возрастает с 1960-х годов до 1990 г. (от характерных значений, равных около 3.5 до почти 4.5 м), затем резко снижается в 1991–1992 гг. и далее опять постепенно увеличивается. Такое поведение говорит о существенном изменении условий генерации волн, которое, по-видимому, произошло в рассматриваемом районе в начале 1990-х годов. Отметим, что именно в это время среднегодовая высота волн заметно выросла на западном побережье Эстонии, но значительно упала на побережье Литвы [28]. Умозрительное объяс-

нение здесь может быть связано с тем, что направление ветра во время сильных штормов существенным образом изменилось примерно на десятилетие. Это предположение согласуется с данными о повсеместном изменении направлений ветра в северо-восточной части Балтийского моря [16, 29].

Еще одна интересная особенность – годовая максимальная высота измеренных волн почти точно совпадает с предсказаниями RS-моделирования в 1992–1995 гг., но заметно различается в последующее время. Любопытное свойство состоит еще и в том, что тренд годовых самых высоких измеренных волн и порог для 1 % высоких волн, рассчитанный по данным измерений, существенно различны. В середине 1990-х годов максимальная высота волн постепенно увеличиваются, тогда как 1 %-ный порог существенно уменьшается с 2.8 до 2–2.2 м.

***

Волновой климат в районе порога Дарс повторяет некоторые хорошо известные особенности волн в полузакрытых бассейнах Балтийского моря: относительно умеренные долгосрочные значения высоты волн, периоды обычно в диапазоне 2–4 с и наиболее частая высота волн – около 0.5 м. Модели волнения разумно воспроизводят как среднюю высоту волн, так и распределение волн различных высот. Моделями, учитывающими воздействие ветра с высоким разрешением, также адекватно воспроизводится детальное поведение высоты волны во времени. Модели, включающие ветровые поля низкого разрешения (например, геострофический ветер), также воспроизводят основную статистику волнения, но часто не могут воспроизвести волновые поля во время сильных штормов. Поэтому результаты моделирования даже на основе ветровых полей низкого разрешения могут с успехом использоваться для приложений, которые базируются исключительно на статистических распределениях параметров волнения (например, при оценках интенсивности прибрежных процессов или суммарного вдольберегового транспорта наносов методом CERC).

Измеренные и модельные данные свидетельствуют о заметных отличиях в распределениях периодов волн, особенно при значительном волнении. Расхождение измеренных и рассчитанных периодов при сильных штормах доходит до 2 с, что может заметно влиять на оценки степени интенсивности взаимодействия волн с дном, а также рефракционные характеристики для некоторых глубин и, следовательно, на оценки частоты нелинейной генерации экстремально высоких гребней при взаимодействиях пересекающихся систем волн [4].

Пилообразное поведение моделируемых годовых максимальных волн, хотя и обусловлено в значительной мере межгодовой изменчивостью, показывает, что основной скачок свойств штормов в южной части Балтийского моря произошел в начале 1990-х годов. Так как максимальная высота волны в рамках модельных RS-расчетов составила 6.23 м, и при этом имело место совпадение модельных и измеренных условий волнения для многих штормов, это означает, что здесь может возникать более экстремальное волнение, чем, например, в Рижском или даже в Финском заливах. Основная причина заключается в том, что в отличие от этих акваторий район порога Дарс и находящийся вблизи бассейн Аркона ориентированы вдоль преобладающих при сильных штормах направлений ветра. Эта особенность наглядно проявляется в 20 %-ной разнице наиболее высоких волн за все время наблюдений (5.2 м измерено в Финском заливе [2], 6.23 м – ретроспективный прогноз над порогом Дарс), причем в бассейне Аркона еще сохраняется некоторый потенциал даже для больших высот волн.

Также очень интересная черта сравниваемых данных – несовпадение временных изменений для средней высоты волн, характерных свойств умеренно высоких (порог для

10 % наиболее высоких) и свойств наиболее высоких волн. Свойства средних и умеренно высоких волн демонстрируют идентифицируемые изменения за последние полвека [17], а порог для 1 % наиболее высоких волн, оцениваемый по экспериментальным данным, заметно падает в последние два десятилетия. Этот процесс противоположен недавно обнаруженному для северо-восточной части Финского залива увеличению этого порога [16] на фоне отсутствия изменений в средних высотах волн. Тем не менее оба варианта изменений согласуются с постепенным увеличением по сравнению с другими направлениями частоты юго-западных и западных ветров [29, 30] на больших участках Балтийского моря. Анализ также указывает на некоторые признаки (хотя и статистически не значимые) того, что высота волн при наиболее сильных штормах не изменяется в течение последних 20 лет, но увеличивается частота штормов с очень высокими волнами.

Авторы выражают благодарность за предоставленные данные: Ральфу Вейссе (Institute for Coastal Research, Helmholtz-Zentrum Geesthacht) – результаты моделирования 1957–2002, Хеинцу Гюнтхеру, Ингеборг Нёрен (Institute for Coastal Research) – экспериментальные данные и Андрусу Ряямету (Institute of Cybernetics, Tallinn University of Technology) – результаты расчетов волнения.

Работа поддержана целевым финансированием Министерства образования и науки Эстонии (грант SF0140007s11), Научным фондом Эстонии (грант № 7413), BONUS+ проект BalticWay и Российским фондом фундаментальных исследований (гранты № 10-05-00199-а, 09-05-00204, 11-0200483).

Литература

1. *Лопатухин Л.И., Бухановский А.В., Иванов С.В., Чернышева Е.С.* Справочные данные по режиму ветра и волнения Балтийского, Северного, Черного, Азовского и Средиземного морей // Российский морской регистр судоходства. СПб., 2006. 450 с.
2. *Soomere T.* Extremes and decadal variations of the northern Baltic Sea wave conditions // Extreme Ocean Waves. Pelinovsky E., Kharif Ch. (eds.). Springer. 2008. P.139–157.
3. *Kharif C., Pelinovsky E.* Physical mechanisms of the rogue wave phenomenon // Eur. J. Mech. B Fluids. 2003. 22. P.603–634.
4. *Peterson P., Soomere T., Engelbrecht J., van Groesen E.* Interaction soliton as a possible model for extreme waves in shallow water // Nonlin. Proc. Geophys. 2003. V.10. P.503–510.
5. *Didenkulova I.* Shapes of freak waves in the coastal zone of the Baltic Sea (Tallinn Bay) // Boreal Env.Res. 2011. V.16 (Suppl. A). P.138–148.
6. *Walker D.A.G., Taylor P.H., Taylor R.E.* The shape of large surface waves on the open sea and the Draupner New Year wave // Appl. Ocean Res. 2004. V.26. P.73–83.
7. *Lavrenov I.V., Porubov A.V.* Three reasons for freak wave generation in the non-uniform current // Eur. J. Mech. B Fluids 2006 V.25. P.574–585.
8. *Soomere T.* Rogue waves in shallow water // Eur. Phys. J. Special Topics 2010. V.185. C.81–96.
9. *Soomere T., Engelbrecht J.* Weakly two-dimensional interaction of solitons in shallow water // Eur. J. Mech. B Fluids 2006. V.25. P.636–648.
10. *Ryabchuk D., Kolesov A., Chubarenko B., Spiridonov M., Kurennoy D., Soomere T.* Coastal erosion processes in the eastern Gulf of Finland and their links with long-term geological and hydrometeorological factors // Boreal Env. Res. 2011. V.16. (Suppl.A.) P.117–137.
11. *Soomere T., Behrens A., Tuomi L., Nielsen J.W.* Wave conditions in the Baltic Proper and in the Gulf of Finland during windstorm Gudrun // Nat. Hazards Earth Syst. Sci. 2008. V.8. P.37–46.
12. *Ryabchuk D., Leont'yev I., Sergeev A., Nesterova E., Sukhacheva L., Zhamoida V.* The morphology of sand spits and the genesis of long-shore sand waves on the coast of the eastern Gulf of Finland // Baltica. 2011. V.24. C.13–24.
13. Атлас волнения и ветра Финского залива / Отв. ред. Г.В.Ржеплинский Л.: Гидрометеоиздат, 1967. 48 с.
14. *Лопатухин Л.И., Миронов М.Е., Померанец К.С., Трапезников Ю.А., Чернышева Е.С.* Оценки экстремального ветра и волнения в восточной части Финского залива // Изв. ВНИИГ. 2006. 245. С.145–155.
15. *Räämet A., Soomere T.* The wave climate and its seasonal variability in the northeastern Baltic Proper // Estonian J. Earth Sci. 2010. V.59. P.100–113.
16. *Соомере Т., Зайцева-Пярнасте И., Ряямет А., Куренной Д.* О пространственно-временной изменчивости полей волнения Финского залива // Фундаментальная и прикладная гидрофизика. 2010. V.4(10). С.90–101.
17. *Soomere T., Weisse R., Behrens, A.* Wave climatology in the Arkona basin, the Baltic Sea // Ocean Sci. Discus. 2011. 8 (6). P.2237–2270.

18. *Weisse R., Günther H.* Wave climate and long-term changes for the Southern North Sea obtained from a high-resolution hindcast 1958–2002 // Ocean Dyn. 2007. V.57. P.161–172.
19. *Weisse R., von Storch H., Callies U.* et al. Regional meteorological marine reanalyses and climate change projections: results for Northern Europe and potential for coastal and offshore applications // Bull. Am. Meteor. Soc. 2009. V.90. P.849–860.
20. *Komen G.J., Cavaleri L., Donelan M., Hasselmann K., Hasselmann S. Janssen P.A.E.M.* Dynamics and modelling of ocean waves. Cambridge Univ. Press, 1994. 339 p.
21. *Augustin, J.* Das Seegangsklima der Ostsee zwischen 1958–2002 auf Grundlage numerischer Daten (Sea state climate of the Baltic Sea 1958–2002 based on numerical data) // Diploma Thesis. Institute for Coastal Research, GKSS Research Center Geesthacht, Geesthacht, Germany [in German]. 2005.
22. *Feser F., Weisse R., von Storch H.* Multi-decadal atmospheric modeling for Europe yields multi-purpose data // Eos Transactions. 2001. V.82. P.305–310.
23. *Kalnay E., Kanamitsu M., Kistler R.* et al. The NCEP/NCAR reanalysis project // Bull. Am. Meteorol. Soc. 1996. V.77. P.437–471.
24. *Kistler R., Kalnay E., Collins W.* et al. The NCEP/NCAR 50-year reanalysis: monthly means CD-ROM and documentation // Bull. Am. Meteorol. Soc. 2001. V.82. P.247–267.
25. *Soomere T.* Wind wave statistics in Tallinn Bay // Boreal Env. Res. 2005. V.10. P.103–118.
26. *Soomere T., Keevallik S.* Directional and extreme wind properties in the Gulf of Finland // Proc. Estonian Acad. Sci. Eng. 2003. V.9. P.73–90.
27. *Soomere T., Räämet A.* Spatial patterns of the wave climate in the Baltic Proper and the Gulf of Finland // Oceanologia 2011. V.53(1-TI). P.335–371.
28. *Zaitseva-Pärnaste I., Soomere T., Tribštok O.* Spatial variations in the wave climate change in the eastern part of the Baltic Sea // J. Coast. Res. 2011. Special Issue 64. P.195–199.
29. *Jaagus J.* Long-term changes in frequencies of wind directions on the western coast of Estonia. Institute of Ecology, Tallinn University. Publications. 2009. [in Estonian]. V.11. P.11–24.
30. *Lehmann A., Getzlaff K., Harlass J.* Detailed assessment of climate variability in the Baltic Sea area for the period 1958 to 2009 // Clim. Res. 2011. V.46. P.185–196.

Статья поступила в редакцию 10.09.2011 г.

DISSERTATIONS DEFENDED AT TALLINN UNIVERSITY OF TECHNOLOGY ON *CIVIL ENGINEERING*

1. **Heino Mölder**. Cycle of Investigations to Improve the Efficiency and Reliability of Activated Sludge Process in Sewage Treatment Plants. 1992.
2. **Stellian Grabko**. Structure and Properties of Oil-Shale Portland Cement Concrete. 1993.
3. **Kent Arvidsson**. Analysis of Interacting Systems of Shear Walls, Coupled Shear Walls and Frames in Multi-Storey Buildings. 1996.
4. **Andrus Aavik**. Methodical Basis for the Evaluation of Pavement Structural Strength in Estonian Pavement Management System (EPMS). 2003.
5. **Priit Vilba**. Unstiffened Welded Thin-Walled Metal Girder under Uniform Loading. 2003.
6. **Irene Lill.** Evaluation of Labour Management Strategies in Construction. 2004.
7. **Juhan Idnurm**. Discrete Analysis of Cable-Supported Bridges. 2004.
8. **Arvo Iital**. Monitoring of Surface Water Quality in Small Agricultural Watersheds. Methodology and Optimization of monitoring Network. 2005.
9. **Liis Sipelgas**. Application of Satellite Data for Monitoring the Marine Environment. 2006.
10. **Ott Koppel**. Infrastruktuuri arvestus vertikaalselt integreeritud raudtee-ettevõtja korral: hinnakujunduse aspekt (Eesti peamise raudtee-ettevõtja näitel). 2006.
11. **Targo Kalamees**. Hygrothermal Criteria for Design and Simulation of Buildings. 2006.
12. **Raido Puust**. Probabilistic Leak Detection in Pipe Networks Using the SCEM-UA Algorithm. 2007.
13. **Sergei Zub**. Combined Treatment of Sulfate-Rich Molasses Wastewater from Yeast Industry. Technology Optimization. 2007.
14. **Alvina Reihan**. Analysis of Long-Term River Runoff Trends and Climate Change Impact on Water Resources in Estonia. 2008.
15. **Ain Valdmann**. On the Coastal Zone Management of the City of Tallinn under Natural and Anthropogenic Pressure. 2008.

16. **Ira Didenkulova**. Long Wave Dynamics in the Coastal Zone. 2008.
17. **Alvar Toode**. DHW Consumption, Consumption Profiles and Their Influence on Dimensioning of a District Heating Network. 2008.
18. **Annely Kuu**. Biological Diversity of Agricultural Soils in Estonia. 2008.
19. **Andres Tolli**. Hiina konteinerveod läbi Eesti Venemaale ja Hiinasse tagasisaadetavate tühjade konteinerite arvu vähendamise võimalused. 2008.
20. **Heiki Onton**. Investigation of the Causes of Deterioration of Old Reinforced Concrete Constructions and Possibilities of Their Restoration. 2008.
21. **Harri Moora**. Life Cycle Assessment as a Decision Support Tool for System optimisation – the Case of Waste Management in Estonia. 2009.
22. **Andres Kask**. Lithohydrodynamic Processes in the Tallinn Bay Area. 2009.
23. **Loreta Kelpšaitė**. Changing Properties of Wind Waves and Vessel Wakes on the Eastern Coast of the Baltic Sea. 2009.
24. **Dmitry Kurennoy.** Analysis of the Properties of Fast Ferry Wakes in the Context of Coastal Management. 2009.
25. **Egon Kivi**. Structural Behavior of Cable-Stayed Suspension Bridge Structure. 2009.
26. **Madis Ratassepp**. Wave Scattering at Discontinuities in Plates and Pipes. 2010.
27. **Tiia Pedusaar**. Management of Lake Ülemiste, a Drinking Water Reservoir. 2010.
28. **Karin Pachel**. Water Resources, Sustainable Use and Integrated Management in Estonia. 2010.
29. **Andrus Räämet**. Spatio-Temporal Variability of the Baltic Sea Wave Fields. 2010.
30. **Alar Just**. Structural Fire Design of Timber Frame Assemblies Insulated by Glass Wool and Covered by Gypsum Plasterboards. 2010.
31. **Toomas Liiv**. Experimental Analysis of Boundary Layer Dynamics in Plunging Breaking Wave. 2011.
32. **Martti Kiisa**. Discrete Analysis of Single-Pylon Suspension Bridges. 2011.
33. **Ivar Annus**. Development of Accelerating Pipe Flow Starting from Rest. 2011.
34. **Emlyn D.Q. Witt**. Risk Transfer and Construction Project Delivery Efficiency – Implications for Public Private Partnerships. 2012.